



HEINRICH HEINE
UNIVERSITÄT DÜSSELDORF

**The Kinetics of α -Synuclein Aggregation:
Single Fibril Growth, β 1- β 2 Contacts, Membrane
Environments and Dityrosine Formation**

Inaugural-Dissertation

zur Erlangung des Doktorgrades der
Mathematisch-Naturwissenschaftlichen Fakultät der
Heinrich-Heine-Universität Düsseldorf

vorgelegt von
Michael Marius Wolfram Würdehoff
aus Viersen

Düsseldorf, Juli 2017

aus dem Institut für Physikalische Biologie
der Heinrich-Heine-Universität Düsseldorf

Gedruckt mit der Genehmigung der
Mathematisch-Naturwissenschaftlichen Fakultät der
Heinrich-Heine-Universität Düsseldorf

Berichtersteller:

1. Prof. Dr. Dieter Willbold
2. Dr. Wolfgang Hoyer

Tag der mündlichen Prüfung: 08.08.2017

“It’s like catching a fish, you know what I mean? It’s the fish
that’s beautiful, not the fisherman.”

Joshua Michael Homme

Contents

Summary	iii
Zusammenfassung	v
List of Figures	vii
List of Tables	ix
1 Introduction	1
1.1 Protein Misfolding Diseases	1
1.2 Protein Misfolding and Amyloid Aggregation	1
1.2.1 Amyloid Structures and Toxicity	3
1.2.2 Detection of Amyloid Aggregation	5
1.3 Parkinson's Disease	7
1.4 α -Synuclein	9
1.4.1 Physiological Aspects	9
1.4.2 α -Synuclein and Membranes	11
1.4.3 α -Synuclein in Disease	12
1.5 Oxidative Stress in PD	15
1.5.1 Dityrosine Formation	16
1.6 Aim of This Work	18
2 Articles	21
2.1 Single Fibril Growth Kinetics of α -Synuclein	21
2.1.1 Article Information	21
2.1.2 Abstract	21
2.1.3 Introduction	22
2.1.4 Results	23
2.1.5 Discussion	27
2.1.6 Materials and Methods	28
2.1.7 Supplement	30
2.2 Contacts between β 1- β 2 Segments in α -Synuclein	33
2.2.1 Article Information	33
2.2.2 Abstract	33
2.2.3 Article	33
2.2.4 Materials and Methods	38
2.2.5 Supplement	40
2.3 Interaction of α -Synuclein with Lipid Bilayer Nanodiscs	43
2.3.1 Article Information	43

Contents

2.3.2	Abstract	43
2.3.3	Introduction	43
2.3.4	Results and Discussion	45
2.3.5	Conclusion	56
2.3.6	Methods	58
2.3.7	Supplement	62
2.4	Dityrosine formation in α -Synuclein	69
2.4.1	Article Information	69
2.4.2	Abstract	69
2.4.3	Introduction	69
2.4.4	Results	71
2.4.5	Discussion	77
2.4.6	Materials and Methods	80
2.4.7	Supplement	83
3	General Discussion	85
	Bibliography	93
	Appendix	109
	List of Abbreviations	111
	Danksagung	115
	Erklärung	117

Summary

Parkinson's disease (PD) is the second most common neurodegenerative disease. In PD, aggregation of the protein α -synuclein (α -syn) in the *substantia nigra* is the central hallmark of pathogenesis. Therefore, understanding the aggregation process itself as well as identifying factors that influence it is crucial. In this respect, this cumulative PhD thesis investigates the aggregation kinetics of α -syn in dependence of several factors in a comprehensive and detailed manner in four dedicated chapters.

In [chapter one](#), the aggregation of α -syn is studied by high-resolution fluorescence microscopy. This *in situ* real-time analysis of aggregation led to the detection of a stop-and-go mechanism of fibril growth, where growth phases were consistently interrupted by stop phases. Stop and growth phases were isoenergetic and interconverted with rate constants $k_{+/-}$ of $\sim 1.5 \times 10^{-4} \text{ s}^{-1}$. On average, α -syn fibrils grew with a growth rate of $\sim 8.5 \text{ nm min}^{-1}$, which corresponded to a growth rate constant of $8.6 \times 10^{-3} \text{ M}^{-1} \text{ s}^{-1}$. The development of this *in situ* assay enables the detailed study of the aggregation process and factors that influence it.

[Chapter two](#) covers the influence of a covalent linkage of $\beta 1$ - and $\beta 2$ -fragments of α -syn on its aggregation and the aggregation of amyloid- β and IAPP. A covalent disulfide linkage of $\beta 1$ - and $\beta 2$ -fragments (called α -synCC) inhibited its aggregation, both *de novo* and seeded aggregation. α -SynCC also inhibited the aggregation of other amyloid proteins substoichiometrically and greatly reduced cytotoxicity of α -syn, amyloid- β and IAPP in SH-S5Y5 cell culture. The identification of this inhibitory conformation that abolishes amyloid aggregate formation harbours great potential for the development of therapeutic molecules.

In [chapter three](#), the effect of membrane-binding on α -syn aggregation is investigated, as α -syn is both a cytosolic and a membrane-associated protein. To mimic physiological lipid bilayers, we used nanodiscs (ND) composed of different lipids (different head group charge, fatty acid type, size) framed by a membrane scaffold protein. By using several biophysical methods we deciphered kinetic, thermodynamic and mechanistic properties of α -syn interaction with membranes, e.g. the higher the negative charge and available membrane surface area, the more α -syn residues were bound and aggregation was inhibited. In low membrane surface area conditions however, α -syn aggregation was stimulated. This study provided detailed, residue-resolved insights into membrane-binding of α -syn and concomitant aggregation behaviour.

[Chapter four](#) deals with the influence of oxidative-stress-associated dityrosine (DiY)-crosslinking in α -syn, as increased oxidative stress is another hallmark of PD. We used UV-irradiation-assisted DiY formation as a model system to specifically form dityrosines. α -Syn as an intrinsically disordered protein showed a high tendency to form both intra- and intermolecular dityrosine crosslinks, independent from tyrosine position. Intermolecular DiY dimers strongly inhibited both *de novo* and seeded aggregation of wildtype α -syn substoichiometrically. DiY-crosslinking of preformed α -syn aggregates stabilized them against dissolution, partly dissolved DiY-crosslinked aggregates acted as efficient on-pathway seeds for α -syn aggregation. This study showed that dityrosine formation can both inhibit aggregation but also stabilize toxic aggregates of α -syn.

Zusammenfassung

Die Parkinson-Krankheit (PD) ist die zweithäufigste neurodegenerative Krankheit. Das zentrale pathogenetische Merkmal der PD ist die Aggregation des Proteins α -Synuklein (α -Syn) in der *Substantia nigra*. Das Verständnis des Aggregationsprozesses sowie die Identifizierung beeinflussender Faktoren ist somit von wesentlicher Bedeutung. Deshalb wird in dieser kumulativen Dissertation die Aggregation von α -Syn detailliert und in Abhängigkeit zahlreicher Faktoren in vier Kapiteln untersucht.

In [Kapitel eins](#) wird die Aggregation von α -Syn mithilfe hochauflösender Fluoreszenzmikroskopie untersucht. Diese *in situ*-Echtzeitanalyse führte zur Identifizierung eines "stop-and-go" Mechanismus des Fibrillenwachstums, in welchem das Fibrillenwachstum durch Stopphasen unterbrochen war. Die Wachstums- und Stopphasen waren isoenergetisch und wechselten mit Ratenkonstanten von $k_{+/-}$ von $\sim 1.5 \times 10^{-4} \text{ s}^{-1}$. Im Durchschnitt wuchsen α -Syn-Fibrillen mit einer Wachstumsrate von $\sim 8.5 \text{ nm min}^{-1}$, dies entspricht einer Wachstumskonstante von $8.6 \times 10^{-3} \text{ M}^{-1} \text{ s}^{-1}$. Die Entwicklung dieses *in situ* Assays ermöglicht die detaillierte Untersuchung von α -Syn-Aggregation und Faktoren, die sie beeinflussen.

[Kapitel zwei](#) behandelt den Einfluss der kovalenten Bindung zwischen den $\beta 1$ - und $\beta 2$ -Fragmenten in α -Syn auf seine Aggregation und die Aggregation von Amyloid- β und IAPP. Die kovalente Disulfidbrücke zwischen den $\beta 1$ - und $\beta 2$ -Fragmenten (α -SynCC) verhindert *de novo* und keiminduzierte Aggregation. α -SynCC inhibierte auch die Aggregation von anderen Proteinen substöchiometrisch und reduzierte die Cytotoxizität von α -Syn, Amyloid- β und IAPP in SH-S5Y5-Zellkultur stark. Die Identifizierung dieser inhibitorischen Konformation, die amyloide Aggregation verhindert, birgt großes Potential bei der Entwicklung von Therapeutika.

In [Kapitel drei](#) wird der Effekt von Lipidmembranen auf die α -Syn-Aggregation untersucht. Um physiologische Lipidmembranen nachzustellen, benutzten wir Nanodisks (ND) mit verschiedenen Lipiden (unterschiedliche Ladung, Fettsäuren und Größe), eingefasst von einem Gerüstprotein. Mithilfe von mehreren biophysikalischen Methoden wurden kinetische, thermodynamische und mechanistische Eigenschaften der Interaktion von α -Syn mit Membranen bestimmt, z.B. je höher die negative Ladung und verfügbare Membranoberfläche, desto mehr Aminosäuren von α -Syn wurden gebunden und die Aggregation war inhibiert. Eine geringe Membranoberfläche hatte einen stimulierenden Effekt auf die Aggregation. Zusammenfassend haben wir in dieser Studie detaillierte, aminosäurespezifische Erkenntnisse in die Membranbindung und damit einhergehende Aggregation von α -Syn geschaffen.

[Kapitel vier](#) beschäftigt sich mit oxidativem-stress-assoziiertes Dityrosinbildung in α -Syn. UV-Bestrahlung diente als Modellsystem, um Dityrosine (DiY) spezifisch zu bilden. α -Syn als intrinsisch ungefaltetes Protein zeigte eine starke Tendenz, intra- und intermolekulare Dityrosine unabhängig von der Tyrosinposition zu bilden. Intermolekulare DiY Dimere inhibierten die *de novo* und keiminduzierte Aggregation von α -Syn substöchiometrisch. DiY-verbrückte α -Syn-Aggregate waren stabil gegenüber Denaturierung und teilweise aufgelöste DiY-Aggregate waren effiziente Keime für die α -Syn-Aggregation. Diese Studie zeigte, dass DiY-bildung die Aggregation verhindert, allerdings toxische Aggregate von α -Syn stabilisiert.

List of Figures

1.1	Protein folding funnel with misfolding pathways and chaperones	2
1.2	The amyloid aggregation process	3
1.3	Structures of amyloid oligomers and amyloid fibrils	4
1.4	Thioflavin T in its free state and bound to amyloid fibrils and ThT assay	6
1.5	Monitoring amyloid aggregation by AFM and TIRFM	7
1.6	Midbrain sections of a healthy brain and a PD patient's brain	8
1.7	Schematic of α -syn with highlighted regions, posttranslational modifications, familial mutations and tyrosines	10
1.8	Amphipathic repeats and α -helical structures of α -syn upon membrane-binding	11
1.9	Structures of α -syn oligomers and α -syn fibrils	13
1.10	Oxidative stress in PD	16
1.11	Reaction scheme of dityrosine formation	17
2.1	Direct observation of α -syn fibril growth by TIRFM	23
2.2	Elongation of an individual fibril and identification of stop states	24
2.3	Time dependence of fibril lengths and growth rates	25
2.4	Two-state model of α -syn fibril elongation	26
2.5	Seeded fibrillation of α -syn in a test tube	27
2.6	AFM images of α -syn seeds used for real-time monitoring of fibrillation	30
2.7	Growth rates of fibrils f1-f10 plotted over time	31
2.8	Probability distribution of growth states and stop states over time	31
2.9	Kinetic analysis of reentry into the growth state	32
2.10	Protein engineering and characterization of α -synCC	35
2.11	α -SynCC inhibits aggregation and toxicity of wt α -syn, A β and IAPP	36
2.12	Representation of the inhibitory effect of tertiary contacts in the β 1– β 2 region of α -syn on the aggregation of amyloidogenic IDPs	37
2.13	SEC analysis of aggregation of α -synCC and wt α -syn	41
2.14	The positions of the exchanges to cysteine (yellow) in α -synCC are identical to those in A β CC in relation to the β -hairpin	41
2.15	ThT time course of fibrillation of wt α -syn in the presence of preformed wt α -syn fibril seeds, with addition of α -synCC at the time points indicated by arrows	41

2.16 SEC analysis of A β aggregation in absence and presence of α -synCC	42
2.17 Lipid charge content modulates α S membrane binding modes and different binding modes show different effects on α S aggregation properties	46
2.18 Nanodiscs binding induces α -helical structure in α S	48
2.19 α S-lipid interaction is favored by, and potentially modulates, membrane plasticity	49
2.20 Limited but highly charged lipid surface area can induce an α S binding mode capable of promoting aggregation through induction of primary nucleation	52
2.21 Moderately charged membrane surfaces interact more transiently with α S and do not induce primary nucleation	54
2.22 Model of the influence of different NDs on the α S aggregation pathways and its potential implication in the context of cell/vesicle membranes	57
2.23 Formation of lipid mixtures in NDs, lipid phase transitions and stability of α S association	63
2.24 α S-ND interactions using different MSP constructs, lower pH and higher temperature	64
2.25 Lipid properties and α S-membrane interactions as seen by MD simulations	65
2.26 Amyloid fibril nucleation and elongation in the presence of 50% POPG ND and rational for normalization of ThT data	66
2.27 DiY formation kinetics of WT α -syn and Y-to-A mutants	72
2.28 DiY formation kinetics of α -syn WT and ribonuclease A	73
2.29 Influence of DiY- α -syn and other DiY species on the aggregation of α -syn	74
2.30 Influence of DiY- α -syn dimers and monomers on α -syn aggregation	75
2.31 DiY-crosslinking stabilizes α -syn fibril seeds	76
2.32 Scheme of the effects of DiY formation on α -syn aggregation	78
2.33 Tyrosine and DiY spectra of α -syn WT and α -syn Y39A-Y125A-Y133A-Y136A (Tyr KO) mutant before and after UV-irradiation	83
3.1 Summarizing scheme of factors that influence the aggregation kinetics of α -syn .	92

List of Tables

2.1	Estimated kinetic parameters for α -syn fibril growth	26
2.2	Summary of NMR samples used in the study	67
2.3	Summary of MD simulations used for the study	68
2.4	Tyrosine and DiY fluorescence emission of α -syn variants before and after DiY formation	84
2.5	Rate constants of DiY formation in α -syn	84

1 Introduction

1.1 Protein Misfolding Diseases

Protein Misfolding Diseases (PMDs) or amyloidoses are diseases that are caused by the misfolding of soluble endogenous proteins into insoluble protein aggregates, called amyloid fibrils. The misfolding/aggregation process is detrimental to cells in direct and indirect ways. Today, there are around 50 different PMDs described, ranging from several neurodegenerative diseases like Alzheimer's disease (AD), Parkinson's disease (PD) or Transmissible spongiform encephalopathies (TSEs) to systemic amyloidoses like AL amyloidosis and localized amyloidoses like type II diabetes mellitus (T2D) [1]. AD, PD and diabetes mellitus alone accounted for ~3 million deaths in 2013, constituting 5.6% of all deaths around the world [2]. In developed high income countries, AD is mostly within the top five causes of death, which will become an even bigger socioeconomical issue, as society ages and a therapy is not available.

In PMDs, the protein misfolding process is seen as the central causative event that initiates pathology. This is supported by genetic studies, where mutations leading to increased production of the protein or mutations that increase the aggregation propensity of the protein cause early-onset or severe forms of the disease. A corresponding genetic background and amyloid pathology has e.g. been described for AD [3], PD [4], Amyotrophic Lateral Sclerosis (ALS) [5] and Huntington's disease [6]. In the case of AD, this central protein aggregation process is called the amyloid cascade and has already been formulated in 1992 by Hardy and Higgins [7].

1.2 Protein Misfolding and Amyloid Aggregation

The misfolding of endogenous proteins is a normal process that can happen during protein folding, as there are often metastable intermediate or stable alternative protein structures on the way to the native, functional protein. When looking at the energy landscape of protein folding, there are often several possible structures that are energetically favorable. These structures represent kinetic traps with a local energy minimum within the protein folding funnel (fig. 1.1) [8]. Once misfolded, proteins can either be correctly folded by the help of chaperones, or degraded by either the ubiquitin-proteasome system or the lysosomal pathway (autophagy) [9, 10].

In PMDs, these pathways are challenged by an overproduction of aggregation-prone proteins or by mutated proteins with a very high aggregation propensity [11]. This results in increased aggregate and amyloid fibril formation which then further inhibits the ubiquitin-proteasome system [12]. Misfolding and aggregate formation can either occur in highly structured proteins like superoxide dismutase in ALS [13] or in intrinsically disordered proteins (IDPs) like α -synuclein in PD [14].

In globular, structured proteins, complete misfolding and aggregation is often preceded by partial misfolding, where certain domains of the protein unfold and misfold locally, as has been e.g. been described for human lysozyme [15]. In IDPs like α -synuclein, there is no need for

unfolding and because of their high flexibility, aggregation-prone β -sheet structures are within their normal transient structural fluctuations [16].

Protein misfolding and aggregation leads to an increase in β -sheets, especially in the late stages, when aggregated proteins form amyloid fibrils. The term "amyloid" has been originally coined by Rudolph Virchow in 1854, who found dense inclusions in brain specimens that could be stained with iodine and therefore called them starch-like (amyloid). In 1859, Friedrich and Kekulé then showed that these inclusions are composed of proteins instead of carbohydrates, thereby first defining amyloid as protein aggregates [17]. Amyloid fibrils are basically arrays of β -strands that are organized into β -sheet-rich fibres. It has been proposed that amyloid formation is not a rare event restricted to a few proteins, but rather that every polypeptide chain has a certain tendency to form an amyloid β -sheet structure as an alternative to its native state [18]. Interestingly, amyloid fibrils are not only associated with diseases, there are several proteins that form functional amyloid fibrils, e.g. URE2p from *Saccharomyces cerevisiae*, Curli from *Escherichia coli* or Pmel17 in *Homo sapiens* [19].

Aggregation of a protein usually follows a nucleation-dependent polymerization process, where the first step is the formation of aggregation nuclei that then seed the aggregation of monomers [20]. This is a continuous process that starts with the misfolding of the monomeric protein to an aggregation-prone conformation. Several monomers can then cluster to oligomers, which can be quite heterogenous, with structures that are on-pathway or off-pathway to amyloid fibrils. Certain on-pathway oligomers, e.g. called protofibrils are then highly seeding-competent amyloid structures that can polymerize and reorganize to amyloid fibrils (fig. 1.2).

The process of aggregation from a monomer to an oligomer and finally an amyloid fibril is called primary nucleation, as the aggregate just forms from associating monomers. There are however two additional secondary processes which influence the aggregation kinetics of amyloid proteins. Once the first fibrils are formed they can break, thereby creating additional fibril ends that are accessible for elongation by monomer addition [21]. This mechanism is called fibril fragmentation and leads to an increase in aggregation speed, as the broken fibrils act as efficient aggregation seeds. A second process that is dependent on preformed aggregates is secondary nucleation. Secondary nucleation describes when β -sheet-rich aggregates cause the aggregation of nearby monomeric proteins by catalyzing aggregation on their surface

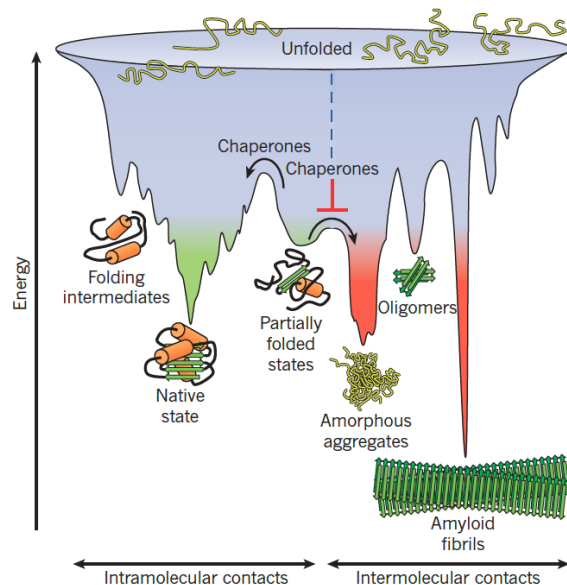


Figure 1.1: Protein folding funnel with misfolding pathways and chaperones. Red areas depict problematic outcomes of protein misfolding that will be subjected to degradation by the Ubiquitin-Proteasome system or the autophagy-lysosome pathway. From Hartl et al., 2011 [8].

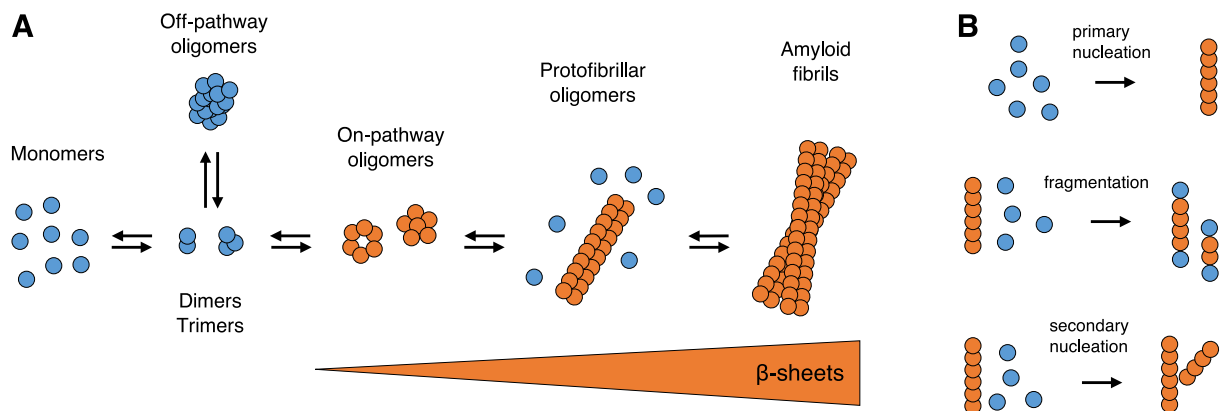


Figure 1.2: The amyloid aggregation process. A: Aggregation of a protein from monomer to amyloid fibril. B: Three main processes that happen during amyloid aggregation. Blue species are non- β -sheet-rich structures (yet) or are off-pathway aggregates, orange species are β -sheet-rich and can be denoted as amyloid structures.

(fig. 1.2B). This process has been described to be the main factor governing the aggregation kinetics of $A\beta$ once enough aggregates have been formed by primary nucleation [22].

1.2.1 Amyloid Structures and Toxicity

Generally speaking, protein aggregates are detrimental to cells in indirect and direct ways. Indirect toxicity arises, when the aggregation of a protein leads to depletion of the native functional protein, which can then no longer exert its physiological function. Increased aggregation of a certain protein can also trigger the aggregation of other aggregation-prone proteins, thereby multiplying the detrimental effect [23, 24]. Accumulation of such protein aggregates directly leads to proteostatic stress that compromises several organelles and cellular processes, e.g. the ubiquitin-proteasome system [12] and the endoplasmic reticulum (ER). ER stress causes a build-up of unfolded and misfolded (membrane-)proteins, which then can no longer be post-translationally modified and/or shuttled to the cell membrane. Persistent ER stress finally results in autophagy and apoptosis [25].

Various aggregation intermediates on the pathway to an amyloid fibril have been described to be toxic to cells. Whereas the monomeric form of an aggregation-prone protein is usually non-toxic, already dimeric assemblies have been reported to be highly synaptotoxic, e.g. in the case of the AD-associated protein $A\beta$ [26]. Trimers of $A\beta$ also greatly impair long-term potentiation [27]. Higher number oligomers of amyloid proteins can be quite heterogenous in structure, but many structural investigations of toxic oligomers show a dominance of β -sheets. For $A\beta$, several β -sheet-rich structures have been suggested, e.g. an antiparallel β -sheet structure, a β -barrel conformation and, similar to amyloid fibrils, a cross- β -architecture (fig. 1.3A,B) [28–30].

Other amyloidogenic proteins like PD-associated α -synuclein or T2D-associated IAPP also form β -sheet rich oligomeric structures on their way to the amyloid fibril [31, 32]. Many of these β -oligomers are believed to consist of β -strands arranged around central cavity, which could lead to membrane disruption and cell death by uncontrolled ion flux. It has also been proposed that small oligomers of amyloid proteins, that do not yet possess an extensive β -sheet structure, can

form annular molecules that act as unspecific ion channels within the cell membrane, thereby causing cell death (fig. 1.3C) [33–35].

Besides the fact that β -oligomers disrupt cell membranes, $A\beta$ oligomers have also been shown to cause synaptotoxicity by binding to membrane-bound prion protein and activating a cascade which leads to reduced NMDA receptors on the cell surface [36]. It has also been reported that $A\beta$ -oligomers induce hyperphosphorylation of the microtubule-stabilizing tau protein and subsequently cause dendritic spine loss, which is another hallmark of AD [37].

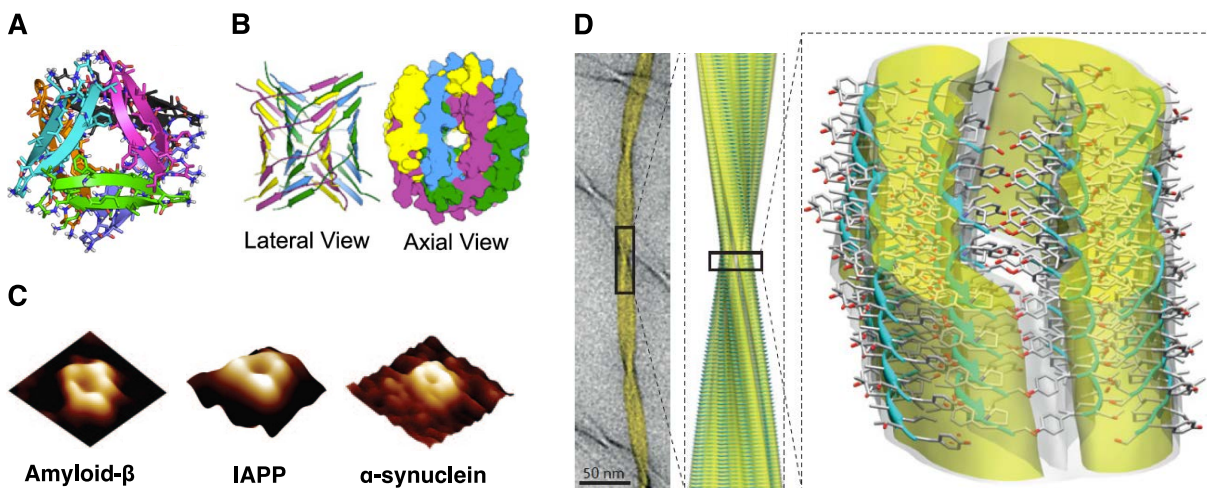


Figure 1.3: Structures of amyloid oligomers and amyloid fibrils. A: X-ray structure of a hexameric oligomer of a modified $A\beta_{17-36}$ peptide from Spencer et al., 2014 [38]. B: Model of a toxic 20-meric oligomer of $A\beta$ with cross- β structure from Stroud et al., 2012 [30]. C: AFM micrographs of small pore-forming oligomers of amyloidogenic proteins $A\beta$, IAPP and α -synuclein from Quist et al., 2005 [35], copyright (2005) National Academy of Sciences. D: TEM (left), MAS NMR structure fitted into the cryo-EM reconstruction of transthyretin₁₀₅₋₁₁₅ fibrils (middle) with zoom (right) from Fitzpatrick et al., 2013 [39].

In contrast to the heterogenous nature of amyloid oligomer structures, the structure of amyloid fibrils is highly similar between numerous amyloidogenic proteins [40]. Amyloid fibrils are fibres with a diameter of around 2 nm to 20 nm and a variable length, which can go up to tens of micrometers. They usually consist of several filaments, which are twisted around each other (fig. 1.3D). When examined by X-ray diffraction, amyloid fibrils of different amyloidogenic proteins exhibit a cross- β diffraction pattern [41]. The so-called cross- β -structure of amyloid fibrils describes a structure, where arrays of β -strands are organized perpendicular to the fibril axis, with stabilizing hydrogen bonds between β -strands (fig. 1.3D).

Whereas amyloid fibrils have been seen as the toxic protein conformation in PMDs, this hypothesis has changed somewhat in recent years, with the focus currently lying on oligomeric aggregation intermediates. Amyloid fibrils are now often seen as the final outcome of protein aggregation with little pathological relevance, once fibrils are deposited intra- or extracellularly in aggresomes or large aggregates like Lewy bodies in PD or amyloid plaques in AD [1]. However, several studies point out that amyloid fibrils are also toxic. On the one hand, fibrils are

in an equilibrium with oligomers and monomers, so they can be a source of toxic oligomers that are dissociating from the fibril [42]. On the other hand, amyloid fibrils of α -synuclein and huntingtin have been shown to actually be more toxic to cells than on-pathway oligomers, when the concentration is accurately taken into account, as they cause membrane permeabilization and apoptosis through caspase-3 activation [43]. Also, fibrils of α -synuclein, tau and superoxide dismutase (SOD1) are able to spread between neurons, thereby triggering the aggregation of monomeric protein and spreading disease throughout the brain [44–46].

1.2.2 Detection of Amyloid Aggregation

Dyes

The first staining and detection method for amyloid aggregates in histological specimens was the iodine staining applied by Rudolph Virchow in 1854. Iodine staining was however not specific for amyloid protein aggregates, as it is usually a staining method for starch. In 1927, Divry and Florkin discovered an amyloid-specific staining method that is still considered the gold-standard of amyloid staining in histological samples today, the Congo red staining [47]. Congo red stains amyloid aggregates red and exhibits a apple-green birefringence when examined under polarized light. Today, especially for staining and detecting amyloid aggregation *in vitro*, the fluorescent dye Thioflavin T (ThT) is widely used. It was discovered by Vassar and Culling in 1959 and has certain advantages over Congo red [48]. In contrast to Congo red, Thioflavin T is a fluorescent dye that greatly enhances its fluorescence emission when bound to amyloid fibrils (~ 100 fold), which makes a laborious staining and washing procedure as well as a polarized light source obsolete. When bound to amyloid fibrils, ThT also changes its excitation and emission wavelengths, from λ_{ex} : 385 nm (free) to λ_{ex} : 450 nm (bound) and from λ_{em} : 445 nm (free) to λ_{em} : 482 nm (bound), respectively.

Thioflavin T is a benzothiazole dye that can be seen as a molecular rotor, where the benzothiazole and aniline moieties can rotate freely around their shared C-C bond in solution, thereby effectively quenching fluorescence (fig. 1.4A). When ThT is bound within the cross- β architecture of amyloid fibrils however, it gets locked in a planar conformation that greatly increases its fluorescence (fig. 1.4B) [49].

Monitoring protein aggregation with Thioflavin T has become a very popular tool for *in vitro* studies, as it is very sensitive and can easily be used in high-throughput screens in multi-wellplates. The so called ThT assay has been pioneered by Harry LeVine III in 1993 [50]. ThT is added in concentrations of around 1 μM to 50 μM to solutions of aggregation-prone proteins that are then subjected to specific aggregation conditions (e.g. 37 $^{\circ}\text{C}$ and shaking, low or high pH, low or high ionic strength etc.). After a variable lag phase, where the first aggregates form by primary nucleation, the ThT signal rises exponentially, proportional to the increase in β -sheets until it reaches a saturation, when all monomers are aggregated to amyloid fibrils (fig. 1.4C). ThT assays are a suitable tool to generally monitor the aggregation of a protein. It has however its limitations, as it can only describe the complete aggregation process. For example, no in-

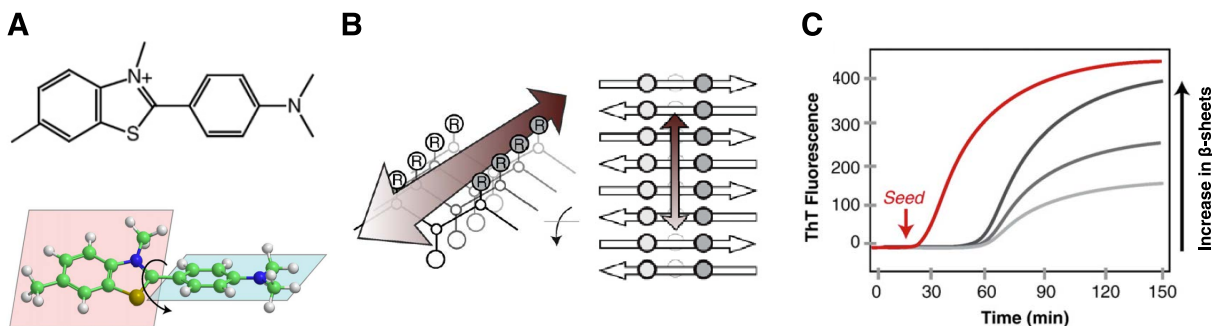


Figure 1.4: Thioflavin T in its free state and bound to amyloid fibrils and ThT assay. A: Thioflavin T in its free state. The benzothiazole and aniline moieties can rotate freely, thereby quenching fluorescence. B: Thioflavin T bound within the cross- β architecture of amyloid fibrils. ThT can bind along surface side-chain grooves in a β -sheet. C: Conventional ThT assay to monitor the aggregation (increase in β -sheets) of proteins. Modified from Biancalana et al., 2010 [48].

formation on the growth kinetics of a single fibril can be retrieved. It has also been shown that several compounds can interfere with ThT binding to fibrils [51].

Besides ThT, 8-Anilino-naphthalene-1-sulfonic acid (ANS) and 4-(dicyanovinyl)-julolidine (DCVJ) are also used to detect amyloid aggregates in solution. ANS is a fluorescent dye which is used to detect exposed hydrophobic patches in proteins, making it a suitable tool to detect protein un-/misfolding and early stages of aggregation [52]. It has indeed been reported that ANS can selectively detect toxic oligomers of A β that do not yet show a marked ThT fluorescence [53]. DCVJ is a molecular rotor like ThT, it can be used as a viscosity or solvent probe and it also binds to hydrophobic patches of proteins. Similar to ANS, DCVJ has been shown to be more sensitive for small oligomeric aggregate detection than ThT [54].

Microscopy

To gain deeper insight into amyloid aggregation kinetics on a molecular level, several microscopic methods have been employed. When aggregation on a single fibril level should be measured *in situ* and in real-time, the measurement has to take place in a buffered solution with free monomers. For that reason, two microscopic methods are especially suitable, atomic force microscopy (AFM) and fluorescence microscopy. AFM is a type of scanning probe microscopy, where a very thin cantilever tip (nanometer radius) scans a sample that has been deposited on a planar carrier, e.g. a mica surface. Because it is not an optical method, the diffraction limit does not have to be taken into account, so it can provide a resolution down to <0.1 nm, which is around 1000 times lower than the optical diffraction limit [55]. As amyloid fibrils are around 2 nm to 20 nm in diameter, AFM is suitable for imaging of amyloid aggregation. It did indeed provide new and detailed insights into the aggregation kinetics of e.g. IAPP and α -synuclein [56, 57]. Studying amyloid formation by AFM enabled the measurement of individual fibril growth rates (e.g. 1.1 nm min^{-1} for IAPP and around 10 nm min^{-1} for α -synuclein) as well as structural rearrangements and stop phases during fibril growth. Figure 1.5A shows seeded α -synuclein growth studied by AFM.

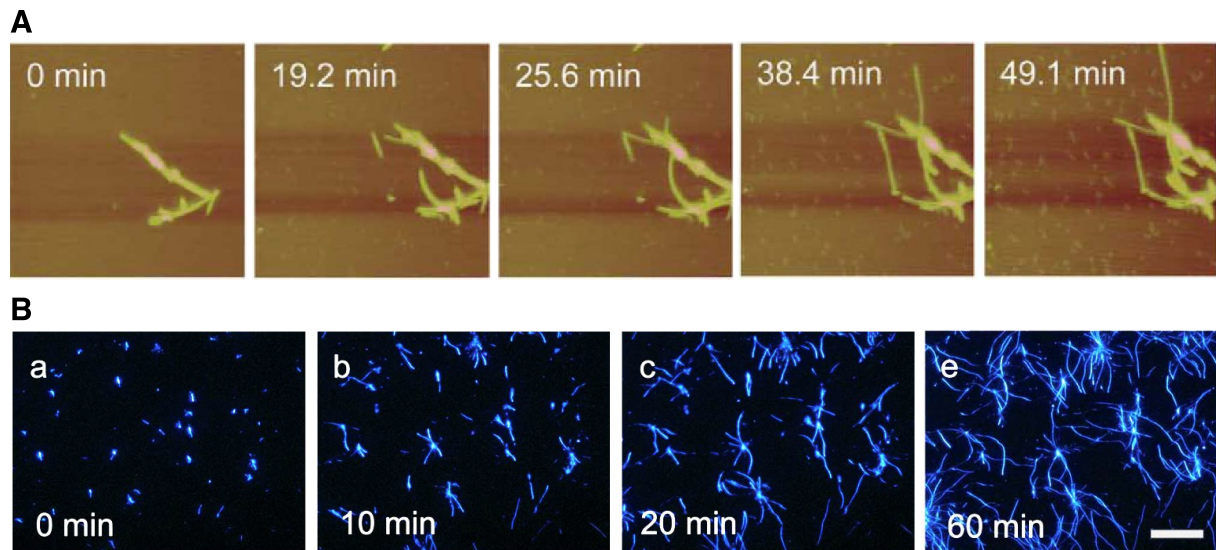


Figure 1.5: Monitoring amyloid aggregation by AFM and TIRFM. A: AFM images of seeded α -synuclein fibril growth performed at 50 °C, pH 7, and 8 μ M monomer concentration, individual images are 1.4 μ m x 1.4 μ m. Modified from Hoyer et al., 2004 [57]. B: TIRFM images of seeded A β ₄₀ fibril growth performed at 37 °C, pH 7.5, 50 μ M monomer and 5 μ M Thioflavin T. Scale bar represents 10 μ m. Modified from Ban et al., 2004 [58].

Besides AFM, high-resolution fluorescence microscopy has been successfully used to study amyloid aggregation. Total internal reflection fluorescence microscopy (TIRFM) has been proven to be especially useful for this application. In TIRFM, the excitation laser light is completely internally reflected at the interface to the sample, thereby creating an evanescent wave of excitation light, which only enters around 150 nm into the sample. Because of that very thin layer of illumination, TIRFM offers a high signal-to-noise ratio (background fluorescence can be reduced down to a factor of 2000 compared to conventional fluorescence microscopy) for objects that are directly near the glass surface of the glass slide [59]. Naturally this requires that fibrillation happens directly at the glass surface. The study of amyloid aggregation has so far provided insights into detailed fibrillation kinetics of β ₂-microglobulin [60], A β ₄₀ [58], glucagon [61, 62], IAPP [63] and α -synuclein in the article included in this thesis (see [section 2.1](#)) [64]. In the TIRFM experiments, Thioflavin T was used as the amyloid staining dye for the growing fibrils.

Alongside TIRFM, super-resolution microscopy like dSTORM has also been used to study the fibrillation of α -synuclein [65]. In all real-time experiments, preformed fibril seeds were included in the reaction to speed up the fibrillation process.

1.3 Parkinson's Disease

Parkinson's disease (PD) is the second most common neurodegenerative disease, the lifetime risk to develop PD is around 2% for men and 1.3% for women [66]. In 2013, 102,500 people died of PD worldwide [2]. PD symptoms have been first described in 1817 by English surgeon James Parkinson who termed the disease "shaking palsy" [67]. It has received worldwide attention

by well-known sufferers like Muhammad Ali, Pope John Paul II and Michael J. Fox, whose foundation is one of the largest funders of PD research today.

The most characteristic symptoms of PD are four motor symptoms which are also the main diagnostic criteria: rigor (muscle stiffness), bradykinesia (slow movement), tremor and postural instability [68]. Alongside these motor symptoms, several non-motor symptoms like depression, apathy and dementia are also known and common, although not as characteristic. Several sensory problems accompany PD, e.g. olfactory dysfunction might be an early preclinical sign of PD [69]. Sleep disorders are also very common in PD patients and greatly affect quality of life. Strikingly, Rapid-eye-movement sleep behavior disorder (RBD) might be a very early sign of PD patients, years before any motor deficits can be diagnosed [70].

PD pathophysiology shows a degeneration of dopaminergic cells in the *substantia nigra*, a region of the midbrain that is involved in motor control and reward. Death of the dopaminergic system and loss of the neurotransmitter dopamine leads to the characteristic motor deficits seen in PD [71]. The loss of dopaminergic neurons in the *substantia nigra* can easily be seen in *post mortem* analysis of a PD-patient's brain, as the usually dark-colored *substantia nigra* region is strongly destained because of the cell loss (fig. 1.6). Dopaminergic neurons are dark-colored because of their high content of neuromelanin, a darkbrown pigment which is highly enriched in these cells [72].

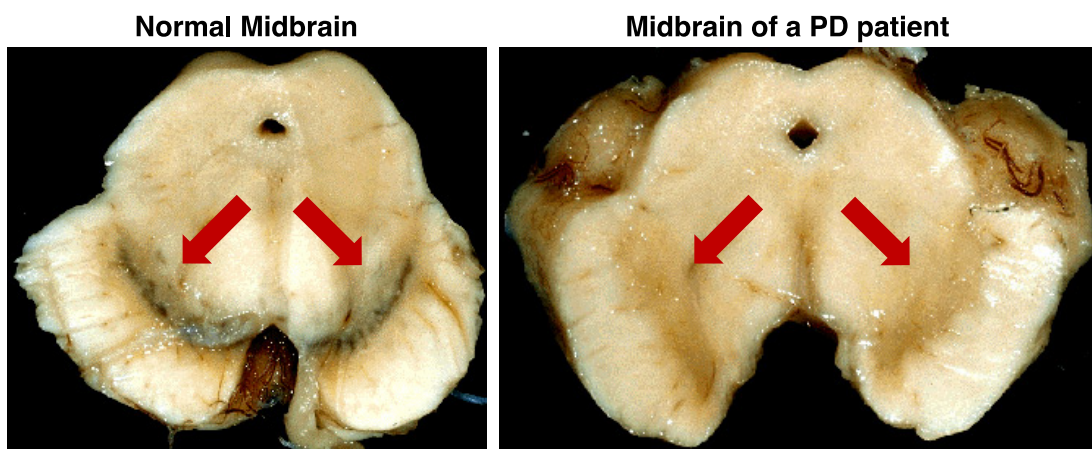


Figure 1.6: Midbrain sections of a healthy brain and a PD patient's brain. Left side: midbrain section of a healthy brain. Right side: midbrain section of a PD patient's brain. Red arrows indicate the *substantia nigra*. Modified from <http://neuropathology-web.org/chapter9/chapter9dPD.html> [73].

Parkinson's disease, alongside other Lewy body diseases like Dementia with Lewy Bodies (DLB) or Multiple System Atrophy (MSA) feature intraneuronal inclusions of aggregated protein called Lewy bodies. They are named after German neurologist Friedrich Heinrich Lewy, who discovered these inclusions in 1912 [74]. Lewy bodies mostly consist of aggregates of an endogenous protein called α -synuclein (α -syn) [75], although other proteins like the tau protein may also be present in smaller amounts [76].

Most cases (>90%) of PD are idiopathic, meaning that disease onset can not be traced to a known cause like a genetic background/familial history or environmental risk factors. Around 5-10% of PD cases can be conclusively traced to monogenetic backgrounds of mutations in at least five genes: *LRRK2*, *SNCA*, *PRKN*, *PINK1* and *PARK7* [77]. In the last years, advances in DNA sequencing techniques and large-scale genome data analysis have revealed that there are likely several more risk loci for Parkinson's disease [78]. The *SNCA* locus codes for α -syn, whose aggregation is heavily associated with PD (see section 1.4). Multiplications of the *SNCA* locus as well as five missense mutations (A30P, E46K, H50Q, G51D and A53T) have been found to cause hereditary early-onset forms of PD [4]. The *LRRK2* locus codes for a protein called leucine-rich repeat kinase 2 that phosphorylates proteins and is abundantly expressed in dopaminergic regions of the brain. Mutations in this protein, e.g. the G2019S mutation alone causes 4% of hereditary forms of PD and 1% of PD cases that have been denoted as idiopathic [79]. *PRKN*, *PINK1* and *PARK7* are autosomal-recessive PD genes, which code for proteins that are involved in the protection of neurons from oxidative stress (*PARK7*) and involved in initiation of autophagy of damaged mitochondria (*PRKN*, *PINK1*) [4].

To this day, no causative therapy for PD is available, but several approaches, e.g. immunotherapy targeting α -syn, are currently developed [80]. Symptomatic treatment of PD is accomplished mainly by replenishing the reduced dopamine pool in the brain. As dopamine does not cross the Blood-Brain-Barrier (BBB) and can cause peripheral adverse side effects, the dopamine precursor Levodopa (L-3,4-dihydroxyphenylalanine) is given as a drug. Levodopa crosses the BBB, where it is converted to dopamine by aromatic L-amino acid decarboxylase [81]. Levodopa therapy is most effective in the first years of the disease. In later stages, when Levodopa treatment loses its effectiveness and/or causes side effects, surgical implantation of electrodes for Deep Brain Stimulation (DBS) can alleviate PD symptoms [82].

1.4 α -Synuclein

1.4.1 Physiological Aspects

α -Synuclein (α -syn) is an endogenous protein of 140 amino acids and 14.5 kDa that is abundantly expressed in the central nervous system (CNS), but e.g. also found in red blood cells, muscle, liver, lung and heart [83]. α -Syn consists of an amphipathic, lysine-rich N-terminus (residues 1-60), a hydrophobic, aggregation-prone middle region (NAC region, residues 61-95) and a highly charged and flexible C-terminus (residues 96-140) [84]. Whereas the NAC region is rather uncharged at physiological pH (-1), the N-terminus carries a positive net charge (+3) and the C-terminus a negative net charge (-12) (fig. 1.7). There are two main posttranslational modifications described for α -syn, the first is that it is ubiquitously acetylated at the N-terminus [85], the second is phosphorylation at different positions, the most frequent phosphorylation sites are serine 87 and serine 129 [86]. Several C-terminal truncations have been described for α -syn, e.g. at positions 119 (aspartic acid), 115 (aspartic acid), 133 (tyrosine) or 135 (aspartic acid) [85]. Truncation of the acidic C-terminus greatly increases the aggregation

propensity of α -syn [87]. Besides that, aggregated α -syn extracted from Lewy bodies is often phosphorylated, poly-ubiquitinated, and glycosylated [83]. As the *substantia nigra* is a brain region with increased oxidative (and nitrative) stress, oxidative and nitrative modifications of α -syn, especially at the four tyrosine residues (Y39, Y125, Y133, Y136), are common (see section 1.5).

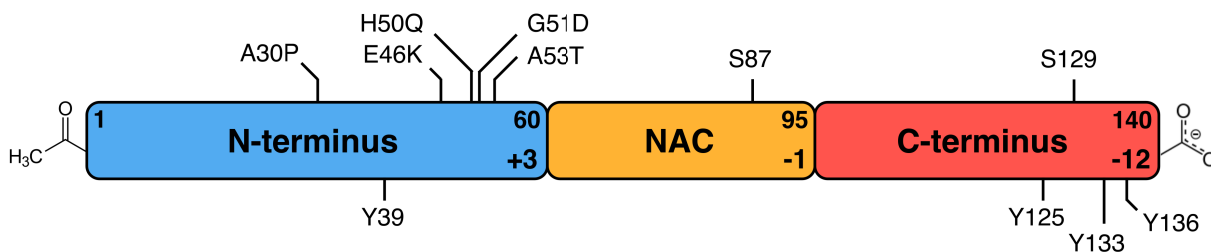


Figure 1.7: Schematic of α -syn with highlighted regions, posttranslational modifications, familial mutations and tyrosines. Blue: Positively-charged, lysine-rich N-terminus with acetyl group and familial PD mutations. Orange: Aggregation-prone NAC region with phosphorylation site serine (S) 87. Red: Negatively-charged C-terminus with phosphorylation site serine (S) 129. Tyrosines are also labelled as a reference for section 2.4.

The function of α -syn is not yet fully understood. *Snca*-knockout mice show a general impairment in synaptic function. When hippocampal slices of *Snca*-knockout mice are subjected to persistent high-frequency stimulation, the synaptic responses are impaired. As this persistent stimulation depletes the pool of docked and reserve vesicles in synapses, α -syn seems to play a role in refilling and trafficking of synaptic vesicles [84, 88]. Indeed, α -syn has been shown to be located in presynaptic terminals, where it is associated with the synaptic vesicle pool [89, 90]. Additionally, α -syn can also bind to synaptic proteins that are involved in vesicle exocytosis, such as phospholipase D2 and RAB small GTPases [91, 92]. α -Syn can also function as a chaperone, e.g. by controlling assembly, degradation and maintenance of the vesicle-associated soluble N-ethylmaleimide-sensitive-factor attachment receptor (SNARE) complex [93, 94]. Besides being associated with the synaptic vesicle pool, α -syn is also associated with mitochondria, both loss and overexpression of α -syn cause mitochondrial dysfunction [95–97]. Localization within the nucleus, the Golgi complex, the endoplasmic reticulum and binding to components of the cytoskeleton have also been reported for α -syn, highlighting a complex role of α -syn both in its physiological function and in disease [83].

α -Syn is a protein that is both cytosolic and membrane-associated [83]. The cytosol-membrane equilibrium may well be directly related to its function in vesicle trafficking, as it has to rapidly associate with - and dissociate from membranes. In its cytosolic form, α -syn is an intrinsically disordered protein (IDP), meaning that it does not exhibit a stable secondary structure in solution, but rather an unfolded structure (random coil). This structural disorder is preserved in several neuronal and non-neuronal cell types [98]. It can however form transient structures, e.g. transient contacts between amino acids that form β -strands in α -syn fibrils [16]. Also, the formation of an N-terminal α -helix has been described for α -syn, especially when α -syn is associated with lipid membranes (see subsection 1.4.2).

1.4.2 α -Synuclein and Membranes

As mentioned before, α -syn is in an equilibrium between a cytosolic and a membrane-associated state. This might be directly linked to its function in synaptic vesicle trafficking, where both membrane-binding and cytosolic solubility are needed. Whereas cytosolic α -syn is intrinsically disordered and only forms transient structural elements, the presence of lipid membranes induces an α -helical fold in α -synuclein [99]. The N-terminus and the NAC region of α -syn contain seven imperfect repeats of an 11-residue lysine-rich sequence (KTKEGVXXXXX) interspaced with hydrophobic residues, which can form an amphipathic, positively charged α -helix (fig. 1.8A). Upon binding to (negatively-charged) lipid bicelles or detergent micelles, α -syn forms an α -helix that spans residues 3 to 92. The helix is either an extended helix, e.g. when the membrane area is large enough and not highly curved (fig. 1.8C) [100, 101], or a "broken" helix with two helices spanning residues 3-37 and 45-92, separated by a turn spanning residues 38-44 (fig. 1.8B) [102]. This amphipathic helix of polar/charged and hydrophobic residues is e.g. a known feature of lipid-associated apolipoproteins, supporting α -syn's role as a lipid-binding protein [103].

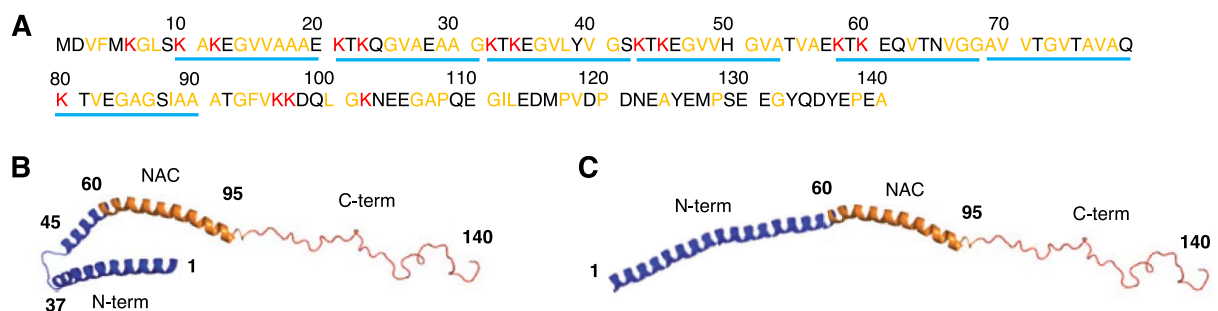


Figure 1.8: Amphipathic repeats and α -helical structures of α -syn upon membrane-binding. A: α -Syn sequence with highlighted KTKEGVXXXXX repeats (underlined in blue), positively-charged lysines (red) and hydrophobic residues (yellow), modified from Ulmer et al., 2005 [102]. B: "Horseshoe" conformation of α -helical α -syn with two helices, N-helix (3-37) and C-helix (45-92), separated by a short linker (38-44), modified from Ulmer et al., 2005 and Lashuel et al., 2013 [84, 102]. C: Extended helix conformation of textalpha-helical α -syn with one continuous helix spanning the first \sim 90 residues, modified from Georgieva et al., 2008, Robotta et al., 2011 and Lashuel et al., 2013 [84, 100, 104]. N-terminus, NAC region and C-terminus are denoted as in fig. 1.7.

It has been shown that α -syn tightly binds to negatively-charged lipids like phosphatidylserine, phosphatidylinositol or phosphatidylglycerol and to a much lesser extent to neutral lipids like phosphatidylcholine or phosphatidylethanolamine [105, 106]. This fits well to a largely electrostatic model of binding, where the positively-charged amphipathic helix of α -syn binds to negatively-charged lipid head groups. This is supported by the observation, that α -syn binding to membranes can be abolished e.g. by a high ionic strength in the buffer [107]. Besides its preference for negatively-charged lipid head groups, α -syn also preferentially binds to phospholipid membranes that are in a fluid phase, e.g. lipids with long unsaturated fatty acids or short saturated fatty acids [108]. Upon binding to liposomal membranes, α -syn is able to rear-

range membrane organization by increasing curvature and tubule formation [109]. In a similar manner, α -syn senses lipid packing defects in curved membranes like vesicles and reorganizes them e.g. by membrane thinning [110].

Binding of α -syn to membranes is not only related to its native function, but also plays a role in PD pathogenesis. Oligomeric or fibrillar α -syn has been shown to destabilize membranes, e.g. by membrane disruption or by formation of ion pores [111, 112]. Oligomeric α -syn can also damage mitochondria and fragment mitochondrial membranes by binding to cardiolipin, a lipid that is part of the inner mitochondrial membrane [113]. In general, the presence of lipids influences and modulates the diseases-associated aggregation kinetics of α -syn (see [subsection 1.4.3](#) and [section 2.3](#)).

1.4.3 α -Synuclein in Disease

The aggregation of α -synuclein is the central pathogenic hallmark of synucleinopathies like Parkinson's Disease or Multiple System Atrophy (MSA). Several studies show that α -syn aggregation is a central event. Known familial mutations like A30P, E46K and A53T increase the aggregation propensity (oligomerization and/or fibrillation) of α -syn and thereby cause early-onset of PD [114–116]. Multiplication of the *SNCA* locus leading to higher α -syn expression also causes severe, early-onset pathology [117, 118]. On the other hand, an artificial mutation (S87E), mimicking phosphorylation at serine 87, greatly decreases both the aggregation propensity and the neurotoxicity of α -syn in rat brains [119].

In respect to pathophysiology, aggregation of α -syn is indirectly toxic to cells, as the aggregation process depletes monomers that then no longer can fulfill their function in vesicle trafficking. In general, aggregation of α -syn, analogous to other amyloid proteins, overexerts the cellular protein degradation machinery, the ubiquitin-proteasome pathway, which finally leads to increased apoptosis [120]. α -syn overexpression and aggregation has been shown to be detrimental to several cell organelles, e.g. by causing severe endoplasmic reticulum stress, fragmenting the Golgi complex and leading to mitochondrial dysfunction [121, 122]. α -Syn aggregation and mitochondrial dysfunction generate oxidative stress that is also detrimental to cells (see [section 1.5](#)). As mentioned before, several oligomeric intermediates of α -syn have been proposed to form annular pores in the membranes, thereby disrupting ion homeostasis [112, 123, 124]. Fibrillar α -synuclein has also been shown to extract lipids from membranes and form coaggregates, thereby destabilizing the membrane [125]. Rather in contrast to other amyloid proteins, there is clear evidence for α -syn that both oligomeric aggregation intermediates as well as mature amyloid fibrils are toxic to cells. Although α -syn oligomers are difficult to isolate and/or purify and sometimes require artificial protein sequence alteration, there is evidence that oligomeric species are toxic to cells, cause oxidative stress and permeabilize membranes [126–128]. On the other hand, there is substantial evidence that α -syn fibrils are toxic to cells and also migrate through the extracellular space between neurons, thereby spreading aggregation and disease throughout the brain [44, 129, 130].

On a structural level, aggregation leads to the formation of β -sheets in α -syn. Whereas amyloid fibrils of α -syn exhibit a distinct β -sheet structure, oligomers show an intermediate structure between monomers (random coil) and amyloid fibrils (β -sheets) when observed by solid-state nuclear magnetic resonance spectroscopy (ssNMR) [124]. Certain α -syn oligomers have been investigated structurally, a low resolution structure of membrane-permeabilizing α -syn oligomers has been obtained by the combination of small-angle X-ray scattering (SAXS) and modeling (fig. 1.9A) [131]. Cryo-EM of an off-pathway, membrane-permeabilizing oligomer showed a pore-like topology (fig. 1.9B) [128].

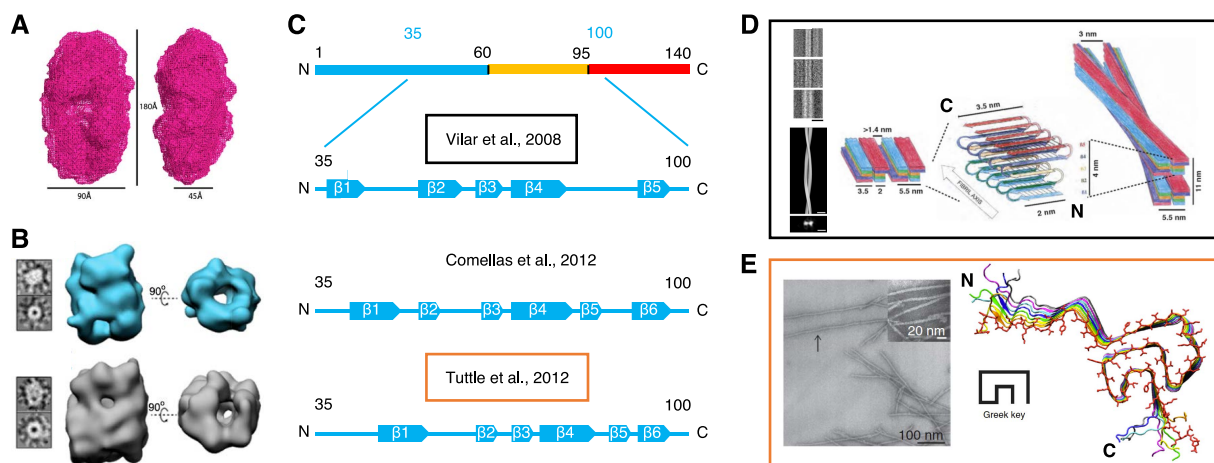


Figure 1.9: Structures of α -syn oligomers and α -syn fibrils. A: Low-resolution SAXS structure of a wreath-shaped, membrane-permeabilizing α -syn oligomer from Giehm et al., 2011 [131]. B: Cryo-EM structure of pore-like oligomer from Chen et al., 2015 [128]. C: Distribution of β -strands in α -syn (35-100) from three different ssNMR structural studies, Vilar et al., 2008 [132], copyright (2008) National Academy of Sciences, Comellas et al., 2012 [133] and Tuttle et al., 2016 [134]. D: Electron micrographs of two different (straight and twisted) fibrils, model of arrangement of α -syn β -strands in a protofilament (middle) and organization of two protofilaments in a straight fibril (left) and twisted fibril (right) from Vilar et al., 2008. E: Electron micrographs of α -syn fibrils and "greek key" model of α -syn fibrils from Tuttle et al., 2016.

Several ssNMR studies have investigated the structure of α -syn fibrils and identified the distribution of β -strands within the fibril [132, 133, 135, 136]. Figure 1.9C shows the distribution of β -strands from selected publications. The β -sheet fibril core of α -syn fibrils is located between residues 35-100 in all selected publications. Whereas Vilar et al. identified five β -strands in α -syn fibrils, Comellas et al. and the most recent and elaborate structure from Tuttle et al. contain six β -strands, although the exact locations within the sequence vary between the different models. Vilar et al. found two fibril morphologies when screening multiple EM pictures, a straight fibril morphology and a twisted morphology (fig. 1.9D). In the proposed model, mature α -syn fibrils are built by two protofilaments, that are either twisted around each other or are ordered in parallel. Each protofilament is built by one α -syn monomer per layer that connects its β -strands with turns in an antiparallel fashion. The most recent and precise model of α -syn fibrils is shown

in [fig. 1.9E](#). Tuttle et al. only observed one fibril morphology by EM, the β -strands of the fibril core are organized in a so called "greek key" motif.

Kinetics of α -Synuclein Aggregation

Aggregation of α -syn generally follows a nucleation-dependent polymerisation process, where secondary nucleation only plays role in certain conditions ([section 1.2](#), [fig. 1.2](#)). There are several biophysical methods that can measure the aggregation kinetics of α -syn, e.g. ThT assays, SAXS, quartz crystal microbalance (QCM) or dynamic light scattering (DLS) [[137](#), [138](#)]. To obtain detailed single fibril kinetics, high resolution techniques like AFM ([fig. 1.5](#)) or TIRFM (see [section 2.1](#)) have to be used [[57](#), [64](#)]. The application of AFM has e.g. detected a stop-and-go growth mechanism of α -syn fibrils, where continuous growth phases are interrupted by stop times, during which fibrils did not grow anymore.

There are a lot of factors that influence the kinetics (and also thermodynamics) of α -syn aggregation *in vitro*. α -Syn aggregation at physiological pH and 37 °C is markedly slower than e.g. the aggregation of amyloid- β or IAPP when studied by ThT assays ([section 2.2](#), [[139](#)]). The kinetics can however be accelerated by many factors. Lowering the pH to <6 greatly accelerates α -syn aggregation, as secondary nucleation becomes a substantial factor that increases aggregation speed [[138](#)]. Increasing the ionic strength of the used buffer or addition of divalent cations like Mg^{2+}/Ca^{2+} has been reported to increase aggregation velocity in α -syn [[140](#)]. The addition of polyvalent heavy metal ions like Al^{3+} or Cu^{2+} also drastically enhanced aggregation speed [[141](#)]. Analogous to the effect of polyvalent cations like Mg^{2+} and Al^{3+} , polycationic molecules like putrescine or spermidine distinctly accelerate α -syn aggregation [[142](#)]. The stimulatory effect of cations or low pH (increase in H_3O^+) highlight the inhibitory effect of the negatively-charged C-terminus on α -syn aggregation - when the negative charges at the C-terminus get neutralized, the aggregation velocity increases substantially. This is confirmed by the observation, that α -syn lacking the highly acidid C-terminus (α -syn₁₋₁₀₈) aggregates much faster than the wildtype protein, aggregation speed of this mutant is also independent from the addition of cations [[87](#)].

As mentioned before, lipids and membranes have a marked effect on the aggregation of α -syn. Whereas neutral phospholipids do not exert a strong effect on α -syn aggregation, highly negatively-charged membranes strongly inhibit the aggregation of α -syn, when the lipid-to- α -syn ratio is high (see [section 2.3](#)). On the other hand, with lower lipid-to- α -syn ratios, negatively-charged membranes can stimulate the aggregation of α -syn by increasing primary nucleation (see [section 2.3](#) and [[107](#)]). Studies using small unilamellar vesicles (SUVs) shed light on the influence of several lipids in respect to lipid head group and fatty acid type on the aggregation of α -syn [[108](#)]. It has e.g. been shown that α -syn aggregation is stimulated the most in the presence of (negatively-charged) lipids with short saturated fatty acid chains like lauric acid (12:0) and myristic acid (14:0) in the fluid phase.

Oxidative modifications of α -syn have also been reported to influence the aggregation kinetics of α -syn in different ways (see [section 1.5](#) and [section 2.4](#)).

1.5 Oxidative Stress in PD

Besides α -syn aggregation, oxidative stress (OS) is another hallmark of Parkinson's disease, as it is highly increased in the *substantia nigra* [143]. The *substantia nigra* naturally is a brain region of increased OS for several reasons. Its high dopamine content is a source of oxidative stress, as dopamine metabolism generates reactive oxygen species, both the deamination of dopamine by monoamine oxidase as well as its autooxidation produce H_2O_2 , superoxide ($O_2^{\cdot-}$) and hydroxyl ($\cdot OH$) radicals [144, 145]. Additionally, the *substantia nigra* contains high amounts of iron (Fe^{2+} and Fe^{3+}) which catalyzes the production of reactive oxygen species (ROS) from H_2O_2 via the Fenton reaction in a cyclic process [146].

Mitochondrial dysfunction is a major source of increased ROS production and has been identified as a critical element in the pathogenesis of PD [147]. Mitochondria naturally produce ROS, e.g. the superoxide anion, as a byproduct of the electron transport chain across complex I to IV. This ROS production can be highly elevated in PD, when complex I is inhibited or deficient and electrons are transferred onto oxygen instead of ubiquinone [148]. The direct link between complex I inhibition and PD can be seen in an inducible PD model: the (unintentional) administration of 1-methyl-4-phenyl-1,2,3,6-tetrahydropyridine (MPTP), originally an unwanted byproduct of meperidine analogue synthesis, causes PD symptoms and classical PD pathology i.e. cell death in the *substantia nigra*, although without without Lewy body pathology. MPTP localizes to mitochondria and has been identified as a potent complex I inhibitor. This specific action of MPTP has made it a drug-inducible animal model for PD [148, 149].

There are also several genetic links between mitochondrial dysfunction/oxidative stress and PD [4]. Loss-of-function mutations in the genes *PRKN*, *PINK1* and *PARK7* cause early-onset PD. *PRKN* and *PINK1* code for the proteins PTEN-induced protein kinase 1 and parkin (RBR E3 ubiquitin protein ligase). These proteins are involved in mitochondrial quality control, as they initiate the degradation of damaged mitochondria. PINK1 senses mitochondrial stress and damage and subsequently recruits parkin to the mitochondrion. Parkin then polyubiquitinates several mitochondrial proteins, thereby tagging the mitochondrion to be degraded by the proteasome and macroautophagy [150]. *PARK7* codes for the protein DJ-1, which is directly linked to prevention of OS. DJ-1 is a neuroprotective, anti-oxidant, anti-apoptotic and anti-inflammatory protein that e.g. directly quenches ROS and acts as a molecular chaperone [151]. Overexpression of DJ-1 e.g. protects from MPTP-induced PD, whereas DJ-1 knockout or loss-of-function mutations increases susceptibility to oxidative stress and finally causes degeneration of nigral cells and PD [147]. Mutations in *LRRK2* that codes for leucine-rich repeat kinase 2 are among the most frequent familial mutations found in PD, most of which are gain-of-function mutations that increase kinase activity of LRRK2 [152]. LRRK2 is a cytosolic protein, but is also known to associate with the outer mitochondrial membrane. Overexpression of LRRK2 and expression LRRK2-mutants with increased kinase activity have been shown to lead to an increase in oxidative-stress mediated cell death [153, 154].

α -Synuclein is also involved in PD-associated OS in a diverse fashion. Aggregation of α -syn directly causes oxidative stress in several ways. For example, overexpression of α -syn causes

increased ROS production and cell death in SH-S5Y5 cells [155]. Additionally, when α -syn can no longer exert its function in vesicle/neurotransmitter recycling and trafficking e.g. due to aggregation, cytosolic dopamine content and metabolism, being a source of ROS, increases. Increased cytosolic dopamine content and subsequent OS is also a result of pore-forming α -syn aggregates that permeabilize vesicles [147, 156]. Besides that, α -Syn can also localize to the inner mitochondrial membrane, where it inhibits complex I and releases cytochrome c, both resulting in increased OS [157]. α -Syn (aggregation) also directly recruits and activates microglia that actively produce ROS and cause OS, thereby promoting neuroinflammation [158].

On the other hand, oxidative (and nitrate) stress has also been reported to promote α -syn aggregation [159]. Oxidative adducts of α -syn protofibrils with dopamine were shown to possess a high kinetic stability, meaning that toxic protofibrils do not polymerize further to mature fibrils that are believed to be less toxic [160]. *In vitro*, oxidative modifications of α -syn have been reported both to increase and decrease the aggregation propensity of the wildtype protein [161, 162]. An aggregate-stabilizing effect of oxidative crosslinking of α -syn fibrils has also been reported [163].

Taken together, these findings suggest that oxidative stress and α -syn aggregation act together in a vicious cycle that further accelerates neurodegeneration in the *substantia nigra*. A summary of oxidative stress pathways in PD is shown in fig. 1.10. Oxidative stress in general is harmful to cells in many ways, as ROS react with biomolecules leading to lipid peroxidation, DNA damage and crosslinking (e.g. by dityrosine formation) and fragmentation of proteins (see subsection 1.5.1 and [147]).

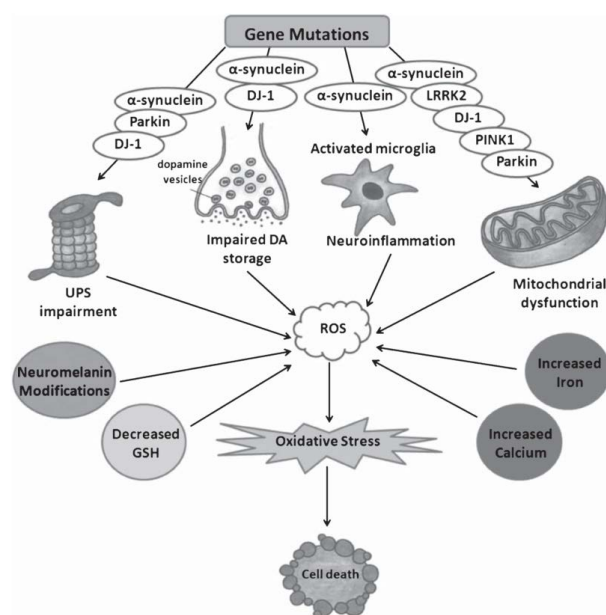


Figure 1.10: Oxidative stress in PD. Various pathways that produce ROS and lead to oxidative stress in PD. From Dias et al., 2013 [147].

1.5.1 Dityrosine Formation

Oxidative stress can lead to several reversible and irreversible protein modifications. Reactive oxygen/nitrogen species can e.g. oxidize methionine residues, lead to polypeptide backbone cleavage, form protein carbonyls, modify tryptophan and tyrosine residues to nitrotryptophan or nitrotyrosine and crosslink proteins by the formation of dityrosines [164]. Dityrosine is a covalent adduct of two tyrosine residues, where a covalent bond forms between the two phenol moieties as a result of hydrogen abstraction and can be used as a marker for oxidative stress [165, 166]. Hydrogen abstraction and subsequent dityrosine formation can either be initiated by reactive oxygen species or by electron ejection through UV-irradiation of about

280 nm [167]. The ejected electron is usually transferred to O_2 , thereby forming the superoxide anion $O_2^{\cdot-}$. Hydrogen abstraction in tyrosine leads to the formation of a tyrosyl radical that can either react with superoxide back to tyrosine, form tyrosine hydroperoxides with superoxide and H^+ or, when two tyrosyl radicals come together, form dityrosine [165]. The reaction of tyrosine to dityrosine proceeds through four steps: 1) tyrosyl radical formation through H^+ -abstraction, 2) radical isomerization from O^\bullet to $^\bullet C$, 3) two tyrosyl radicals form a covalent 3-3'-bond, 4) dityrosine enolization (fig. 1.11) [166].

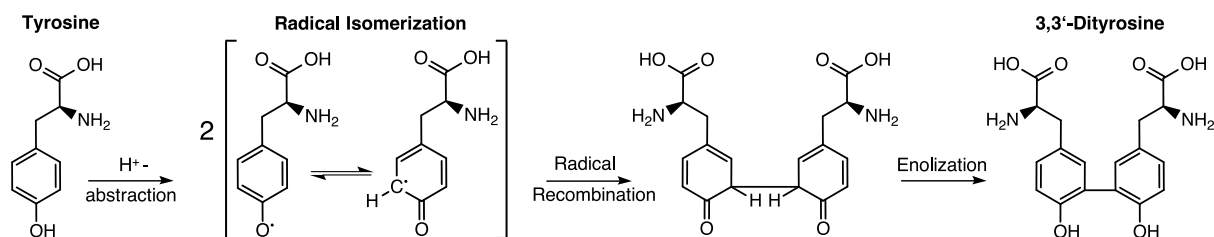


Figure 1.11: Reaction scheme of dityrosine formation. The reaction from tyrosine to 3,3'-dityrosine can be divided into four steps: 1) H^+ -abstraction, 2) radical isomerization, 3) radical recombination of two tyrosyl radicals, 4) dityrosine enolization.

The formation of dityrosine (DiY) due to oxidative stress has been studied for several proteins like calmodulin, insulin, β -casein, bovine serum albumin and β -lactoglobulin [168–171]. Crosslinking between two tyrosine residues have been reported to occur both intra- and inter-molecularly, the latter leading to protein DiY dimer formation. In flexible and rather unstructured proteins like β -casein, dityrosine formation is favored, as close contact of two tyrosyl radicals is more probable. In globular proteins like β -lactoglobulin, reaction of a tyrosyl radical to 3,4-dihydroxyphenylalanine (DOPA) is favoured, as it is more unlikely that two tyrosyl radicals are unlikely to find each other [171]. DOPA is the product of the reaction of one tyrosyl radical with a hydroxyl radical [172].

Dityrosine has unique spectral characteristics that differ from tyrosine, therefore its formation can be studied by the change in fluorescence emission of a solution. At neutral pH, dityrosine has two excitation maxima at 283 nm (unionized form) and 315 nm (ionized form) and an emission maximum of 409 nm [165]. These spectral characteristics also allow that dityrosine formation can be initiated by UV-irradiation at 280 nm and traced/verified simultaneously in a single experimental setup (see section 2.4).

Dityrosine-crosslinking has been studied mechanistically with tyrosine and in proteins like calmodulin, insulin and milk proteins, but it has also been studied in aggregation-prone proteins like amyloid- β and α -syn. In the brain, both amyloid- β and α -syn aggregates (amyloid plaques and Lewy bodies) can be co-stained with an dityrosine antibody, indicating that dityrosine formation is a process that happens naturally during pathogenesis of AD and PD [163, 173]. In the case of amyloid- β , oxidative-stress-induced DiY dimer formation has been reported to in-

crease the aggregation propensity of the protein and stabilize already formed aggregates *in vitro* [173]. For α -syn, various oxidative stress conditions have been used to form dityrosines and/or nitrotyrosine, e.g. incubation with tris-(bipyridine)ruthenium(II) chloride/ammonium persulfate, peroxyxynitrite/ CO_2 , $\text{CuCl}_2/\text{H}_2\text{O}_2$, cytochrome *c*/ H_2O_2 or just prolonged incubation of the protein [161, 162, 174–176]. Dityrosine formation in α -syn has been reported to either increase aggregation propensity or decrease aggregation propensity, depending on the preparation method, and to stabilize preformed fibrils. In [section 2.4](#), the influence of DiY formation in α -synuclein on its aggregation kinetics is covered in detail.

1.6 Aim of This Work

Aggregation of α -synuclein is a central hallmark of Parkinson's disease. The prevention or modification of α -syn aggregation is therefore a central target for the development of causal therapies for PD [177]. In this respect it is crucial to study the aggregation process itself and factors that influence aggregation kinetics in detail, both for the fundamental understanding of protein aggregation and to identify molecular starting points to develop efficient therapeutics. In this thesis, the aggregation process of α -syn is studied on a single molecule level by high-resolution TIRF microscopy. Besides that, several factors that influence the aggregation process of α -syn are investigated: 1) the influence of contacts between $\beta 1$ and $\beta 2$ fragments of α -syn, 2) the influence of different membrane environments and lipid binding and 3) the influence of oxidative-stress-associated dityrosine formation on α -syn aggregation kinetics (and thermodynamics). As this thesis is a cumulative thesis, it comprises four chapters that describe several aspects of α -syn aggregation as single publications.

In [section 2.1](#), the aggregation process of α -syn is studied in detail on a single molecule level with high-resolution TIRF microscopy. The application of this technique to study aggregation of amyloid proteins has been pioneered by Ban and coworkers in 2003 and e.g. provided insights into the aggregation process of $\beta 2$ -microglobulin and amyloid- β_{1-40} [58,60]. We apply this technique to study the aggregation process and kinetics of α -syn on a single aggregate/fibril level, thereby deciphering mechanistic features of α -syn aggregation and determining essential kinetic parameters of α -syn fibril growth.

In [section 2.2](#), the influence of a covalent disulfide linkage of the $\beta 1$ and $\beta 2$ -fragments of α -syn (see [fig. 1.9C](#)) on the aggregation kinetics of α -syn and also on other amyloidogenic proteins, IAPP and $\text{A}\beta$, is examined. It has been shown before, that a β -wrapin affibody protein binds α -syn and thereby inhibits its aggregation substoichiometrically [178]. When bound within a β -wrapin, α -syn adopts a structure that features contacts between the $\beta 1$ and $\beta 2$ fragments of α -syn that usually form β -strands in the amyloid fibril.

In [section 2.3](#) we elucidate the effect of membrane environments, i.e. nanodiscs on the aggregation of α -syn. Nanodiscs are small patches of planar lipid bilayers that are packed into a lipodisc by a membrane scaffold protein. As α -syn is also a membrane-associated protein (see [subsection 1.4.2](#)), studying the influence of lipid bilayers on α -syn aggregation is crucial. In

this publication we evaluate the binding of α -syn to nanodiscs of different charge contents and fluidity in a residue-resolved way and correlate these results with the aggregation propensity of the protein and propose models for α -syn-nanodisc binding and lipid-associated aggregation.

[Section 2.4](#) focusses on the influence of oxidative-stress-associated dityrosine-crosslinking in α -syn on its aggregation propensity. Oxidative stress is another hallmark of PD besides α -syn aggregation. In oxidative stress conditions, tyrosyl radicals are formed that can subsequently form a covalent dityrosine crosslink, when two tyrosyl radicals find each other. In this publication we study dityrosine formation in α -syn by UV-irradiation and a fluorometric assay, compare intra- and intermolecular dityrosine crosslinks and their effect on α -syn aggregation. We also study the effect of dityrosine crosslinks on preformed α -syn aggregates.

2 Articles

2.1 Single Fibril Growth Kinetics of α -Synuclein

2.1.1 Article Information

Title: Single Fibril Growth Kinetics of α -Synuclein

Michael M. Wördehoff¹, Oliver Bannach^{1,2,*}, Hamed Shaykhalishahi¹, Andreas Kulawik^{1,2}, Stephanie Schiefer¹, Dieter Willbold^{1,2}, Wolfgang Hoyer^{1,2}, and Eva Birkmann^{1,2}

¹Institut für Physikalische Biologie, Heinrich-Heine-Universität Düsseldorf, Universitätsstr. 1, 40225 Düsseldorf, Germany

²Institute of Complex Systems (ICS-6), Research Centre Jülich, Wilhelm-Johnen-Straße, 52428 Jülich, Germany

* corresponding author, bannacho@hhu.de

Published in: **Journal of Molecular Biology**, Vol. 427, Issue 6, Part B, pp. 1428–1435, 2015 [64]

DOI: [10.1016/j.jmb.2015.01.020](https://doi.org/10.1016/j.jmb.2015.01.020)

Journal Impact Factor (2015): 4.517.

Contribution: **75%**. M.M.W. designed and performed the experiments, evaluated the data and wrote the manuscript. For further details see the [appendix](#).

2.1.2 Abstract

Neurodegenerative disorders associated with protein misfolding are fatal diseases that are caused by fibrillation of endogenous proteins like α -synuclein (α -syn) in Parkinson's disease (PD) or amyloid- β in Alzheimer's disease. Fibrils of α -syn are a major pathological hallmark of PD and certain aggregation intermediates are postulated to cause synaptic failure and cell death of dopaminergic neurons in the *substantia nigra*. For the development of therapeutic approaches, the mechanistic understanding of the fibrillation process is essential. Here we report real-time observation of α -syn fibril elongation on a glass surface, imaged by total internal reflection fluorescence microscopy using Thioflavin T fluorescence. Fibrillation on the glass surface occurred in the same time frame and yielded fibrils of similar length as fibrillation in solution. Time-resolved imaging of fibrillation on a single fibril level indicated that α -syn fibril elongation follows a stop-and-go mechanism, i.e. fibrils either extend at a homogenous growth rate or stop to grow for variable time intervals. The fibril growth kinetics were compatible with a model featuring two states, a growth state and a stop state, which were approximately isoenergetic and interconverted with rate constants of $\sim 1.5 \times 10^{-4} \text{ s}^{-1}$. In the growth state, α -syn monomers were incorporated into the fibril with a rate constant of $8.6 \times 10^{-3} \text{ M}^{-1} \text{ s}^{-1}$. Fibril elongation of α -syn is slow compared to other amyloidogenic proteins.

2.1.3 Introduction

Protein misfolding diseases are fatal disorders that include neurodegenerative diseases like Parkinson's disease (PD) or Alzheimer's disease (AD). These diseases are caused by misfolding and aggregation of endogenous proteins into amyloid fibrils. This process can either start from mainly disordered proteins, like α -synuclein (α -syn) [84], or highly structured proteins like lysozyme that undergo partial unfolding [179]. Aggregation of such disease-associated proteins usually follows a nucleation-dependent polymerization process, starting from monomers that first assemble into oligomeric fibrillation nuclei. Further polymerization occurs by monomer addition, resulting in protofibrils and mature amyloid fibrils as found in amyloid deposits like Lewy bodies in PD or amyloid plaques in AD [1, 75, 180, 181]. The primary nucleation step is bypassed in the presence of preformed fibrils, which serve as seeds for the conversion of monomers from the soluble to the fibrillary state [20, 44].

In PD, the deposition of α -syn aggregates is the major pathophysiological hallmark [84]. α -Syn is a 14.5 kDa protein mainly found in the central nervous system [89]. Studies have shown that α -syn plays a crucial role in synaptic trafficking. Both the knockout and the overexpression of α -syn, respectively, lead to synaptic failure, thus supporting its role in neurotransmitter trafficking [88, 182]. During progression of PD, fibrillar aggregates of α -syn accumulate in the brain, predominantly in the *substantia nigra*, coinciding with the loss of dopaminergic neurons [156]. The resulting deficiency of the neurotransmitter dopamine leads to the characteristic symptoms of PD including bradykinesia, rigor, and tremor [183]. Certain fibrillation intermediates of α -syn are neurotoxic, e.g. by an amyloid pore forming mechanism [112]. Additionally, mature α -syn fibrils are proven to be detrimental to cells as they provide a source of neurotoxic oligomers [42] and spread disease between neurons [44].

Studying the fibrillation process of amyloid proteins has long been and still is of great importance, both for the development of reliable and early stage diagnostic methods, and for the identification of compounds that interfere with the protein misfolding process. The fluorescent dye Thioflavin T (ThT) is often used to measure amyloid fibrillation *in vivo* and *in vitro* [48]. ThT binds amyloid fibrils with a K_D ranging from 0.033 μ M to 23 μ M, depending on the fibril forming protein [184], and exhibits a hundredfold increase in fluorescence emission at \sim 485 nm when bound within the cross- β -sheet architecture of amyloid fibrils. Usually, ThT assays are conducted in solution with agitation throughout the experiment [50]. The resulting fluorescence curve reflects fibrillation within the whole sample as an integrated value. Due to the experimental setup, no information on the single aggregate or fibril morphology can be obtained. Furthermore, the determined fibrillation kinetics only reflect the mean situation of an ensemble of molecules in different assembly states. Kinetic information on the single fibril level cannot be attained. To gain a deeper insight into the aggregation mechanism at the molecular level, the application of high resolution imaging techniques which allow for monitoring the elongation of single fibrils has proven successful in order to gain a deeper insight into the aggregation mechanism at the molecular level [56, 59].

Combination of ThT staining with total internal reflection fluorescence microscopy (TIRFM) was pioneered by Ban et al. [60]. This method provided kinetic insights on a single fibril level into fibrillation of the amyloidogenic proteins β 2-microglobulin [60], amyloid- β 40 (A β 40) [58], glucagon [61, 62], and amylin [63]. Here we report the direct observation and kinetic analysis of α -syn fibril growth that is associated with PD, studied by TIRFM.

2.1.4 Results

Direct Observation of α -Syn Fibrillation by TIRFM

The fibrillation of α -syn was monitored in the presence of seeds prepared by sonication of preformed fibrils. Seed particles were imaged by atomic force microscopy (AFM) as bundles of short (length <200 nm) fibrils (fig. 2.6) and therefore contained multiple potential fibrillation sites. Direct observation of α -syn fibril elongation was performed on conventional $130\ \mu\text{m}$ to $160\ \mu\text{m}$ thick glass carriers, covered with a smaller coverslip and sealed with wax (valap) to prevent evaporation. Images from seven different positions were taken every ten minutes for 40 h. The obtained images from these seven positions did not show any significant difference in terms of fibrillation kinetics, fibril morphology and seed distribution. Images of fibril elongation from an individual fibril seed are shown in fig. 2.1.

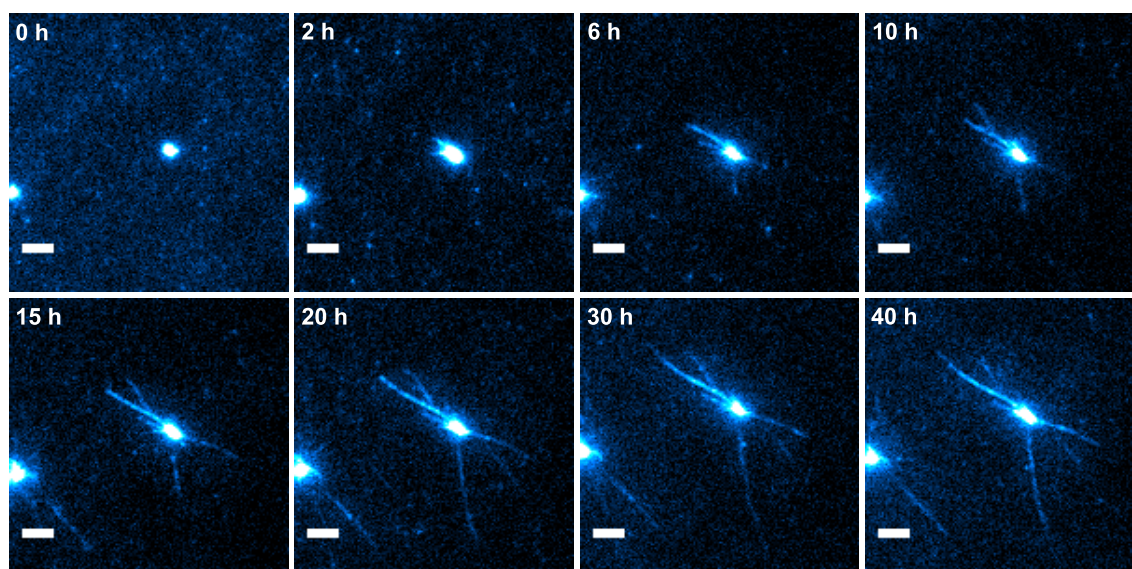


Figure 2.1: Direct observation of α -syn fibril growth by TIRFM. Time series of TIRFM images of a $160\ \mu\text{M}$ solution of monomeric α -syn in the presence of $15\ \mu\text{g ml}^{-1}$ seeds and $7\ \mu\text{M}$ ThT. Excitation of ThT fluorescence with 405 nm laser, filtering of fluorescence emission through a 450/50 bandpass filter. Scale bar: $2\ \mu\text{m}$.

A time lapse video of the elongation of multiple fibrils is provided in the Supplemental Materials. Figure 2.2A shows the elongation of a single fibril. The background fluorescence is sufficiently low to allow determination of the time course of fibril length.

Kinetics of the Elongation of Single α -Syn Fibrils Studied by TIRFM

For the analysis of fibrillation kinetics, the time-dependent length of 25 individual fibrils was studied. Final fibril lengths were ranging from $\sim 4 \mu\text{m}$ to $\sim 9 \mu\text{m}$ with most fibrils having a length of around $7 \mu\text{m}$ after 40 h of fibrillation (fig. 2.3A). Fibril elongation was not a continuous process but a combination of growth states and stop states (fig. 2.2B, fig. 2.3A).

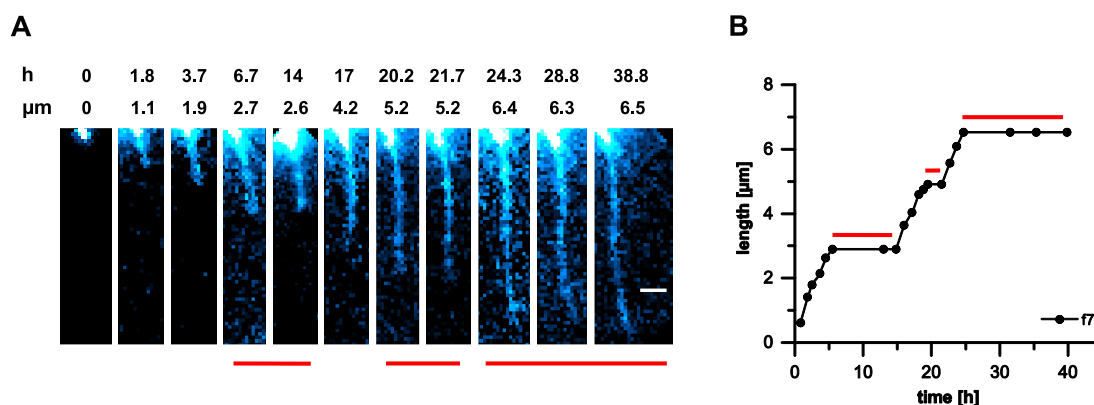


Figure 2.2: Elongation of an individual fibril and identification of stop states. A: Elongation of a single fibril (f7). Experiment time and corresponding length are indicated above, detected stop states are designated by a red line beneath the images, scale bar: $1 \mu\text{m}$. B: Corresponding length measurement of f7 over time. Stop states were defined as periods with growth rates $< 2 \text{ nm min}^{-1}$, a value approximately corresponding to the error of length determinations. The three stop states detected during elongation of f7 are indicated by a red line.

This stop-and-go mechanism of amyloid fibril elongation has been observed before [57, 58, 62, 185]. To depict growth and stop states accurately, the fibril length was measured approximately every 30 min to 60 min during growth states and less frequently during stop states. More frequent sampling did not provide additional information due to the limited pixel resolution of the TIRFM images. Growth rates (g) were determined as the increase in length from the previous time point divided by the measurement time between the two time points (fig. 2.3B).

During growth states, most fibrils were growing with a growth rate g of about 4 nm min^{-1} to 12 nm min^{-1} (fig. 2.3B). The mean rate of α -syn fibril elongation proved to be $8.5 \pm 3.7 \text{ nm min}^{-1}$ (table 2.1). The growth rate of individual fibrils exhibited a high inter- and intrafibrillar variability over time (fig. 2.7), the mean growth rate, however, did not change significantly during the experiment (fig. 2.3B). A growth rate of $\sim 8.5 \text{ nm min}^{-1}$ corresponds to the addition of $\sim 1.2 \alpha$ -syn monomer to the growing fibril per second, assuming a structure of α -syn fibrils as proposed by Vilar et al. [132] and a distance of 0.47 nm between β -strands in an amyloid fibril [186]. Vilar et al. suggest that mature α -syn fibrils consist of four protofilaments twisted around each other, with each protofilament comprising a single α -syn molecule per β -strand layer, which is equivalent to 8.5 monomers per nm fibril length. Addition of 1.2α -syn monomers per second corresponds to a rate constant of fibril elongation k_{on} of $8.6 \times 10^3 \text{ M}^{-1} \text{ s}^{-1}$, assuming an average monomer concentration of $140 \mu\text{M}$ during the 40 h experiment time (see below and fig. 2.5B).

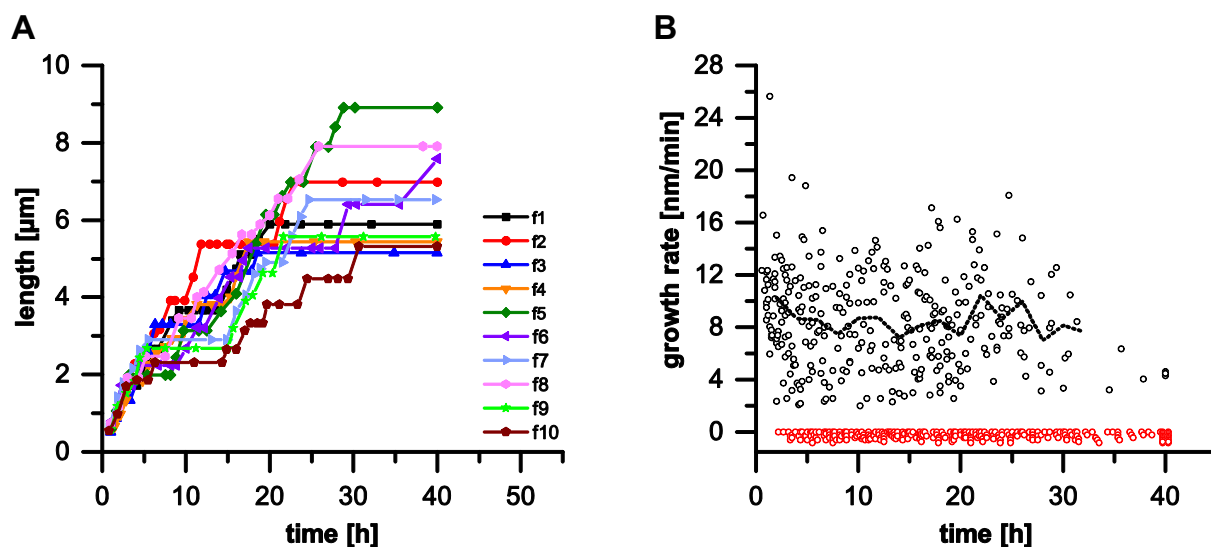


Figure 2.3: Time dependence of fibril lengths and growth rates. A: Time courses of the elongation of ten different fibrils (f1-10) B: Growth rate plot of 25 fibrils, calculated by the increase in fibril length compared to the previous measurement divided by the time interval between the two measurements. Growth rates $< 2 \text{ nm min}^{-1}$ were in the range of the detection limit and were assigned to stop states (red circles). The dashed line indicates mean growth rates, binned to an interval of 2 h. The mean growth rate after 34 h was not determined as there were too few events.

The single fibril growth kinetics data was analyzed with a two state model featuring a growth state and a stop state which interconvert with rate constants k_- and k_+ , respectively, previously applied to fibril elongation data of $\text{A}\beta$ [185] and glucagon [62] (fig. 2.4A). Growth state (fig. 2.4B) and stop state (fig. 2.4C) length distributions were plotted and fitted by a monoexponential decay function to determine k_- and k_+ .

Stop and growth states populated at the end of the experiment were excluded from the analysis, as (i) only a lower limit of their lengths could be specified, and (ii) during the apparent stop states that were not followed by a growth phase, fibril elongation might have proceeded unnoticed outside of the TIRFM focal plane. With a k_- of $1.63 \times 10^{-4} \text{ s}^{-1}$ and a k_+ of $1.27 \times 10^{-4} \text{ s}^{-1}$, the frequency of entry into a stop state or reentry into the growth state was similar.

Consequently, the probabilities of being in the growth state, p_+ , or in a stop state, p_- , determined from the single fibril elongation curves, were both around 0.5 during most of the experiment time (fig. 2.8). Whereas the monoexponential fit to the growth state length distribution is of high quality ($R^2 = 0.998$), the stop state length distribution is not fitted perfectly by a monoexponential decay ($R^2 = 0.976$). A possible explanation would be the existence of different stop states with individual constants k_+ of reentry into the growth state (fig. 2.9). The obtained kinetic parameters of α -syn fibril growth are summarized in table 2.1.

Comparison of Single Fibril Monitoring with Fibrillation in a Test Tube

To compare the real-time monitoring experiment in immediate proximity to the TIRFM glass surface with seeded fibrillation of α -syn in bulk solution, fibrillation reactions were performed in

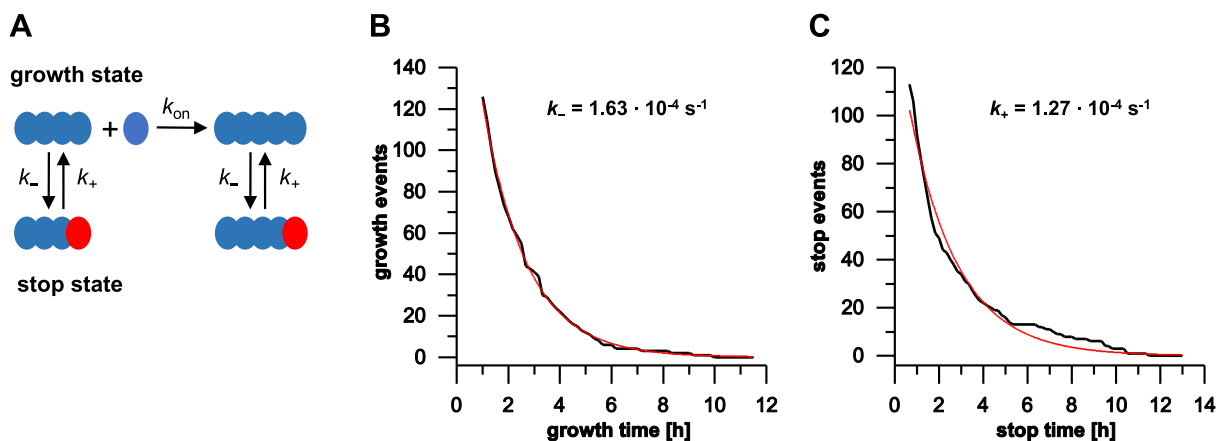


Figure 2.4: Two-state model of α -syn fibril elongation. A: The fibril can adopt a growth state or a stop state which interconvert with rate constant k_- and k_+ . Fibril elongation occurs in the growth state with rate constant k_{on} . B, C: Distributions of the lengths of growth states (B) and stop states (C) (black lines). The number of states was plotted against the minimal length of these events. To determine k_- and k_+ , the plots were fitted by a monoexponential decay function (red lines). R^2 was 0.998 for (B) and 0.976 for (C).

test tubes under identical conditions (identical protein and seed concentrations, no agitation, 25 °C). After 0 h, 24 h, 48 h and 72 h, samples were taken and imaged by TIRFM (fig. 2.5A).

As in the real-time monitoring experiment, concentrations of 15 $\mu\text{g ml}^{-1}$ α -syn seeds and 160 μM monomeric α -syn substrate was effective in triggering fibrillation on the time scale of hours to days. Seeds of α -syn were observed as accumulations of individual fluorescent particles when stained with the amyloid-specific dye ThT. The accumulation of seed particles is probably due to drying of the sample, as it was not observed in the real-time experiment. Comparable to the *in situ* experiment, fibrils grew beam-like in all directions with the seed being the center, as expected for seed particles comprising multiple active fibrillation sites (fig. 2.6). Fibrillation was clearly visible after 24 h with fibril lengths of around 6 μm (fig. 2.5A). After 48 h, fibrils had reached lengths of up to $\sim 10 \mu\text{m}$, which is comparable to the *in situ* experiment.

In parallel to TIRFM, the fibrillation in test tubes was monitored by determining the depletion of soluble α -syn. The test tube samples were centrifuged at 100 000 g for 1 h at 4 °C to pellet

Table 2.1: Estimated kinetic parameters for α -syn fibril growth.

	Parameter	Value	Standard Deviation
Rate of transition into growth state	k_+ (s^{-1})	1.27×10^{-4}	$\pm 0.36 \times 10^{-5}$
Rate of transition into stop state	k_- (s^{-1})	1.63×10^{-4}	$\pm 0.15 \times 10^{-5}$
Probability of growth state	p_+ (3-30 h)	0.48	± 0.12
Probability of stop state	p_- (3-30 h)	0.52	± 0.12
Fibril growth rate	g (nm min^{-1})	8.5	± 3.7
Fibril elongation rate constant	k_{on} ($\text{M}^{-1} \text{s}^{-1}$)	8.6×10^3	$\pm 3.7 \times 10^3$

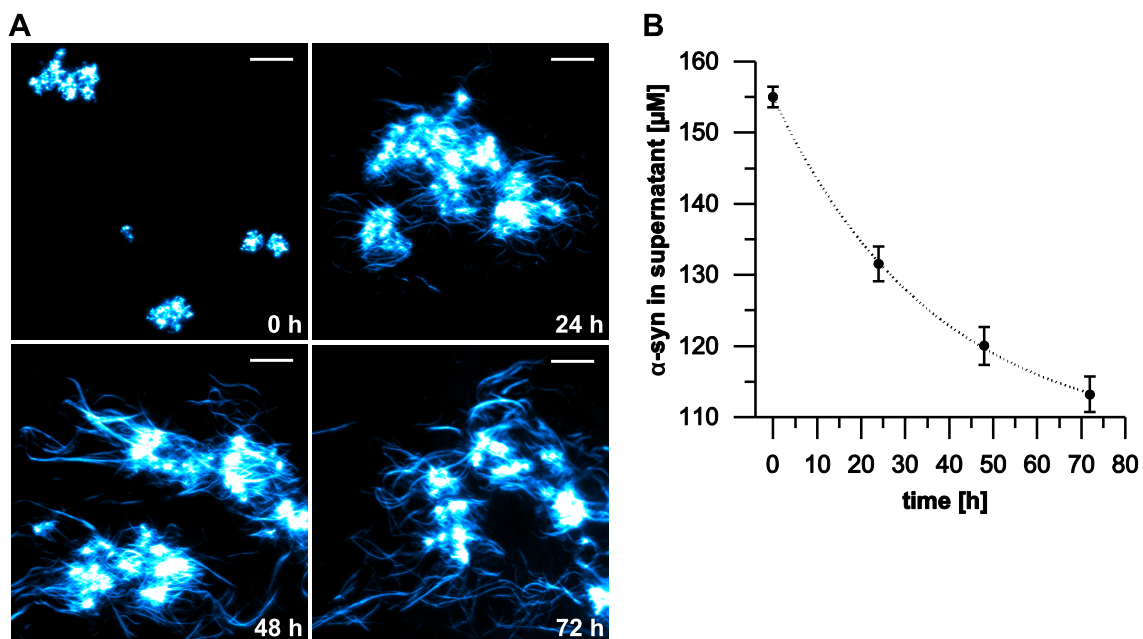


Figure 2.5: Seeded fibrillation of α -syn in a test tube. The test tube experiment was performed under the same conditions as the real-time TIRFM experiment. A: Aliquots (5 μ l) were withdrawn after the indicated times, dried out on a glass slide, and imaged by TIRFM. Scale bar: 10 μ m. B: α -Syn concentration in the supernatant after 100 000 g centrifugation of test tube samples plotted over incubation time.

fibrils. The α -syn concentration in the supernatant was measured by spectrophotometry and plotted over time (fig. 2.5B). The concentration of soluble α -syn decreased only slowly from an initial value of 160 μ M to 115 μ M after 72 h of fibrillation.

In conclusion, the test tube fibrillation data agrees with the real-time monitoring data that α -syn fibril elongation is rather slow under the applied conditions, occurring on the time scale of hours to days.

2.1.5 Discussion

In this study we report the direct observation of α -syn fibrillation in real-time and the analysis of fibrillation kinetics at the single fibril level imaged by TIRFM.

The analysis of α -syn fibrillation kinetics revealed a stop-and-go mechanism for fibril elongation, which is in accordance with previous studies on other amyloidogenic proteins, such as A β and glucagon [57, 58, 62, 185]. The fibril elongation kinetics were compatible with a two-state model featuring a growth state and a stop state. The probabilities of being in the growth state or the stop state are very similar, i.e. the growth state and the stop state are approximately isoenergetic. The interconversion between the states occurs with rate constants of $\sim 1.5 \times 10^{-4} \text{ s}^{-1}$. Very similar rates were reported for the stop-go transition of glucagon fibrillation [62], indicating a common physical origin of the stop-and-go fibrillation mechanisms of different amyloidogenic proteins. Previous suggestions to explain the occurrence of stop states comprise growth-inhibiting interactions of the fibril with physical obstacles [58] and surfaces [57, 185], as well as transitions between templating-competent and templating-incompetent conformations

at the fibril ends [185, 187]. Templating-incompetent conformations could result from incorrect attachment or incorrect conformational conversion of monomers or oligomers at the growing fibril end. To explain the long duration of stop states, the dissociation or reconversion rate of the incorrectly attached unit would need to be sufficiently low [65]. In this context it is worth noting that different regions of the conformational space of amyloid-like structures are separated by significant energy barriers [42]. For example, the rates of dissociation of monomers or soluble oligomers from amyloid fibrils or protofibrils are frequently on the order of or below the stop-go transition rate reported here [188–190].

During growth states, the average fibril growth rate was 8.5 nm min^{-1} , corresponding to a rate of monomer addition of $\sim 9 \times 10^3 \text{ M}^{-1} \text{ s}^{-1}$. α -Syn fibril growth rates of 10 nm min^{-1} (average including stop phases) [57] or between 0 nm min^{-1} and 6 nm min^{-1} [65] were reported previously based on *in situ* AFM or two-color direct stochastic optical reconstruction microscopy data, respectively. The data sets cannot be compared directly due to differences in experimental conditions that are expected to affect the fibrillation kinetics (e.g. protofibril vs. fibril elongation, pH, temperature). However, the data consistently demonstrate a low elongation rate of α -syn in comparison with other amyloidogenic polypeptides. For example, fibril growth rates of A β 40 and glucagon are approximately one order of magnitude higher at similar temperatures and slightly lower monomer concentrations than those used here [58, 62, 191]. Similarly, 8-fold and 20-fold higher elongation rate constants were determined for β 2-microglobulin and the yeast prion protein Sup35, respectively [21, 192]. α -Syn is a comparatively long amyloidogenic protein [193] with a stretch of ~ 70 amino acids that has to be incorporated correctly in an in-register format into the fibril core [132, 194]. The length of the polypeptide chain might be a factor limiting the elongation rate, considering the rugged energy landscape at the monomer-fibril interface [195, 196]. A further characteristic of α -syn is its highly acidic C-terminus. Electrostatic repulsion between the C-termini of α -syn molecules at the fibril end likely reduces the rate of fibril elongation. This is supported by the strong inhibiting effect of the C-terminus on *de novo* fibrillation [87, 197].

2.1.6 Materials and Methods

Fibrillation of α -Syn and Preparation of Fibril Seeds

α -Syn was recombinantly expressed in *Escherichia coli* and purified as previously described [140]. After purification, α -syn was dialyzed against 20 mM 2-(N-morpholino)ethanesulfonic acid (MES) buffer, pH 6.0. Protein concentration was measured by UV/VIS-spectroscopy. α -Syn fibrils were prepared as follows: 300 μl of 150 μM α -syn diluted in 20 mM MES, pH 6.0 with 0.02% sodium azide (NaN_3) were incubated at 300 rpm and 37°C for five days in a 2 ml glass vial containing a magnetic stir bar. Samples of the α -syn fibrillation reaction were taken after different time points followed by addition of 5 μM ThT and imaging by TIRFM to confirm the presence of amyloid fibrils. For the preparation of fibril seeds, the fibril solution was diluted twentyfold (5 μl in 100 μl) in 20 mM MES buffer pH 6.0 in PCR tubes. The PCR tube was then transferred to an ultrasound bath (Bandelin Sonorex RK100H, Bandelin electronic) and sonicated twice for 10 min. Seed solutions were stored at 4°C for a maximum of one week.

Cleaning of Glass Slides and TIRFM

Glass slides for imaging of the seeded fibrillation samples and for the direct observation of fibril elongation were Menzel-Gläser coverslips #1 (0.13 mm to 0.16 mm thickness, hydrolytic class 1), 25 x 60 mm coverslips as carriers and 18 x 18 mm coverslips as covers (Gerhard Menzel GmbH, Braunschweig). Coverslips were cleaned by 45 min sonication in an ultrasound bath (Bandelin Sonorex RK100H, Bandelin electronic) at 60 °C in a container with 2% Hellmanex III solution (Hellma). Afterwards, the coverslips were thoroughly rinsed in Milli-Q H₂O (~ten times) and subsequently stored in absolute ethanol. Prior to use, absolute ethanol was evaporated under a nitrogen stream.

TIRFM was performed on a Leica AF6000LX inverted microscope with a HCX PL APO 100x 1.47 oil objective and a Hamamatsu C9100-02-LNK00 EM-CCD camera (objective-style TIRFM). A 405 nm laser diode was used for the excitation of ThT, the excitation light was filtered from fluorescence signal by a 450/50 bandpass filter. Exposure times and EM gain were set to 100 ms and gain 800-1200 for preview and 1 s to 2 s and gain 200-500 for the final images. Images were analyzed with the open source software ImageJ (available at <http://rsb.info.nih.gov/ij/>; developed by Wayne Rasband, National Institutes of Health, Bethesda, MD). Images were manipulated with regard to changing brightness/contrast, cropping of images and applying the "hot cyan" lookup table as well as insertion of scale bars.

Direct Observation of α -Syn Fibril Elongation by TIRFM

For the direct observation of fibril elongation, a 10 μ l sample was prepared as follows: 15 μ g ml⁻¹ α -syn seeds, 10 mM MgCl₂, 7 μ M ThT and 160 μ M α -syn monomers in 20 mM MES pH 6.0 were mixed in a PCR tube. Seven μ l of this sample were applied onto a 25 x 60 mm glass slide covered with an 18 x 18 mm glass slide with a distance of approx. 15 μ m between the two slides (as confirmed by a z-scan with laser scanning microscopy). The coverslips were sealed with wax (valap: 1 part vaseline, 1 part lanolin, 1 part paraffin wax, recipe from Nikon Imaging Center, Harvard Medical school) to prevent evaporation. Sample preparation time was around ten minutes before the first image was taken. The sample was inserted into the TIRF microscope, seven suitable positions were selected and imaged every ten minutes for 40 h. Penetration depth of the evanescent field was 180 nm, exposure time 1.5 s, EM gain: 500. Temperature was ~25 °C, as measured with an infrared thermometer during the experiment. To analyze growth kinetics of single fibrils, images were loaded into ImageJ image analysis software and fibril lengths were measured with the segmented line tool.

Seeded Fibrillation of α -Syn in a Test Tube

For the seeded fibrillation of α -syn in a test tube, 100 μ l samples per time point were prepared under the same conditions as in the real-time fibrillation TIRFM experiment, except for the absence of ThT. Samples were incubated at 25 °C without shaking. After 0 h, 24 h, 48 h and 72 h, 5 μ l samples were withdrawn from the solutions and dried on a coverslip. Prior to imaging by TIRFM, 5 μ l of 5 μ M ThT was added to the dried spots to dissolve salt crystals and provide the fluorescent dye. The remaining solution (95 μ l) was subjected to ultracentrifugation at 100 000 *g* and 4 °C for one hour. The concentration of soluble protein in the supernatant was measured by absorption at 280 nm in a JASCO V-650 spectrophotometer. Three samples per time point were measured.

Acknowledgements

Michael M. Wördehoff was supported by a fellowship of the Deutschlandstipendium and the Heinrich Heine International Graduate School of Protein Science and Technology (iGRASPseed). We like to thank Dr. Gerhard Steger for fruitful discussion.

Appendix

Supplementary data to this article can be found online at: <http://dx.doi.org/10.1016/j.jmb.2015.01.020>.

Received 19 September 2014, Received in revised form 26 January 2015, Accepted 29 January 2015, Available online 4 February 2015.

Keywords: protein aggregation; amyloid; fibril formation; Parkinson's disease; thioflavin T

2.1.7 Supplement

Contents: Supplementary Figures 2.6-2.9

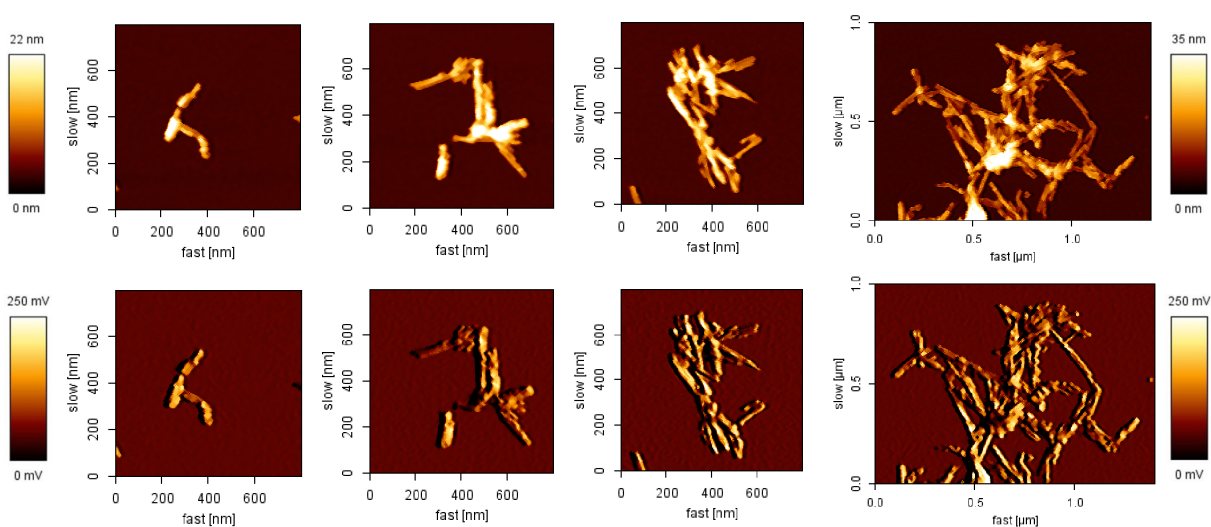


Figure 2.6: AFM images of α -syn seeds used for real-time monitoring of fibrillation. Seeds were prepared by sonication of a $100 \mu\text{g ml}^{-1}$ α -syn fibril solution. $50 \mu\text{l}$ of a $15 \mu\text{g ml}^{-1}$ seed solution in 20 mM MES pH 6.0 containing 10 mM MgCl_2 were deposited on a mica slide and incubated for one hour at room temperature. Afterwards, the slide was washed three times with $100 \mu\text{l}$ dH_2O and dried carefully under a nitrogen stream. AFM images were obtained with tapping mode. The upper row shows the height traces, the lower row shows the amplitude traces of four individual seed spots, the seed image on the right having a different xy and height scale. In AFM, individual seeds were of similar size as in the TIRFM images, covering an area of around $0.5 \times 0.5 \mu\text{m}$. Individual seed particles consisted of multiple fibril fragments, consistent with the observation that fibrils were growing in multiple directions from one seed in the real-time TIRFM experiment.

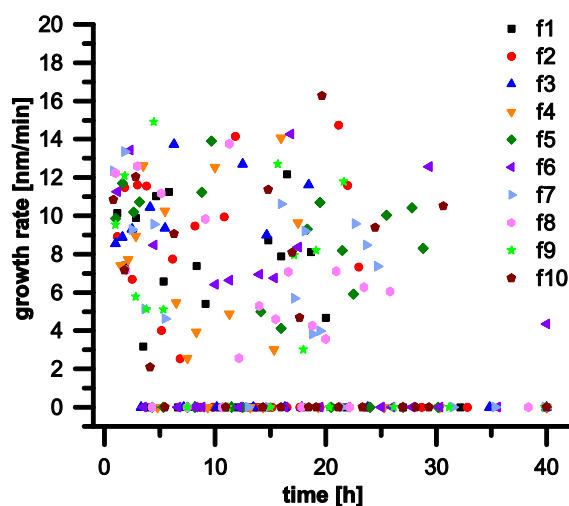


Figure 2.7: Growth rates of fibrils f1-f10 plotted over time. The growth rates of fibrils f1-f10 shown in [fig. 2.3](#) exhibited a high variability over time.

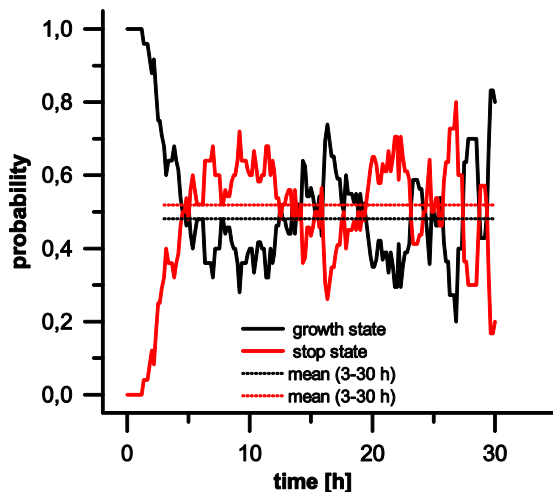


Figure 2.8: Probability distribution of of growth states and stop states over time. Probabilities were determined by dividing the number of growth events and the number of stop events by the total number of events at the respective times. Apparent stop states that were not followed by a growth state (i.e. stop states populated at the end of the experiment) were excluded from the analysis, as fibril growth might have proceeded unnoticed outside of the TIRFM focal plane in these cases. The high growth state probability during the first \sim three hours of the experiment can be explained by a bias stemming from the fact that only initially growing fibrils were selected for analysis. The mean growth rate after 34 h was not determined as there were too few events. The mean probabilities were calculated for the time frame from 3 h to 30 h, as there were very few growth events after 30 h.

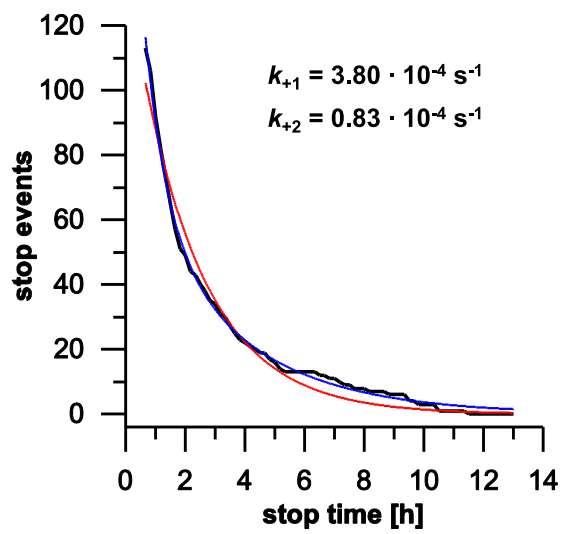


Figure 2.9: Kinetic analysis of reentry into the growth state. Stop state length distribution (black line) fitted to a single exponential (red) or a double exponential (blue) decay. The better fit of the double exponential function suggests the existence of different stop states with individual constants k_+ of reentry into the growth state. R^2 was 0.976 (red) or 0.996 (blue). k_{+1} and k_{+2} represent the constants of reentry into the growth state determined by the double exponential decay fit.

2.2 Contacts between β 1- β 2 Segments in α -Synuclein

2.2.1 Article Information

Title: Contact Between the β 1 and β 2 Segments of α -Synuclein that Inhibits Amyloid Formation

Hamed Shaykhalishahi¹, Aziz Gauhar¹, Michael M. Wördehoff¹, Clara S. R. Grüning¹, Antonia N. Klein², Oliver Bannach^{1,2}, Matthias Stoldt^{1,2}, Dieter Willbold^{1,2}, Torleif Härd³, and Wolfgang Hoyer^{1,2,*}

¹Institut für Physikalische Biologie, Heinrich-Heine-Universität Düsseldorf, 40225 Düsseldorf, Germany

²Strukturbiochemie (ICS-6), Forschungszentrum Jülich, 52425 Jülich, Germany

³Department of Chemistry and Biotechnology, Swedish University of Agricultural Sciences (SLU), 750 07 Uppsala, Sweden

* corresponding author, wolfgang.hoyer@uni-duesseldorf.de

Published in: **Angewandte Chemie International Edition**, Vol. 54, pp. 8837-8840, 2015 [[139](#)]

DOI: [10.1002/anie.201503018](https://doi.org/10.1002/anie.201503018)

Journal Impact Factor (2015): 11.709.

Contribution: **20%**. M.M.W. designed and performed the TIRF microscopy experiments and evaluated the data. For further details see the [appendix](#).

2.2.2 Abstract

Conversion of the intrinsically disordered protein α -synuclein (α -syn) into amyloid aggregates is a key process in Parkinson's disease. The sequence region 35-59 contains β -strand segments β 1 and β 2 of α -syn amyloid fibril models and most disease-related mutations. β 1 and β 2 frequently engage in transient interactions in monomeric α -syn. Here, we evaluate the consequences of β 1- β 2 contacts by disulfide engineering, biophysical techniques, and cell viability assays. The double-cysteine mutant α -synCC, with a disulfide linking β 1 and β 2, is aggregation-incompetent and inhibits aggregation and toxicity of wild-type α -syn. We show that α -syn delays the aggregation of amyloid- β peptide and islet amyloid polypeptide involved in Alzheimer's disease and type 2 diabetes, an effect enhanced in the α -synCC mutant. Tertiary interactions in the β 1- β 2 region of α -syn interfere with the nucleation of amyloid formation, suggesting promotion of such interactions as a potential therapeutic approach.

2.2.3 Article

Protein aggregation and the toxicity of the resulting aggregates are fundamental to the pathogenesis of several human degenerative diseases. For example, aggregates consisting of α -synuclein (α -syn), the amyloid- β peptide (A β), or islet amyloid polypeptide (IAPP) are pathological features of Parkinson's disease (PD), Alzheimer's disease (AD), and type 2 diabetes, respectively [[1](#), [75](#)]. α -Syn is a cytoplasmic protein of 140 amino acids which predominantly exists as an intrinsically disordered protein (IDP) in the cell [[198](#), [199](#)]. The conformational ensemble

of the IDP contains a substantial fraction of conformers that exhibit long-range intramolecular interactions, which may promote or inhibit aggregation [16, 200–204].

According to paramagnetic relaxation enhancement NMR and molecular simulations, contacts between the $\beta 1$ and $\beta 2$ sequence segments are among the most prevalent tertiary interactions in monomeric α -syn [16]. The designations $\beta 1$ and $\beta 2$ refer to two of the approximately five β -strands of α -syn molecules in the amyloid fibril state [132]. The $\beta 1$ - $\beta 2$ region comprises amino acids 35-59, lies outside of the hydrophobic, fibrillation-triggering NAC region [205], and is the most N-terminal sequence region of α -syn incorporated in the fibril core of most of the fibril polymorphs described to date [132, 135, 206, 207]. Several lines of evidence support a critical role of the $\beta 1$ - $\beta 2$ region for α -syn aggregation and pathogenesis: First, it harbors most of the disease-related mutations, which alter the oligomerization and fibrillation propensity of α -syn [208]. Second, it is part of the core of α -syn oligomers, exhibiting particularly high resistance to H/D exchange [209]. Third, it regulates α -syn strain type and seeding efficiency [210]. Fourth, we have recently shown that sequestration of the $\beta 1$ - $\beta 2$ region by the engineered binding protein β -wrapin AS69 potently inhibits α -syn aggregation [178]. In complex with AS69, α -syn locally adopts a β -hairpin conformation with β -strands comprising residues 37-43 and 48-54, respectively, reminiscent of the $\beta 1$ and $\beta 2$ strands of fibrillar α -syn [178]. The tertiary contacts between the β -strands of the AS69-bound β -hairpin agree well with the $\beta 1$ - $\beta 2$ contact map of free, monomeric α -syn [16].

Considering the importance of the $\beta 1$ - $\beta 2$ region for α -syn aggregation, $\beta 1$ - $\beta 2$ tertiary contacts might be crucial regulators of aggregation. Here we investigate the effect of contact between $\beta 1$ and $\beta 2$ on amyloid formation. A stable contact was established by introduction of an intramolecular disulfide bond in the double cysteine mutant G41C/V48C, called α -synCC. The C41-C48 disulfide bond is compatible with the β -hairpin conformation of AS69-bound α -syn (fig. 2.10a).

The two exchanges G41C and V48C are located in the $\beta 1$ and $\beta 2$ strand, respectively, diagonally opposite of each other. The C α -C α distance of G41 and V48 in the α -syn:AS69 complex is 6.1 Å, which is within the C α -C α distance range of cysteine disulfide bonds in X-ray structures (average: 5.6 Å) [211]. The steric demands of two disulfide-bonded cysteine residues (sum of residue volumes 207 Å³) are similar to those of the original glycine-valine combination (sum of residue volumes 203 Å³) [212]. To analyze the conformation of α -synCC, the (¹H-¹⁵N) HSQC NMR spectrum of [U-¹⁵N]- α -synCC was compared to that of [U-¹⁵N]-wt α -syn (fig. 2.10b). The limited resonance dispersion of wt α -syn was retained for α -synCC, demonstrating that the engineered disulfide does not induce folding into a stable conformation. α -synCC showed insignificant secondary chemical shifts, further indicating that it is an IDP like wt α -syn (fig. 2.10c).

Noticeable differences in chemical shifts of α -synCC and wt α -syn were only observed for the amino acid residues adjacent to the two mutation sites; however, secondary chemical shifts did not support formation of any stable secondary structure in this region (fig. 2.10c). Oxidized α -synCC did not form fibrils after prolonged incubation in a fibrillation assay monitored by Thioflavin T (ThT) fluorescence (fig. 2.10d). Breakage of the $\beta 1$ - $\beta 2$ disulfide bond with the reducing agent dithiothreitol (DTT), however, resulted in aggregation kinetics similar to those of wt α -syn (fig. 2.10d). Formation of the $\beta 1$ - $\beta 2$ disulfide bond thus renders α -synCC non-fibrillogenic,

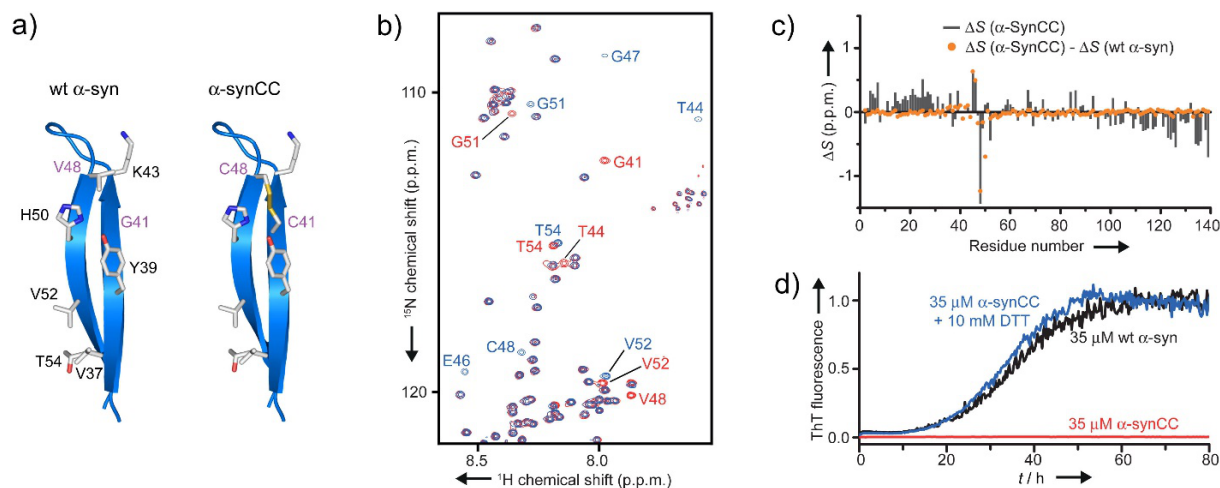


Figure 2.10: Protein engineering and characterization of α -synCC. a) Left: β -Hairpin conformation of the β 1– β 2 region of α -syn bound to β -wrapin AS69 (PDB: 4bx1). The side chains at the front face are shown as sticks. Right: Model of a β -hairpin conformation of α -synCC, in which residues 41 and 48 of wt α -syn have been exchanged to cysteines. b) Section of overlaid $(^1\text{H}-^{15}\text{N})$ -HSQC NMR spectra of $[\text{U}-^{15}\text{N}]$ -wt α -syn (red) and $[\text{U}-^{15}\text{N}]$ - α -synCC (blue) at 10 °C. Assignments of peaks affected by the double cysteine exchange are indicated. c) Averaged $\text{C}\alpha$ and C' secondary chemical shifts of α -synCC and difference in secondary chemical shifts between α -synCC and wt α -syn. d) ThT time course of fibrillation of oxidized and reduced α -synCC compared to wt α -syn.

indicating that β 1- β 2 contacts entail conformations belonging to the pool of autoinhibitory conformations [200]. Size exclusion chromatography (SEC) confirmed that oxidized α -synCC did not form stable oligomers upon incubation but remained monomeric (fig. 2.13). This is in contrast to A β CC, a double cysteine mutant of A β engineered following an analogous strategy (fig. 2.14), which was previously shown to form stable, neurotoxic oligomers [213,214]. This difference might be a consequence of the lower hydrophobicity of the hairpin region of α -synCC compared to the hairpin region of A β CC, with GRAVY (grand average of hydropathy) [215] values of 0.48 for α -synCC(37-54) and 1.27 for A β CC(17-36).

α -SynCC inhibited the aggregation of wt α -syn both at equivalent and at substoichiometric concentrations (fig. 2.11a). The inhibitory effect at substoichiometric ratios indicates that α -synCC interferes with nucleation and/or elongation of wt α -syn fibrils. The inhibitory effect is a consequence of the β 1- β 2 disulfide linkage as it was abolished by disulfide reduction by DTT (fig. 2.11a).

To test if α -synCC inhibits elongation of wt α -syn fibrils, seeded fibrillation reactions of wt α -syn were performed in the absence and presence of α -synCC and monitored either in a fluorescence microplate reader (fig. 2.15) or by total internal reflection fluorescence microscopy (TIRFM) (fig. 2.11d). Ultrasonicated wt α -syn fibrils were used as seeds. Addition of α -synCC entailed a concentration-dependent inhibition of seeded wt α -syn aggregation (fig. 2.15). Wt α -syn fibril seeds were imaged by TIRFM as particles with several fibrillation sites, resulting in a fibril network after quiescent incubation with wt α -syn monomers (fig. 2.11d) [64]. In contrast, fibril networks were not formed when α -synCC was incubated with wt α -syn fibril seeds, in agreement with the finding that α -synCC is non-fibrillogenic (fig. 2.11d). Incubation of wt α -syn monomers with wt α -syn fibril seeds did not lead to the formation of fibril networks when

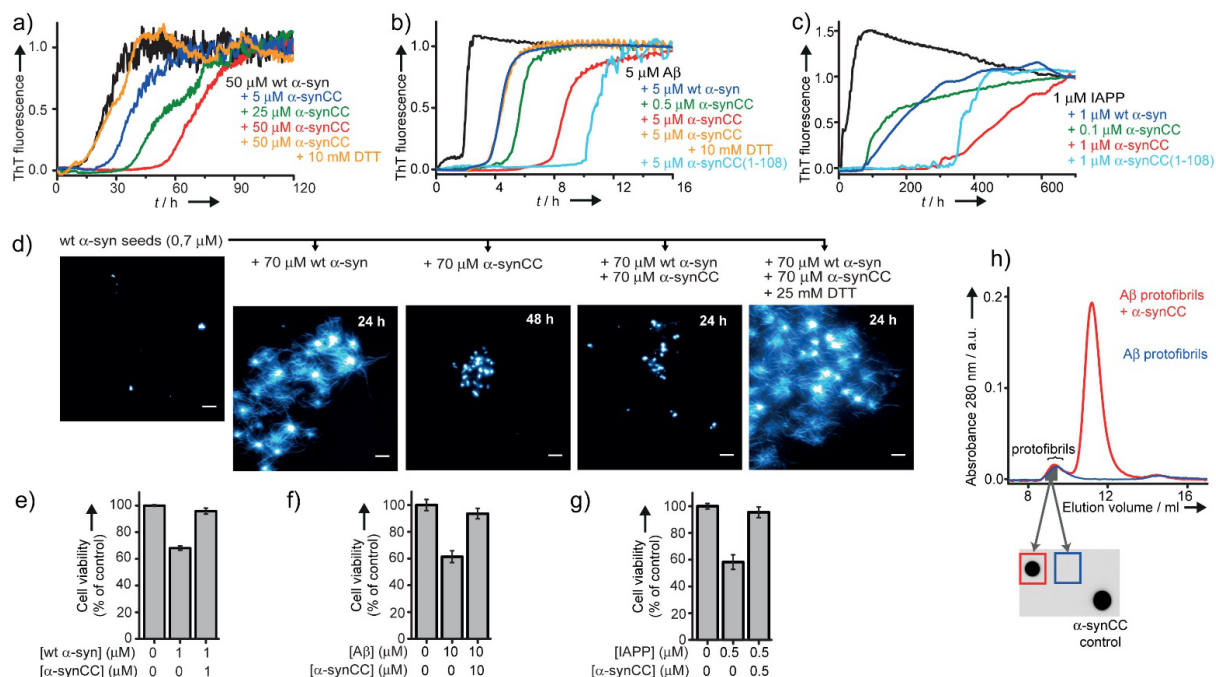


Figure 2.11: α -SynCC inhibits aggregation and toxicity of wt α -syn, A β and IAPP. a)–c) ThT time course of fibrillation of wt α -syn (a), A β (b), and IAPP (c) in the absence and presence of α -synCC. d) TIRF microscopy of fibrillation of α -synCC and wt α -syn in the presence of wt α -syn fibril seeds under quiescent condition. Scale bar: 5 μ m. e)–g) MTT assays to evaluate the toxicity of wt α -syn (e), A β (f), and IAPP (g) aged in the absence and presence of α -synCC to SH-SY5Y neuroblastoma cells. The data are representative of experiments carried out in triplicate (mean \pm s.d.), expressed as percentage relative to the untreated cells (control). h) α -SynCC interacts with A β protofibrils. SEC chromatograms of purified A β protofibril samples re-injected onto the column after 10 min incubation at room temperature in the absence (blue) or presence (red) of a twofold excess (calculated in monomer units) of α -synCC. A β protofibrils elute close to the void volume (ca. 8.5 ml), while the elution peak at circa 11.5 ml corresponds to α -synCC. Dot blot analysis of the protofibril fractions using the anti- α -syn antibody 211 is shown below the chromatogram. Fresh α -synCC served as positive control. A β (1-40) (b,f) or A β (1-42) (h) with an N-terminal methionine [216] was used.

α -synCC was present (fig. 2.11d). The inhibitory effect of α -synCC on wt α -syn fibril elongation was dependent on the β 1- β 2 disulfide linkage as it was abrogated by disulfide reduction by DTT (fig. 2.11d). In summary, the seeded fibrillation experiments indicate that α -synCC interacts with fibril ends. Wt α -syn samples that were aged under aggregation-promoting conditions reduced the viability of human SH-SY5Y neuroblastoma cells, as assessed by an MTT (3-(4,5-dimethylthiazol-2-yl)-2,5-diphenyltetrazolium bromide) assay (fig. 2.11e). However, when ageing of wt α -syn was performed in the presence of α -synCC, the cell viability was rescued (fig. 2.11e).

Different protein aggregation disorders, associated with amyloidogenic proteins of non-homologous sequences, frequently overlap clinically and pathologically, suggesting a mutual interference of the aggregation reactions of the involved proteins [210,217]. While A β plaques are often found in PD patients, α -syn Lewy bodies are found in most of the AD cases [218]. Similarly, IAPP oligomers and plaques were identified in the brains of diabetic AD patients [219]. We investigated potential heterotypic interactions of α -synCC with other amyloidogenic proteins by testing its effects on the fibrillation of A β and IAPP. The effects of α -synCC were

compared to those exerted by wt α -syn. Wt α -syn and α -synCC both inhibited fibrillation of A β and IAPP, with more potent inhibition exhibited by α -synCC (fig. 2.11b,c). The lag-time of fibrillation of 5 μ M A β increased by 2- and 4-fold upon addition of an equimolar amount of wt α -syn and α -synCC, respectively (fig. 2.11b). Reduction of the disulfide bond in α -synCC decreased the inhibitory effect of α -synCC to the level of wt α -syn, demonstrating that the β 1- β 2 disulfide linkage is responsible for the higher inhibitory potential of α -synCC (fig. 2.11b). The lag-time of fibrillation of a 1 μ M solution of IAPP increased by 10- and 40-fold in the presence of an equimolar amount of wt α -syn and α -synCC, respectively (fig. 2.11c). A 1:10 ratio of α -synCC:A β or α -synCC:IAPP was sufficient to achieve a significant prolongation of the fibrillation lag time, supporting an impact of α -synCC on the nucleation and/or elongation of A β and IAPP fibrils (fig. 2.11b,c). A chaperone-like activity of α -syn was observed before in thermal-induced and chemical-induced protein aggregation assays [220, 221]. The acidic C-terminal tail was critical for this activity by serving as a solubilizing domain. A C-terminally truncated variant of α -synCC, α -synCC(1-108), however, caused similar increases in the fibrillation lag times of A β and IAPP as full-length α -synCC (fig. 2.11b,c). β 1- β 2-mediated aggregation inhibition does therefore not depend on the acidic C-terminal of α -syn and must act through a different mechanism than the previously reported chaperone-like function. To complement the ThT fluorescence data, A β aggregation was analyzed by SEC and transmission electron microscopy (TEM), demonstrating that α -synCC inhibited the formation of oligomers and fibrils (fig. 2.16). Ageing of solutions of A β and IAPP under aggregation-promoting conditions resulted in cytotoxicity in an MTT assay on SH-SY5Y neuroblastoma cells (fig. 2.11f,g). However, when the cells were treated with A β and IAPP samples aged in the presence of α -synCC they displayed a viability similar to that of untreated cells (fig. 2.11f,g). To identify the molecular species interacting with α -synCC, binding of α -synCC to monomers of wt α -syn, A β , or IAPP, and to A β protofibrils, metastable neurotoxic oligomers, was tested. Biotinylated monomers of the target proteins were coated on streptavidin SA sensor chips. No response indicative of binding was detected for any of the three target proteins when α -synCC was passed as analyte over the sensor surfaces (data not shown). Freshly prepared A β protofibrils were incubated for 10 min with or without α -synCC. The incubated samples were analyzed by reinjection onto the SEC column, isolation of the protofibril fraction, and dot blot using the anti- α -syn antibody 211 (fig. 2.11h).

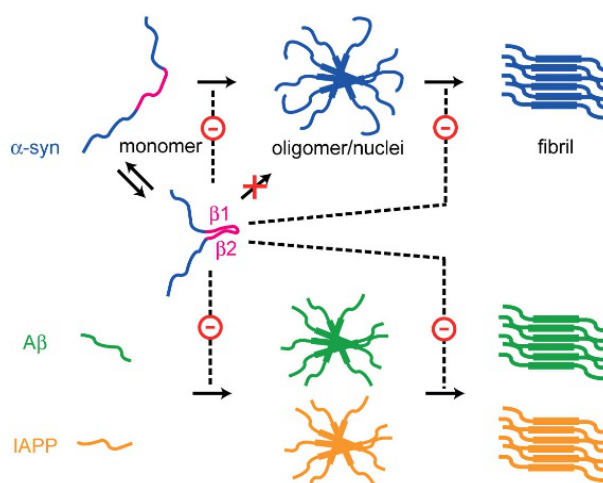


Figure 2.12: Representation of the inhibitory effect of tertiary contacts in the β 1- β 2 region of α -syn on the aggregation of amyloidogenic IDPs. Conformations of α -syn featuring β 1- β 2 contacts are incompetent to form oligomers and fibrils. Furthermore, they inhibit fibril nucleation and elongation of α -syn, A β , and IAPP.

The A β protofibrils sample pre-incubated with α -synCC showed immunoreactivity, indicating binding of α -synCC to A β protofibrils.

The present study shows that α -synCC with established disulfide bond actively interferes with the aggregation of amyloidogenic proteins (fig. 2.12). How does the β 1- β 2 contact lead to inhibition of protein aggregation? Considering the amino acid sequence, formation of β 1- β 2 contacts is likely accompanied by population of conformers with clusters of hydrophobic and aromatic amino acids, including, e.g., Tyr-39 and His-50. These conformers might not be compatible with the fibrillation reaction, but prone to interact with other species on the aggregation pathway that also exhibit hydrophobic patches, such as oligomeric nuclei and fibril ends, eventually precluding further assembly of these species.

This work supports the view that the β 1- β 2 region is an important regulatory element of α -syn aggregation. Tertiary interactions between β 1 and β 2 interfere with aggregation and steer α -syn's capacity to engage in hetero-interactions with other amyloidogenic IDPs. In the search for inhibitors of amyloid formation [222], promotion of β 1- β 2 contacts therefore constitutes a potential approach.

2.2.4 Materials and Methods

Protein Preparation

Wt α -syn and α -syn(1-108) were expressed and purified as described [178]. To generate α -synCC and α -synCC(1-108) constructs, the Gly-41 and Val-48 residues of wt α -syn and α -syn(1-108) were exchanged to cysteines using a site-directed mutagenesis approach. In order to ensure formation of the intramolecular disulfide bond, the purified α -synCC proteins were dialyzed against 100 mM Tris-HCl, pH 8.4, containing 2 μ M CuSO₄ [223]. Oxidized α -synCC was further purified by activated thiol sepharose 4B medium (GE Healthcare). For NMR experiments, both wt α -syn and α -synCC were expressed in M9 minimal medium supplemented with ¹⁵N-NH₄Cl (1 g l⁻¹) and ¹³C₆-glucose (2 g l⁻¹) and purified as described for the unlabeled protein.

A β 40 and A β 42 were produced with an N-terminal methionine by recombinant co-expression with ZA β 3 [216]. The N-terminal methionine is required for translation initiation in the employed expression system. A β with and without N-terminal methionine are highly similar in terms of structure and aggregation properties [216, 224].

Synthetic human IAPP (EMD Millipore), amidated at the C-terminus to correspond to the form with full biological activity [225], was dissolved in 20 mM NaPi, 50 mM NaCl, pH 6.0, containing 6 M Guanidine HCl to dissolve preexisting aggregates. The monomeric fraction was collected after SEC on a Superdex 75 10/300 GL column (GE Healthcare) in 20 mM NaPi, 50 mM NaCl, pH 6.0.

NMR Spectroscopy

NMR data were collected at 10 °C using a 900 MHz spectrometer (Varian) equipped with a cryogenically cooled Z-axis pulse-field-gradient triple resonance probe. (¹H-¹⁵N)-HSQC (heteronuclear single quantum coherence) measurements were performed on samples of ca. 250 μ M [U-¹⁵N]-wt α -syn or [U-¹⁵N]- α -synCC in 20 mM NaPi, 50 mM NaCl, pH 7.4. Backbone assignments were obtained with BEST-TROSY

experiments [226] and standard triple resonance heteronuclear NMR techniques using samples of the [U- ^{13}C , ^{15}N]-labeled proteins. NMR data were processed using NMRPipe [227] and analyzed with CcpNmr [228]. Averaged $\text{C}\alpha$ and C' secondary chemical shifts were calculated as $\Delta\text{S} = (3 \times \Delta\text{S}(\text{C}\alpha) + 4 \times \Delta\text{S}(\text{C}'))/7$ applying random coil shifts according to Kjaergaard et al [229, 230].

Microplate Aggregation Assay

Fibrillation was performed in black round-bottom 96-well plates (Nunc) in an Infinite M1000 plate reader (Tecan). α -Syn fibrillation was done at 37 °C in 20 mM NaPi, 50 mM NaCl, pH 6.0, under orbital shaking with one glass bead (2 mm) per microplate well. $\text{A}\beta$ fibrillation was done at 30 °C (fig. 2.11b,f) or 37 °C (fig. 2.16) in 20 mM NaPi, 50 mM NaCl, pH 7.4, under orbital shaking with one glass bead per microplate well. $\text{A}\beta$ (1-40) with an N-terminal methionine [216] was used in the fibrillation experiments. IAPP fibrillation was done at 30 °C in 20 mM NaPi, 50 mM NaCl, pH 6.0, under quiescent conditions. All samples contained 40 μM ThT and 0.04% NaN_3 . The plates were sealed with polyolefin tape (Nunc) before incubation. Amyloid formation was followed by ThT fluorescence at 480 nm (excitation 440 nm). Seeded-growth fibrillation of α -syn was performed under the same conditions as applied for *de novo* fibrillation, but in the presence of 20% (w/w) α -syn seeds. Seeds were prepared by ultrasonication of preformed α -syn fibrils for 15 min in an ultrasound water bath.

Size Exclusion Chromatography

SEC runs were performed on a Superdex 75 10/300 GL column connected to an Äkta Purifier system (GE Healthcare) at a flow rate of 0.8 ml min $^{-1}$.

TIRF Microscopy

Wt α -syn and α -synCC were incubated in 20 mM MES, 10 mM MgCl_2 , pH 6.0, at 37 °C in PCR tubes in the presence of α -syn seeds, prepared by ultrasonication of preformed α -syn fibrils for 15 min in an ultrasound water bath. After 0 h, 24 h and 48 h, 2 μl samples were withdrawn and dried on a cleaned glass coverslip (Menzel-Gläser coverslips #1, 25 x 60 mm, 0.13 mm to 0.16 mm thickness, hydrolytic class 1, Gerhard Menzel GmbH, Braunschweig, Germany). Directly prior to imaging, 5 μl of 5 μM Thioflavin T in dH_2O were pipetted onto the dried spots. TIRFM was performed on a Leica AF6000LX inverted microscope equipped with a HCX PL APO 100x 1.47 oil objective and a Hamamatsu C9100-02-LNK00 EM-CCD camera (objective-style TIRFM). A 405 nm laser diode was used for the excitation of ThT. Excitation light was filtered from the fluorescence signal by a 450/50 bandpass filter. Exposure times and EM gain were set to 100 ms and 800-1200 for preview and 1 s to 2 s and 200-500 for the final images. Images were processed with ImageJ software (available at <http://rsb.info.nih.gov/ij/>; developed by Wayne Rasband, National Institutes of Health, Bethesda, MD) with respect to brightness and contrast settings, cropping of images, and application of lookup table hot cyan.

Transmission Electron Microscopy

Samples from an A β aggregation assay were diluted to an A β concentration of 5 μ M, and 20 μ l were applied to formvar/carbon coated copper grids (S162, Plano), followed by incubation for 3 min. The grids were washed three times with H₂O and once with 2% aqueous uranyl acetate, followed by 1 min incubation with 2% aqueous uranyl acetate for negative staining. The grids were dried overnight. The samples were examined with a Libra 120 electron microscope (Zeiss) operating at 120 kV.

Toxicity Assay

The viability of SH-SY5Y neuroblastoma cells was assessed with an MTT assay (Cell Proliferation Kit I, Roche Diagnostics) as described before [178]. Protein samples were aged under the conditions of the microplate aggregate assay described above for 48 h (α -syn), 4 h (A β), or 1 h (IAPP) at a protein concentration of 50 μ M (α -syn), 96 μ M (A β), or 50 μ M (IAPP), respectively, and diluted into the cell culture medium to the final concentrations of 1 μ M (α -syn), 10 μ M (A β) and 0.5 μ M (IAPP). The cell cultures were further incubated for 24 h before the MTT assay was carried out.

A β Protofibril Interaction

A β 42 protofibrils were prepared as described before [189]. 480 μ l of freshly SEC-purified A β protofibrils (52 μ M monomer concentration) in 20 mM NaPi buffer, pH 7.0, were mixed with 200 μ l of 283 μ M α -synCC or with 200 μ l of buffer and incubated at room temperature for 10 min. Following re-injection of the samples onto a Superdex 75 10/300 column, A β protofibril fractions were collected for further analysis by dot blotting. The anti- α -syn antibody 211 (Santa Cruz Biotechnology) recognizing a C-terminal epitope was used at a concentration of 0.5 μ g ml⁻¹ to detect α -synCC. A HRP-conjugated goat anti-rabbit IgG antibody was applied to detect bound antibody 211 on a CCD camera, using SuperSignal West Pico chemiluminescent substrate (Thermo Scientific).

Acknowledgements

This work was supported by the Ministerium für Innovation, Wissenschaft und Forschung des Landes Nordrhein-Westfalen.

Appendix

Supporting information for this article is available at <http://dx.doi.org/10.1002/anie.201503018>.

Received: 1 April 2015, Published online: 26 June 2015

Keywords: Aggregation, intrinsically disordered proteins, protein engineering, protein folding, protein–protein interactions.

2.2.5 Supplement

Contents: Supporting Figures 2.13-2.16

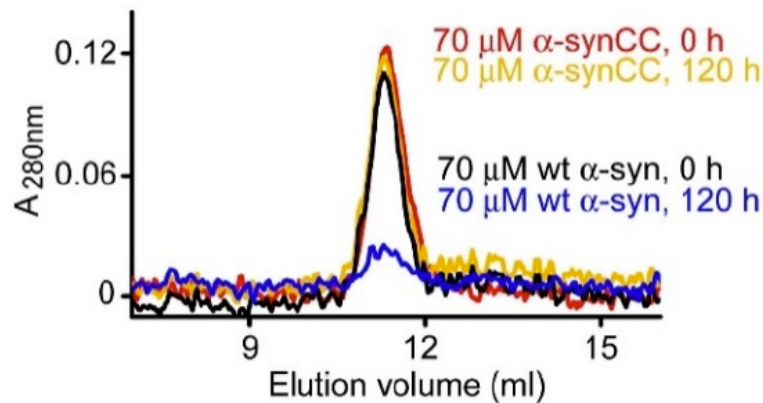


Figure 2.13: SEC analysis of aggregation of α -synCC and wt α -syn. Protein samples subjected to an aggregation assay for the indicated times were loaded onto a Superdex 75 10/300 GL column (void volume \sim 8.5 ml. For wt α -syn, the elution peak was greatly reduced after 120 h incubation due to the formation of amyloid fibrils which do not enter the column bed.



Figure 2.14: The positions of the exchanges to cysteine (yellow) in α -synCC are identical to those in A β CC [214] in relation to the β -hairpin. Backbone hydrogen bonding across the strands is indicated with black dots.

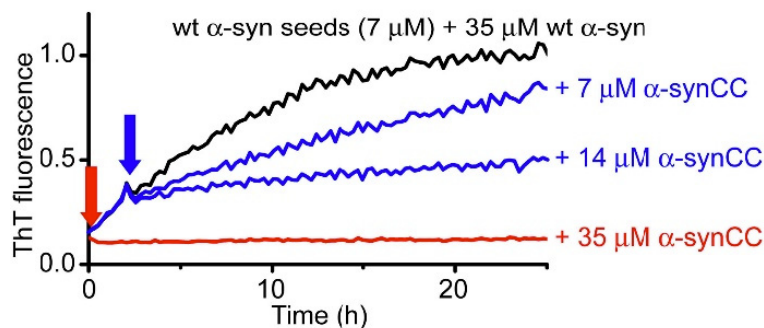


Figure 2.15: ThT time course of fibrillation of wt α -syn in the presence of preformed wt α -syn fibril seeds, with addition of α -synCC at the time points indicated by arrows.

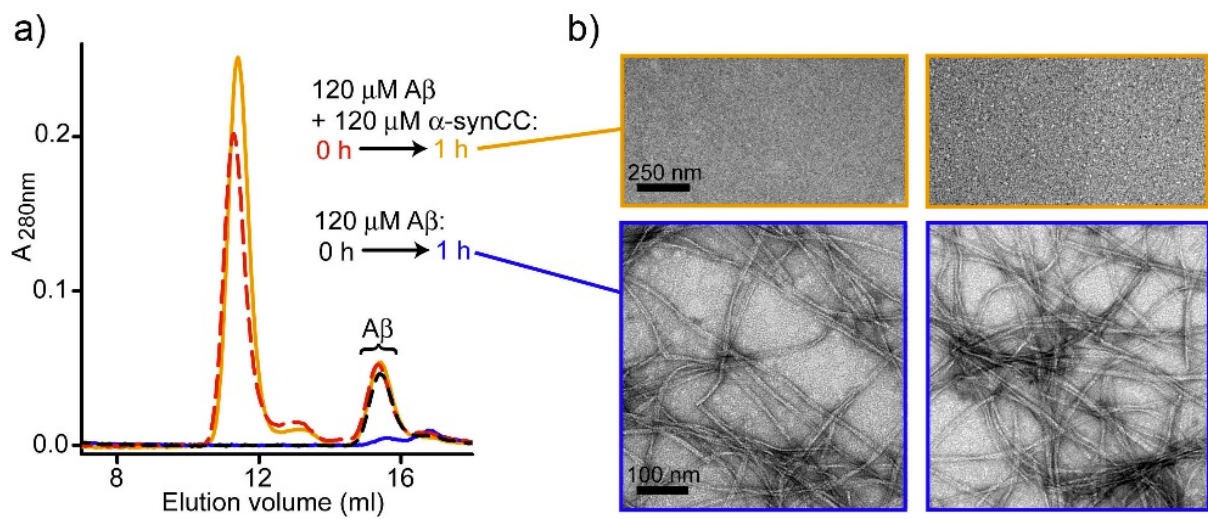


Figure 2.16: a) SEC analysis of A β aggregation in absence and presence of α -synCC. Protein samples were subjected to an aggregation assay for the indicated times and loaded on a Superdex 75 10/300 GL column (void volume \sim 8.5 ml). In the absence of α -synCC, the elution peak of A β was strongly reduced after 1 h incubation (blue trace) due to the formation of amyloid fibrils which do not enter the column bed. b) Two representative TEM images of each of the 1 h incubation samples analyzed in a).

2.3 Interaction of α -Synuclein with Lipid Bilayer Nanodiscs

2.3.1 Article Information

Title: A Structural and Kinetic Link Between Membrane Association and Amyloid Fibril Formation of α -Synuclein

Thibault Viennet^{1,2}, Michael M. Wördehoff¹, Boran Uluca^{1,2}, Chetan Poojari^{2,3,4}, Hamed Shaykhalishahi¹, Dieter Willbold^{1,2}, Birgit Strodel², Henrike Heise^{1,2}, Alexander K. Buell¹, Wolfgang Hoyer^{1,2} & Manuel Etzkorn^{1,2,*}

¹Institute of Physical Biology, Heinrich-Heine-University Düsseldorf, Germany

²Institutue of Complex Systems, Forschungszentrum Jülich, Germany

³Department of Physics, Tampere University of Technology, Finland

⁴Department of Physics, University of Helsinki, Finland

* corresponding author, manuel.etzkorn@hhu.de

Submitted to: **Nature Chemical Biology**, 12.05.2017.

Journal Impact Factor (2016/2017): 15.066.

Contribution: **35%**. M.M.W. prepared unlabelled and ¹⁵N-labelled α -synuclein, performed aggregation assays and evaluated the data. For further details see the [appendix](#).

2.3.2 Abstract

The protein α -Synuclein (α S) is linked to Parkinson's disease through its abnormal aggregation, which is thought to involve an interplay between cytosolic and membrane-bound forms of α S. Therefore, better insights into the molecular determinants of membrane association and their implications for protein aggregation may help deciphering the pathogenesis of Parkinson's disease. Following previous studies using micelles and vesicles, we present a comprehensive study of α S interaction with phospholipid bilayer nanodiscs. Using a combination of NMR-spectroscopic and complementary biophysical as well as computational methods we structurally and kinetically characterize α S interaction with defined stable planar membranes in a quantitative and site-resolved way. We probe the role of α S acetylation as well as membrane charge, plasticity and available surface area in modulating α S membrane binding modes and directly link these findings to their consequences for the nucleation and elongation process of α S amyloid fibril formation.

2.3.3 Introduction

The protein α -Synuclein (α S) is associated with various synucleinopathies including Parkinson's disease through its abnormal aggregation, fibril formation and formation of Lewy bodies [44, 75, 136, 231]. While the exact native function is yet not fully understood, α S is found in synaptic vesicles and supposed to be involved in membrane interactions, e.g. in synaptic

vesicle homeostasis [232, 233] and SNARE-like vesicle-to-vesicle or vesicle-to-membrane fusion [234, 235]. Membrane association of α S has been shown to modulate its aggregation propensity [236, 237], and α S oligomeric species have been proposed to be the toxic species in Parkinson's disease, especially through membrane pore formation mechanisms [238, 239]. α S has been shown to be N-terminally acetylated, which is thought to act as an important mode of regulation of protein-membrane association [98, 240, 241]. Previous data recorded using micelle and vesicle preparations already provided valuable information of the α S-membrane interactions, including binding and lipid specificity [105, 106, 242], effect of mutations on membrane association [235, 243], micelle-bound structure [102], vesicle-bound structural insights [244–246] and conformational dynamics [14, 235, 246]. Two structural models of lipid-bound α S were proposed, i.e. the “extended helix” consisting of one roughly 100-residue long α -helix [100] and the “horse-shoe”, consisting of two helices with different lipid affinities separated by a kink at residues 42-44 [247]. Furthermore, various effects of lipids for α S aggregation were reported including inhibition of aggregation [248], triggering of fibrillation [107, 249] and modification of fibril structure [133]. Membrane binding and its effect on aggregation have been shown to be strongly dependent on chemical properties of the lipids including head group charge content [247] and fatty acid type [108].

The intrinsic features of the phospholipid bilayer nanodisc (ND) system [250] offer the potential to provide additional insights that are complimentary to the information obtained on micelle and vesicle preparations. Notably, NDs have been used before to study the effect of calcium ions on the membrane interaction of α S [251] as well as lipid and monomer specificity of the Alzheimer's associated A β peptide [252]. In general, NDs are very homogenous, stable in a wide buffer range [253] and allow the preparations of well-defined lipid mixtures with an accurate estimate of the bilayer size [254], charge [255], and lipid molarity [256]. The increased stability offers e.g. the possibility to consistently determine the interaction with a stable planar bilayer surface. In contrast, it is known for small unilamellar vesicles (SUVs) that the interaction with α S can considerably and rapidly change the lipid environment (e.g. from homogenous SUVs to rather heterogeneous particles [110, 133, 235, 257]). Additionally, the smaller size of the NDs should, in theory, allow the detection of the lipid-bound state using suitable solution NMR techniques [253, 258, 259]. In general, the well-defined size and lipid composition of NDs, paired with their accessibility, homogeneity and stability should therefore permit quantitative insights into membrane association as well as its role in aggregation.

Here we make use of this potential and report on a comprehensive NMR investigation of the effects of lipid charge, bilayer fluidity and α S acetylation on the structural aspects of α S membrane association. We corroborate these insights with molecular dynamics (MD) simulations as well as a series of complementary biophysical measurements to further characterize membrane plasticity, overall affinities as well as binding and aggregation kinetics. Based on this data we correlate structural insights, such as residue specific affinities and competition for accessible membrane surface area, to their potential role in modulating α S aggregation properties. Our study provides insights into (i) the different lipid binding modes of α S to stable planar bilayers of defined lipid quantity and composition, (ii) the effect of membrane plasticity for α S binding,

(iii) the modulation of membrane plasticity through α S, and (iv) the connection between binding modes and their effect on α S aggregation. Additionally, it gives an initial estimate of the number of lipid-associated α S molecules that are required to induce/promote nucleation, and allows to develop a basic structural, thermodynamic and kinetic model of the modulation of α S aggregation through its interaction with different membrane surfaces. Our *in vitro* data help to better understand the molecular determinants of α S-membrane association and point to possible *in vivo* implications in the context of Parkinson's disease.

2.3.4 Results and Discussion

Effects of Phospholipid Head-group Charge on the α S Membrane Binding Mode

To obtain residue specific insights into the interaction of α S with lipid bilayer nanodiscs (NDs) of various composition, we recorded a series of solution NMR 2D TROSY-HSQC spectra (see Supplementary Table 2.2 for full list of measured samples). The NMR spectrum of α S in the presence of NDs containing only DMPC lipids perfectly overlays with the spectrum of α S in the absence of NDs (fig. 2.17a-d). This finding provides additional evidence that α S does not interact with non-charged lipid bilayers [105], a point that is still controversial in the literature [99]. Additionally, it also shows that α S does not interact with the membrane scaffold protein (MSP), confirming that the effects described in the following are not biased by (unspecific) α S-MSP interactions.

In a similar way as reported previously using liposomes [247, 260], we further tested the influence of increasing amounts of negatively charged lipid head groups on α S membrane association, keeping a molar ratio of one α S molecule per membrane leaflet (fig. 2.17a-d). Note that lipid ratios and proper mixing of the different lipid types inside the nanodiscs was also observed by NMR spectroscopy (Supplementary Figure 2.23a). Our NMR data show a gradually increasing bilayer interaction of α S with increasing lipid charge content, dividing the protein into rather distinct regions with different binding behaviors (fig. 2.17e). The first region spans the N-terminal residues 1-38, which are already weakly interacting at 25% content of negatively charged lipids and strongly interact at 50% (or higher) charge content. The region of residues 38-60 interacts more gradually at 50% charge content. Amino-acids 60-98, corresponding approximately to the aggregation-prone non-amyloid- β component (NAC region), displays some interactions with membranes containing 75% anionic lipids and strongly interacts at 100% anionic lipid content. The 98-120 region is (partly) affected by 100% net charge content only. Finally, the last 20 C-terminal residues never show any membrane interaction. This data is largely in line with an expected predominantly electrostatic model (the first 60 residues displaying a net positive charge, the last 40 residues a net negative charge, and the NAC region being mostly hydrophobic), as well as the three regions dynamic model reported before using SUVs [246].

Using Thioflavin T (ThT) fluorescence as a reporter for fibril formation, we also measured aggregation kinetics of α S in the absence and presence of the different ND compositions (fig. 2.17f-g). These experiments were performed under conditions where α S amyloid fibrils form spontaneously and therefore mainly report on the potential interference of nanodiscs with

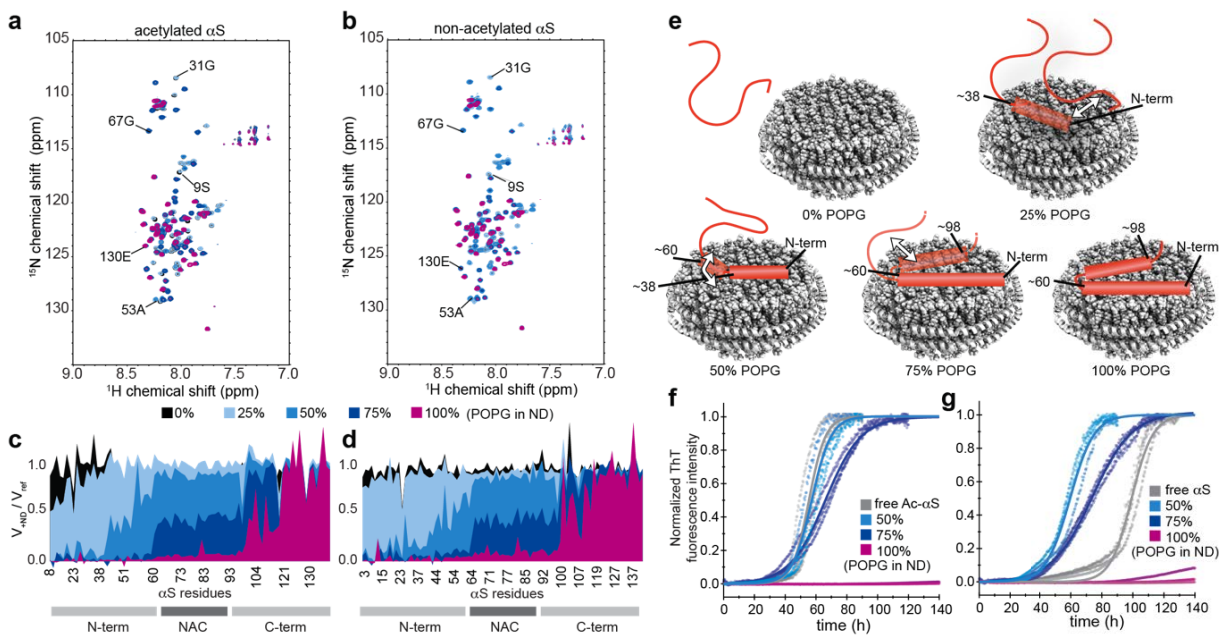


Figure 2.17: Lipid charge content modulates α S membrane binding modes and different binding modes show different effects on α S aggregation properties. NMR spectra of $[^{15}\text{N}]\text{-}\alpha$ S ($50\ \mu\text{M}$) in the absence or in the presence of $25\ \mu\text{M}$ NDs of different POPG (negative charges) contents. $[^{15}\text{N}\text{-}^1\text{H}]\text{-TROSY-HSQC}$ spectra of acetylated (a) and non-acetylated (b) α S. Spectra in the absence (grey) or in the presence of NDs containing 0% POPG (black), 25% POPG (light blue), 50% POPG (blue), 75% POPG (dark blue) and 100% POPG (purple) are displayed. Selected residue assignments corresponding to differently affected parts of α S are indicated. Corresponding NMR attenuation profiles, i.e. the ratio of peak volumes in the presence and absence of NDs, are plotted against α S primary sequence for acetylated (c) and non-acetylated (d) α S. (e) Molecular model visualizing the gradual binding of different parts of α S to NDs with increasing charge content. (f,g) α S aggregation assays (normalized ThT fluorescence) in the absence and presence of NDs with indicated POPG charge content for acetylated (f) and non-acetylated (g) α S (data of triplicate measurements until reaching saturation and their respective fits are shown, color code as in a-d).

the lipid-independent aggregation pathway of α S [138, 261–263]. Interestingly, despite the fact that the NMR data show interaction, the presence of NDs up to an anionic lipid content of 50% does not appear to affect aggregation kinetics (note that the free non-acetylated α S reference (fig. 2.17g, gray) shows a different behavior, this point will be discussed below). When increasing the negative charge content to 75% the aggregation half-time slightly increases (fig. 2.17f,g, dark blue) and a strong aggregation-inhibiting effect is detected in the presence of NDs with 100% anionic lipids (fig. 2.17f,g, purple).

While the NMR data visualize the modes of α S binding to membranes of different charge contents, the ThT kinetic data allow to directly link these molecular determinants to their effect on α S aggregation. In this respect, one of the most striking connections is that α S interaction with NDs comprising up to 50% negatively charged lipids does not involve the NAC region and that under the same conditions no detectable effect on the aggregation behavior of (acetylated) α S is found in ThT assays. When further increasing the charge density above 50% negatively charged lipids, NMR data show first a partial (75% POPG, fig. 2.17a-d, dark blue) and then a full (100% POPG, fig. 2.17a-d, purple) signal attenuation of the NAC region. This correlates well with a slight inhibitory effect of the 75% charged NDs on α S aggregation (fig. 2.17f,g, dark

blue) and a very strong inhibitory effect of 100% charged NDs (fig. 2.17f,g, purple). Our data strongly suggest that for the tested conditions (high anionic lipid content and high lipid-to- α S ratios) membrane association of the NAC region seems to be the dominant factor for protecting α S from aggregation.

Nanodisc-bound State of α S is Predominantly α -Helical

It is worth noting that the NMR results described above mainly refer to the decrease in peak intensity as a reporter for interactions, which is in line with the effects seen before using SUVs [242]. While it is clear that SUVs have particle sizes (associated with slow tumbling rates) well above the detection limit of conventional solution NMR techniques, the smaller size of the ND system should, in principle, allow detection of NMR signals, as has been reported before for several ND-bound or ND-integrated proteins [253]. Nonetheless, neither the usage of Transverse Relaxation Optimized Spectroscopy (TROSY) [264] with increased signal accumulation (i.e. 10-fold longer as for spectra shown in fig. 2.17a-b) nor the measurement at increased temperatures (35 °C) and the usage of an NMR-optimized smaller membrane scaffold protein (MSP1D1 Δ H5) [258] forming NDs of smaller size and higher tumbling rates, resulted in appearance of a new set of peaks indicative for the bound state (and the presence of slow exchange processes) or a collective shift of peaks indicative of fast on-off exchange processes (see e.g. Supplementary Figure 2.24). In theory, three effects may explain this observation and obstruct detection of the ND-bound residues of α S: (i) the bound-to-free exchange rate is in the order of the NMR time scale (so-called intermediate exchange), (ii) the presence of a non-negligible part of α S protruding out of the ND (namely at least residues 98-140), slowing down molecular tumbling and increasing relaxation leading to line broadening beyond the detection limit, and/or (iii) membrane-bound α S shows a significant amount of plasticity leading to inhomogeneous broadening of the NMR lines.

While intermediate exchange can be largely ruled out due to the observed binding kinetics (vide infra, fig. 2.20a-b, t_{on} and t_{off} of around 4 μ s and 65 s, respectively) it is at this point difficult to further distinguish between slower tumbling and molecular plasticity (or a combination thereof) that interfere with solution NMR detection of the bound conformation. In order to still gain insight into the conformation of α S bound to NDs, we used magic angle spinning (MAS) solid-state NMR which is not subject to size effects. Moreover, we took advantage of the very low temperatures (100 K) used in Dynamic Nuclear Polarization (DNP) to additionally eliminate exchange processes, as well as to increase the sensitivity of the experiment. To avoid problems of signal overlap arising from severe inhomogeneous line broadening often seen in this range of temperatures [265], we used a sparse isotope labelling scheme [266], leading to the simplification of ^{13}C - ^{13}C spectra to secondary structure sensitive $\text{C}\alpha$ - $\text{C}\beta$ cross-correlations of valines (and leucine $\text{C}\beta$ - $\text{C}\gamma$). Notably according to the α S primary sequence (fig. 2.18, top) and our solution NMR observations (fig. 2.17a-b), 95% of the valine residues (i.e. 18 out of the 19) should be membrane-bound at the used charge content and α S-to-ND ratio.

While in the absence of NDs the DNP ^{13}C - ^{13}C spectrum (fig. 2.18, black) shows a continuous distribution of the Valine C α -C β cross peaks reflecting the carbon chemical shifts of the allowed Ramachandran space (expected for an intrinsically disordered protein such as αS), a very strong peak shift to a defined chemical shift range typical for α -helical structure is visible after addition of NDs (fig. 2.18b, red). The DNP data thus show that αS binds the ND lipid surface in α -helical conformation corroborating previous studies using CD and vesicles, solution NMR and detergents micelles and solid-state NMR and SUVs [102, 107, 246].

Membrane Plasticity and αS -membrane Interaction: A Two-way Street?

While Figure 2.17 shows the effect of gradually increasing the level of POPG in DMPC lipids it should be noted that both lipids do not only differ in their head group charge but also in their hydrocarbon chain length and number of unsaturated bonds, i.e. 16:0-18:1 PG and 14:0 PC for POPG and DMPC, respectively (nomenclature refers to 'number of carbons in the fatty acid': 'number of unsaturations'). Both of these features will affect the fluidity and phase transition temperature T_m of the lipid bilayer. In general, native membranes are heterogeneous mixtures of numerous different lipids and proteins, both of which can strongly influence lipid phase properties. In this respect it was also suggested before that the MSP-lipid interactions may not only be seen as an artificial border of the bilayer, but may partly mimic protein-lipid interaction occurring in native membranes [267]. While the usage of additional transmembrane proteins is rather restricted due to the limited bilayer area of the NDs, the usage of different heterogeneous lipid mixtures may generate a suitable mimetic for rather heterogeneous physiological membranes.

To further investigate the effect of different lipid properties we recorded additional NMR spectra of αS in the presence of NDs containing different lipids and lipid mixtures. The data recorded with 100% POPC NDs do not show interaction (fig. 2.19a, grey), comparable to 100% DMPC NDs (fig. 2.17a-d, black) and demonstrates that in the absence of negative net charges on the head groups, properties such as an increased chain length and unsaturation, do not induce a significantly stronger interaction. We also used lipid mixtures where charged and uncharged

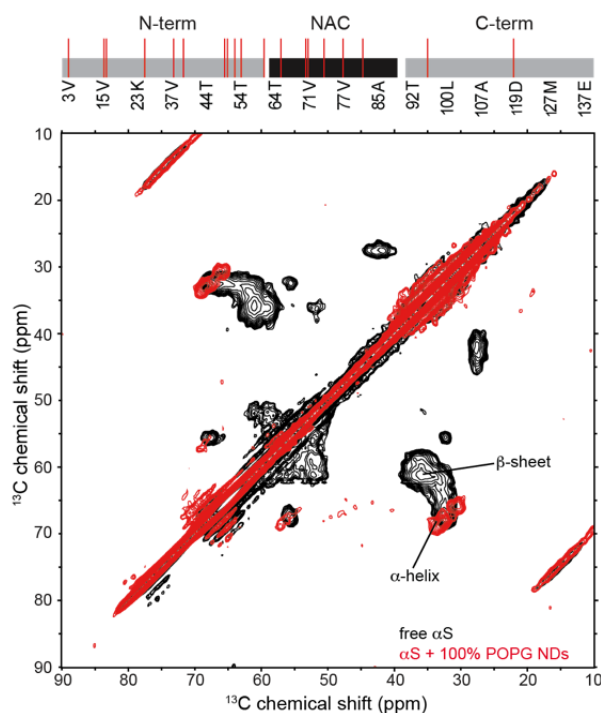


Figure 2.18: Nanodiscs binding induces α -helical structure in αS . [^{13}C - ^{13}C]-Proton Driven Spin Diffusion MAS-DNP spectra of free αS in frozen solution (black) and when bound to NDs with 100% POPG lipids (red). Selective isotope labelling was used to specifically monitor Valine C α -C β chemical shift distribution. Peaks position indicative of the β -sheet and α -helical secondary structure are labelled. Occurrence of Valine residues in the αS sequence is shown on top (18 out of 19 Valines are present in the expected binding site of the used ND).

2.3 Interaction of α -Synuclein with Lipid Bilayer Nanodiscs

lipids have the same fatty acid chains (i.e. POPC/POPG and DMPG/DMPC) or mixtures where the position of negative charge and hydrocarbon chain is swapped (i.e. DMPG/POPC vs. POPG/DMPC). In these mixtures, we kept the overall net charge content constant at 50%. Our data show that the heterogeneous mixtures DMPG/POPC and POPG/DMPC behave very similarly (fig. 2.19a, turquoise and dark blue, respectively) suggesting that the position of charge with respect to chain length and unsaturation is not critical in the tested conditions. Also, when using a more homogenous mix of POPG/POPC, a similar pattern is found (fig. 2.19a, yellow), suggesting that ‘surface roughness’ of the membrane, as potentially introduced by the heterogeneous lipid chain lengths, does not significantly change the α S-membrane interaction.

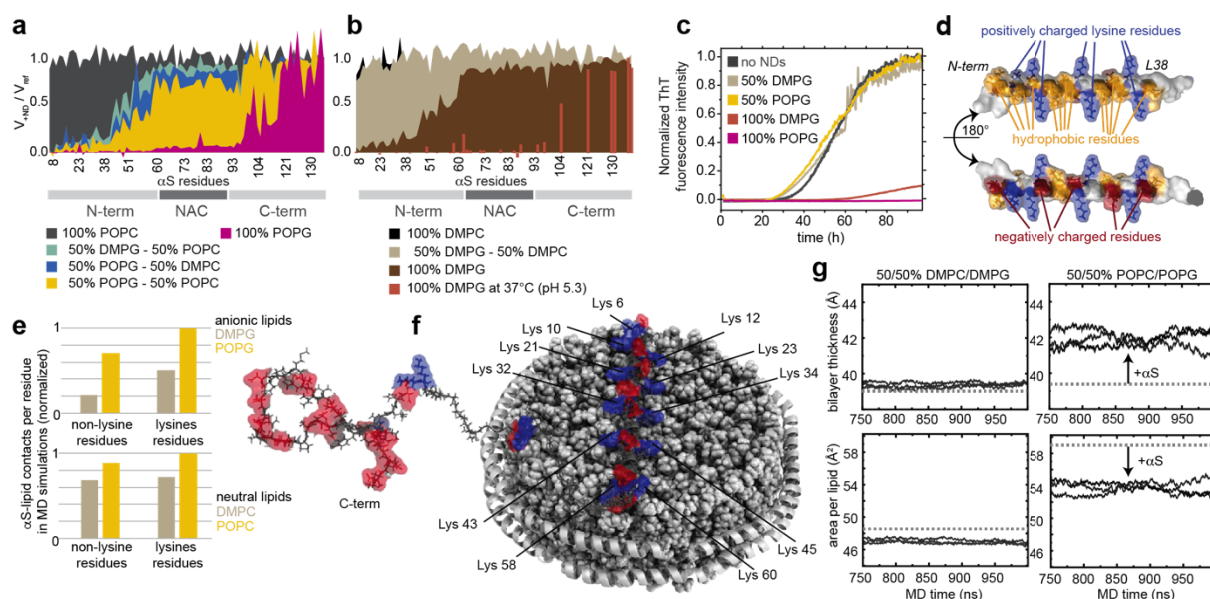


Figure 2.19: α S-lipid interaction is favored by, and potentially modulates, membrane plasticity. α S NMR attenuation profiles in the presence of NDs with indicated lipid composition (molar ratio 2:1, α S-to-NDs) for bilayers that are in a more fluid (a) or gel phase (b) at 10 °C. Note that all NMR data, except the indicated 100% DMPG measurement (b, red bars), are recorded at 10 °C. (c) Corresponding ThT aggregation assays for selected conditions (color code as in (a,b), for better visibility only the mean values of triplicate measurements are shown). (d) α S structural model of key lipid binding mode (see text for more details). Periodically and symmetrically appearing lysine residues (blue) form a positively charged ‘grid’. (e) α S-to-lipid contacts (<0.4 nm) per residue as occurring during the time course of MD simulations. Normalized values for interactions of either lysine or all other residues with anionic lipids (upper diagram) or neutral lipids (lower diagram) for gel/fluid-phase membranes (beige/yellow bars) are shown, respectively. (f) Model of α S-ND interaction, lysine (blue) and negatively charged residues (red) are highlighted. (g) Effect of α S interaction in MD simulations on the two different membrane systems. Bilayer thickness (upper panels) and area per lipid (lower panels) in the presence (solid lines, three independent simulations) and in the absence of α S (dashed line, one simulation) are shown.

Interestingly, when using a homogeneous mix with fully saturated lipids (DMPC/DMPG), albeit having the same net charge content of 50%, a very different pattern in line with no significant interaction with α S, is visible (fig. 2.19b, beige). Notably, at the temperature of the NMR experiments (10 °C) the bilayer formed by DM-lipids is in the gel phase (T_m around 28 °C,

Supplementary Figure 2.23d). This data is in line with previous data on SUVs that identified an important role of the lipid phase for α S-lipid interaction [108]. When increasing the charge content to 100%, but remaining in the gel phase (100% DMPG, fig. 2.19b, brown) the first 60 residues of α S show a clear interaction with the membrane resembling a binding mode that is found for 50% charge content in the fluid phase (e.g. fig. 2.19a, yellow). While increasing the temperature for the NMR measurements above T_m leads to a previously observed loss of NMR signals due to amide-water exchange processes for most residues relevant for the interaction (Supplementary Figure 2.24c-d), lowering the pH from 7.4 to 5.3 (Supplementary Figure 2.24e-f) can counter this effect and allows to confirm that when measuring the interactions to DMPG lipids in the fluid phase, a much larger binding interface is found (fig. 2.19b, brown-red), comparable to the binding mode found for 100% POPG (fig. 2.19a, purple). Consequently, when the lipid charge density is high enough, the lipid phase state and related bilayer fluidity in a stable planar bilayer plays an important role in α S association. Taken together, these data on α S-lipid association can be summarized as follows: (i) unsaturations in the hydrocarbon chains, leading to increased membrane fluidity, are not sufficient to induce binding, (ii) the presence of heterogeneity in fatty acid chains and the combination of charge and unsaturation on the same lipid molecule are not critical and (iii) in addition to charge, a lipid phase state that introduces an increased membrane fluidity is important for binding.

We also performed ThT aggregation assays with NDs containing selected lipid mixtures as investigated by NMR, again under conditions in which spontaneous aggregation of α S is observed in the absence of lipids. All mixtures that contain 50% negatively charged lipids, independently of tail heterogeneity or charge position show consistently unaffected aggregation behavior (fig. 2.19c). However, α S aggregation is drastically impeded in the presence of 100% DMPG NDs (fig. 2.19d, red-brown). Since aggregation assays were measured at 37 °C (i.e. above the DMPG phase transition) this is well in line with the corresponding NMR attenuation profile (fig. 2.19c, red-brown) suggesting that under this conditions α S is in a lipid binding mode that involves the NAC region and thus inhibits aggregation.

From the evaluation of the different membrane interaction modes of α S with NDs observed in this study, it is clear that in particular the initial about 38 residues comprise a central lipid binding motif. Based on previously reported solid-state NMR data [246] and CD data [106, 107] of vesicle preparations as well as the DNP solid-state NMR data of α S in the presence of NDs that we report here, it is also clear that the lipid interacting residues of α S form a helical secondary structure. Analysis of the primary sequence and secondary structure of this interacting region highlights key features of its architecture which is highly suitable for interactions with charged lipid (bi)layers (fig. 2.19d) [99]. These features include the very exposed and symmetric distribution of positively charged lysine side chains (fig. 2.19d, blue), the occurrence of hydrophobic residues on one side of the helix (fig. 2.19d, yellow) and the distribution of negative charges on the opposite side (fig. 2.19d, red). Based on this architecture it is tempting to speculate that the positively charged residues will interact with negatively charged lipid head groups, the hydrophobic residues will be oriented towards the hydrophobic lipid chains and the negatively charged residues will be oriented towards the solvent (and compensate the net charge of the

protein). Noteworthy these protein features are again found in the next binding region (residue 39-60). In this picture, it would be likely that the lipids as well as the lysine side chains (partly) rearrange, from their 'unbound' conformation, to ideally accommodate electrostatic interactions in the bound conformation. This rearrangement may be favored by a more fluid lipid phase, which would explain the lower interaction found for NDs with DMPG lipids below the phase transition.

To test this hypothesis, we performed molecular dynamics (MD) simulations of α S-membrane interactions. Our simulations focus on the first 61 residues of α S and its interactions with membranes formed by a mixture of either 50% POPG - 50% POPC lipids in the fluid phase or a 50% DMPG - 50% DMPC mix in the gel phase (see methods for more details). Indeed, the MD data confirm that the lysine residues play a key role in the membrane interaction, as e.g. visible by promoting considerably more contacts to anionic lipids than other residues during the time course of the simulations (fig. 2.19e, upper diagram). Additionally, the MD data also show a generally stronger interaction of α S with the anionic lipids in the fluid membranes (POPG) as compared to the gel-phase membranes (DMPG) (fig. 2.19e, yellow vs. beige). Noteworthy, these effects are much less pronounced for contacts to the neutral lipids (fig. 2.19e, lower diagram). These findings correlate well with the effects of lipid charge and membrane plasticity seen in the NMR and aggregation assays.

Interestingly the MD data also report on the effect of α S interaction from the lipid point of view. According to this data, the already well ordered DMPC/PG-lipids (gel phase) experience only very small effects due to the presence of α S. On the other hand, the less ordered POPC/PG-lipids (fluid phase) are strongly affected. Here the presence of α S induces a considerably more ordered lipid state as evident by an increased bilayer thickness, reduced surface area per lipid and increased order parameters for the hydrocarbon chains (fig. 2.19g and Supplementary Figure 2.25). Generally, the MD data suggest that α S-membrane interaction is (initially) facilitated by increased membrane plasticity (e.g. more contacts for fluid phase). The increased plasticity may facilitate reorientations of the lipids to support favorable interactions with α S. This view is supported by our MD data showing significantly higher occurrence of short lysine-lipid distances, which would allow lipid-mediated salt bridges, in the simulations with more fluid membranes (see Supplementary Figure 2.25). These interactions may consequently confine lipids and lead to a reduced membrane plasticity. The latter is in line with recent experimental data showing that α S binding can increase lipid packing [268], an effect that has also been suggested to play a role in α S function as chaperone for SNARE-mediated vesicle fusion [93].

NDs Can Simultaneously Interact With Multiple α S Proteins Facilitating Formation of Aggregation Seeds

While our NMR data clearly reveal binding modes with different contributions of the α S primary sequence, we were also interested in the overall affinity of the protein for NDs. We therefore measured interaction kinetics using bio-layer interferometry (BLI) with immobilized NDs of

different charge content. In line with the NMR data, no α S binding was detected when NDs containing 100% DMPC were immobilized (data not shown).

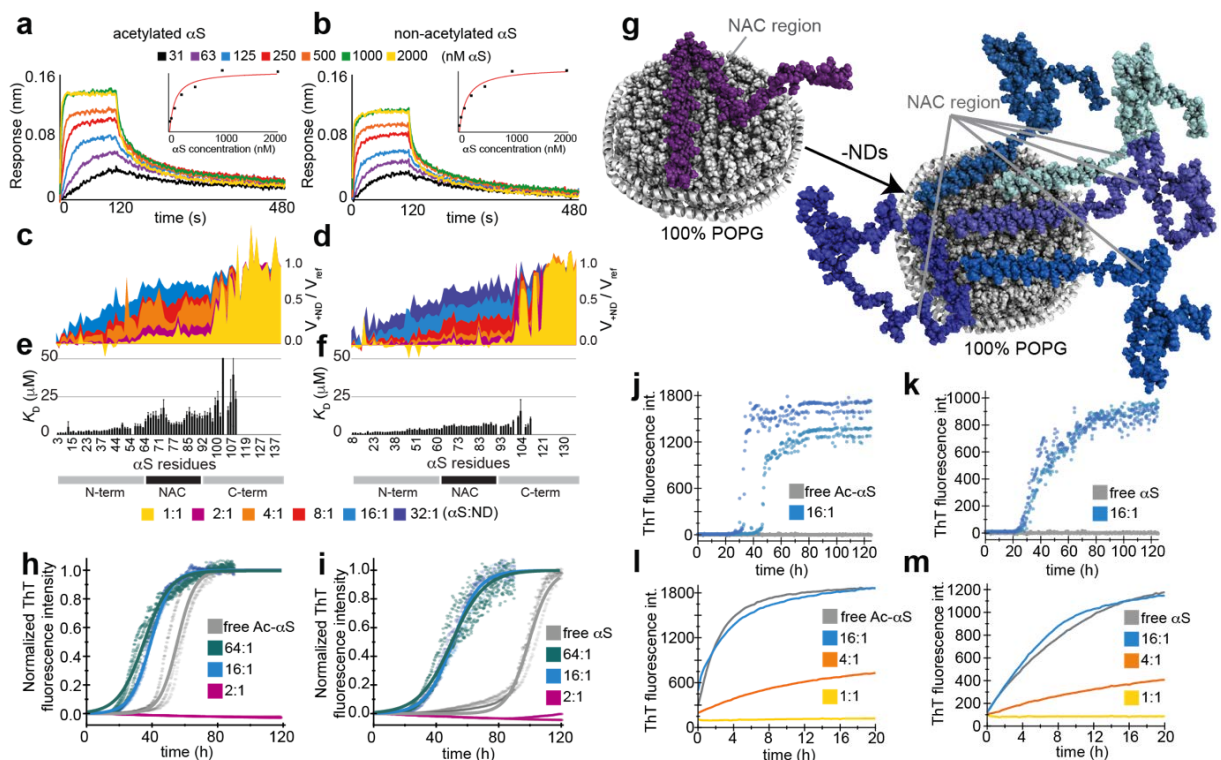


Figure 2.20: Limited but highly charged lipid surface area can induce an α S binding mode capable of promoting aggregation through induction of primary nucleation. BLI sensorgrams using 100% POPG immobilized NDs and acetylated α S (a) or non-acetylated α S (b) in different concentrations ranging from 31 (black) to 2000 nM (yellow). Corresponding steady-state response plots are shown as inserts. The extracted global affinities (K_D) are about 60 and 100 nM, respectively. NMR attenuation profiles of a titration of 50 μ M acetylated (c) or non-acetylated (d) α S with varying concentrations of 100% POPG NDs (α S-to-NDs molar ratios ranging from 32:1 to 1:1, see color code). (e,f) Corresponding residue-specific affinities (K_D) extracted from NMR titration data shown in (c,d), respectively. (g) Model of different α S-lipid binding modes in the presence of excess (upper picture) or limited amount (lower picture) of highly charged NDs (for simplicity only one side of the bilayer is occupied by α S). (h,i) Normalized ThT fluorescence kinetic curves for selected α S-to-ND ratios for acetylated (h) and non-acetylated (i) α S. While high amount of NDs (upper binding mode in g) inhibit aggregation, limited amount of highly charged membrane surface (lower binding mode in g) enhances aggregation. (j,k) Normalized kinetic data in quiescent conditions and absence of preformed seeds at pH 5.3 for acetylated (j) or non-acetylated (k) α S. While under these conditions no aggregation (nucleation) is observed in the absence of NDs (grey) the presence of 16:1 molar ratio of 100% POPG NDs (lower binding mode in g) induces primary nucleation. (l,m) Raw data of quiescent ThT fluorescence aggregation assay in the presence of 2.5% preformed seeds for acetylated (l) or non-acetylated (m) α S for different molar ratios (see color code) of 100% POPG NDs.

In the case where NDs with 100% anionic lipid content were immobilized, a clear response upon addition of different α S concentrations was observed (fig. 2.20a,b) and dissociation constants K_D in the order of 60 nM to 100 nM (one α S to one ND) were calculated. In addition, kinetic information could be extracted which shows a tight binding with a fast association and a slow off-rate of approximately 10^{-2} s^{-1} .

In order to obtain residue-specific insights into the membrane affinity of α S, we additionally conducted NMR titration experiments using 100% negatively charged NDs (fig. 2.20c-f). In general, dissociation constants can be extracted from NMR titrations attenuation profiles by fitting the concentration dependency of the attenuation with a single exponential decay for each resolved peak (corresponding to one assigned residue) (fig. 2.20e-f). Our data reveal differential membrane affinities for different regions of the α S primary sequence. The regions with differential affinities largely overlap with the regions of the different binding modes identified before, i.e. four distinct regions of decreasing affinity range (1-38, 39-60, 61-98, 99-140).

Importantly, it appears that one ND with 100% negatively charged lipids can simultaneously interact with up to 16 α S molecules (8 per bilayer side) in the course of the NMR time scale, as seen from the almost complete disappearance of the signals of the very N-terminal residues (fig. 2.20e-f, light blue). Moreover, while these first residues are interacting with the membrane, independently of the number of α S molecules bound to one ND, the binding of the NAC region is strongly modulated by the number of bound α S molecules. This suggests that, due to the higher lipid affinity of the N-terminal region as compared to the NAC region, the free energy of the system is minimized by favoring N-terminal interactions in cases where the accessible membrane surface is limited. Note that due to the geometry of the used nanodiscs up to five α S molecules can simultaneously bind with a 38-residue long α -helix (first binding mode) to one side of one ND. If 8 molecules are accommodated together on the surface, (on average) a 23-residue long helix per monomer could be formed.

To characterize the effect of the accessible membrane surface area (as given by the α S-to-ND ratio) and the resulting stoichiometry on α S aggregation behavior, we measured ThT aggregation kinetics on samples with different α S-to-ND ratios ranging from 2:1 to 64:1 by varying the ND concentration at constant α S concentrations (fig. 2.20h-i). Interestingly, a higher ratio of α S-to-ND leads to a prominent decrease in aggregation lag-times when using 100% POPG NDs (fig. 2.20h,i, blue and cyan). These data show, in line with previously reported behavior on SUVs [107, 133, 249], that under specific conditions lipid bilayers can accelerate the fibrillation process. Here, these conditions represent a limited membrane surface area with a high charge density. According to our NMR data this will introduce an α S-lipid binding mode that brings several α S molecules with exposed NAC regions in close proximity. Noteworthy, unlike in the case of SUVs [107], AFM images of α S fibrils formed in the absence or presence of NDs do not show different morphology (data not shown).

We additionally carried out the same BLI measurements, NMR titrations and ThT assays for ND containing only 50% POPG lipids. For these NDs no clear signature of binding could be obtained in the BLI measurements (data not shown), suggesting a weak affinity and/or too fast off rates to allow detection via BLI. This is in line with size exclusion chromatography (SEC) profiles that also point to a more transient interaction (Supplementary Figure 2.23b,c). NMR titrations, however, show clear concentration dependent attenuation profiles that allow the calculation of residue specific affinities (fig. 2.21a-d). Noteworthy, the affinities for the α S residues in the first binding region (residues 1-38) are comparable to the values obtained for 100% charged NDs (fig. 2.20e-f). In contrast, for the following binding regions much lower

affinities are found (at the edge of detection for residues 39-60, and no interaction for residues >60), including the absence of interactions of the NAC region.

In line with an exposed NAC region the ThT data for NDs with 50% negatively charged lipids at low α S-to-ND ratios are consistently showing no effect on aggregation half-times. The data at higher ratios are less reproducible and show a slight tendency to prolonged half-times (fig. 2.21e-f). At this point, it is not clear whether this feature has mechanistic relevance or is just an artefact caused by the limited reproducibility of this condition.

The Molecular, Thermodynamic and Kinetic Determinants of Membrane-modulated α S Aggregation

It has recently been shown in a systematic study that under appropriate conditions, which minimize the intrinsic nucleation rate (quiescent conditions and protein repellent plate surfaces), lipid bilayers in the form of small unilamellar vesicles can largely accelerate the nucleation of α S amyloid fibrils [107]. In order to determine whether NDs can have a similarly accelerating effect, we performed ThT aggregation experiments under similar conditions, i.e. where no α S aggregation should be detected in the absence of lipids (see methods for more details). These experiments were performed at mildly acidic pH (5.3), as it was recently shown that under these conditions, α S amyloid fibrils can amplify autocatalytically through surface-catalyzed secondary nucleation [138,269]. This should in principle enable even very low primary nucleation rates to be detected through autocatalytic amplification. Membrane binding behavior of α S at these buffer conditions was also checked by NMR for 100% POPG NDs and comprises the same region (residues 1-96 at low α S-to-ND ratios) as seen for neutral pH (see Supplementary Figure 2.24c,d).

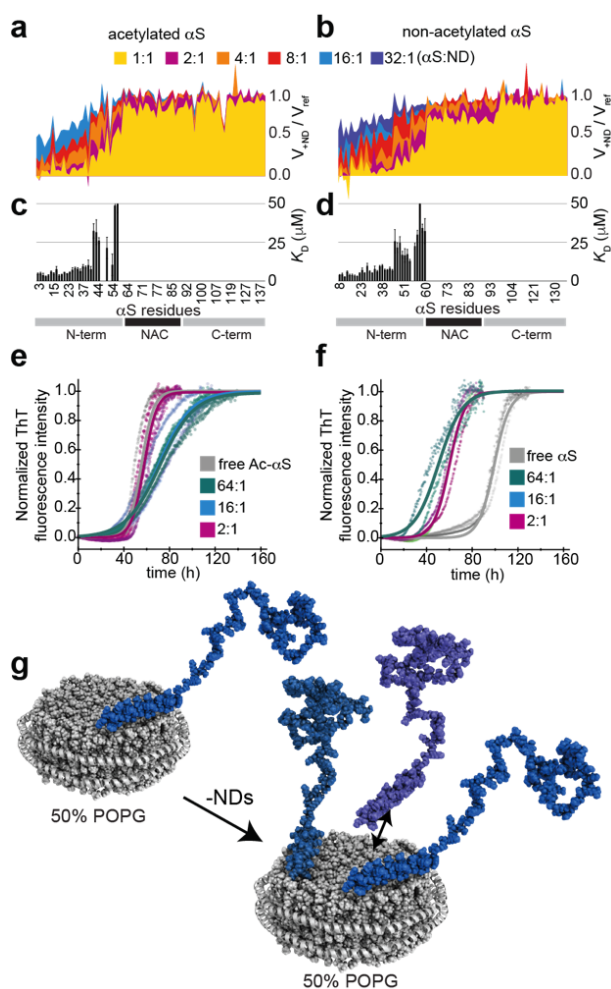


Figure 2.21: Moderately charged membrane surfaces interact more transiently with α S and do not induce primary nucleation. NMR attenuation profiles of a titration of 50 μ M acetylated (a) or non-acetylated (b) α S with varying concentrations of 50% POPG NDs (α S-to-NDs molar ratios ranging from 32:1 to 1:1, see color code). (c,d) Corresponding residue-specific affinities (K_D) extracted from NMR titration data shown in (a,b), respectively. (e,f) Normalized ThT fluorescence kinetic curves for selected α S-to-ND ratios for acetylated (e) and non-acetylated (f) α S. (g) Model of α S-lipid binding modes in the presence of excess (upper picture) or limited amount (lower picture) of moderately charged NDs (for simplicity only one side of the bilayer is occupied by α S).

As expected, the ThT assay under the quiescent conditions does not show any aggregation in the absence of NDs (fig. 2.20j,k, grey). However, the samples with 100% POPG NDs (in a α S-to-ND ratio of 16:1) do display aggregation, indicating that this type of membrane is indeed enhancing primary nucleation to a degree sufficient that the subsequent secondary nucleation leads to detectable quantities of amyloid fibrils (fig. 2.20j,k, blue). Interestingly, since our data also allow an estimation of the total number of α S monomers that are brought in close proximity due to their interaction with the same ND, this result may also provide a first approximation of the number of α S monomers needed for the formation of a nucleus. Our data suggest that this 'minimal critical nucleation number' has an upper limit of around 8 α S molecules.

In order to further disentangle the effect of NDs on the various individual steps in the α S aggregation pathway, we next designed strongly seeded aggregation assays under quiescent conditions at neutral pH, where fibril elongation is the only process that occurs at a significant rate. Seeding experiments carried out in the presence of 100% charged (POPG) NDs show a clear reduction in elongation rate with increasing ND concentration (fig. 2.20l,m). While at high molar excess of α S (16:1, α S-to-ND), according to our NMR data, nearly all α S monomers should interact through their most N-terminal regions with the NDs, no significant effect on the elongation rate was observed (fig. 2.20l,m, blue). At molar ratios of 4:1 (fig. 2.20l,m, orange) a decrease in elongation is observed, however at this ratio our NMR data clearly indicate that all α S monomers are interacting with the NDs. Nevertheless, in both cases (molar ratios of 16:1 and 4:1) larger fractions of the monomer population should still have accessible NAC regions, which may explain their ability to participate in the fibril elongation process. However, the limited interaction surface may also influence the dynamic nature of membrane association leading to a certain population of free monomeric α S at any given time.

Unlike for 100% POPG NDs (fig. 2.20j-l) and in line with the previously discussed moderate effects of 50% POPG NDs on the overall aggregation process (fig. 2.17f,g, blue, fig. 2.19d, yellow and beige, fig. 2.21e,f), we did not observe accelerated α S nucleation in the presence of NDs with 50% POPG nor a clear perturbation of fibril elongation in seeded experiments (see Supplementary Figure 2.26 for data and a more detailed discussion).

N-terminal Acetylation Has Moderate Effect on Membrane Association and Leads to Different Behavior in Aggregation Assays

As visible in Figure 2.17, Figure 2.19, Figure 2.20, and Figure 2.21, in addition to using the N-terminally acetylated form of α S, which represents the native post-translational modification of α S and is known to be relevant for membrane association [98, 240], we also recorded most experiments with the non-acetylated form of α S. In line with previous findings [270], N-terminal acetylation leads to clear chemical shift perturbations in the NMR spectra for the first 10 residues of α S (fig. 2.17a,b).

Overall, most of the above discussed features of α S membrane interaction are rather similar in acetylated and non-acetylated α S, however there are a number of distinct differences. For instance, the peaks which are already shifted in free α S due to the acetylation are also the

ones that are affected most by the presence of nanodiscs with low amount of charges (close to physiological concentration). Our data (fig. 2.17a-d) show a rather small but significant increase in the membrane association of the first 15 residues due to the N-terminal acetylation, which is in line with previous observation using SUVs [241, 271]. α S acetylation is known to increase N-terminal helix propensity [270, 272], which may facilitate formation of the initial binding mode and be of significance for naturally occurring processes.

A similar effect is also seen for the global binding as determined by BLI, which shows a (slightly) higher membrane affinity of the acetylated (fig. 2.20a, K_D of 60 nM) as for the non-acetylated α S construct (fig. 2.20b, K_D of 100 nM). When looking deeper into the NMR titration data, it appears that another effect takes place, namely a slightly increased membrane affinity of the NAC region for the non-acetylated α S NAC region (fig. 2.20e vs. f and fig. 2.21c vs. d). At current stage, it is not easy to explain why a modification at the N-terminus will affect the lipid interaction of a protein region that is sequentially separated by roughly 60 residues. Such a behavior could however either be related to intermolecular interactions and/or long range intramolecular interactions (in a 'horseshoe'-conformation) that may or may not be artificially introduced by the limited surface area of the NDs.

Strikingly, the reference kinetic curve of non-acetylated α S reproducibly shows under the applied conditions a strongly delayed aggregation as compared to the acetylated reference. In the setup used, primary nucleation processes are likely to happen at the air-water or plate-water interface [262, 263], thus a lower hydrophobic propensity of non-acetylated α S could explain this effect. While this may be the dominant process in the absence of lipids, it may not be the case anymore in the presence of NDs [107], either because NDs shield these interfaces or because nucleation happens primarily at the membrane surface. The much lower differences due to acetylation state in the presence of NDs fit this explanation, as well as additional tests we ran using different types of plates (data not shown). Higher order processes, namely different fragmentation behaviors, can however not be excluded.

It appears that the biggest effect of acetylation is related to assay parameters that are normally not the matter of interest, which nevertheless may be important for future studies [260]. Still the results from systematic measurement of the effects of N-terminal acetylation via different methods point to subtle changes in membrane interaction in respect to NAC region specific affinities at high lipid charge densities as well as to N-terminal binding at a lipid charge density comparable with the overall composition found for membranes in e.g. synaptic vesicles [246]. Hence, both effects may be of particular importance under physiological conditions.

2.3.5 Conclusion

Overall our data demonstrate that the nanodisc system allows to study the interaction of α S with stable, planar membranes in a quantitative and site-resolved way. It also provides insights into the correlation between the identified membrane binding modes as well as binding kinetics and their consequences for α S amyloid fibril formation, both in respect to the nucleation and elongation process.

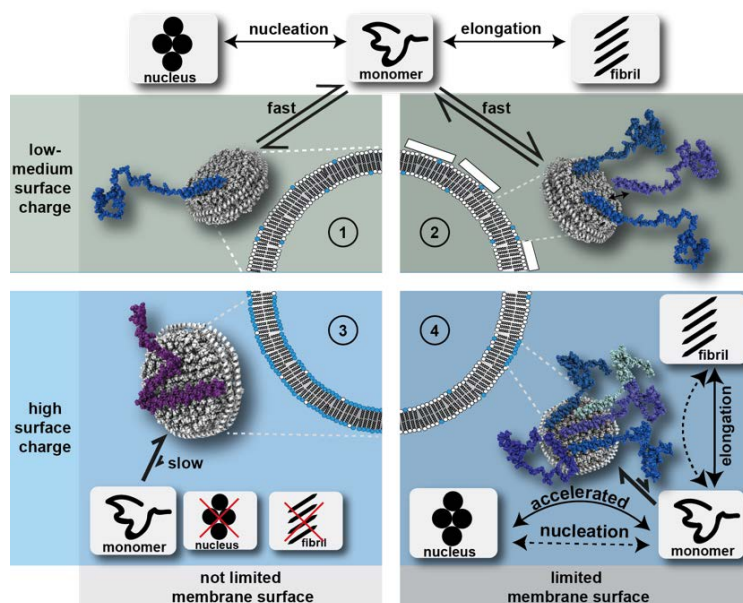


Figure 2.22: Model of the influence of different NDs on the α S aggregation pathways and its potential implication in the context of cell/vesicle membranes. Four scenarios are depicted according to their membrane surface charge and accessibility, respectively. In cases where membranes/NDs with only low charge densities are present (scenario 1 and 2) α S interacts with its N-terminal residues and most likely forms a fast exchanging equilibrium between soluble and membrane associated α S monomers. This equilibrium does not seem to strongly interfere with the slow process of α S nucleation, it may however (slightly) decrease the pool of free monomers available for fibril formation. Notably these conditions are more likely to better resemble the average charge densities found in physiological membranes. However, specific, abnormal and/or stochastic processes may also lead to highly charged membrane surfaces with limited (scenario 4) or not limited surface access (scenario 3). α S will strongly interact with the latter in a binding mode that will largely inhibit both, α S nucleation and fibril elongation. In cases where several α S monomers compete for a limited highly charged membrane surface area (scenario 4), the amyloid fibril nucleation process can be accelerated, most likely due to an α S binding mode that brings exposed NAC regions of several α S monomers in close proximity. Under these conditions the fibril elongation rate is largely unperturbed, probably due to sufficient monomers with limited membrane association and/or due to induction of higher order processes.

In summary, our data show that (i) residue specific α S-membrane affinities are rather similar for the N-terminal α S region for 100% and 50% negatively charged NDs, (ii) for 100% anionic lipids the α S can adopt a substantially expanded binding mode as compared to 50% anionic lipids content, leading to considerably higher global affinities, (iii) the exchange rate between free α S in solution and membrane-bound α S is rather slow in the 100% charged case and likely to be rapid in the 50% case, (iv) region-specific membrane affinities (especially the NAC region) are correlated with aggregation properties, (v) with sufficient excess of lipids and sufficient charge density, NDs can inhibit primary nucleation as well as fibril elongation by sequestering monomers out of solution, (vi) competition of α S monomers for highly charged lipid surface generates a membrane-bound α S conformation that can induce primary nucleation, and (vii) the number of α S monomers that are brought together on one ND and which can promote amyloid fibril nucleation is in the order of 8 α S molecules. [Figure 2.22](#) summarizes these molecular, thermodynamic and kinetic determinants of membrane-modulated α S aggregation.

While our *in vitro* data show strongest effects at lipid charge densities well above the average lipid compositions of native membranes, the membrane composition may vary locally

in physiological membranes. Due to the normally found high lipid diffusion rates, clusters of higher negative charges may form spontaneously and/or be induced by an initially transient α S interaction. For the latter, the N-terminal acetylation may play an important role, since it increases membrane interaction at average native lipid charge densities. Our data suggest that clusters of around 60-80 negatively charged lipids suffice to form a strong interaction (this may however not be the lower limit). Sporadically formed lipid charged clusters could also induce a competition of several α S monomers for the accessible surface area. Our data show that due to the different residue-specific membrane affinities this will generate a binding mode that, once the rather low α S critical oligomerization number is reached, can act as an aggregation seed. Such a scenario could promote the initial step of primary nucleation in the pathogenesis of Parkinson's disease and is in line with recent *in vivo* findings suggesting that shielding α S from membrane interactions can inhibit initial steps of amyloid fibril formation including the formation of cell toxic species [273].

2.3.6 Methods

α S and N-terminally Acetylated α S Expression and Purification

Codon-optimized α S in the pT7-7 vector was expressed in *E. coli* BL21 DE3. For acetylated α S, the N-terminal acetylation enzyme NatB from *Schizosaccharomyces pombe* was coexpressed in a second vector, pNatB [274]. pNatB (pACYCduet-naa20-naa25) was a gift from Dan Mulvihill (Addgene plasmid # 53613). Expression was conducted in 50 mM phosphate-buffered 2YT-medium (pH 7.2) with 0.4% glycerol and 2 mM MgCl₂, protein production was induced at OD 1-1.2 with 1 mM IPTG and run for 4 h at 37 °C. For ¹⁵N-labelled protein, α S or acetylated α S was expressed in M9 medium with 0.2% ¹⁵NH₄Cl.

Sparsely labelled α S for DNP experiments was non-acetylated, expression was done in a similar way, in M9 medium using 0.4% [2-¹³C]-glucose and 0.2% ¹⁵NH₄Cl. Isotope labelling of Phe, Gln, Glu, Pro, Asn, Asp, Met, Thr, Lys, and Ile was suppressed by supplementing sufficient quantities (150 μ g ml⁻¹ of each) of these unlabeled amino acids in the expression media as reported previously [266].

Purification of α S or acetylated α S was carried out as previously described [140], some changes to the original protocol have been made. Except for sparse labelled α S for which previous lysis in 20 mM Tris-HCl pH 8.0, 1 mM EDTA was done, cell lysis and release of α S or acetylated α S was performed by directly boiling the frozen cell pellet at 95 °C in a threefold volume of 20 mM sodium phosphate buffer, pH 7.4, for 30 min. Thermostable α S or acetylated α S remained in the supernatant after 30 min of centrifugation at 15 000 g and 4 °C and was subsequently subjected to an ammonium sulfate precipitation by slowly adding saturated ammonium sulfate solution to 50% saturation at 4 °C. Precipitated protein was pelleted at 15 000 g and 4 °C, dissolved in 50 ml of 50 mM Tris-HCl pH 8, sterile-filtered and loaded onto an ion exchange chromatography column (HiTrap Q FF, GE Healthcare), where α S or acetylated α S eluted at around 300 ml NaCl in 50 mM Tris-HCl pH 8. Elution fractions containing α S or acetylated α S were subjected to another ammonium sulfate precipitation and finally purified by a SEC run (Superdex 75 10/300, GE Healthcare) in 20 mM sodium phosphate pH 7.4, 50 mM NaCl. N-terminal acetylation of acetyl- α S was checked by HPLC, mass spectrometry, and NMR, proved to be about 95% when coexpressed with NatB.

Membrane Scaffold Proteins Expression and Purification

As reported before [275], *E. coli* BL21 (DE3) were transformed with MSP1D1 or MSP1D1 Δ H5 plasmid DNA in vector pET28a. Cells were grown in LB medium, induced by 1 mM IPTG at an optical density of 0.7 and incubated 5 h to 6 h at 37 °C, then pelleted down. Cells were resuspended in 50 mM Tris-HCl pH 8, 500 mM NaCl (buffer B) supplemented with 6 M GdnHCl and EDTA-free Complete protease inhibitors (Macherey-Nagel) lysed by sonication (Bandelin Sonopuls MS72 probe), centrifuged at 17 000 g for 1 h (Beckman J2-21 rotor JA-20.1) and incubated 1 h with previously equilibrated 2.5 ml Ni-NTA agarose resin/3 L culture (Macherey-Nagel). Column was washed with 4 CV buffer B, 4 CV buffer B supplemented with 1% Triton X-100, 4 CV buffer B + 60 mM Na-cholate, 4 CV buffer B, 4 CV buffer B + 20 mM imidazole. Four fractions of 1 CV were eluted with 250 mM imidazole. The whole process was kept at 4 °C in a cold room. The elution fractions were pooled and dialysed against 100-fold 200 mM Tris-HCl pH 7.5, 100 mM NaCl. N-terminal His-tag was cleaved using TEV protease incubated overnight at 4 °C. Δ His-MSP was separated from MSP by IMAC and concentrated to the desired molarity using a Vivaspin centrifugal device of 10 kDa MWCO.

Nanodiscs Assembly

Nanodiscs were assembled according to established protocols [250]. In short, lipids chloroform stocks were dried under nitrogen flow to obtain a lipid film and stored under vacuum overnight. Δ His-MSP1D1 or MSP1D1 Δ H5 and the appropriate amount of lipids (Avanti Polar Lipids) solubilized in 60 mM Na-cholate were mixed together in 20 mM Tris-HCl pH 7.5, 100 mM NaCl, 5 mM EDTA. The scaffold-to-lipids molar ratio was calculated from geometrical considerations. 20% w/v of previously washed Biobeads SM-2 (Biorad) were added and the mixture incubated at room temperature overnight. The Biobeads were removed by centrifugation and once again 20% w/v were added for an additional 4 h to 5 h. Finally, they were purified by SEC on a HiLoad 16/600 Superdex 200 pg column (GE Healthcare) equilibrated with 20 mM sodium phosphate pH 7.4, 50 mM NaCl using a Äkta pure device at a flow rate of 1 ml min⁻¹. The quality of NDs preparation was check by the SEC chromatogram as well as by DLS (PSS Nicomp). NDs were concentrated to the desired molarity using a Vivaspin centrifugal device of 10 kDa MWCO.

Bio-layer Interferometry (BLI)

NDs were immobilized on the sensor surface of amine reactive biosensors (AG2R) (fortéBIO, PALL Life Science) after EDC/NHS activation to a final level between 1.2 nm to 1.8 nm depending on the NDs type using an Octet RED96 instrument (fortéBIO, PALL Life Science). All biosensors were quenched with 1 M ethanolamine for 3 min. All experiments were carried out in multi cycle kinetics at 25 °C. Association of α S in running buffer (20 mM sodium phosphate pH 7.4, 50 mM NaCl) on NDs and reference biosensors was recorded for 120 s, followed by a dissociation phase of 360 s. Sensorgrams were double referenced using the reference biosensors and a buffer cycle. Steady-state analysis was realized by fitting the α S concentration dependency of the highest response against with a simple 1:1 binding model. After normalization, all on and off curves were fitted against simple exponential build-up or decays and led to similar on- and off-rates.

Solution NMR Spectroscopy

Solution NMR experiments were performed on a Bruker Avance III HD spectrometer operating at 600 MHz ^1H Larmor frequency, equipped with a triple resonance TCI (^1H , ^{13}C , ^{15}N) cryoprobe and shielded z-gradients. If not stated otherwise, all experiments data were recorded at 10 °C with an αS concentration of 50 μM in 20 mM sodium phosphate pH 7.4, 50 mM NaCl, 10% (v/v) $^2\text{H}_2\text{O}$ and ND concentration was set to 25 μM (one αS per membrane leaflet). All [^1H - ^{15}N]-TROSY-HSQC NMR spectra were acquired with 32 scans and 256 indirect increments, processed with TOPSPIN 3.2 (Bruker) and analyzed with CCPN [228]. Peaks were automatically integrated and the ratio of volumes in the presence and absence of NDs plotted against the primary sequence. Outliers as results of peak overlap and/or ambiguities were removed.

ThT Fluorescence Aggregation Assays

50 μM of αS or acetylated αS was mixed with either 25 μM (2:1), 3.125 μM (16:1) or 0.781 μM (64:1) nanodiscs with different lipid mixtures. Assays were conducted in 20 mM sodium phosphate buffer pH 7.4 or 20 mM acetate buffer pH 5.3 with 50 mM NaCl, 0.02% NaN_3 and 10 μM Thioflavin T. Unless otherwise stated, triplicates of 120 μl were pipetted into 96-well half area well plates with non-binding surface (Corning No. 3881, black, clear bottom) containing a glass ball for mixing and incubated at 37 °C for up to 7 days. Orbital shaking at 217 rpm was used for 15 s every 20 min. Thioflavin T fluorescence was excited at 445 nm and measured at 485 nm every 20 min with 15 s of shaking prior to the measurement in a plate reader (Tecan Spark 10M or Tecan infinite M1000PRO).

For the seeded experiments, fibril seeds of αS or acetylated αS were prepared as follows: 300 μl of 100 μM αS or acetylated αS was fibrillated at 37 °C and 800 rpm for 3 days in a 2 ml tube containing a glass ball in a Thermomixer (Eppendorf). The fibril solution was diluted to 50 μM and sonicated with a tip sonicator (Bandelin Sonopuls HD3200, BANDELIN electronic) at 10% power (20 W) for 60 s, with 1 s pulses on and 4 s off in between. Seed solution was diluted 20-fold for the aggregation assays (2.5 μM , 5%).

Kinetic curves were corrected by subtracting the curve of buffer (containing NDs) in the presence of ThT and normalized to highest fluorescence intensity (in line with comparable fibril mass seen in SDS-PAGE after the aggregation assay). The corresponding triplicates are shown as transparent circles in order to visualize the reproducibility of each experiment. In the case of quiescent nucleation and seeded assays no normalization was applied and data were recorded without the presence of glass balls and without plate shaking.

Sodium Dodecylsulfate – Polyacrylamide Gel Electrophoresis (SDS-PAGE)

In order to compare the amounts of soluble and fibrillated αS or acetylated αS in the aggregation samples, 100 μl of each triplicate sample were taken out of the well plate, combined in 1.5 ml tubes and spun down at 20 000 g and 20 °C for 30 min. Supernatants (\sim 290 μl) was removed and pellets were re-suspended in 280 μl buffer and SDS-sample buffer (4-fold) was added. Samples were boiled for 15 min at 98 °C and subsequently 10 μl were loaded onto a 15% SDS-gel together with standards of αS or acetylated αS and nanodiscs.

Dynamic Nuclear Polarization (DNP) NMR Spectroscopy

Magic-angle spinning solid-state DNP experiments were performed on a Bruker Avance III HD spectrometer operating at 600 MHz, equipped with a 395.18 GHz second-harmonic gyrotron and a 3.2 mm ^1H , ^{13}C , ^{15}N triple resonance low-temperature MAS probe. Data were collected at 100 K, 9 kHz MAS speed and 9 W continuous-wave microwave power. The samples were prepared from sparsely labelled non-acetylated αS (250 μg) in the presence or in the absence of 2:1 molar ratio of 100% POPG nanodiscs and filled into 3.2 mm sapphire rotors. Final sample conditions were 15 mM sodium phosphate pH 7.4, 25 mM sodium chloride, 30% $^2\text{H}_2\text{O}$, 60% glycerol- d_6 and 2.5 mM AMUPOL [276]. Two-dimensional [^{13}C - ^{13}C]-Proton-Driven Spin Diffusion (PDS) experiments with 1 s mixing time were performed. ^1H decoupling using SPINAL [228] with a decoupling field of 104 kHz was employed during evolution and detection periods. Both experiments were conducted using 300 t_1 increments with 16 and 48 scans each for αS in the absence and in the presence of nanodiscs, respectively. A recycle delay of 5 s was used in both experiments. Both spectra were processed using Topspin 3.2 (Bruker) using identical parameters with squared and shifted sine bell function (qsine 2.5) for apodization.

Molecular Dynamics Simulations

As starting conformation for the MD simulations, the NMR structure of micelle-bound αS (PDB 1XQ8) was used, considering only the first 61 residues in order to concentrate on the membrane binding region of αS .

The protein was placed either 0.5 nm or 1.5 nm above the membrane surface. A starting orientation with the negatively charged side chains pointing away from the membrane and the lysine side chains being oriented towards the membrane surface was chosen (fig. 2.19d). For modeling the lipid bilayer, membrane patches consisting of POPC/POPG (1:1) or DMPC/DMPG (1:1) involving 512 lipids (256 lipids per leaflet) were built and modeled with Slipids force field parameters [277], while the Amber99sb-ILDN force field [278] was used for αS . Before αS was added, both lipid bilayers were solvated and simulated for 500 ns (POPC/POPG) or 1000 ns (DMPC/DMPG) to obtain relaxed membranes. The protein was then placed above the membrane, the protein-membrane system solvated using the TIP3 water model [279], Na^+ and Cl^- added to neutralize the system and to mimic the Na^+ concentration used in the experiments. After energy minimization and equilibration, MD production runs of 500 ns or 1000 ns length were performed in the NPT ensemble at 10 $^\circ\text{C}$ and 1 bar using the GROMACS 4.6 molecular dynamics package [280]. For the analysis, which was performed using Gromacs and Membrainy tools [281], only the last 250 ns of each production run was used. More details on the simulation procedure, including an overview of the production runs, can be found in the Supplementary Information, table 2.3.

Differential Scanning Calorimetry (DSC)

Samples of approximately 5 μM NDs of different types (and if stated 10 μM αS) were degassed for at least 20 min at 30 $^\circ\text{C}$ and measured in a Microcal VP-DSC instrument (Malvern Instruments). The thermograms were acquired up-scan from 5 $^\circ\text{C}$ to 45 $^\circ\text{C}$ at a scanning rate of 0.5 $^\circ\text{C min}^{-1}$ and corrected by subtracting the thermogram of buffer.

Acknowledgements

The authors acknowledge access to the Jülich-Düsseldorf Biomolecular NMR Center and thank the CSC – IT Center for Science, Finland, for computational resources. Financial support from an Emmy Noether grant of the DFG ET103/2-1 to M.E. and an ERC consolidator grant to W.H. is gratefully acknowledged. T.V. and M.M.W. acknowledge support from the International Graduate School of Protein Science and Technology (iGRASPseed) granted by the Ministry of Innovation, Science and Research of the state North Rhine-Westphalia. This work was supported by the DFG (HE 3243/4-1) and by the Ministry of Innovation, Science and Research within the framework of the NRW Strategieprojekt BioSC (BioSc seed fund). We thank Dr. Aldino Viegas for help with NMR data acquisition and Dr. Céline Galvagnion for fruitful discussions.

Author Contributions

H.H., B.S., D.W., W.H., A.K.B. and M.E. designed the experiments. T.V., M.M.W., H.S., B.U. and C.P. performed the experiments. T.V. and M.M.W. analyzed the data. T.V. and M.E. wrote the manuscript. All authors commented on the manuscript.

2.3.7 Supplement

Contents: Supplementary Figures 2.23-2.26 and Supplementary Tables S1 and S2.

2.3 Interaction of α -Synuclein with Lipid Bilayer Nanodiscs

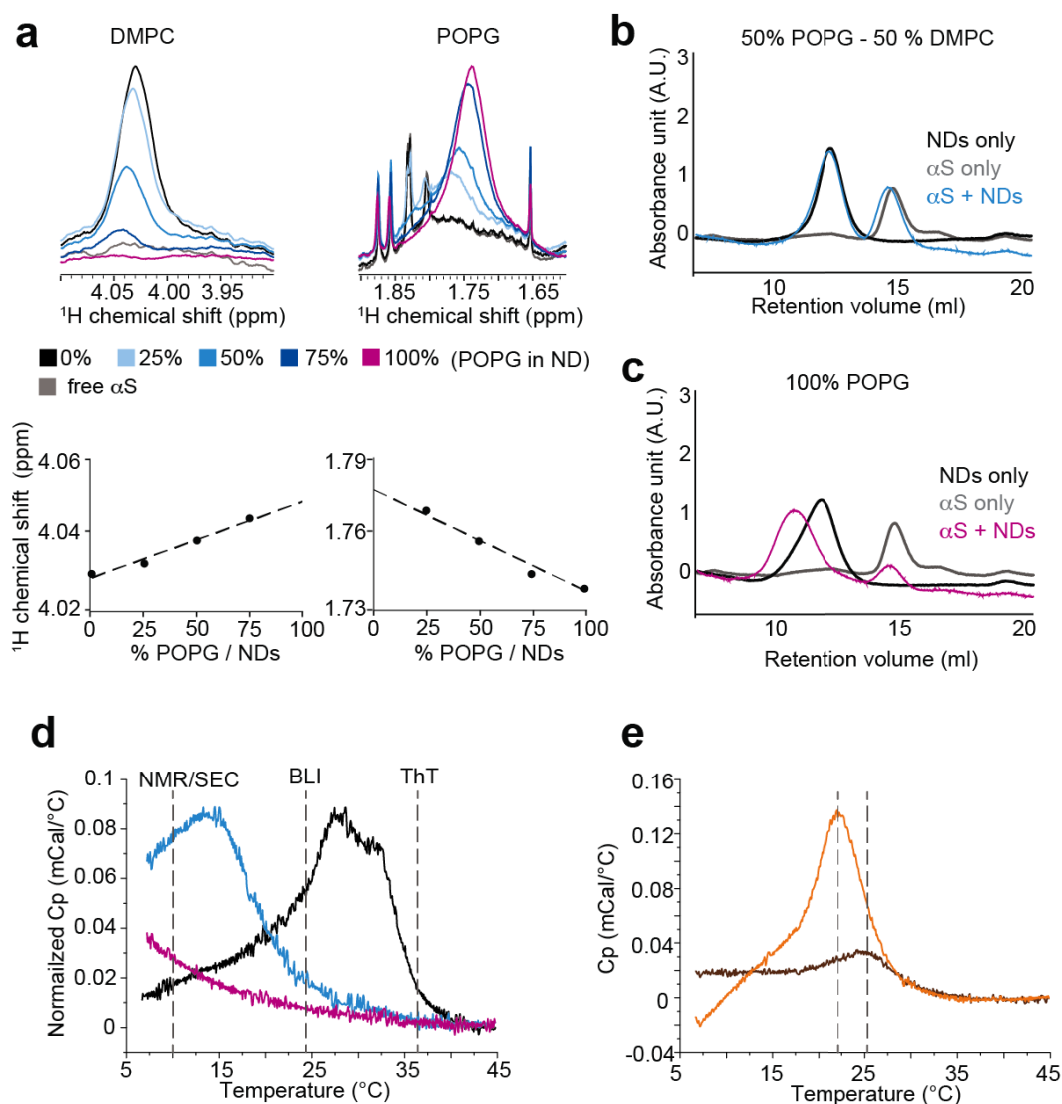


Figure 2.23: Formation of lipid mixtures in NDs, lipid phase transitions and stability of αS association. (a) NMR ^1H -1D spectra of αS in the presence of NDs containing different POPG-to-DMPC ratios corresponding to the samples shown in [fig. 2.17a-b](#). Chemical shifts ranges for signals from either DMPC (left, choline methyl groups) or POPG (right, ^1H next to the unsaturation) are displayed. The volumes of the peaks reflect within an error of approximately 10% the aimed lipid compositions. In addition to volume changes also chemical shifts perturbations for both lipid specific peaks are visible and follow a rather linear dependence on the composition. The NMR data therefore report on both the presence and mixing of both lipid types in single nanodiscs. (b) Size exclusion chromatography (SEC) profiles (Superdex 200 13/300 gl, GE Healthcare) of αS alone (grey), 50% POPG NDs alone (black) and both after mixing (same amounts as in the isolated case) and incubation for 24 h at room temperature (blue). The clear separation of αS from NDs in the mixture points to a fast-kinetic exchange between free and bound αS . The conserved total absorbance additionally confirms the stability of the NDs in the presence of αS . (c) Same as in (b) but using 100% POPG NDs. The SEC profile of the mixture of αS with 100% POPG NDs shows a clear reduction of free αS and a size increase of the ND peak, pointing to a strong interaction between the two components. (d) Differential scanning calorimetry (DSC) thermograms of nanodiscs prepared with either 100% DMPC (black), 100% POPG (purple) or a 50%-50% mixture thereof (blue), showing phase transitions temperatures around 28 $^{\circ}\text{C}$, below 5 $^{\circ}\text{C}$ and 13 $^{\circ}\text{C}$, respectively. Temperatures at which different measurements were performed are highlighted. (e) DSC profile of 100% DMPG NDs in the absence (brown) or presence of αS (orange). While the presence of αS leads to a lower phase transition temperatures of the lipid bilayer, in line with what was reported using SUVs [107], the transition temperature differences is much smaller for NDs ($\Delta T_m = 2.5$ $^{\circ}\text{C}$) as compared to SUVs ($\Delta T_m = 11$ $^{\circ}\text{C}$) in line with a largely increase stability of the NDs.

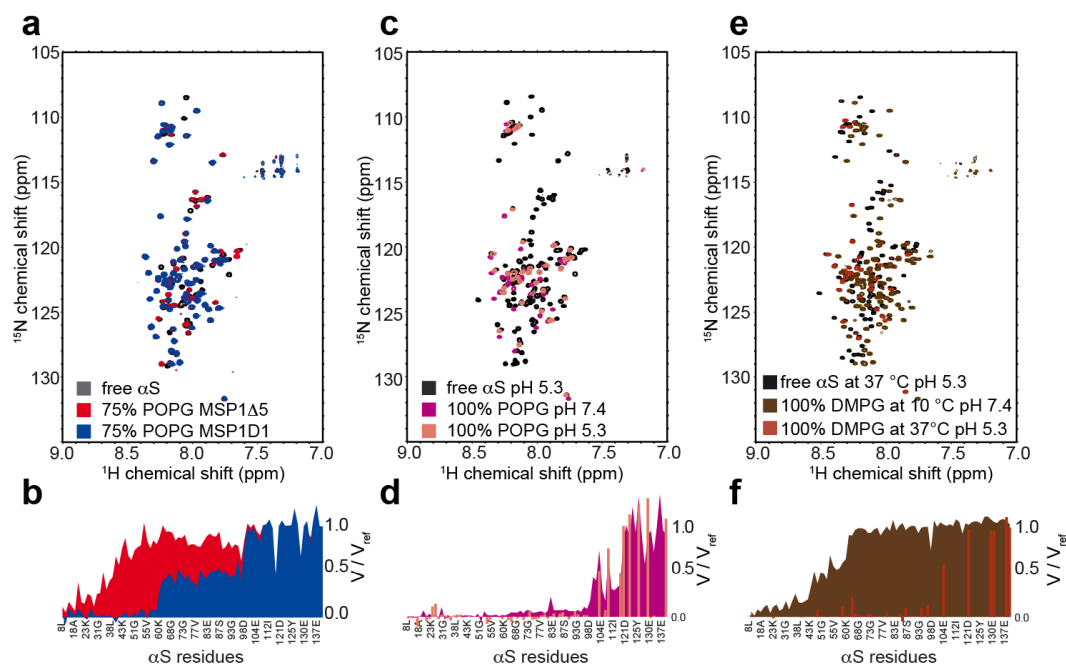


Figure 2.24: αS -ND interactions using different MSP constructs, lower pH and higher temperature. NMR spectra (a) and the respective attenuation profiles (b) of [^{15}N]-acetylated- αS (50 μM) in the absence or in the presence of 25 μM NDs with 75% POPG content, assembled using the regular MSP1D1 construct (blue) or with the smaller MSP1 Δ 5 (red). Spectra (c) and attenuation profiles (d) corresponding to the binding of αS to NDs containing 100% POPG lipids at pH 7.4 (purple) and pH 5.3 (pale orange). Transferable assignments (bars) show that no significant difference in binding mode is visible upon pH variation. Spectra (e) and attenuation profiles (f) corresponding to the binding of αS to NDs containing 100% DMPG lipids in their gel phase (10 $^{\circ}\text{C}$, brown) or their fluid phase (37 $^{\circ}\text{C}$, red). Since normally measurement at 37 $^{\circ}\text{C}$ leads to considerable peak loss of N-terminal αS residues due to water exchange processes, the spectrum was recorded at pH 5.3 (counteracting water exchange). Note that the pH shift alone has no significant effect on binding (see (c) and (d)). Reference spectra of respective free αS are shown in dark grey.

2.3 Interaction of α -Synuclein with Lipid Bilayer Nanodiscs

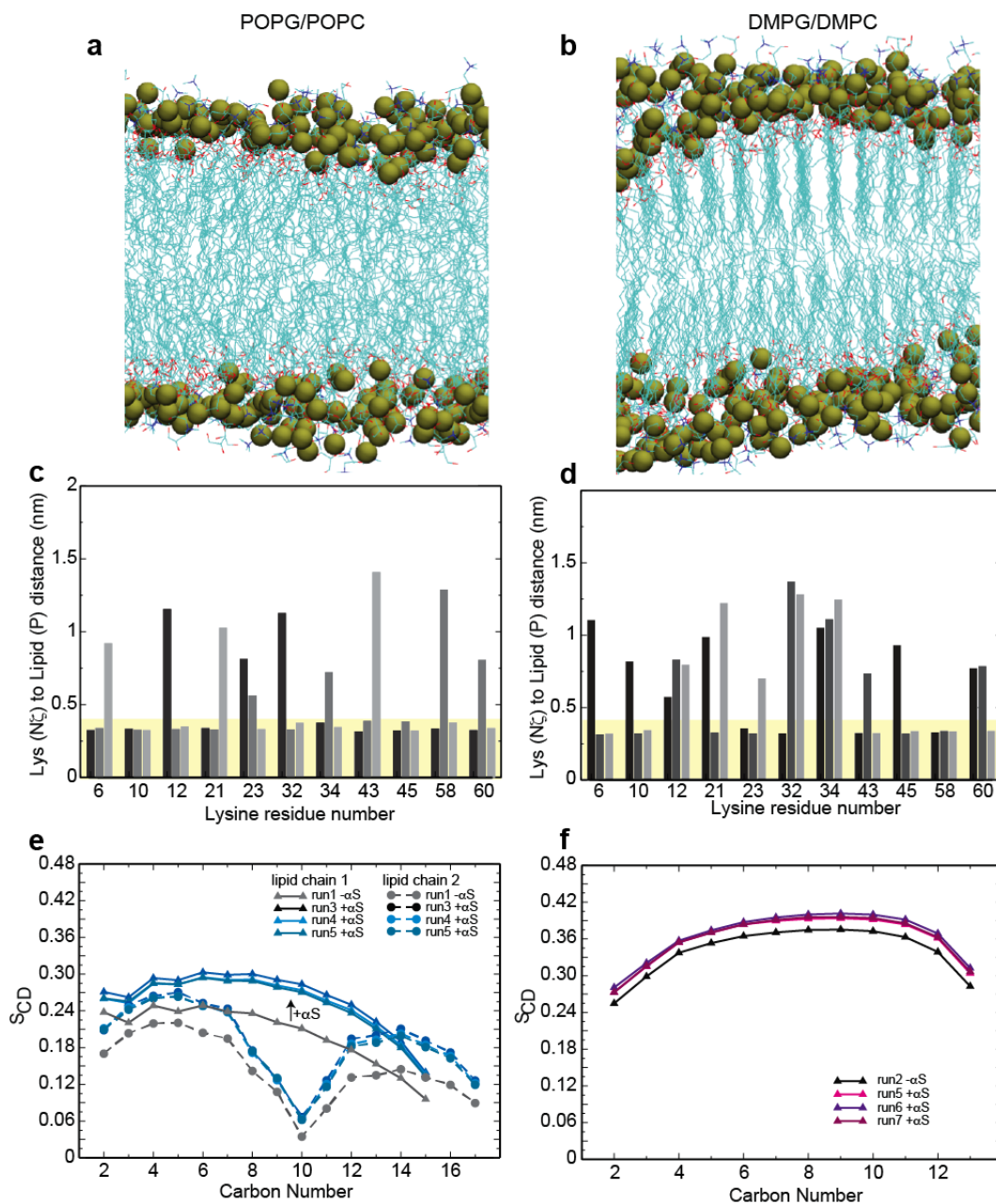


Figure 2.25: Lipid properties and α S-membrane interactions as seen by MD simulations. (a,b) Molecular arrangement of lipid bilayer in the absence of α S for POPG/POPC lipids in fluid phase (a) and DMPG/DMPC lipids in gel phase (b) (end of run1/run2, [table 2.3](#)). (c,d) Distances for indicated lysine residues from Lys-N ζ to the phosphorus atom of the next anionic lipid as found in different runs of MD simulations for POPG/POPC (c, individual bars for run3-5, [table 2.3](#)) and DMPG/DMPC (d, individual bars for run5-7, [table 2.3](#)) membranes. Distances that could promote lipid-mediated salt bridges are highlighted in yellow. (e,f) Calculated order parameters for indicated carbon atoms of the lipid fatty acids with and without α S for POPG/POPC (e) and DMPG/DMPC (f) membranes.

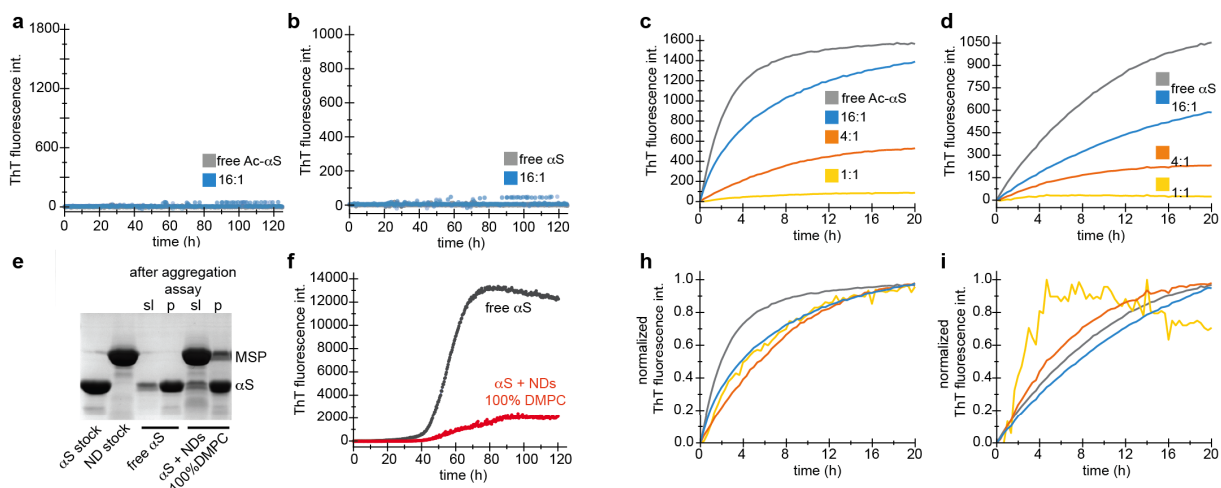


Figure 2.26: Amyloid fibril nucleation and elongation in the presence of 50% POPG ND and rational for normalization of ThT data. (a,b) Quiescent nucleation assay of acetylated α S (a) and non-acetylated (b) α S in the absence (grey) and presence of 50% POPG NDs (conditions analog to data shown in fig. 2.20j,k, for 100% POPG NDs). (c,d,) Seeded aggregation assays under conditions analog to data shown in fig. 2.20m,l, but using 50% POPG NDs. Surprisingly, the 50% charged NDs do show an effect on the ThT signal as a reporter for fibril elongation in seeded experiments. This data is difficult to explain given that elongation is, in all cases of amyloid formation, responsible for the generation of the bulk of fibril mass. Hence, its inhibition should slow down the overall aggregation kinetic, also under non-seeded conditions. Noteworthy, we observe that ThT signal intensity can be strongly affected by the presence of NDs and that the absolute ThT intensity does not correlate with absolute fibril mass when comparing data recorded in the absence or presence of NDs. This is visible by comparing SDS-PAGE results (e) with ThT intensities (f) of identical samples. After the aggregation assay the α S-band for soluble (sl) and insoluble (p) protein show very similar intensities in the absence and presence of 100% DMPC NDs. Although our NMR data show that these NDs do not interact with the α S, the corresponding ThT signal (of the identical samples) show very different intensities (f). It is therefore likely that the ThT (unspecifically) interacts with NDs, leading to an overall decrease in ThT intensities. We therefore normalized most ThT assays. Noteworthy, this effect is less pronounced for ND with 100% POPG (as e.g. visible in the data in fig. 2.20m,l), which we attribute to the high coverage of the lipid surface by α S molecules that may reduce the unspecific ThT-ND interactions. In line with our other data recorded using 50% POPG NDs, albeit significantly reduced ThT sensitivity, only very moderate effects of the NDs on the fibril elongation process are visible after normalizing ThT intensities in the seeded aggregation assays (h,i).

2.3 Interaction of α -Synuclein with Lipid Bilayer Nanodiscs

Table 2.2: Summary of NMR samples used in the study.

α S type	pH	MSP type	Lipids in ND	α S-to-ND ratio
acetylated	5.3	-	-	-
	7.4	-	-	-
	7.4	D1	100% DMPC	2:1
	7.4	D1	25% POPG - 75% DMPC	2:1
	7.4	D1	50% POPG - 50% DMPC	1:1, 2:1, 4:1, 8:1, 16:1
	7.4	D1	75% POPG - 25% DMPC	2:1
	7.4	Δ 5	75% POPG - 25% DMPC	2:1
	5.3	D1	100% POPG	2:1
	7.4	D1	100% POPG	1:2, 1:1, 2:1, 4:1, 8:1, 16:1
	7.4	D1	100% POPC	2:1
	7.4	D1	50% POPG - 50% POPC	2:1
	7.4	D1	50% DMPG - 50% POPC	2:1
	7.4	D1	50% DMPG - 50% DMPC	2:1
	7.4	D1	100% DMPG	2:1
	5.3	D1	100% DMPG, 37 °C	2:1
non-acetylated	7.4	D1	100% DMPC	2:1
	7.4	D1	100% DMPC	2:1
	7.4	D1	25% POPG - 75% DMPC	2:1
	7.4	D1	50% POPG - 50% DMPC	1:1, 2:1, 4:1, 8:1, 16:1, 32:1
	7.4	D1	75% POPG - 25% DMPC	2:1
	7.4	D1	100% POPG	1:1, 2:1, 4:1, 8:1, 16:1, 32:1

Table 2.3: Summary of MD simulations used for the study. As starting conformation for the MD simulations, the NMR structure of micelle-bound α S (PDB 1XQ8) was used, considering only the first 61 residues in order to concentrate on the membrane binding region of α S. The Amber99sb-ILDN force field [277] was used for α S, which was simulated in its non-acetylated form (i.e., with NH_3^+ at the N-terminus) and with a C-terminal N-methyl amide capping group to account for the fact that α S would continue beyond residue 61. All lysine side chains were modeled as positively charged, glutamate and aspartate as negatively charged, while glutamine and histidine residues were considered to be neutral corresponding to a pH of 7.4. The protein was placed either 0.5 nm or 1.5 nm above the membrane surface. A starting orientation with the negatively charged side chains pointing away from the membrane and the lysine side chains being oriented towards the membrane surface were chosen (fig. 2.19d). For modeling the lipid bilayer, membrane patches consisting of POPC/POPG (1:1) or DMPC/DMPG (1:1) involving 512 lipids (256 lipids per leaflet) were built using CHARMM-GUI [282] and modeled with Slipids force field parameters [278, 283]. Before α S was added, both lipid bilayers were solvated and simulated for 500 ns (POPC/POPG) or 1000 ns (DMPC/DMPG) to obtain relaxed membranes. Here, the same simulation procedure was employed as described below. α S was placed above the membrane, the protein-membrane complex solvated using the TIP3 water model, Na^+ and Cl^- added to neutralize the system and to mimic the Na^+ concentration used in the experiments. The ion parameters of Smith and Dang [284] were used. The system was then subjected to steepest descent energy minimization, followed by MD equilibration in the NVT ensemble for 1 ns at 10 °C using the V-rescale thermostat [285] with a time constant of 0.5 ps and separate temperature coupling for the protein, membrane and water/ions. Afterwards, 1 ns of NPT equilibration was performed using the Nose-Hoover thermostat [286, 287] and Parrinello-Rahman barostat [288] with semiisotropic pressure scaling, a reference pressure of 1 bar, a time constant of 10 ps and an isothermal compressibility of $4.5 \times 10^{-5} \text{ bar}^{-1}$. During both equilibration steps, restraints were applied to the positions of the P-atoms of the lipids and terminal C-atoms of their tails with a force constant of $1000 \text{ kJ mol}^{-1} \text{ nm}^{-2}$. All bond lengths were constrained using the Lincs algorithm [289]. The Coulombic interactions were calculated using the Particle mesh Ewald (PME) method [290, 291] with a cut-off of 1 nm for the short-range interactions and a Fourier spacing of 0.12 nm. The cut-off for the van der Waals interactions was set at 1.4 nm. Periodic boundary conditions were employed in all directions. For the MD production runs the same settings as for the NPT equilibration were used, except that all position restraints were removed. All MD simulations were performed at 10 °C with a time step of 2 fs for integration using the GROMACS 4.6 molecular dynamics package [280]. For the analysis, which was performed using Gromacs and Membrainy tools [281], only the last 250 ns of each production run was used.

Membrane models	Systems	α S initial distance to the membrane surface [nm]	Time [ns]
POPC/POPG*	RUN1	-	500
DMPC/DMPG*	RUN2	-	1000
POPC/POPG	RUN3	0.5	1000
POPC/POPG	RUN4	0.5	1000
POPC/POPG	RUN5	1.5	1000
DMPC/DMPG	RUN6	0.5	1000
DMPC/DMPG	RUN7	1.5	1000
DMPC/DMPG	RUN8	1.5	1000

2.4 Dityrosine formation in α -Synuclein

2.4.1 Article Information

Title: **Opposed Effects of Dityrosine Formation in Soluble and Aggregated α -Synuclein on Fibril Growth**

Michael M. Wördehoff¹, Hamed Shaykhalishahi¹, Luca Groß¹, Lothar Gremer^{1,2}, Mathias Stoldt^{1,2}, Alexander K. Buell¹, Dieter Willbold^{1,2} and Wolfgang Hoyer^{1,2,*}

¹Institut für Physikalische Biologie, Heinrich-Heine-Universität Düsseldorf, Universitätsstr. 1, 40225 Düsseldorf, Germany

²Institute of Complex Systems (ICS-6), Research Centre Jülich, Wilhelm-Johnen-Straße, 52428 Jülich, Germany

* corresponding author, wolfgang.hoyer@hhu.de

Submitted to: **Journal of Molecular Biology**, 30.06.2017.

Journal Impact Factor (2016/2017): 4.632.

Contribution: **75%**. M.M.W. designed and performed the experiments, evaluated the data and wrote the manuscript. For further details see the [appendix](#).

2.4.2 Abstract

Parkinson's disease (PD) is the second most common neurodegenerative disease. It is characterized by aggregation of the protein α -synuclein (α -syn) in Lewy bodies, mitochondrial dysfunction, and increased oxidative stress in the *substantia nigra*. Oxidative stress leads to several modifications of biomolecules including dityrosine (DiY)-crosslinking in proteins, which has recently been detected in α -syn in Lewy bodies from PD patients. Here we report that α -syn is highly susceptible to UV-induced DiY formation. We investigated DiY formation of α -syn and nine tyrosine-to-alanine mutants and monitored its effect on α -syn fibril formation *in vitro*. UV irradiation of intrinsically disordered α -syn generates DiY-modified monomers and dimers, which inhibit fibril formation of unmodified α -syn by interfering with fibril elongation. The inhibition depends on both the DiY group and its integration into α -syn. When preformed α -syn fibrils are crosslinked by DiY formation they gain increased resistance to denaturation. DiY-stabilized α -syn fibrils retain their high seeding efficiency even after being exposed to denaturant concentrations that completely depolymerise non-crosslinked seeds. Oxidative stress-associated DiY crosslinking of α -syn therefore entails two opposing effects: (i) inhibition of aggregation by DiY-modified monomers and dimers, and (ii) stabilization of fibrillar aggregates against potential degradation mechanisms, which can lead to promotion of aggregation, especially in the presence of secondary nucleation.

2.4.3 Introduction

Parkinson's disease (PD) is the second most common neurodegenerative disease with a prevalence of around 1% of people over the age of 65 [292], resulting in approximately 100,000 deaths in 2013 [2]. The lifetime risk to develop PD is around 2% for men and 1.3% for women with a tendency to increase in an aging society [66]. On the molecular level, PD pathophysiology

shows abnormal aggregation of the intrinsically disordered protein α -synuclein (α -syn) [84], as well as increased oxidative stress (OS), especially in dopaminergic neurons of the *substantia nigra* [143]. Aggregation of α -syn into amyloid fibrils and finally intracellular Lewy body deposits is a central feature of PD and other Lewy body diseases [84]. This is reflected in the genetics of familial forms of PD, where multiplication of or point mutations (A53T, A30P, E46K, G51D) in the *SNCA* gene (encoding α -syn) cause hereditary early-onset forms of PD [4]. Aggregation of α -syn is detrimental to cells in many ways as it decreases the free α -syn monomer pool, thereby disturbing the physiological function of α -syn, i.e. maintenance of the synaptic vesicle pool [240,293] and dopamine trafficking and homeostasis [182]. Moreover, various aggregated species of α -syn have been shown to form pores in the cell membrane [112], damage mitochondria [294], destabilize microtubules [295,296] and cause endoplasmic reticulum stress [297]. Besides α -syn aggregation, OS is a central hallmark of PD [143]. The *substantia nigra* is a brain region with increased OS. Firstly, its high dopamine content is a source of reactive oxygen species (ROS), as the deamination of dopamine by monoamine oxidase generates H_2O_2 which is a strong oxidizing agent [144]. Besides that, dopamine autooxidates to dopamine o-quinone and aminochrome, thereby creating toxic superoxide and hydroxyl radicals [145]. Moreover, dopaminergic neurons contain high amounts of iron which is known to catalyze ROS production via the Fenton reaction [146]. Also, mitochondrial dysfunction, e.g. inhibition of complex I, is part of PD pathophysiology [298]. Complex I inhibition results in increased production of ROS [299]. This can e.g. be triggered by 1-methyl-4-phenyl-1,2,3,6-tetrahydropyridine (MPTP), a drug that inhibits complex I and thereby leads to characteristic PD symptoms, making it an animal model for PD [149]. Besides that, familial early-onset forms of PD are caused by mutations in *PINK1* [300], *PRKN* [301] and *PARK7* [302] which code for proteins that usually associate with mitochondria in OS conditions and either prevent oxidative damage [303] or initialize autophagy of already damaged mitochondria [304]. Oxidative stress is harmful to cells in many ways, as it leads to lipid peroxidation, DNA damage and dityrosine (DiY) formation in proteins [165]. DiY crosslinks are formed when two tyrosyl radicals react with each other to form a C_{ortho}-C_{ortho} covalent bond between the two phenol moieties [166]. Elevated DiY levels have been shown to exist in the brains of Alzheimer's disease patients [305], and DiY-crosslinking of amyloid- β (A β) increases its toxicity by enhanced aggregation propensity and stabilization of already aggregated A β fibrils [173]. In PD, DiY and α -syn are colocalized in Lewy bodies of *substantia nigra* brain sections [163]. Moreover, DiY is present in ROS-induced α -syn aggregates in dopaminergic SH-SY5Y cells [306] and is a marker of oxidative stress in a MPTP model of Parkinson's disease [307]. DiY-crosslinking of α -syn *in vitro* has been performed by incubating α -syn with peroxynitrite/CO₂ [174, 175, 308], CuCl₂/H₂O₂ [163, 175], cytochrome c/H₂O₂ [176], by prolonged incubation [161] or upon purification [309]. To specifically achieve DiY-modification of α -syn, photosensitization of tris(bipyridine)-ruthenium(II) chloride in presence of ammonium persulfate was performed, demonstrating toxicity of the photoinduced oligomeric species to SH-SY5Y cells [162]. The *in vitro* studies have consistently linked DiY formation to stabilization of preformed aggregates [161, 162, 174, 176]. In contrast, the reported effects on α -syn fibril formation varied, comprising complete inhibition of fibril formation [175], reduction of the fibril

amount [162], formation of off-pathway aggregates [176] and increased fibril formation [163]. In previous *in vitro* studies, extensive crosslinking typically resulted in α -syn multimers up to high-n oligomers [162, 163, 174–176]. An alternative method for DiY generation is direct photolysis by UV irradiation at a wavelength of around 280 nm, which generates tyrosyl radicals by photo-ejection of electrons [167]. DiY formation can in this case be directly followed by an increasing fluorescence emission at 410 nm, as has been applied in studies of the DiY formation characteristics of, e.g., calmodulin [169] and insulin [170]. Here we show that α -syn is highly susceptible to DiY formation by UV irradiation, resulting in DiY-modified α -syn monomers and dimers but not higher-n oligomers. We compare UV-induced DiY formation of wildtype (WT) α -syn and several tyrosine-to-alanine (Y-to-A) mutants. We investigate the consequences of DiY formation for α -syn fibril formation and observe both inhibitory and stabilizing effects, depending on whether soluble or aggregated α -syn is DiY-modified.

2.4.4 Results

α -Syn is Highly Susceptible to DiY Formation upon UV Irradiation at 280 nm Wavelength

To study the effect of DiY crosslinks on α -syn aggregation we generated DiY-modified α -syn by UV irradiation. α -Syn was expressed and purified with an N-terminal acetyl group, corresponding to the physiological state [85]. We chose UV-irradiation-induced DiY formation, as it allows online monitoring of DiY formation kinetics by fluorescence spectroscopy and enables preparation of sufficient amounts of DiY-crosslinked protein for biophysical studies. As there are no tryptophanes and cysteines in α -syn and only two phenylalanines ($\lambda_{\text{Ex (max)}}$: 258 nm), its four tyrosine residues are the major target for photooxidative modifications [170]. We therefore applied UV irradiation at 280 nm, using the xenon lamp of a spectrofluorometer as the light source, to selectively excite tyrosine and transform it into a radical, which leads to the formation of DiY, its most abundant photooxidation product [310]. The kinetics of DiY formation were simultaneously recorded by monitoring DiY fluorescence emission at 410 nm. WT α -syn rapidly formed DiY upon irradiation in the spectrofluorometer, reaching a DiY fluorescence intensity plateau within minutes (fig. 2.27a, black trace, fig. 2.33). The set of α -syn species resulting from UV-induced DiY formation was analyzed by size exclusion chromatography (SEC) and SDS-PAGE (fig. 2.27e,f). Monomers and dimers but no higher-n oligomers were detected.

In order to test if the four tyrosine residues in α -syn possess different propensities for DiY formation we created nine tyrosine-to-alanine (Y-to-A) mutants of α -syn, the single mutants Y39A, Y125A, Y133A, Y136A, double mutants Y125A-Y133A, Y125A-Y136A, Y133A-Y136A, the triple mutant Y125A-Y133A-Y136A, and a quadruple tyrosine knockout mutant. All single Y-to-A mutants exhibited similar DiY formation kinetics, with Y39A reaching a slightly higher final fluorescence intensity compared to the other single mutants (fig. 2.27a,b blue traces). Similarly, the three double mutants showed comparable DiY formation kinetics (fig. 2.27a, red traces). This indicates that the DiY formation propensity does not differ greatly between the four tyrosines in α -syn. The extent of DiY formation as judged from the final DiY fluorescence intensities increased with the number of tyrosine contained in the α -syn variant (fig. 2.27 and

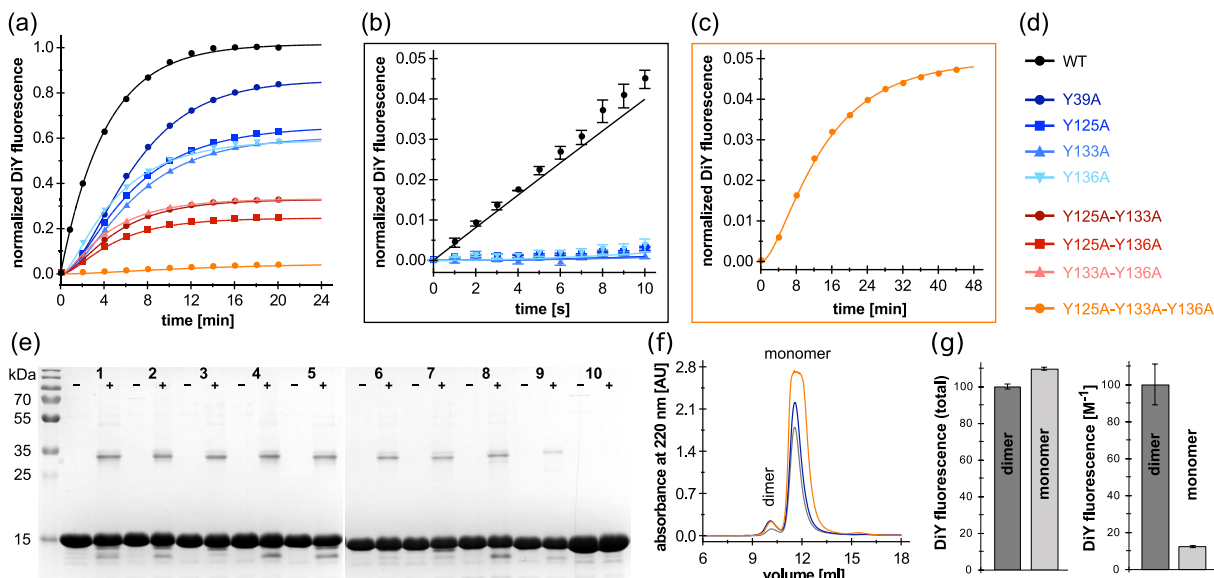


Figure 2.27: DiY formation kinetics of WT α -syn and Y-to-A mutants. (a) DiY formation kinetics of WT α -syn and single/double/triple Y-to-A mutants upon UV irradiation at 280 nm wavelength, monitored by DiY fluorescence at 410 nm. Fluorescence intensities were normalized by setting the highest fluorescence value of WT DiY- α -syn to unity. All curves are means of triplicate measurements. Solid lines represent fits to a consecutive two-step reaction, except for WT α -syn, for which a one-step first order model was applied. (b) Zoom into the first 10 seconds of the kinetics of WT α -syn and single Y-to-A mutants. (c) Zoom into the DiY formation kinetics of the triple Y-to-A mutant, Y125A-Y133A-Y136A. (d) α -Syn variants investigated in this study. (e) SDS-PAGE of WT α -syn and Y-to-A mutants before (-) and after (+) UV irradiation. 1: WT α -syn, 2-9: single/double/triple Y-to-A mutants in the same order as in (d), 10: quadruple Y-to-A tyrosine knockout mutant. (f) SEC of WT DiY- α -syn, C-term DiY- α -syn (Y39A), and N-term DiY- α -syn (Y125A-Y133A-Y136A). (g) DiY fluorescence in dimer and monomer peak after SEC of WT DiY- α -syn, total fluorescence and fluorescence intensity normalized to protein concentration are shown as means of triplicates.

table 2.4). As expected, the quadruple Y-to-A mutant of α -syn devoid of tyrosines did not show tyrosine or DiY fluorescence (fig. 2.33 and table 2.4). For all tyrosine-containing variants, the occurrence of DiY fluorescence was accompanied by a decrease in tyrosine fluorescence in the range of 17-28%, suggesting that only \sim 20% of tyrosines are converted to DiY after UV irradiation (fig. 2.33 and table 2.4). A limited yield of DiY formation upon UV irradiation has been observed before, with \sim 6% conversion to DiY in the case of calmodulin, and has been attributed to competing reactions [165].

In the case of WT α -syn containing four tyrosines, a strong increase in DiY fluorescence was observed directly from the beginning of UV irradiation (fig. 2.27b), with kinetics in agreement with a one-step first order reaction (fig. 2.27a). In contrast, all other variants, containing three or less tyrosines, showed a sigmoidal profile of DiY formation, and could be fit to the reaction scheme of a consecutive two-step reaction (fig. 2.27a, rate constants are given in table 2.5). The difference in the reaction profile of WT and mutant α -syn indicates that WT α -syn is exceptionally susceptible to DiY formation. The present data does not report on the step in the DiY formation mechanism responsible for this effect. However, the clear difference between WT α -syn and the single Y-to-A mutants suggests that its four tyrosines concertedly prime WT α -syn for DiY formation.

One factor that may promote rapid DiY formation in α -syn is the structural flexibility of the intrinsically disordered protein (IDP), which enables contacts between all tyrosines [174]. Ribonuclease A is a globular protein containing six tyrosine and no tryptophan residues, with the capacity to form DiY-linked dimers [311]. When UV-irradiated at the same conditions, DiY formation is much slower in ribonuclease A compared to α -syn (fig. 2.28), supporting a role of α -syn's conformational flexibility in facilitating DiY formation. To evaluate the ratio of inter- to intramolecular DiY formation, dimers and monomers of UV-irradiated WT α -syn were purified by size exclusion chromatography (SEC) (fig. 2.27f). The dimer fraction contained only $\sim 5\%$ of the total protein according to absorbance at 220 nm, yet exhibited nearly the same DiY fluorescence intensity as the monomer fraction (fig. 2.27g). The lower DiY content per protein in the monomer fraction is in agreement with the limited conversion of tyrosines to DiY. UV-irradiation induced α -syn dimers could also be visualized by SDS-PAGE for all α -syn variants apart from the quadruple Y-to-A mutant of α -syn devoid of tyrosines (fig. 2.27e).

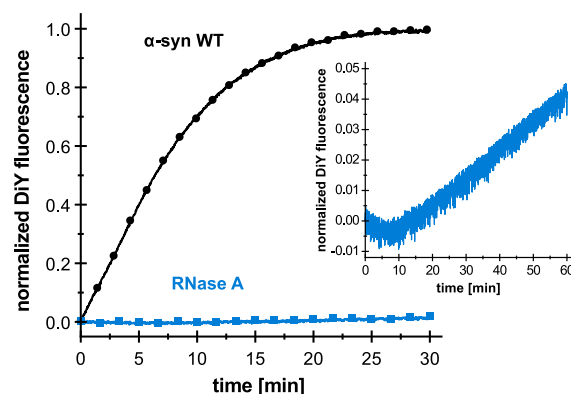


Figure 2.28: DiY formation kinetics of α -syn WT and ribonuclease A. DiY formation kinetics of 100 μ M α -syn WT and 100 μ M ribonuclease A (RNase A). A zoom into the DiY formation kinetics of RNase A for a longer time (1 h) is also shown. The mean curve of triplicate measurements was normalized by setting the highest fluorescence intensity of α -syn WT to unity.

DiY-modified Monomers and Dimers Inhibit Fibril Formation of Unmodified α -Syn by Interfering with Fibril Elongation

We next evaluated the effect of DiY crosslinks on α -syn aggregation. To this end, UV-irradiated solutions of WT and Y-to-A mutant α -syn that had achieved the final plateau of DiY fluorescence intensity (referred to hereafter as DiY- α -syn) were added to non-UV-irradiated WT α -syn, and aggregation was monitored by Thioflavin T (ThT) fluorescence. The solutions contained 25 μ M WT α -syn and 25 μ M DiY- α -syn (total protein concentration, DiY-containing protein molecules were not further enriched). WT and Y-to-A mutant DiY- α -syn greatly inhibited aggregation of WT α -syn, manifested in a prolonged lag-time and a reduced slope of the aggregation time course in the observed growth phase (fig. 2.29a and b). WT DiY- α -syn and all tyrosine-containing Y-to-A mutant DiY- α -syn variants inhibited aggregation to a similar extent. In contrast, the UV-irradiated quadruple Y-to-A mutant devoid of tyrosines did not inhibit α -syn aggregation (fig. 2.29c).

To investigate the specificity of aggregation inhibition by DiY- α -syn, we evaluated the inhibitory potential of free DiY and of a UV-irradiated, DiY-containing fragment of the tau protein, TauK18 Δ 280AA [312]. Like α -syn, tau is an IDP involved in neurodegenerative diseases, and interactions of α -syn and tau have been reported [210]. Free DiY did not show a significant effect on α -syn aggregation (fig. 2.29c). DiY-TauK18 Δ 280AA led to a prolonged lag-time of α -syn

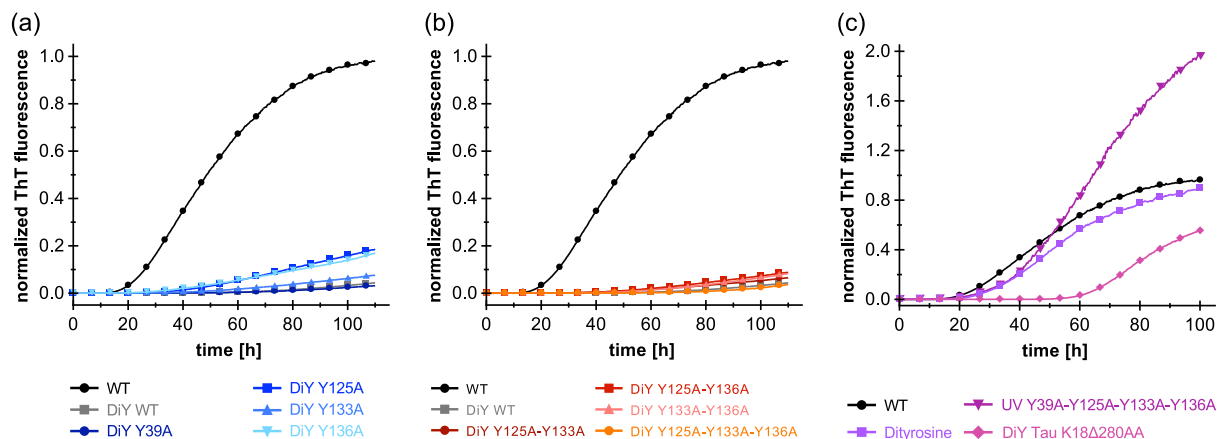


Figure 2.29: Influence of DiY- α -syn and other DiY species on the aggregation of α -syn. Kinetics of fibril formation of 25 μ M non-irradiated WT α -syn in the presence of (black) 25 μ M of non-irradiated WT α -syn, or in the presence of 25 μ M of the indicated DiY species: (a) single Y-to-A mutants, (b) double/triple Y-to-A mutants, (c) quadruple tyrosine knockout mutant, DiY/tyrosine mix (prepared as DiY α -syn), and DiY-TauK18 Δ 280AA. Mean curves of triplicates are shown (with the exception of the black curve which is the mean of 15 experiments), normalized by setting the highest fluorescence intensity in the aggregation reaction of non-irradiated WT α -syn to unity.

aggregation, but did not have a strong effect on the slope of the aggregation time course in the observed growth phase (fig. 2.29c). These observations demonstrate that the specific protein environment of DiY determines the effect on aggregation, and that DiY- α -syn is particularly potent at inhibiting α -syn aggregation.

The efficient aggregation inhibition entailed by the triple mutant Y125A-Y133A-Y136A, which can only form intermolecular DiY crosslinks through its sole tyrosine residue Y39, suggests that DiY-crosslinked α -syn dimers are the main inhibitory species (fig. 2.29b). To compare the inhibitory potential of DiY- α -syn dimers and monomers, the dimeric and monomeric DiY- α -syn fractions were separated by SEC (fig. 2.27f) and added to WT α -syn aggregation reactions (fig. 2.30a,b). Apart from WT DiY- α -syn, the single Y-to-A mutant Y39A DiY- α -syn, which can form inter- and intramolecular DiY only in the C-terminal domain (thus denoted C-term DiY- α -syn), and the triple Y-to-A mutant Y125A-Y133A-Y136A, which can only form intermolecular DiY in the N-terminal domain (thus denoted N-term DiY- α -syn), were included in this experiment. DiY- α -syn dimers were added at a concentration of 1.25 μ M to 25 μ M WT α -syn, i.e. at a substoichiometric ratio of 1:20 or 1:10 with regard to the dimer concentration or subunit concentration, respectively. To achieve the same DiY concentration in the case of DiY- α -syn monomers, they were added at a total protein concentration of 10 μ M, accounting for the approximately eight-times lower DiY fluorescence compared to DiY- α -syn dimers (fig. 2.27g). Addition of the N-term DiY- α -syn monomer fraction resulted in only minor effects on WT α -syn aggregation, in agreement with the fact that this construct cannot form intramolecular DiY crosslinks. In contrast, all DiY- α -syn dimers as well as WT and C-term DiY- α -syn monomers strongly inhibited WT α -syn aggregation (fig. 2.30a). Dimers, irrespective of the domain location of the DiY crosslinks, achieved a higher inhibitory effect than monomers, supporting a dominant role of dimers in DiY- α -syn-associated aggregation inhibition.

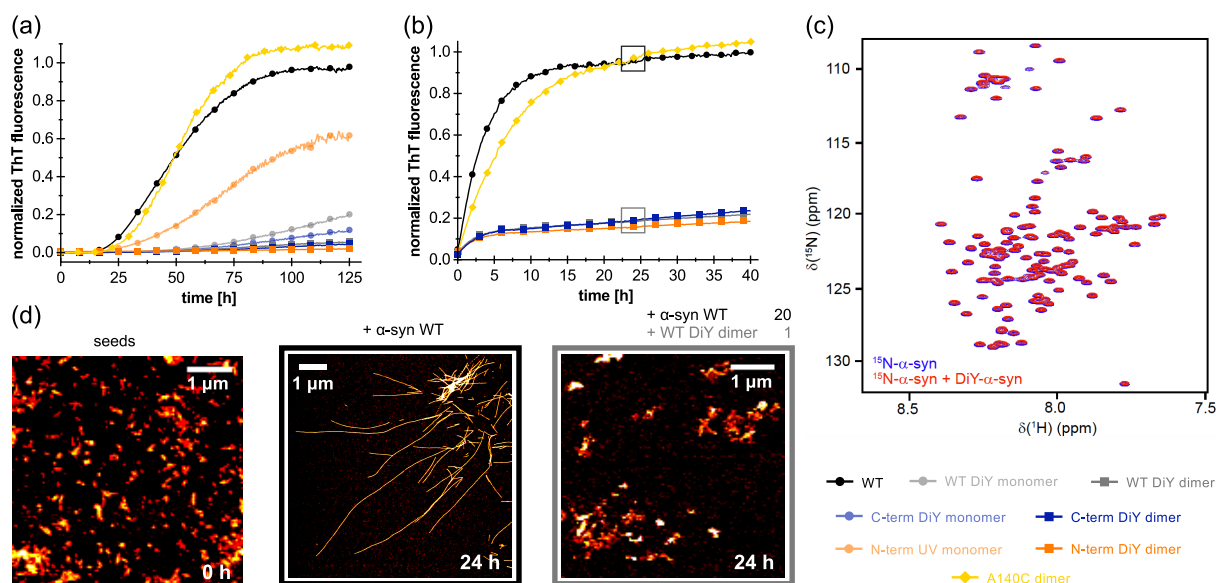


Figure 2.30: Influence of DiY- α -syn dimers and monomers on α -syn aggregation. (a) Kinetics of fibril formation of 25 μM of non-irradiated WT α -syn in the presence of either 1.25 μM DiY- α -syn dimers (WT, C-term, N-term), 1.25 μM A140C dimers, or 10 μM DiY- α -syn monomers (WT, C-term, N-term). (b) Seeded aggregation of 25 μM WT α -syn in the presence of 1.25 μM DiY dimers (WT, C-term, N-term) or 1.25 μM A140C dimers and 10% (in monomer equivalents, 2.5 μM) sonicated preformed α -syn fibril seeds. Seeded aggregation was performed without agitation to disfavor formation of new nuclei or fibril fragmentation. (c) (^1H - ^{15}N) HSQC NMR spectra of 100 μM [^{15}N]- α -syn in the absence and presence of 400 μM unlabeled (natural abundance) WT DiY- α -syn. (d) AFM micrographs of samples taken from the seeded aggregation assay shown in (b) with/without WT DiY- α -syn dimers after 0 h and 24 h.

To test the effect of DiY- α -syn on the elongation of α -syn fibrils, WT α -syn aggregation was monitored in the presence of ultrasonicated α -syn WT fibrils seeds, under conditions disfavoring formation of new nuclei or fibril fragmentation [269]. As expected under these conditions, WT α -syn aggregation proceeded rapidly without a discernible lag phase (fig. 2.30b). In the presence of DiY- α -syn dimers at a substoichiometric ratio of 1:20, however, this process is halted, resulting in a \sim 5-fold lower final ThT fluorescence compared to aggregation reactions in the absence of DiY- α -syn dimers (fig. 2.30b). The inhibitory effect of DiY- α -syn on fibril elongation was confirmed by atomic force microscopy (AFM). Sonicated seed particles were imaged as bundles of short (length $<$ 200 nm) fibrils of WT α -syn [64] (fig. 2.30d). After quiescent incubation of seeds with WT α -syn monomers in the absence of WT DiY- α -syn dimers, long fibrils formed (fig. 2.30d). In contrast, after quiescent incubation of seeds with WT α -syn monomers in the presence of WT DiY- α -syn dimers, the seed fibril bundles appeared unchanged and long fibrils could not be observed (fig. 2.30d). We investigated if the inhibitory effect of DiY- α -syn dimers depends on the nature of the crosslink, by comparing the effect of α -syn dimers crosslinked through a C-terminal disulfide bond. Dimers of α -syn A140C had only minor effects on *de novo* and seeded aggregation of WT α -syn (fig. 2.30a and b). This demonstrates that the DiY crosslink exerts specific effects.

The substoichiometric inhibition entailed by DiY- α -syn indicates that it interferes with nucleation and/or elongation of α -syn fibrils by interacting with higher-order α -syn assemblies such as oligomers, fibril surfaces, or fibril ends. We tested if DiY- α -syn also has an effect on the

conformation of monomeric α -syn. For this purpose, the (^1H - ^{15}N) HSQC NMR spectra of [^{15}N]- α -syn in the absence and presence of a 4-fold excess of [NA]-DiY- α -syn were compared (fig. 2.30c). The spectra perfectly superimposed, suggesting the absence of an effect of DiY- α -syn on α -syn monomer conformation.

DiY Formation Stabilizes On-pathway Aggregation Seeds

OS-associated DiY-crosslinking can stabilize preformed aggregates [161, 162, 174, 176]. We evaluated the stabilization of preformed α -syn fibrils by UV-induced DiY-crosslinking against chemical denaturation, and examined if DiY-stabilized α -syn aggregates retain the ability to seed α -syn fibrillation. To this end, we preformed α -syn fibrils and split the fibril sample in two halves, one of which was UV-irradiated for DiY-crosslinking. The samples were subsequently incubated in 4 M guanidinium chloride (GdnHCl), a potent denaturant of non-crosslinked α -syn fibrils [313]. The non-irradiated sample experienced a rapid decline in ThT fluorescence under these conditions (fig. 2.31a) and eluted in SEC almost exclusively as a monomer after 90 min of incubation (fig. 2.31b). In contrast, the decrease in ThT fluorescence was less pronounced for the DiY-crosslinked sample, which eluted in SEC as a mixture of monomers, low-n oligomers, and high molecular weight aggregates of >600 kDa (fig. 2.31a,b). AFM imaging of the void volume fraction of 4 M GdnHCl-treated DiY-crosslinked fibrils revealed small fibril fragments of about 30-200 nm length (fig. 2.31c). These stabilized fibril fragments were subsequently added to an aggregation reaction of monomeric α -syn under conditions disfavoring formation of new nuclei or fibril fragmentation, demonstrating seeding activity of DiY-stabilized α -syn fibrils (fig. 2.31d). The void volume fraction of 4 M GdnHCl-treated non-crosslinked fibrils, on the other hand, did not seed α -syn fibrillation (fig. 2.31d), in agreement with the absence of stabilized fragments in this case (fig. 2.31b).

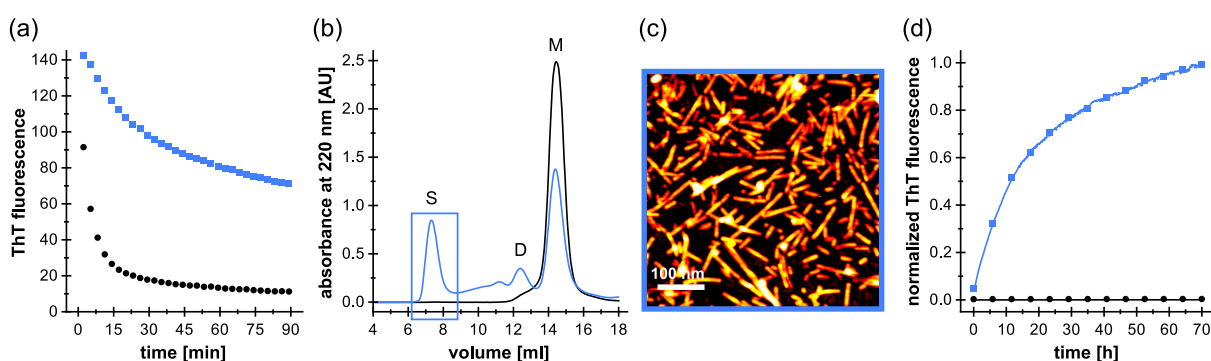


Figure 2.31: DiY-crosslinking stabilizes α -syn fibril seeds. (a) Chemical denaturation in 4 M GdnHCl of WT α -syn fibrils that were (blue) or were not (black) subjected to DiY-crosslinking by UV irradiation at 280 nm before, monitored by ThT fluorescence. (b) SEC after 90 min of denaturation, performed on a Superdex 200 column. S: void volume peak containing seeds (>600 kDa); D: DiY dimer peak; M: α -syn monomer peak. The void volume fractions collected for further characterization are indicated by a blue box. (c) AFM micrograph (height image) of purified DiY-stabilized fibril seeds. (d) Seeding capacity of DiY-stabilized fibril fragments evaluated by addition to a fibril formation assay of 25 μM non-irradiated α -syn monomer under conditions disfavoring formation of new nuclei or fibril fragmentation.

In conclusion, OS-associated DiY-crosslinking in α -syn fibrils leads to a substantial increase in resistance to denaturation. When DiY-crosslinked fibrils are partially denatured and subsequently separated again from the denaturant, they still exhibit a strong seeding efficiency for α -syn monomers.

2.4.5 Discussion

Several post-translational modifications of α -syn have been identified in Lewy bodies, potentially with critical impact on α -syn aggregation [86]. One of these modifications is DiY formation, which is special in its capacity to establish novel covalent bonds between sites that are distant in the primary sequence, as well as between two protein molecules. In the case of intrinsically disordered proteins (IDPs) like α -syn, these crosslinks will strongly influence the ensemble of conformations adopted by the polypeptide chain [176]. We find that α -syn is highly susceptible to UV-induced DiY formation. This is likely another consequence of its IDP nature [174], as the globular protein ribonuclease A, which like α -syn contains tyrosines and no tryptophan, shows insignificant levels of DiY formation in comparison (fig. 2.28). This is in accordance with studies on the IDP β -casein, which has a dramatically increased propensity for DiY formation compared to the globular proteins BSA and β -lactoglobulin [171].

Strikingly, WT α -syn containing 4 tyrosines exhibits a different time course of DiY formation than all mutants containing 3 or less tyrosines, achieving a far higher initial rate of DiY production (fig. 2.27b). The very significant difference in rates cannot simply be explained by statistical arguments. Assuming that the rate of production of the tyrosine radical, as well as its lifetime are not the limiting factors of DiY formation, but rather the encounter of two tyrosine radicals, we would expect a ratio of the rates of 6 to 3 to 1, corresponding to the number of possible intramolecular DiY pairs if a total of 4, 3, and 2 tyrosines are present per molecule of α -syn. In addition, the WT sequence with 4 tyrosines can in principle form 2 DiY crosslinks, so that the upper bound of the ratios of the intramolecular DiY formation kinetics of a purely statistical treatment is 12 to 3 to 1. Therefore, the much larger difference in response to irradiation between the WT sequence and the tyrosine deletion mutants is most likely due to differences in the efficiency in radical generation, radical lifetime and the rates of potential side reactions other than DiY formation that the tyrosyl radicals can undergo. The distinct changes from the 4 tyrosine-containing WT to the 3 tyrosine-containing mutants suggests significant differences in the collective photophysical properties of the tyrosines in these constructs. These properties are likely decisively affected by the high local concentration of tyrosine in α -syn (60 mM, assuming a radius of 3 nm for the α -syn molecule) [314], and by the particular capability of tyrosine residues to establish intra- and intermolecular contacts of IDPs [315, 316].

Analysis of the Y-to-A mutants furthermore indicates that the propensity for UV-induced DiY formation does not differ greatly between the four tyrosines. This is reminiscent of a study on peroxynitrite-induced DiY formation, which arrived at the same conclusion by analyzing a set of tyrosine-to-phenylalanine mutants [175]. In contrast, other studies have observed dominant roles of Tyr-125 [308], Tyr-133/Tyr-136 [176], or have prevalently detected Tyr-39 in DiY

crosslinks [162,309], suggesting that the method of tyrosyl radical formation affects the residue-specific DiY formation propensity.

We observe opposing effects of DiY formation on α -syn fibrillation, depending on whether monomers or fibrils are DiY-modified (fig. 2.32). UV-induced DiY-modification of α -syn monomers led to intra- and intermolecular DiY crosslinks, with similar amounts of DiY in the monomer and dimer fractions, but insignificant formation of higher-n oligomers (fig. 2.27e,f,g). Substoichiometric amounts of DiY-modified monomers and dimers inhibited *de novo* fibril formation as well as seeded fibril growth of unmodified α -syn (fig. 2.32b). This demonstrates that at least the fibril elongation step of the aggregation reaction is inhibited. Since free DiY and a DiY-containing fragment of the tau protein showed no or only weak effects on α -syn fibrillation, respectively, specific interactions between DiY-modified and unmodified α -syn molecules seem to be critical for aggregation inhibition. The hydrophobic NAC region might be a key interaction site in this context, as it is critical for α -syn self-assembly. At the same time, the inhibitory effect is not a general phenomenon linked only to dimer formation, as a dimer linkage through a C-terminal disulfide bond could not reproduce the effect of C-terminal DiY-crosslinking (fig. 2.30a,b). This suggests that DiY is not just serving as a linker that modulates the conformational ensemble of α -syn, but that the DiY group is actively involved in interactions that lead to an inhibition of fibril elongation.

The substoichiometric inhibition of fibril elongation suggests that these interactions occur preferentially at the fibril end. With fibril ends, DiY-modified monomers and dimers establish interactions that are incompatible with fibril elongation.

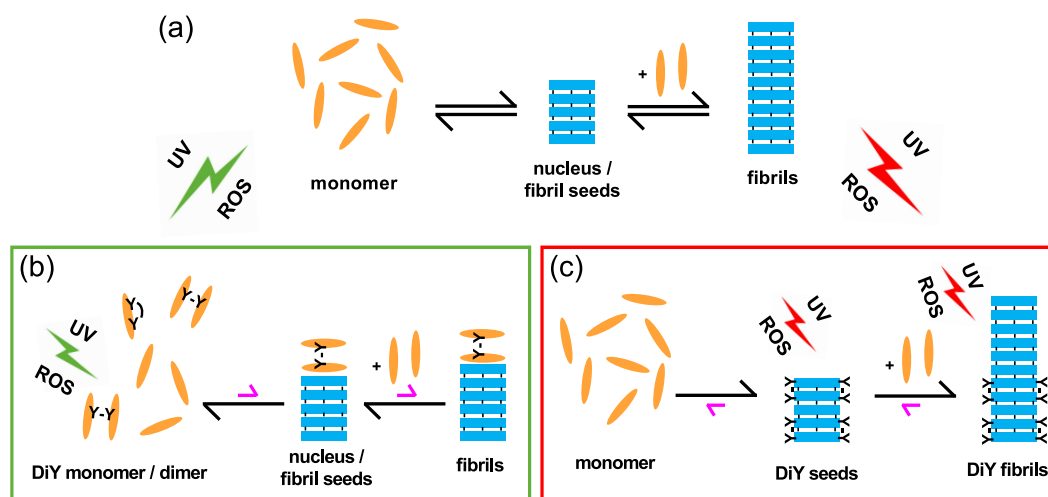


Figure 2.32: Scheme of the effects of DiY formation on α -syn aggregation. (a) Pathogenic aggregation process of α -syn from monomers to nuclei/fibril seeds and mature fibrils. (b) Inhibition of α -syn aggregation. When α -syn monomers are DiY-modified by UV irradiation or reactive oxygen species (ROS), resulting in DiY-crosslinked dimers and monomers, both nucleation and fibril elongation are inhibited. (c) Stabilization of α -syn fibril seeds by DiY formation. When α -syn nuclei/fibrils are modified by DiY-crosslinking they gain increased resistance to denaturation and retain the capacity to seed fibril growth.

The stronger inhibitory effect of the dimer compared to the monomer could be due to the larger number of sites in the dimer that are involved in such off-pathway interactions (e.g. two NACs regions in the dimer vs. one in the monomer), or due to the increased topological challenge to correctly incorporate a dimer into the in-register fibril core. We note again, however, that the specific DiY crosslink is critical for the enhanced inhibition of the dimer, as a dimer linkage through a C-terminal disulfide bond did not show a significant inhibitory effect. Previous studies have shown that DiY-crosslinking stabilizes preformed α -syn aggregates against chemical denaturation [161, 162, 174, 176]. We find that preformed α -syn fibrils stabilized by UV-induced DiY modification are effective at seeding α -syn fibril growth (fig. 2.31d, fig. 2.32c). Stabilization of α -syn fibril seeds by DiY-crosslinking might consequently be a factor that counteracts their cellular degradation and hence supports the persistence and even spreading of α -syn pathology.

In contrast to the consistent observation of stabilization of preformed α -syn aggregates [176], previous studies reported different effects of DiY-crosslinking on *de novo* fibril formation. In agreement with the inhibitory effect of DiY-modified α -syn monomers and dimers reported here, Norris et al. found that α -syn did not polymerize into fibrils after peroxyxynitrite treatment [175]. Tris(bipyridine)ruthenium(II) chloride photosensitization led to a reduction in fibril yield [162]. In contrast, formation of off-pathway aggregates or increased fibril formation was observed upon treatment with cytochrome c/H₂O₂ [176] or CuCl₂/H₂O₂ [163], respectively. Specifically for DiY-crosslinked α -syn dimers, a reducing effect on the fibril yield of non-crosslinked α -syn [162] or a role as critical on-pathway intermediate [161] have been reported. The disparate findings suggest that the conditions of tyrosyl radical generation modulate the effects of DiY- α -syn on fibril formation, for example by determining the extent of DiY modification and the set of DiY-modified α -syn species. In fact, we observe exclusively DiY-modified α -syn monomers and dimers after UV irradiation, whereas previous protocols generated α -syn multimers up to high oligomers [162, 163, 174–176].

We find that DiY-modified monomers and dimers strongly inhibit fibril elongation, whereas DiY-stabilization of fibril seeds promotes fibril elongation in the presence of a degradation/destabilization process. DiY modification of α -syn might therefore protect from aggregation in the absence of aggregates, or when low aggregate amounts are present. However, as aggregation proceeds in the course of disease progression, DiY formation might switch from an aggregation-inhibiting to an aggregation-promoting factor above a critical level of aggregate formation. In the presence of secondary nucleation processes that lead to autocatalytic proliferation of fibrils [269], the rate of which depends on the total mass of fibrils, DiY-induced stabilization of fibrils could ultimately result in the initiation of a positive feedback loop of α -syn aggregation.

2.4.6 Materials and Methods

Expression and Purification of Acetyl- α -syn and Acetyl- α -syn Mutants

Acetyl- α -syn wildtype (WT), acetyl- α -syn tyrosine-to-alanine (Y-to-A) mutants and acetyl- α -syn-A140C were expressed in *E. coli* BL21DE3 carrying codon-optimised α -syn in pT7-7 vector and the pNatB vector with the N-terminal acetylation enzyme NatB from *Schizosaccharomyces pombe* [274]. PNatB (pACYCduet-naa20-naa25) was a gift from Dan Mulvihill (Addgene plasmid #53613). Y-to-A mutants were generated by QuikChange site-directed mutagenesis. Expression was conducted in phosphate-buffered (50 mM, pH 7.2) 2YT-medium with 0.4% glycerol and 2 mM MgCl₂, protein production was induced at \sim OD 1.2 with 1 mM IPTG and run for 4 h at 37 °C. Purification of α -syn was performed as previously described [140] with modifications to the original protocol: Cell lysis and release of thermostable α -syn was carried out by boiling the frozen cell pellet in a fourfold volume of dH₂O at 95 °C for 30 min. After centrifugation at 15 000 *g* and 4 °C for 30 min, the protein in the supernatant was precipitated by gradually adding saturated ammonium sulfate solution until 50% saturation was reached. Protein was pelleted at 15 000 *g* and 4 °C for 30 min and resuspended in 50 ml of 50 mM Tris-HCl, pH 8, sterile-filtered and loaded onto a 5 ml HiTrap QFF anion exchange chromatography column (GE Healthcare). Acetyl- α -syn eluted at \sim 300 mM NaCl in a 0-500 mM NaCl gradient. The elution fractions were precipitated by adding saturated ammonium sulfate solution to 50% saturation, the protein pelleted as before, resuspended in dH₂O and finally purified by size exclusion chromatography (SEC) on a Superdex 75 16/60 column (GE Healthcare) in 25 mM K-phosphate buffer, pH 7.3, 100 mM KCl. Final yields were \sim 40-60 mg l⁻¹ culture for acetyl- α -syn WT and Y-to-A mutants, and around 20 mg l⁻¹ for acetyl- α -syn A140C. Protein concentrations were determined by absorbance measurement at 275 nm using an extinction coefficient of 5600 M⁻¹ cm⁻¹ if not stated otherwise.

DiY Formation by UV-irradiation

For DiY formation, 100 μ M solutions of α -syn WT and α -syn Y-to-A mutants as well as tauK18 Δ 280AA, tyrosine, and ribonuclease A in 25 mM K-phosphate buffer, pH 7.3, 100 mM KCl were loaded into a fluorescence cuvette with a magnetic stir bar. All spectra and DiY formation kinetics were recorded on a JASCO FP-6500 spectrofluorometer at 20 °C. Before and after DiY formation, tyrosine spectra ($\lambda_{\text{Ex}} = 274$ nm, bandwidth 5 nm; $\lambda_{\text{Em}} = 290$ –350 nm) and DiY spectra ($\lambda_{\text{Ex}} = 320$ nm, bandwidth 5 nm; $\lambda_{\text{Em}} = 350$ –480 nm) were recorded. DiY formation was induced at $\lambda_{\text{Ex}} = 280$ nm (bandwidth 20 nm) and monitored every second at $\lambda_{\text{Em}} = 410$ nm (bandwidth 20 nm). UV irradiation and fluorescence readings were stopped when a fluorescence intensity plateau was reached to prevent excessive photobleaching. For evaluation, buffer fluorescence was subtracted and the mean of triplicate measurements was normalized by setting the highest fluorescence of WT DiY- α -syn to unity. The kinetics of DiY formation were fit to a consecutive two-step reaction or a one-step first order reaction, using Abscissa 2D plot and fit tool by Rüdiger Brühl (<http://rbruehl.macbay.de/>).

Separation of DiY- α -syn Dimers and DiY- α -Syn Monomers

To compare the inhibitory potential of DiY- α -syn dimers and monomers, the dimeric and monomeric fractions of WT DiY- α -syn, the single Y-to-A mutant Y39A DiY- α -syn (C-term DiY- α -syn), and the triple Y-to-A mutant Y125A-Y133A-Y136A (N-term DiY- α -syn) were separated by SEC. DiY formation was carried out in solutions of 200 μ M WT α -syn, 267 μ M Y39A α -syn, and 800 μ M Y125A-Y133A-Y136A α -syn, i.e., at equivalent tyrosine concentration. After DiY formation by UV irradiation, 500 μ l of each sample were loaded onto a Superdex 75 10/300 column (GE Healthcare) and separated by SEC in 25 mM K-phosphate buffer, pH 7.3, 100 mM KCl. For analytical SEC, 200 μ l samples with half the protein concentration were loaded. As DiY formation significantly changed the absorption of α -syn at 275 nm and to ensure comparability of the different Y-to-A mutants, protein concentrations were measured at 220 nm using extinction coefficients of 105 344 M⁻¹ cm⁻¹ for monomers and 210 688 M⁻¹ cm⁻¹ for dimers. These extinction coefficients were determined by measuring the absorbance at 220 nm of a WT α -syn sample of known concentration (determined by absorbance at 275 nm). For determination of the dimer and monomer yields, SEC peaks were integrated by the UNICORN evaluation software (GE Healthcare). For the measurement of DiY fluorescence in the dimer and monomer peaks, three \sim 400 μ l samples of 100 μ M WT DiY- α -syn were separated by SEC, the protein concentrations of dimer and monomer peaks were measured as before, and the fluorescence was measured at 410 nm with $\lambda_{\text{Ex}} = 320$ nm. The mean DiY fluorescence of triplicate samples was calculated.

Aggregation Assays

Thioflavin T (ThT) aggregation assays were conducted in Corning half area 96-well plates with non-binding surface (Corning No. 3881). For the assays starting from monomeric α -syn, 25 μ M of non-irradiated WT α -syn was mixed with either 25 μ M DiY- α -syn, 25 μ M of UV-irradiated tyrosine, or 25 μ M of UV-irradiated tauK18 Δ 280AA. Aggregation assays were run for five days with measurement of ThT fluorescence every 20 min ($\lambda_{\text{Ex}} = 450$ nm, bandwidth 5 nm; $\lambda_{\text{Em}} = 482$ nm, bandwidth 10 nm) with 15 s of orbital shaking before the measurement in Tecan Infinite 200PRO and Tecan Infinite M1000PRO plate readers. The assays were conducted at 37 °C in 25 mM K-phosphate buffer, pH 7.3, 100 mM KCl, 1 mM MgCl₂, 10 μ M Thioflavin T (ThT) and 0.05% NaN₃, reflecting intracellular potassium and magnesium concentration as well as intracellular pH and ionic strength. A glass ball was added per well to improve mixing. Per well, 125 μ l sample was used. To evaluate the effect of DiY- α -syn dimers and A140C dimers on α -syn aggregation, 1.25 μ M dimers (WT DiY- α -syn dimer, C-terminal DiY- α -syn dimer, N-terminal DiY- α -syn dimer, A140C dimer) were added to 25 μ M of WT monomers (1:20 stoichiometry). DiY- α -syn monomer fractions were used at a total α -syn concentration of 10 μ M in order to achieve the same DiY concentration as in the dimer experiments, considering the eight-times lower DiY fluorescence compared to DiY- α -syn dimers. For seeded aggregation assays, 10% (in monomer units, 2.5 μ M) of WT α -syn fibril seeds were added to 25 μ M WT α -syn aggregation reactions. The seed solution was prepared as follows: 300 μ l of 100 μ M α -syn was fibrillated at 37 °C and 800 rpm for 3 days in a 2 ml tube containing a glass balls in a Thermomixer (Eppendorf). The fibril solution was diluted to 50 μ M and sonicated with a tip sonicator (Bandelin Sonopuls HD3200, BANDELIN electronic) at 10% power (20 W) for 60 s, with 1 s pulses separated by 4 s pause. In seeded aggregation experiments samples were not shaken prior

to measurement to disfavor formation of new nuclei or fibril fragmentation. For evaluation, the mean of triplicate measurements was referenced to the highest fluorescence of 25 μM WT $\alpha\text{-syn}$.

Nuclear Magnetic Resonance Spectroscopy (NMR)

NMR spectra were acquired at 10 °C using a 750 MHz Avance III spectrometer (Bruker) equipped with a cryogenically cooled Z-axis pulse-field-gradient triple resonance probe. The NMR samples contained [$U\text{-}^{15}\text{N}$]- $\alpha\text{-syn}$ at a concentration of 100 μM in 20 mM Na-phosphate buffer, pH 7.4, 50 mM NaCl, 8% D_2O , with or without addition of 400 μM [NA]-DiY- $\alpha\text{-syn}$.

Atomic Force Microscopy (AFM)

For AFM imaging, 20 μl of the indicated samples shown in figure 4 and 5 were incubated for 30 min on a gold-coated mica surface, the solution was taken off, shortly washed with dH_2O , and dried under a nitrogen stream. The samples were imaged by tapping mode on a JPK Instruments Nanowizard 3.

Denaturation and Seeding Capacity of DiY-crosslinked $\alpha\text{-Syn}$ Fibrils

For the fibril denaturation experiments, 3 ml of 150 μM $\alpha\text{-syn}$ WT in 25 mM K-phosphate buffer, pH 7.3, 100 mM KCl, 1 mM MgCl_2 and 0.1% NaN_3 were fibrillated at 37 °C in a 15 ml tube under stirring with a magnetic stir bar for 3 days. Four aliquots of 700 μl were directly frozen in liquid nitrogen and stored at -80 °C. One half of each aliquot was subjected to DiY-crosslinking by UV irradiation as described before. Subsequently, 300 μl of the fibril solutions (with and without DiY crosslinks) were mixed with 20 μM ThT and 4 M guanidinium chloride, pH 8, in a glass cuvette with a stir bar (total volume: 600 μl) and incubated for 90 min at 20 °C inside the fluorometer. ThT fluorescence was measured every minute at 485 nm ($\lambda_{\text{Ex}} = 445 \text{ nm}$). Buffer fluorescence was subtracted. After 90 min of denaturation, 500 μl of the solutions were loaded onto a Superdex 200 10/300 column (GE Healthcare) and separated at a flow rate of 0.5 ml min^{-1} in 25 mM K-phosphate buffer, pH 7.3, 100 mM KCl. Void volume fractions ($\sim 1.5 \text{ ml}$) were collected and directly evaluated for their capacity to seed fibril formation by addition (80% v/v) to aggregation reactions of 25 μM non-irradiated WT $\alpha\text{-syn}$ at 37 °C. Fibril formation was followed without shaking to disfavor formation of new nuclei or fibril fragmentation.

Keywords

Protein aggregation, amyloid, Parkinson's disease, oxidative stress, intrinsically disordered proteins.

Acknowledgements

We acknowledge support from the European Research Council (WH) and the International Graduate School of Protein Science and Technology (iGRASPseed) granted by the Ministry of Innovation, Science and Research of the state North Rhine-Westphalia (MMW). We acknowledge access to the Jülich-Düsseldorf Biomolecular NMR Center.

Author Contributions

W.H., M.M.W., A.K.B. designed the experiments. M.M.W., H.S., Lu.G., Lo.G., and M.S. performed the experiments. M.M.W., W.H., M.S., A.K.B., D.W. analyzed and interpreted the data. M.M.W. and W.H. drafted the manuscript. All authors contributed to the submitted version of the manuscript.

Additional Information

Competing financial interests: The authors declare no competing financial interests.

2.4.7 Supplement

Contents: Supplementary Figure S1 and Supplementary Table S1 and S2.

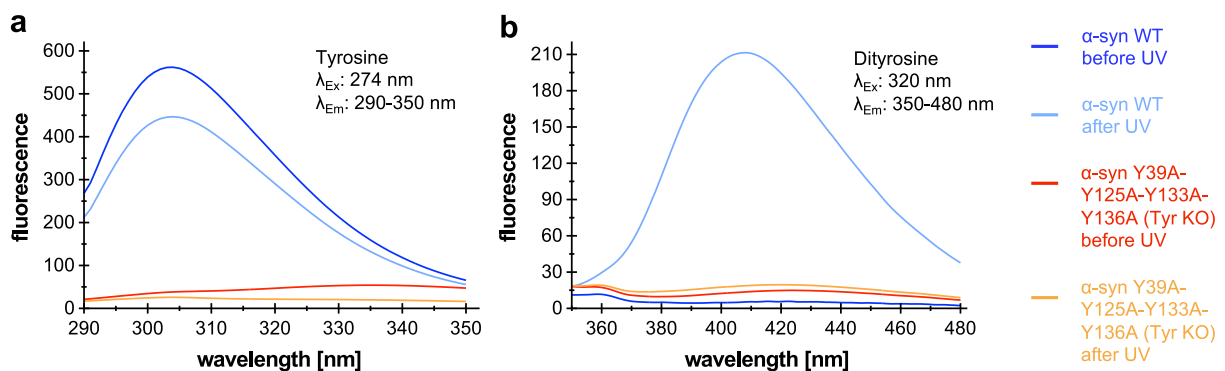


Figure 2.33: Tyrosine and DiY spectra of α -syn WT and α -syn Y39A-Y125A-Y133A-Y136A (Tyr KO) mutant before and after UV-irradiation. (a) Tyrosine spectra of WT and Tyr KO mutant before and after UV-irradiation recorded at $\lambda_{Ex} = 274$ nm and at $\lambda_{Em} = 290-350$ nm. Whereas α -syn WT shows a marked tyrosine spectrum with a peak at 303 nm that decreases $\sim 20\%$ after UV-irradiation, the Tyr KO mutant does not exhibit a marked tyrosine spectrum. (b) DiY spectra of WT and Tyr KO mutant before and after UV-irradiation recorded at $\lambda_{Ex} = 320$ nm and at $\lambda_{Em} = 350-480$ nm. α -Syn WT shows a high DiY fluorescence increase at 410 nm after UV-irradiation, the Tyr KO mutant does not show a peak at 410 nm after UV irradiation.

Table 2.4: Tyrosine and DiY fluorescence emission of α -syn variants before and after DiY formation. For the quadruple mutant, tyrosine and DiY spectra could not be measured properly because of the absence of tyrosines; n. o.: not observed.

Protein	Tyrosine fluorescence $\lambda_{\text{EX}}: 274 \text{ nm}, \lambda_{\text{EM}}: 303 \text{ nm}$			Dityrosine fluorescence $\lambda_{\text{EX}}: 320 \text{ nm}, \lambda_{\text{EM}}: 410 \text{ nm}$	
	before	after	decrease [%]	before	after
	WT	560	451	19.5	13
Y39A	376	288	23.3	6	109
Y125A	453	378	16.7	7	138
Y133A	514	410	20.2	9	136
Y136A	465	367	21.0	12	215
Y125A-Y133A	399	329	17.4	9	146
Y125A-Y136A	340	279	18.1	11	108
Y133A-Y136A	395	320	18.9	10	134
Y125A-Y133A-Y136A	243	176	27.6	5	27
Y39A-Y125A-Y133A-Y136A (Tyr KO)	n.o.	n.o.	-	n.o.	n.o.

Table 2.5: Rate constants of DiY formation in α -syn. The kinetics data was fit to a consecutive two stage reaction $A \xrightarrow{k_1} B \xrightarrow{k_2} C$. The rate constants obtained from the fit cannot be assigned to reaction steps 1 or 2 and have therefore been labeled k_m and k_n .

Protein	Rate constants	
	$k_m [\text{s}^{-1}]$	$k_n [\text{s}^{-1}]$
WT	1.67×10^4	4.01×10^{-3}
WT (monoexponential fit)	-	4.02×10^{-3}
Y39A	4.58×10^{-3}	4.58×10^{-3}
Y125A	1.01×10^{-2}	2.95×10^{-3}
Y133A	7.75×10^{-3}	3.09×10^{-3}
Y136A	2.01×10^{-2}	3.34×10^{-3}
Y125A-Y133A	1.23×10^{-2}	3.77×10^{-3}
Y125A-Y136A	1.40×10^{-2}	3.82×10^{-3}
Y133A-Y136A	2.38×10^{-2}	3.77×10^{-3}
Y125A-Y133A-Y136A	5.33×10^{-3}	1.33×10^{-3}

3 General Discussion

In this PhD thesis, several kinetic parameters of α -synuclein aggregation were determined and different factors that influence the aggregation process were disentangled. We analyzed the effects of protein modifications of α -syn on its aggregation properties, i.e. the effect of a covalent disulfide linkage of the aggregation-prone β 1- and β 2-regions in α -syn and the effect of oxidative-stress-associated intra- and intermolecular dityrosine-crosslinking. Moreover, the interaction of α -syn with different artificial lipid bilayer membrane mimetics, called nanodiscs (ND), has been studied in detail, including the consequences of interaction for aggregation.

We also gained detailistic insights into the aggregation process itself, by analyzing aggregation of α -syn by high-resolution fluorescence microscopy on a single molecule level. This *in situ* observation of aggregation in real-time enabled us to precisely determine aggregation speed in nm/min, which directly relates to the amount of attaching α -syn monomers/second (to the fibril end) and, by considering the protein concentration, yields the kinetic parameter k_{on} for α -syn fibril growth. In our case, the mean single fibril aggregation speed of α -syn averaged over 25 fibrils and 34 h proved to be around $8.5 \pm 3.7 \text{ nm min}^{-1}$, which corresponds to ~ 1.2 α -syn monomer incorporating into the fibril per second, assuming an α -syn fibril structure as proposed by Vilar et al., and a distance between β -sheets within a fibril of 0.47 nm [132, 186]. This aggregation speed results in an α -syn fibril elongation rate constant of $8.6 \times 10^3 \text{ M}^{-1} \text{ s}^{-1}$. Other high-resolution microscopy methods like atomic force microscopy (AFM) or two-color direct stochastic optical reconstruction microscopy (dSTORM) have also analyzed α -syn fibril growth and measured growth rates between 1 to 10 nm min^{-1} [57, 65]. These growth rates are within one order of magnitude with our determined growth rate of $8.5 \pm 3.7 \text{ nm min}^{-1}$, the slight variances in growth rate can e.g. be explained by different experimental conditions, e.g. different buffer/pH, protein concentration and temperature. The fibril growth rates of other amyloidogenic proteins like amyloid- β 40, glucagon, β 2-microglobulin and Sup35 are between 8 to 40-fold higher, indicating that α -syn fibril elongation is a rather slow process [21, 58, 62, 192]. In comparison to these other proteins, α -syn is a long protein of 140 amino acids which might explain that the incorporation of a monomer into the fibril takes longer.

Besides growth rates, we also observed stop phases during fibril growth, which has been observed before in comparable *in situ* experiments [57, 58, 62, 185]. Our high-resolution data enabled us to study interconversion rates between growth and stop phases in detail, based on 25 fibrils. Growth and stop phases interconverted with rates of about $1.5 \times 10^{-4} \text{ s}^{-1}$ (k_- : $1.63 \times 10^{-4} \text{ s}^{-1}$, k_+ : $1.27 \times 10^{-4} \text{ s}^{-1}$), thereby demonstrating that growth and stop phases are approximately isoenergetic. These stop phases of fibril growth have been hypothesized to result from contacts of fibrils with obstacles or surfaces like the glass surface in microscopy carriers or the surface of a mica chip for AFM [57, 58, 185] or incorporation of a templating-incompetent monomer or oligomer [185, 187]. Indeed, this might well be the case. In section 2.4 we describe the formation dityrosine (DiY)-crosslinked dimers in α -syn that potently inhibit fibril elongation in a substoichiometric fashion. A low substoichiometric ratio of 1:20 relating to DiY dimer to α -syn monomer almost completely inhibited fibril elongation (fig. 2.30b,d). The inhibitory effect

on fibril elongation is likely a sterical hindrance, when a DiY-crosslinked dimer docks to the fibril end, the dimer subunits can not both be incorporated into the fibril, so that fibril growth cannot proceed (fig. 3.1). Interestingly, van Maarschalkerweerd et al. have found that DiY-crosslinked dimers are naturally present in recombinant protein preparations of α -syn as they can form during the purification procedure, e.g. in concentration and/or gel filtration steps [309]. Incorporation of this templating-incompetent DiY dimer to the fibril end might be the explanation for our observed stop phases during fibril growth. Adding to this we showed by NMR experiments that DiY dimers (and/or intramolecularly-crosslinked DiY monomers) do not interact with wildtype α -syn monomers, indicating that the inhibitory effect on fibril elongation is indeed based on the interaction with fibrils (fig. 2.30c).

DiY-crosslinking of proteins is a process that happens in oxidative stress conditions, when proteins are exposed to reactive oxygen species such as the H_2O_2 or the hydroxyl radical ($\cdot OH$) [165]. DiY and α -syn are colocalized in the brain of PD patients, indicating that DiY-crosslinked α -syn plays a role in PD pathology [163]. We found that α -syn as an intrinsically disordered protein (IDP) has a high tendency to form dityrosine crosslinks, much more than a globular protein such as ribonuclease A (fig. 2.28). The analysis of DiY formation kinetics of several tyrosine-to-alanine mutants did not show any preference of DiY formation of certain tyrosine positions within the four tyrosines found in α -syn. This is probably because of its high structural flexibility, so all tyrosines can easily be radicalized and two tyrosyl radicals can easily find each other.

In the brain, α -Syn is highly abundant in the cytosol of neurons, e.g. up to 1.2% of total proteins is α -syn in brain regions like the striatum or the hippocampus [89]. Considering an average cytosolic protein concentration of approximately 100 to 270 mg ml⁻¹ [317], α -syn concentration in neurons is at least 1 mg ml⁻¹. The high abundance of α -syn in brain regions that exhibit increased oxidative stress conditions might indicate that oxidative (dityrosine) formation in α -syn is a probable process that happens quite often. This points to the possibility that α -syn, besides its role in synaptic trafficking, is also an antioxidant that functions as a ROS scavenger by readily reacting with hydroxyl radicals [318]. On the other hand, the coexistence of high α -syn concentrations and increased OS also demonstrates that α -syn aggregation and OS can influence each other and act together in a detrimental way that finally causes cell death [155, 319].

Indeed, we found two opposing effects when looking at DiY formation in α -syn (see section 2.4, fig. 2.32). When monomeric solutions of α -syn were irradiated with UV light, a model system of OS-associated tyrosine radicalization and subsequent DiY formation, DiY-crosslinks formed rapidly. These DiY-crosslinks in α -syn markedly inhibited the aggregation of wildtype protein (fig. 2.29a,b, fig. 2.30a,b,d), thereby showing that OS can be quenched by α -syn and that this oxidative modification prevents the toxic aggregation process. We can however not exclude that these DiY-crosslinked α -syn species are cytotoxic, as has been shown for different oxidatively modified α -syn species [162].

On the other hand, we have shown that OS-associated DiY-crosslinking of preformed α -syn aggregates has a stabilizing effect that greatly increases their resistance to dissolution (fig. 2.31a,b,c). These crosslinked aggregates still retain the ability to induce aggregation

of α -syn monomers, thereby showing that OS-associated protein modifications can have an aggregation-promoting effect (fig. 2.31d). As dityrosine and α -syn have been shown to colocalize in Lewy bodies of PD patients' brain, this DiY-stabilization of α -syn fibrils occurs naturally [163]. This indicates that stabilization of aggregation seeds by DiY-crosslinking is another hallmark of PD and can be seen as a vicious cycle of OS and aggregation that increases aggregate toxicity, as stabilized aggregates cannot be dissolved/removed.

Besides the inhibitory effect of DiY dimers on α -syn fibril elongation, we also analyzed the inhibitory effect of a certain structural conformation of α -syn, where the β 1- and β 2-regions has been stabilized by a disulfide bridge (see section 2.2). It has been shown before that certain affibody proteins called β -wrapins can bind α -syn and sequester a β -hairpin conformation spanning the β 1- and β 2-region, thereby potently inhibiting aggregation [178]. The idea of the study presented in section 2.2 was to stabilize this contact between the β 1- and β 2-fragments in α -syn by an intramolecular disulfide bridge and study its consequences for the aggregation of wildtype protein. By mutating glycine at position 41 and valine at position 48 both to cysteine, a disulfide bridge can form between these residues that takes up a comparable space as the glycine and valine residues do when locked in the β -hairpin conformation (0.56 nm vs. 0.61 nm, see fig. 2.10a) [211]. As wildtype α -syn does not contain cysteines in its sequence, disulfide bonds can only form between these two residues in the mutant which we thus denoted α -synCC. α -SynCC retained the disordered structure of wildtype α -syn, indicating that the introduced disulfide bridge did not enforce an artificial conformation in α -syn (fig. 2.10c).

The stabilized β 1- β 2-contacts in α -synCC rendered it aggregation-incompetent and inhibited not only the *de novo* aggregation of α -syn, but also the aggregation of amyloid proteins amyloid- β and IAPP substoichiometrically (fig. 2.11 a-c). α -SynCC also inhibited the seeded aggregation of wildtype α -syn (fig. 2.11 d). This effect might well be analogous to the inhibitory effect on fibril elongation that we have described for DiY dimers and DiY monomers. α -SynCC molecules might dock to the fibril end and may also partly form the β -sheet core of the fibril. However because of the sterical restraints introduced by the covalent linkage of the β 1- and β 2-fragments that are usually also part of the fibril, α -synCC can not be incorporated completely into the fibril. This process results in fibril ends that are incompetent for further monomer docking, leading to stop phases in fibril growth, which we have observed in section 2.1. Before fibril growth can proceed, the templating-incompetent monomer (or dimer in the case of DiY-crosslinking) would have to dissociate from the fibril end, a process that is on the timescale of 10 to 120 min in the case of amyloid- β [188, 189]. Considering that the aggregation of α -syn and amyloid- β *in vitro* is completely finished within 3 to 30 h (fig. 2.11 a,b), the substantial inhibitory effect of the incorporation of templating-incompetent species becomes evident.

Also, both in the case of DiY-crosslinked dimers/monomers and α -synCC, the substoichiometric inhibition of fibril elongation can easily be explained by the direct interaction of templating-incompetent species with the fibril ends. When we call this inhibition a substoichiometric effect, we compare the concentration of monomeric protein that goes into the fibrillation reaction with the concentration of the monomeric (or dimeric) inhibitor. However this is no longer a substoichiometric effect when we consider that the inhibition takes place at the fibril

end. The concentration of fibril ends is much lower than the concentration of monomeric protein that goes into the fibrillation reaction, e.g. even as low as 1/1000 of the total initial monomer concentration [43], pointing to a rather stoichiometric inhibition of fibril elongation. The effects of templating-incompetent α -syn-species like DiY dimers and α -synCC on fibril elongation are summarized in figure 3.1 (right hand side).

In relation to the aggregation-inhibiting α -synCC, we also showed that cell viability in an MTT-assay with SH-S5Y5 cells is increased when cells are treated with solutions of α -syn, amyloid- β and IAPP that have been coaggregated in the presence of α -synCC, compared to the aggregated proteins without α -synCC (fig. 2.11e-g). This not only shows that reduced aggregation is directly linked to reduced cytotoxicity, but also that molecules that dock to the fibril ends and render them templating-incompetent have the potential to prevent aggregate toxicity. Alongside other therapeutic routes to inhibit amyloid toxicity like reduction of amyloid protein production [320], stabilization of monomers/nucleation inhibitors [321] and clearance of aggregates [322], specific fibril elongation inhibitors that induce (ideally constant) stop phases in fibril growth might be another promising strategy. These fibril elongation inhibitors can be molecules that stabilize conformations of amyloid proteins that can dock to the fibril end but are then templating-incompetent. In the case of α -syn, a molecule that e.g. stabilizes non-fibrillogenic contacts between β 1- and β 2-fragments may be a promising therapeutic candidate. As we have shown a substoichiometric mode of action for fibril elongation inhibitors, they might be effective in quite low concentrations. As most amyloidoses are diseases that develop slowly and manifest in the last quarter of life (60 years plus), decreasing aggregation velocity by a factor of two might actually prevent disease onset.

Besides the detailed analysis of the α -syn aggregation process and the analysis of influencing factors related to modification of α -syn itself by DiY formation or protein engineering, we also studied the effect of an important binding partner of α -syn, i.e. lipid membranes, on its aggregation (section 2.3). In its physiological state, α -syn is in an equilibrium between a cytosolic and a membrane-associated form [83]. Therefore, its interaction with lipid membranes definitely has consequences in respect to aggregation propensity and velocity. Aggregation of α -syn in the presence of lipid membranes has been studied before *in vitro*, several membrane mimetics have been used, e.g. detergent micelles or lipid vesicles [107, 133, 236, 249]. In our study we chose lipid bilayer nanodiscs (ND) that are composed of a phospholipid bilayer surrounded by a membrane scaffold protein (MSP). NDs have several advantages over lipid vesicles, e.g. a homogenous, well defined size and membrane area [254], a high stability [253] and their lipid composition and charge can easily be modified by introducing different lipids as well as gangliosides, cholesterol and sphingomyelin [252, 255]. The size of NDs can also easily be tuned by choosing a specific MSP construct of a defined length. In contrast to lipid vesicles, NDs provide a planar lipid bilayer surface which might have a different effect on α -syn binding and aggregation than curved lipid vesicles. It has e.g. been shown, that α -syn binding remodels curved lipid vesicles, thereby forming lipoprotein particles that also coaggregate [110, 125, 257]. This might be very different for stable, planar lipid bilayer NDs.

We studied the residue-specific binding of α -syn to differently charged nanodiscs e.g. using liquid-state NMR. Therefore, the content of negatively charged 1-palmitoyl-2-oleoyl-sn-glycero-3-phosphoglycerol (POPG) was varied from 0% to 100% in 25% steps in a molar ratio of one α -syn molecule per ND bilayer side. An interaction of α -syn with nanodiscs results in a reduced residue peak intensity in NMR, i.e. a complete disappearance of residue peaks in NMR means a strong binding of these residues to nanodiscs. This disappearance of peaks due to immobilization of α -syn on the membrane surface has been used before to study the residue-resolved interaction of α -syn with vesicles [242]. We therefore analyzed binding by calculating the reduction of peak intensity over the 140 residues of α -syn in presence of NDs (fig. 2.17). At 0% negative charge, α -syn did not interact with nanodiscs at all, the NMR spectrum remained unchanged in respect to the reference spectrum without nanodiscs. At 25% negative charge, which is close to the negative charge content in physiological membranes, e.g. synaptic vesicles [323], residues 1-38 of α -syn were interacting with nanodiscs. The higher the negative charge, the more α -syn residues were bound. At 100% negative charge, α -syn residues 1-98 interacted strongly with NDs. The residue-resolved analysis of nanodisc binding lead us to the conclusion, that there are four regions in α -syn in relation to ND-binding: region one spans residues 1-38 and weakly interacts with NDs at 25% negative charge, region two comprises residues 38-60 and interacts at 50% negative charge with NDs. The aggregation-prone central NAC region of α -syn spanning residues 60-95 (region three) begins to interact with NDs at 75% charge and strongly interacts at 100% negatively-charged lipids in NDs. Region four (residues 98-120) is only weakly affected by NDs with 100% negative charge. The last 20 amino acids of α -syn never interact with NDs. This four region model fits to the three region model that has been proposed by Fusco et al. using lipid vesicles [246]. The binding of α -syn to NDs is probably facilitated by electrostatic interactions. As the first 60 residues of α -syn with its lysine-rich repeat sequences carry a positive net charge, a strong interaction with negatively-charged NDs is logical. Interestingly, the practically neutral NAC region is also strongly bound to NDs at 100% negative charge. (fig. 2.17).

We next wanted to find out how the interaction with NDs influences the aggregation kinetics of α -syn, we hypothesized for example that strong binding of the aggregation-prone NAC region of α -syn to nanodiscs would result in a prominent change in aggregation behavior. Therefore we performed Thioflavin T aggregation assays with α -syn in the presence of NDs of different charge content and also different concentrations of NDs (fig. 2.17, fig. 2.20, fig. 2.21). We found that NDs with a negative charge of 50% in a 1:1 stoichiometry with α -syn did not influence aggregation kinetics, aggregation halftimes were the same as for the wildtype protein without NDs (fig. 2.17f). This fits to the observations from the NMR experiments, where the NAC region of α -syn was still unaffected by the presence of NDs with 50% POPG, therefore aggregation can take place, although many synuclein molecules are anchored to NDs with their N-terminus. As obvious from the NMR experiments, The NAC region of α -syn starts to interact gradually with NDs of 75% negative charge. Consequently, the aggregation kinetics of α -syn begin to be affected, with slightly longer aggregation halftimes (fig. 2.17f). At 100% negative charge, aggregation of α -syn is completely inhibited in a 1:1 ratio for 140 h. This is explained by the fact

3 General Discussion

that the complete aggregation-triggering NAC region of α -syn is bound to NDs as evident from the NMR experiments (fig. 2.17c, purple). From this data we concluded that binding of α -syn to highly-negatively charged membranes with a high surface area, i.e. a high lipid-to- α -syn-ratio prevents the aggregation of α -syn. This has also been reported before in a study using small unilamellar vesicles made of the negatively-charged lipid 1,2-dimyristoyl-sn-glycero-3-phospho-L-serine (DMPS) [107].

However, this situation (100% negatively-charged lipids and a large available membrane surface area) is likely not a physiological scenario. It is much more likely that there is a limited membrane surface available for interaction. Most negatively-charged lipids of the plasma membrane (phosphatidylserine, phosphatidylinositol and phosphatidic acid) are located at the cytosolic side (inner leaflet) of the membrane, where they can interact with cytosolic proteins like α -syn [324]. A further clustering of negatively-charged lipids may result in small membrane patches with a limited interaction surface but very high charge. We therefore also tested the influence of low ND(lipid)-to- α -syn-ratios on the aggregation of α -syn. Interestingly, low ND(lipid)-to- α -syn-ratios, e.g. 1:16 or 1:64 had a stimulating effect on aggregation (fig. 2.20h). When coaggregated in the presence of small amounts of NDs with 100% negatively-charged POPG lipids, aggregation halftimes were approximately reduced by a factor of two. A 1:16 stoichiometry of 100% POPG NDs to α -syn was also the only tested condition which could induce aggregation in quiescent conditions, where α -syn aggregation is usually very slow (fig. 2.20j). A similar ambivalent effect of lipid-induced aggregation-inhibition and aggregation-stimulation, depending on the lipid-to- α -syn-ratio, has been reported before for lipid vesicles [107]. This shows that membrane curvature only plays a subordinate role when it comes to the influence on α -syn aggregation.

We think that the aggregation-triggering effect of a small, negatively-charged membrane surface area results from many α -syn molecules that cluster together on the membrane surface. The high negative charge binds α -syn molecules tightly to the membrane surface, but as the surface is only limited, they do not bind with residues 1-100 (including NAC region) as is the case when the membrane surface area is not limited. Several α -syn molecules rather bind with their very N-terminal residues on the ND surface, as their affinity for negatively-charged lipids is the highest, i.e. higher than the affinities of the NAC region residues (fig. 2.20e). When several α -syn molecules are bound on the ND surface, the NAC regions of these molecules come in close proximity to each other (fig. 2.20g, fig. 2.22). This leads to an accelerated aggregation, as nuclei form faster in this way than in solution. As a 16:1 ratio of α -syn to NDs (i.e. eight α -syn molecules per bilayer side) promotes aggregation, we deduce that eight molecules of α -syn can form a nucleus that is promoting aggregation.

In contrast to highly-charged NDs with 100% anionic POPG lipids and a limited surface, NDs with a low-to-medium charge (e.g. 50% POPG), did not show an aggregation-triggering effect, even in low ND-to- α -syn ratios (fig. 2.21e). When comparing this effect with the NMR data on the interaction of α -syn with 50% POPG NDs (fig. 2.21a), we see e.g. in the case of a 16:1 α -syn-to-ND ratio that interaction of the N-terminal residues is only transient, as approximately 50% of residue peaks are still visible. This only transient interaction does not

seem to be enough to bring the NAC region of several α -syn molecules in close proximity to each other and stimulate aggregation. Aggregation therefore seems to proceed on a longer time-scale than the transient on-off-interactions of α -syn with membranes of low-to-medium charge (fig. 2.21g).

What does this mean now in respect to α -syn's physiological function and its role in the pathogenesis of Parkinson's disease? In our study we used planar lipid bilayer mimetics to study α -syn's interaction and aggregation. Although α -syn exerts its function in synaptic vesicle trafficking and preferentially binds to small, highly-curved vesicles [83, 99], it has also been shown to bind to (rather) planar bilayers, thereby forming an extended helix conformation rather than a broken helix conformation [100]. A switching between a broken, kinked helix and extended helix has been reported before and might actually be directly related to its function, as this extension e.g. might trigger vesicle fusion/rearrangement [325]. With our highly tunable and stable planar lipid bilayer ND system we were able to reproduce the strong binding and aggregation-inhibition properties of negatively-charged lipid membranes previously reported using curved lipid vesicles [107, 236]. Our planar bilayer ND approach therefore combines the reproducibility of physiological lipid-binding features of α -syn with the advantages of NDs, e.g. in NMR experiments like small size, high stability and homogeneity, to name a few [253].

In contrast to the aggregation-inhibition and membrane interaction of α -syn in high lipid-to- α -syn ratios, the situation in Parkinson's disease pathogenesis is likely a different one, where membrane environments actually promote aggregation. It has been shown that PD is caused and/or initiated by an increased expression of α -syn or the expression of α -syn mutants that show an increased aggregation propensity and/or different lipid binding properties [4, 243]. The α -syn-to-lipid ratio therefore is likely much higher in PD patients than in healthy individuals. This would shift the effect of membrane interaction from an aggregation-inhibiting to an aggregation-promoting effect as has been observed in our study. Notably, it has recently been demonstrated that molecules that reduce membrane interaction of α -syn actually reduce cytotoxicity [273, 326]. Therefore, the combination of NMR and aggregation analysis (in high α -syn-to-lipid ratios) established with our ND system is well suited to screen and assess molecules that inhibit aggregation of α -syn in a membrane environment and subsequently reduce cytotoxicity.

Figure 3.1 summarizes selected findings of ND membrane interaction of α -syn and its consequences for aggregation (left hand side).

In conclusion, this PhD thesis with its four distinct publications unraveled several kinetic determinants and features of α -syn aggregation. Besides identifying key kinetic parameters of α -syn fibril growth on a single molecule level, we found different conformers of α -syn that potently inhibit aggregation. These conformers are either species that arise from natural oxidative modifications of α -syn (in the case of DiY dimers and monomers) or conformers that are likely within the normal structural flexibility of the IDP α -syn and can be stabilized by protein engineering (α -synCC). The identification of these efficient aggregation inhibitors harbours great potential for the finding and development of therapeutic aggregation inhibitors that e.g. exhibit their function by stabilizing aggregation-incompetent conformers of α -syn. We have also established a highly tunable and defined ND system for studying membrane interaction and aggregation of α -syn.

3 General Discussion

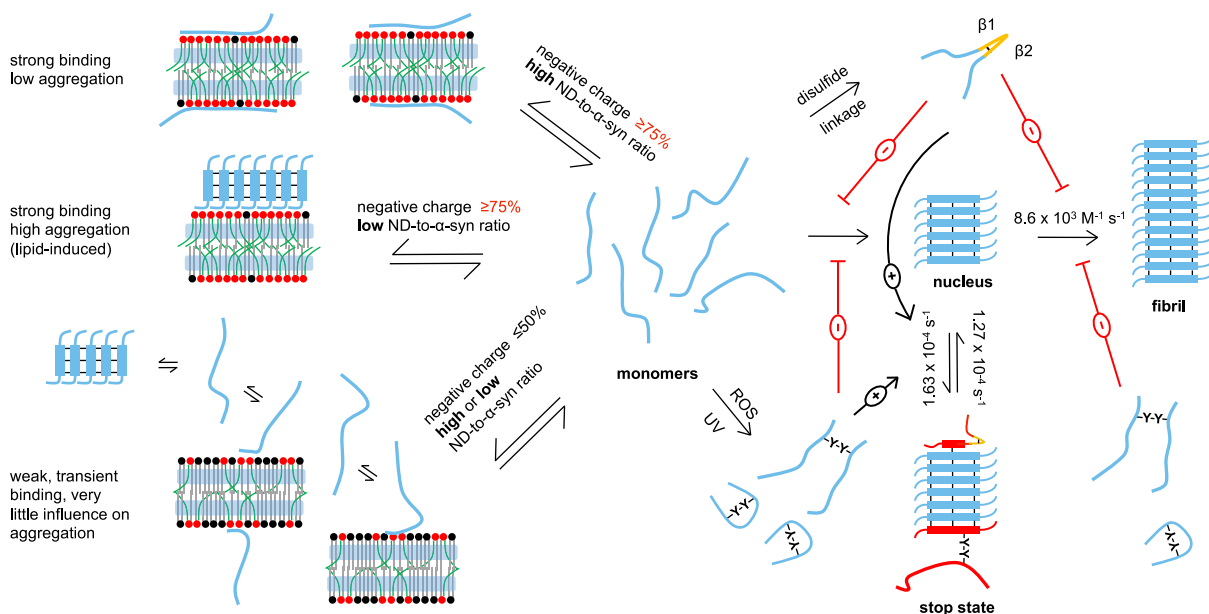


Figure 3.1: Summarizing scheme of factors that influence the aggregation kinetics of α -syn. On the right hand side, the detailed kinetics from monomers over nuclei to fibrils including stop phases are shown. Rate constants of individual steps are given beside the respective reaction arrow (see section 2.1). On the right upper side, the inhibitory effect of $\beta 1$ - $\beta 2$ -linked α -syn monomers on aggregation is shown (see section 2.2). On the right lower side, the inhibitory effect of dityrosine (dimers) on aggregation is displayed, e.g. also by leading to stop phases of fibril growth, when dityrosine dimers dock to fibril ends (see section 2.4). On the left hand side, the interaction of α -syn with lipid bilayer nanodiscs is shown. Red lipid head groups are negatively-charged, black head groups are neutral. Green fatty acid chains are oleyl-chains, grey fatty acid chains are palmitoyl- or myristoyl-chains. The membrane scaffold protein of nanodiscs (NDs) is depicted in translucent blue. Highly-negatively-charged lipid bilayer NDs can either prevent aggregation by strong binding of α -syn (residues up to 120), when there is a high lipid-to- α -syn ratio, or promote aggregation by strong binding of only the N-terminal residues of many molecules, thereby bringing a lot of aggregation-prone α -syn molecules in close proximity, when there is a low lipid-to- α -syn ratio. Low-to-medium-charged NDs only weakly and transiently interact with α -syn, thereby not exhibiting a marked effect on aggregation (see section 2.3).

Besides identifying key kinetic and thermodynamic residue-resolved properties of the α -syn-ND interaction, we were able to recapitulate the ambivalent influence of negatively-charged membranes on the aggregation of α -syn. As a reduction of α -syn-membrane interaction has been shown to reduce cytotoxicity, our ND system offers the potential to identify and assess aggregation inhibitors of α -syn in a more physiological membrane environment setting.

Bibliography

- [1] Knowles, T. P. J., Vendruscolo, M., and Dobson, C. M. The amyloid state and its association with protein misfolding diseases. *Nature Reviews Molecular Cell Biology* **15**(6), 384–396 (2014).
- [2] Naghavi, M., Wang, H., Lozano, R., et al. Global, regional, and national age–sex specific all-cause and cause-specific mortality for 240 causes of death, 1990–2013: a systematic analysis for the Global Burden of Disease Study 2013. *The Lancet* **385**(9963), 117–171, jan (2015).
- [3] Karch, C. M., Cruchaga, C., and Goate, A. M. Alzheimer’s disease genetics: From the bench to the clinic. *Neuron* **83**(1), 11–26 (2014).
- [4] Lill, C. M. Genetics of Parkinson’s disease. *Molecular and Cellular Probes* **30**(6), 386–396 (2016).
- [5] Blokhuis, A. M., Groen, E. J. N., Koppers, M., et al. Protein aggregation in amyotrophic lateral sclerosis. *Acta Neuropathologica* **125**(6), 777–794 (2013).
- [6] Walker, F. O. Huntington’s disease. *Lancet* **369**(9557), 218–228 (2007).
- [7] Hardy, J. A. and Higgins, G. A. Alzheimer’ s Disease: The Amyloid Cascade Hypothesis. *Science* **256**, 182–185 (1992).
- [8] Hartl, F. U., Bracher, A., and Hayer-Hartl, M. Molecular chaperones in protein folding and proteostasis. *Nature* **475**, 324–332 (2011).
- [9] Rubinsztein, D. C. The roles of intracellular protein-degradation pathways in neurodegeneration. *Nature* **443**(7113), 780–786 (2006).
- [10] Glickman, M. H. and Ciechanover, A. The Ubiquitin-Proteasome Proteolytic Pathway: Destruction for the Sake of Construction. *Physiological Reviews* **82**(2), 373–428 (2002).
- [11] Hipp, M. S., Park, S. H., and Hartl, U. U. Proteostasis impairment in protein-misfolding and -aggregation diseases. *Trends in Cell Biology* **24**(9), 506–514 (2014).
- [12] Bence, N. F., Sampat, R. M., and Kopito, R. R. Impairment of the ubiquitin-proteasome system by protein aggregation. *Science* **292**(5521), 1552–5 (2001).
- [13] Ivanova, M. I., Sievers, S. a., Guenther, E. L., et al. Aggregation-triggering segments of SOD1 fibril formation support a common pathway for familial and sporadic ALS. *Proceedings of the National Academy of Sciences of the United States of America* **111**(1), 197–201 (2014).
- [14] Eliezer, D., Kutluay, E., Bussell, R., et al. Conformational properties of alpha-synuclein in its free and lipid-associated states. *Journal of molecular biology* **307**(4), 1061–73 (2001).
- [15] Chiti, F. and Dobson, C. M. Amyloid formation by globular proteins under native conditions. *Nature chemical biology* **5**(1), 15–22 (2009).
- [16] Esteban-Martín, S., Silvestre-Ryan, J., Bertoncini, C. W., et al. Identification of fibril-like tertiary contacts in soluble monomeric α -synuclein. *Biophysical Journal* **105**(5), 1192–1198 (2013).
- [17] Sipe, J. D. and Cohen, A. S. Review: History of the Amyloid Fibril. *Journal of Structural Biology* **130**(2-3), 88–98 (2000).
- [18] Chiti, F. and Dobson, C. M. Protein Misfolding, Functional Amyloid, and Human Disease. *Annual Review of Biochemistry* **75**(1), 333–366 (2006).
- [19] Fowler, D. M., Koulov, A. V., Balch, W. E., et al. Functional amyloid - from bacteria to humans. *Trends in Biochemical Sciences* **32**(5), 217–224 (2007).
- [20] Jarrett, J. T. and Lansbury, P. T. Seeding "one dimensional cristallization" of amyloid: a pathogenic mechanism in Alzheimer’s disease and scrapie? *Cell* **73**, 1055–1058 (1993).
- [21] Collins, S. R., Dougllass, A., Vale, R. D., et al. Mechanism of prion propagation: Amyloid growth occurs by monomer addition. *PLoS Biology* **2**(10) (2004).

Bibliography

- [22] Cohen, S. I. A., Linse, S., Luheshi, L. M., et al. Proliferation of amyloid- β 42 aggregates occurs through a secondary nucleation mechanism. *Proceedings of the National Academy of Sciences of the United States of America* **110**(24), 9758–63 (2013).
- [23] Dubey, K., Anand, B. G., Temgire, M. K., et al. Evidence of rapid coaggregation of globular proteins during amyloid formation. *Biochemistry* **53**(51), 8001–8004 (2014).
- [24] Oskarsson, M. E., Paulsson, J. F., Schultz, S. W., et al. In vivo seeding and cross-seeding of localized amyloidosis: A molecular link between type 2 diabetes and Alzheimer disease. *American Journal of Pathology* **185**(3), 834–846 (2015).
- [25] Ogen-Shtern, N., Ben David, T., and Lederkremer, G. Z. Protein aggregation and ER stress. *Brain Research* **1648**, 658–666 (2016).
- [26] Shankar, G. M., Li, S., Mehta, T. H., et al. Amyloid-beta protein dimers isolated directly from Alzheimer's brains impair synaptic plasticity and memory. *Nature medicine* **14**(8), 837–42 (2008).
- [27] Townsend, M., Shankar, G. M., Mehta, T., et al. Effects of secreted oligomers of amyloid beta-protein on hippocampal synaptic plasticity: a potent role for trimers. *The Journal of Physiology* **572**(Pt 2), 477–92 (2006).
- [28] Cerf, E., Sarroukh, R., Tamamizu-Kato, S., et al. Antiparallel beta-sheet: a signature structure of the oligomeric amyloid beta-peptide. *The Biochemical journal* **421**(3), 415–423 (2009).
- [29] Shafir, Y., Durell, S. R., Anishkin, A., et al. Beta-barrel models of soluble amyloid beta oligomers and annular protofibrils. *Proteins: Structure, Function and Bioinformatics* **78**(16), 3458–3472 (2010).
- [30] Stroud, J. C., Liu, C., Teng, P. K., et al. Toxic fibrillar oligomers of amyloid- β have cross- β structure. *PNAS* **109**(20), 7717–7722 (2012).
- [31] Paslawski, W., Andreasen, M., Nielsen, S. B., et al. High stability and cooperative unfolding of α -synuclein oligomers. *Biochemistry* **53**(39), 6252–63 (2014).
- [32] Buchanan, L. E., Dunkelberger, E. B., Tran, H. Q., et al. Mechanism of IAPP amyloid fibril formation involves an intermediate with a transient beta-sheet. *PNAS* **110**(48), 19285–19290 (2013).
- [33] Ahmed, M., Davis, J., Aucoin, D., et al. Structural conversion of neurotoxic amyloid-beta(1-42) oligomers to fibrils. *Nature structural & molecular biology* **17**(5), 561–7 (2010).
- [34] Lashuel, H. a. and Lansbury, P. T. Are amyloid diseases caused by protein aggregates that mimic bacterial pore-forming toxins? *Quarterly reviews of biophysics* **39**(2), 167–201 (2006).
- [35] Quist, A., Doudevski, I., Lin, H., et al. Amyloid ion channels: a common structural link for protein-misfolding disease. *PNAS* **102**(30), 10427–10432 (2005).
- [36] Um, J. W., Nygaard, H. B., Heiss, J. K., et al. Alzheimer amyloid-beta oligomer bound to postsynaptic prion protein activates Fyn to impair neurons. *Nat Neurosci* **15**(9), 1227–1235 (2012).
- [37] Mairet-Coello, G., Courchet, J., Pieraut, S., et al. The CAMKK2-AMPK Kinase Pathway Mediates the Synaptotoxic Effects of A β Oligomers through Tau Phosphorylation. *Neuron* **78**(1), 94–108 (2013).
- [38] Spencer, R. K., Li, H., and Nowick, J. S. X-ray crystallographic structures of trimers and higher-order oligomeric assemblies of a peptide derived from A β 17-36. *Journal of the American Chemical Society* **136**(15), 5595–5598 (2014).
- [39] Fitzpatrick, A. W. P., Debelouchina, G. T., Bayro, M. J., et al. Atomic structure and hierarchical assembly of a cross- β amyloid fibril. *PNAS* **110**(14), 5468–5473 (2013).
- [40] Eisenberg, D. and Jucker, M. The amyloid state of proteins in human diseases. *Cell* **148**(6), 1188–1203 (2012).
- [41] Sunde, M., Serpell, L. C., Bartlam, M., et al. Common core structure of amyloid fibrils by synchrotron X-ray diffraction. *Journal of Molecular Biology* **273**(3), 729–739 (1997).
- [42] Cremades, N., Cohen, S. I. A., Deas, E., et al. Direct observation of the interconversion of normal and toxic forms of α -synuclein. *Cell* **149**(5), 1048–1059 (2012).

-
- [43] Pieri, L., Madiona, K., Bousset, L., et al. Fibrillar α -synuclein and huntingtin exon 1 assemblies are toxic to the cells. *Biophysical Journal* **102**(12), 2894–2905 (2012).
- [44] Luk, K. C., Kehm, V., Carroll, J., et al. Pathological α -synuclein transmission initiates Parkinson-like neurodegeneration in nontransgenic mice. *Science* **338**(November), 949–954 (2012).
- [45] Kfoury, N., Holmes, B. B., Jiang, H., et al. Trans-cellular propagation of Tau aggregation by fibrillar species. *Journal of Biological Chemistry* **287**(23), 19440–19451 (2012).
- [46] Münch, C., O'Brien, J., and Bertolotti, A. Prion-like propagation of mutant superoxide dismutase-1 misfolding in neuronal cells. *Proceedings of the National Academy of Sciences of the United States of America* **108**(9), 3548–53 (2011).
- [47] Kyle, R. A. Amyloidosis: A convoluted story. *British Journal of Haematology* **114**(3), 529–538 (2001).
- [48] Biancalana, M. and Koide, S. Molecular mechanism of Thioflavin-T binding to amyloid fibrils. *Biochimica et Biophysica Acta (BBA) - Proteins and Proteomics* **1804**(7), 1405–1412 (2010).
- [49] Stsiapura, V. I., Maskevich, A. A., Kuzmitsky, V. A., et al. Computational study of thioflavin T torsional relaxation in the excited state. *Journal of Physical Chemistry A* **111**(22), 4829–4835 (2007).
- [50] LeVine, H. Thioflavine T interaction with synthetic Alzheimer's disease beta-amyloid peptides: detection of amyloid aggregation in solution. *Protein science : a publication of the Protein Society* **2**(3), 404–10 (1993).
- [51] Jameson, L. P., Smith, N. W., and Dzyuba, S. V. Dye-binding assays for evaluation of the effects of small molecule inhibitors on amyloid (A β) self-assembly. *ACS Chemical Neuroscience* **3**(11), 807–819 (2012).
- [52] Hawe, A., Sutter, M., and Jiskoot, W. Extrinsic fluorescent dyes as tools for protein characterization. *Pharmaceutical Research* **25**(7), 1487–1499 (2008).
- [53] Bolognesi, B., Kumita, J. R., Barros, T. P., et al. ANS binding reveals common features of cytotoxic amyloid species. *ACS Chemical Biology* **5**(8), 735–740 (2010).
- [54] Lindgren, M. and Hammarström, P. Amyloid oligomers: Spectroscopic characterization of amyloidogenic protein states. *FEBS Journal* **277**(6), 1380–1388 (2010).
- [55] Jalili, N. and Laxminarayana, K. A review of atomic force microscopy imaging systems: Application to molecular metrology and biological sciences. *Mechatronics* **14**(8), 907–945 (2004).
- [56] Goldsberry, C., Kistler, J., Aebi, U., et al. Watching amyloid fibrils grow by time-lapse atomic force microscopy. *Journal of Molecular Biology* **285**(1), 33–39 (1999).
- [57] Hoyer, W., Cherny, D., Subramaniam, V., et al. Rapid self-assembly of α -synuclein observed by in situ atomic force microscopy. *Journal of Molecular Biology* **340**(1), 127–139 (2004).
- [58] Ban, T., Hoshino, M., Takahashi, S., et al. Direct observation of A β amyloid fibril growth and inhibition. *Journal of Molecular Biology* **344**(3), 757–767 (2004).
- [59] Ban, T. and Goto, Y. Direct Observation of Amyloid Growth Monitored by Total Internal Reflection Fluorescence Microscopy. *Methods in Enzymology* **413**, 91–102 (2006).
- [60] Ban, T., Hamada, D., Hasegawa, K., et al. Direct observation of amyloid fibril growth monitored by thioflavin T fluorescence. *Journal of Biological Chemistry* **278**(19), 16462–16465 (2003).
- [61] Andersen, C. B., Yagi, H., Manno, M., et al. Branching in amyloid fibril growth. *Biophysical Journal* **96**(4), 1529–1536 (2009).
- [62] Ferkinghoff-Borg, J., Fonslet, J., Andersen, C. B., et al. Stop-and-go kinetics in amyloid fibrillation. *Physical Review E - Statistical, Nonlinear, and Soft Matter Physics* **82**(1), 7–10 (2010).
- [63] Patil, S. M., Mehta, A., Jha, S., et al. Heterogeneous amylin fibril growth mechanisms imaged by total internal reflection fluorescence microscopy. *Biochemistry* **50**(14), 2808–2819 (2011).
- [64] Wördehoff, M. M., Bannach, O., Shaykhalishahi, H., et al. Single fibril growth kinetics of α -synuclein. *Journal of Molecular Biology* **427**(6), 1428–1435 (2015).

Bibliography

- [65] Pinotsi, D., Büll, A. K., Galvagnion, C., et al. kinetics via two-color super-resolution microscopy Direct observation of heterogeneous amyloid fibril growth kinetics via two-color super-resolution microscopy. *Nano Letters* **14**, 339–345 (2013).
- [66] Elbaz, A., Bower, J. H., Maraganore, D. M., et al. Risk tables for parkinsonism and Parkinson's disease. *Journal of Clinical Epidemiology* **55**(1), 25–31 (2002).
- [67] Parkinson, J. An essay on the shaking palsy. 1817. *The Journal of neuropsychiatry and clinical neurosciences* **14**(2), 223–36; discussion 222 (2002).
- [68] Jankovic, J. Parkinson's disease: clinical features and diagnosis. *J Neurol Neurosurg Psychiatry* **79**(1957), 368–376 (2008).
- [69] Ponsen, M. M., Stoffers, D., Booij, J., et al. Idiopathic hyposmia as a preclinical sign of Parkinson's disease. *Annals of Neurology* **56**(2), 173–181 (2004).
- [70] Schenck, C. H., Boeve, B. F., and Mahowald, M. W. Delayed emergence of a parkinsonian disorder or dementia in 81% of older men initially diagnosed with idiopathic rapid eye movement sleep behavior disorder: A 16-year update on a previously reported series. *Sleep Medicine* **14**(8), 744–748 (2013).
- [71] Obeso, J. A., Rodríguez-Oroz, M. C., Benitez-Temino, B., et al. Functional organization of the basal ganglia: Therapeutic implications for Parkinson's disease. *Movement Disorders* **23**(Suppl. 3), 548–559 (2008).
- [72] Fedorow, H., Tribl, F., Halliday, G., et al. Neuromelanin in human dopamine neurons: Comparison with peripheral melanins and relevance to Parkinson's disease. *Progress in Neurobiology* **75**(2), 109–124 (2005).
- [73] Agamanolis, D. P. Neuropathology, an illustrated interactive course for medical students and residents. <http://neuropathology-web.org/chapter9/chapter9dPD.html>. Accessed: 18.06.2017.
- [74] Holdorff, B. Friedrich Heinrich Lewy (1885 - 1950) and His Work. *Journal of the History of the Neurosciences* **11**(1), 19–28 (2002).
- [75] Spillantini, M. G., Schmidt, M. L., Lee, V. M., et al. Alpha-synuclein in Lewy bodies. *Nature* **388**(6645), 839–840 (1997).
- [76] Ishizawa, T., Mattila, P., Davies, P., et al. Colocalization of tau and α -synuclein epitopes in Lewy bodies. *Journal of Neuropathology and Experimental Neurology* **62**(4), 389–397 (2003).
- [77] Lesage, S. and Brice, A. Parkinson's disease: From monogenic forms to genetic susceptibility factors. *Human Molecular Genetics* **18**(R1), 48–59 (2009).
- [78] Nalls, M. a., Pankratz, N., Lill, C. M., et al. Large-scale meta-analysis of genome-wide association data identifies six new risk loci for Parkinson's disease. *Nature genetics* **056**(9), 1–7 (2014).
- [79] Healy, D. G., Falchi, M., O'Sullivan, S. S., et al. Phenotype, genotype, and worldwide genetic penetrance of LRRK2-associated Parkinson's disease: a case-control study. *The Lancet Neurology* **7**(7), 583–590 (2008).
- [80] Valera, E., Spencer, B., and Masliah, E. Immunotherapeutic Approaches Targeting Amyloid- β , α -Synuclein, and Tau for the Treatment of Neurodegenerative Disorders. *Neurotherapeutics* **13**(1), 179–189 (2016).
- [81] Lewitt, P. A. Levodopa for the Treatment of Parkinson's Disease. *The New England journal of medicine* **359**(23), 2468–2476 (2008).
- [82] Volkmann, J., Albanese, A., Antonini, A., et al. Selecting deep brain stimulation or infusion therapies in advanced Parkinson's disease: An evidence-based review. *Journal of Neurology* **260**(11), 2701–2714 (2013).
- [83] Burré, J., Sharma, M., and Südhof, T. C. Cell Biology and Pathophysiology of α -Synuclein. *Cold Spring Harbor Perspectives in Medicine* **a024091** (2017).
- [84] Lashuel, H. A., Overk, C. R., Oueslati, A., et al. The many faces of α -synuclein: from structure and toxicity to therapeutic target. *Nature reviews. Neuroscience* **14**(1), 38–48 (2013).
- [85] Anderson, J. P., Walker, D. E., Goldstein, J. M., et al. Phosphorylation of Ser-129 is the dominant pathological modification of α -synuclein in familial and sporadic lewy body disease. *Journal of Biological Chemistry* **281**(40), 29739–29752 (2006).

-
- [86] Oueslati, A., Fournier, M., and Lashuel, H. A. Role of post-translational modifications in modulating the structure, function and toxicity of α -synuclein. Implications for Parkinson's disease pathogenesis and therapies. *Progress in Brain Research* **183**(C), 115–145 (2010).
- [87] Hoyer, W., Cherny, D., Subramaniam, V., et al. Impact of the acidic C-terminal region comprising amino acids 109-140 on α -synuclein aggregation in vitro. *Biochemistry* **43**(51), 16233–16242 (2004).
- [88] Cabin, D. E., Shimazu, K., Murphy, D., et al. Synaptic vesicle depletion correlates with attenuated synaptic responses to prolonged repetitive stimulation in mice lacking alpha-synuclein. *The Journal of Neuroscience* **22**(20), 8797–807 (2002).
- [89] Iwai, A., Masliah, E., Yoshimoto, M., et al. The precursor protein of non-A β component of Alzheimer's disease amyloid is a presynaptic protein of the central nervous system. *Neuron* **14**(2), 467–475 (1995).
- [90] Lee, S. J., Jeon, H., and Kandror, K. V. α -Synuclein is localized in a subpopulation of rat brain synaptic vesicles. *Acta Neurobiologiae Experimentalis* **68**(4), 509–515 (2008).
- [91] Payton, J. E., Perrin, R. J., Woods, W. S., et al. Structural determinants of PLD2 inhibition by α -synuclein. *Journal of Molecular Biology* **337**(4), 1001–1009 (2004).
- [92] Dalfó, E. and Ferrer, I. α -Synuclein Binding To Rab3a in Multiple System Atrophy. *Neuroscience Letters* **380**(1-2), 170–175 (2005).
- [93] Burré, J., Sharma, M., Tsetsenis, T., et al. Alpha-synuclein promotes SNARE-complex assembly in vivo and in vitro. *Science* **329**(5999), 1663–7 (2010).
- [94] Burré, J., Sharma, M., and Südhof, T. C. α -Synuclein assembles into higher-order multimers upon membrane binding to promote SNARE. *Proceedings of the National Academy of Sciences of the United States of America* **111**(40), E4274–83 (2014).
- [95] Li, W.-W., Yang, R., Guo, J.-C., et al. Localization of alpha-synuclein to mitochondria within midbrain of mice. *Neuroreport* **18**(15), 1543–1546 (2007).
- [96] Ellis, C. E., Murphy, E. J., Mitchell, D. C., et al. Mitochondrial Lipid Abnormality and Electron Transport Chain Impairment in Mice Lacking α -Synuclein. *Molecular and Cellular Biology* **25**(22), 10190–10201 (2005).
- [97] Martin, L. J., Pan, Y., Price, A. C., et al. Parkinson's Disease α -Synuclein Transgenic Mice Develop Neuronal Mitochondrial Degeneration and Cell Death. *The Journal of Neuroscience* **26**(1), 41–50 (2006).
- [98] Theillet, F.-X., Binolfi, A., Bekei, B., et al. Structural disorder of monomeric α -synuclein persists in mammalian cells. *Nature* **530**(7588), 45–50 (2016).
- [99] Davidson, W. S., Jonas, a., Clayton, D. F., et al. Stabilization of alpha-synuclein secondary structure upon binding to synthetic membranes. *The Journal of biological chemistry* **273**(16), 9443–9 (1998).
- [100] Georgieva, E. R., Ramlall, T. F., Borbat, P. P., et al. Membrane-bound α -synuclein forms an extended helix: Long-distance pulsed ESR measurements using vesicles, bicelles, and rodlike micelles. *Journal of the American Chemical Society* **130**(39), 12856–12857 (2008).
- [101] Trexler, A. J. and Rhoades, E. α -Synuclein binds large unilamellar vesicles as an extended helix. *Biochemistry* **48**(11), 2304–2306 (2009).
- [102] Ulmer, T. S., Bax, A., Cole, N. B., et al. Structure and Dynamics of Micelle-bound Human α -Synuclein. *Journal of Biological Chemistry* **280**(10), 9595–9603 (2005).
- [103] Snead, D. and Eliezer, D. Alpha-Synuclein Function and Dysfunction on Cellular Membranes. *Experimental neurobiology* **23**(4), 292–313 (2014).
- [104] Robotta, M., Braun, P., Van Rooijen, B., et al. Direct evidence of coexisting horseshoe and extended helix conformations of membrane-bound alpha-Synuclein. *ChemPhysChem* **12**(2), 267–269 (2011).
- [105] Rhoades, E., Ramlall, T. F., Webb, W. W., et al. Quantification of alpha-synuclein binding to lipid vesicles using fluorescence correlation spectroscopy. *Biophysical journal* **90**(12), 4692–700 (2006).

Bibliography

- [106] Jo, E., McLaurin, J., Yip, C. M., et al. α -Synuclein membrane interactions and lipid specificity. *Journal of Biological Chemistry* **275**(44), 34328–34334 (2000).
- [107] Galvagnion, C., Buell, A. K., Meisl, G., et al. Lipid vesicles trigger α -synuclein aggregation by stimulating primary nucleation. *Nature chemical biology* **11**(3), 229–234 (2015).
- [108] Galvagnion, C., Brown, J. W. P., Ouberai, M. M., et al. Chemical properties of lipids strongly affect the kinetics of the membrane-induced aggregation of α -synuclein. *Proceedings of the National Academy of Sciences of the United States of America* **113**(26), 7065–70 (2016).
- [109] Westphal, C. H. and Chandra, S. S. Monomeric synucleins generate membrane curvature. *Journal of Biological Chemistry* **288**(3), 1829–1840 (2013).
- [110] Ouberai, M. M., Wang, J., Swann, M. J., et al. α -Synuclein senses lipid packing defects and induces lateral expansion of lipids leading to membrane remodeling. *Journal of Biological Chemistry* **288**(29), 20883–20895 (2013).
- [111] Reynolds, N. P., Soragni, A., Rabe, M., et al. Mechanism of membrane interaction and disruption by α -synuclein. *Journal of the American Chemical Society* **133**(48), 19366–19375 (2011).
- [112] Danzer, K. M., Haasen, D., Karow, A. R., et al. Different species of α -synuclein oligomers induce calcium influx and seeding. *Journal of Neuroscience* **27**(34), 9220–9232 (2007).
- [113] Nakamura, K., Nemani, V. M., Azarbal, F., et al. Direct membrane association drives mitochondrial fission by the Parkinson disease-associated protein α -synuclein. *Journal of Biological Chemistry* **286**(23), 20710–20726 (2011).
- [114] Li, J., Uversky, V. N., and Fink, A. L. Effect of familial Parkinson's disease point mutations A30P and A53T on the structural properties, aggregation, and fibrillation of human α -synuclein. *Biochemistry* **40**(38), 11604–11613 (2001).
- [115] Conway, K. a., Lee, S. J., Rochet, J. C., et al. Acceleration of oligomerization, not fibrillization, is a shared property of both α -synuclein mutations linked to early-onset Parkinson's disease: implications for pathogenesis and therapy. *Proceedings of the National Academy of Sciences of the United States of America* **97**(2), 571–576 (2000).
- [116] Pandey, N., Schmidt, R. E., and Galvin, J. E. The alpha-synuclein mutation E46K promotes aggregation in cultured cells. *Experimental Neurology* **197**(2), 515–520 (2006).
- [117] Eriksen, J. L., Przedborski, S., and Petrucelli, L. Gene dosage and pathogenesis of Parkinson's disease. *Trends in Molecular Medicine* **11**(3), 91–96 (2005).
- [118] Ferese, R., Modugno, N., Campopiano, R., et al. Four Copies of SNCA Responsible for Autosomal Dominant Parkinson's Disease in Two Italian Siblings. *Parkinson's Disease* **2015** (2015).
- [119] Oueslati, A., Paleologou, K. E., Schneider, B. L., et al. Mimicking Phosphorylation at Serine 87 Inhibits the Aggregation of Human α -Synuclein and Protects against Its Toxicity in a Rat Model of Parkinson's Disease. *Journal of Neuroscience* **32**(5), 1536–1544 (2012).
- [120] Stefanis, L., Larsen, K. E., Rideout, H. J., et al. Expression of A53T mutant but not wild-type α -synuclein in PC12 cells induces alterations of the ubiquitin-dependent degradation system, loss of dopamine release, and autophagic cell death. *The Journal of Neuroscience* **21**(24), 9549–60 (2001).
- [121] Smith, W. W., Jiang, H., Pei, Z., et al. Endoplasmic reticulum stress and mitochondrial cell death pathways mediate A53T mutant alpha-synuclein-induced toxicity. *Human Molecular Genetics* **14**(24), 3801–3811, oct (2005).
- [122] Gosavi, N., Lee, H. J., Lee, J. S., et al. Golgi fragmentation occurs in the cells with prefibrillar α -synuclein aggregates and precedes the formation of fibrillar inclusion. *Journal of Biological Chemistry* **277**(50), 48984–48992 (2002).
- [123] Tosatto, L., Andrichetti, A. O., Plotegher, N., et al. Alpha-synuclein pore forming activity upon membrane association. *Biochimica et Biophysica Acta (BBA) - Biomembranes* **1818**(11), 2876–2883, nov (2012).

-
- [124] Kim, H.-Y., Cho, M.-K., Kumar, A., et al. Structural Properties of Pore-Forming Oligomers of α -Synuclein. *Journal of the American Chemical Society* **131**(47), 17482–17489, dec (2009).
- [125] Hellstrand, E., Nowacka, A., Topgaard, D., et al. Membrane Lipid Co-Aggregation with α -Synuclein Fibrils. *PLoS ONE* **8**(10), e77235, oct (2013).
- [126] Karpinar, D. P., Balija, M. B. G., Kügler, S., et al. Pre-fibrillar alpha-synuclein variants with impaired beta-structure increase neurotoxicity in Parkinson's disease models. *The EMBO journal* **28**(20), 3256–68, oct (2009).
- [127] Winner, B., Jappelli, R., Maji, S. K., et al. In vivo demonstration that alpha-synuclein oligomers are toxic. *Proceedings of the National Academy of Sciences of the United States of America* **108**(10), 4194–9, mar (2011).
- [128] Chen, S. W., Drakulic, S., Deas, E., et al. Structural characterization of toxic oligomers that are kinetically trapped during α -synuclein fibril formation. *Proceedings of the National Academy of Sciences of the United States of America* **112**(16), E1994–2003, apr (2015).
- [129] Volpicelli-Daley, L. A., Luk, K. C., Patel, T. P., et al. Exogenous α -synuclein fibrils induce Lewy body pathology leading to synaptic dysfunction and neuron death. *Neuron* **72**(1), 57–71, oct (2011).
- [130] Masuda-Suzukake, M., Nonaka, T., Hosokawa, M., et al. Prion-like spreading of pathological α -synuclein in brain. *Brain* **136**(4), 1128–38, apr (2013).
- [131] Giehm, L., Svergun, D. I., Otzen, D. E., et al. Low-resolution structure of a vesicle disrupting α -synuclein oligomer that accumulates during fibrillation. *Proceedings of the National Academy of Sciences of the United States of America* **108**(8), 3246–51, feb (2011).
- [132] Vilar, M., Chou, H.-T., Lührs, T., et al. The fold of alpha-synuclein fibrils. *Proceedings of the National Academy of Sciences of the United States of America* **105**(25), 8637–42 (2008).
- [133] Comellas, G., Lemkau, L. R., Zhou, D. H., et al. Structural intermediates during alpha-synuclein fibrillogenesis on phospholipid vesicles. *Journal of the American Chemical Society* **134**, 5090–5099 (2012).
- [134] Tuttle, M. D., Comellas, G., Nieuwkoop, A. J., et al. Solid-state NMR structure of a pathogenic fibril of full-length human α -synuclein. *Nature structural & molecular biology* **23**(5), 409–15, may (2016).
- [135] Heise, H., Hoyer, W., Becker, S., et al. Molecular-level secondary structure, polymorphism, and dynamics of full-length alpha-synuclein fibrils studied by solid-state NMR. *Proceedings of the National Academy of Sciences of the United States of America* **102**(44), 15871–15876 (2005).
- [136] Tuttle, M. D., Comellas, G., Nieuwkoop, A. J., et al. Solid-state NMR structure of a pathogenic fibril of full-length human α -synuclein. *Nature Structural & Molecular Biology* **23**(February), 1–9 (2016).
- [137] Giehm, L., Lorenzen, N., and Otzen, D. E. Assays for α -synuclein aggregation. *Methods* **53**(3), 295–305, mar (2011).
- [138] Gaspar, R., Meisl, G., Buell, A. K., et al. Secondary nucleation of monomers on fibril surface dominates α -synuclein aggregation and provides autocatalytic amyloid amplification. *Quarterly Reviews of Biophysics* **50**, 1–12 (2017).
- [139] Shaykhalishahi, H., Gauhar, A., Wördehoff, M. M., et al. Contact between the β 1 and β 2 Segments of α -Synuclein that Inhibits Amyloid Formation. *Angewandte Chemie - International Edition* **54**(30), 8837–8840 (2015).
- [140] Hoyer, W., Antony, T., Cherny, D., et al. Dependence of α -Synuclein aggregate morphology on solution conditions. *Journal of Molecular Biology* **322**(2), 383–393, sep (2002).
- [141] Uversky, V. N., Li, J., and Fink, A. L. Metal-triggered structural transformations, aggregation, and fibrillation of human α -synuclein. *Journal of Biological Chemistry* **276**(47), 44284–44296 (2001).
- [142] Antony, T., Hoyer, W., Cherny, D., et al. Cellular polyamines promote the aggregation of α -synuclein. *Journal of Biological Chemistry* **278**(5), 3235–3240 (2003).

Bibliography

- [143] Blesa, J., Trigo-Damas, I., Quiroga-Varela, A., et al. Oxidative stress and Parkinson's disease. *Frontiers in Neuroanatomy* **9**(July), 1–9 (2015).
- [144] Muñoz, P., Huenchuguala, S., Paris, I., et al. Dopamine oxidation and autophagy. *Parkinson's Disease* **2012** (2012).
- [145] Hermida-Ameijeiras, Á., Méndez-Álvarez, E., Sánchez-Iglesias, S., et al. Autoxidation and MAO-mediated metabolism of dopamine as a potential cause of oxidative stress: Role of ferrous and ferric ions. *Neurochemistry International* **45**(1), 103–116 (2004).
- [146] Lan, A. P., Chen, J., Chai, Z. F., et al. The neurotoxicity of iron, copper and cobalt in Parkinson's disease through ROS-mediated mechanisms. *BioMetals* **29**(4), 665–678 (2016).
- [147] Dias, V., Junn, E., and Mouradian, M. M. The Role of Oxidative Stress in Parkinson's Disease. *Journal of Parkinson's Disease* **3**(4), 461–491 (2013).
- [148] Winklhofer, K. F. and Haass, C. Mitochondrial dysfunction in Parkinson's disease. *Biochimica et Biophysica Acta (BBA) - Molecular Basis of Disease* **1802**(1), 29–44, jan (2010).
- [149] Smeyne, R. J. and Jackson-Lewis, V. The MPTP model of Parkinson's disease. *Molecular Brain Research* **134**(1), 57–66 (2005).
- [150] Narendra, D., Walker, J. E., and Youle, R. Mitochondrial quality control mediated by PINK1 and Parkin: Links to parkinsonism. *Cold Spring Harbor Perspectives in Biology* **4**(11) (2012).
- [151] Kahle, P. J., Waak, J., and Gasser, T. DJ-1 and prevention of oxidative stress in Parkinson's disease and other age-related disorders. *Free Radical Biology and Medicine* **47**(10), 1354–1361 (2009).
- [152] West, A. B., Moore, D. J., Biskup, S., et al. Parkinson's disease-associated mutations in leucine-rich repeat kinase 2 augment kinase activity. *Proceedings of the National Academy of Sciences of the United States of America* **102**(46), 16842–16847 (2005).
- [153] Heo, H. Y., Park, J. M., Kim, C. H., et al. LRRK2 enhances oxidative stress-induced neurotoxicity via its kinase activity. *Experimental Cell Research* **316**(4), 649–656 (2010).
- [154] Nguyen, H. N., Byers, B., Cord, B., et al. LRRK2 mutant iPSC-derived da neurons demonstrate increased susceptibility to oxidative stress. *Cell Stem Cell* **8**(3), 267–280 (2011).
- [155] Junn, E. and Mouradian, M. M. Human α -Synuclein over-expression increases intracellular reactive oxygen species levels and susceptibility to dopamine. *Neuroscience Letters* **320**(3), 146–150 (2002).
- [156] Lotharius, J. and Brundin, P. Pathogenesis of parkinson's disease: dopamine, vesicles and α -synuclein. *Nature Reviews Neuroscience* **3**(12), 932–942 (2002).
- [157] Parihar, M. S., Parihar, A., Fujita, M., et al. Mitochondrial association of alpha-synuclein causes oxidative stress. *Cellular and Molecular Life Sciences* **65**(7-8), 1272–1284 (2008).
- [158] Su, X., Maguire-Zeiss, K. A., Giuliano, R., et al. Synuclein activates microglia in a model of Parkinson's disease. *Neurobiology of Aging* **29**(11), 1690–1701 (2008).
- [159] Paxinou, E., Chen, Q., Weisse, M., et al. Induction of α -Synuclein Aggregation by Intracellular Nitritive Insult. *The Journal of Neuroscience* **21**(20), 8053–61 (2001).
- [160] Conway, K. A., Rochet, J. C., Bieganski, R. M., et al. Kinetic Stabilization of the α -Synuclein Protofibril by a Dopamine- α -Synuclein Adduct. *Science* **294**(5545), 1346–9, nov (2001).
- [161] Krishnan, S., Chi, E. Y., Wood, S. J., et al. Oxidative dimer formation is the critical rate-limiting step for Parkinson's disease alpha-synuclein fibrillogenesis. *Biochemistry* **42**(3), 829–837 (2003).
- [162] Borsarelli, C. D., Falomir-Lockhart, L. J., Ostatná, V., et al. Biophysical properties and cellular toxicity of covalent crosslinked oligomers of α -synuclein formed by photoinduced side-chain tyrosyl radicals. *Free Radical Biology and Medicine* **53**(4), 1004–1015 (2012).
- [163] Al-Hilaly, Y. K., Biasetti, L., Blakeman, B. J. F., et al. The involvement of dityrosine crosslinking in α -synuclein assembly and deposition in Lewy Bodies in Parkinson's disease. *Scientific Reports* **6**(December), 39171 (2016).

-
- [164] Stadtman, E. R. Protein oxidation and aging. *Free Radical Research* **40**(12), 1250–1258 (2006).
- [165] Malencik, D. A. and Anderson, S. R. Dityrosine as a product of oxidative stress and fluorescent probe. *Amino Acids* **25**(3-4), 233–247 (2003).
- [166] Giulivi, C. and Davies, K. [39] Dityrosine: A Marker for Oxidatively Modified Proteins and Selective Proteolysis. *Methods in Enzymology* **233**, 363–371 (1994).
- [167] Lehrer, S. S. and Fasman, G. D. Ultraviolet irradiation effects in poly-L-tyrosine and model compounds. Identification of bityrosine as a photoproduct. *Biochemistry* **6**(3), 757–67 (1967).
- [168] Malencik, D. A. and Anderson, S. R. Dityrosine formation in calmodulin. *Biochemistry* **26**(3), 695–704, feb (1987).
- [169] Malencik, D. a. and Anderson, S. R. Dityrosine formation in calmodulin: conditions for intermolecular cross-linking. *Biochemistry* **33**(45), 13363–72, nov (1994).
- [170] Correia, M., Neves-Petersen, M. T., Jeppesen, P. B., et al. UV-Light Exposure of Insulin: Pharmaceutical Implications upon Covalent Insulin Dityrosine Dimerization and Disulphide Bond Photolysis. *PLoS ONE* **7**(12) (2012).
- [171] Dalsgaard, T. K., Nielsen, J. H., Brown, B. E., et al. Dityrosine, 3,4-dihydroxyphenylalanine (DOPA), and radical formation from tyrosine residues on milk proteins with globular and flexible structures as a result of riboflavin-mediated photo-oxidation. *Journal of Agricultural and Food Chemistry* **59**(14), 7939–7947 (2011).
- [172] Karam, L. R., Dizdaroglu, M., and Simic, M. G. OH radical-induced products of tyrosine peptides. *Int J Radiat Biol Relat Stud Phys Chem Med* **46**(6), 715–724 (1984).
- [173] Al-Hilaly, Y. K., Williams, T. L., Stewart-Parker, M., et al. A central role for dityrosine crosslinking of Amyloid-beta in Alzheimer's disease. *Acta neuropathologica communications* **1**, 83 (2013).
- [174] Souza, J. M., Giasson, B. I., Chen, Q., et al. Dityrosine cross-linking promotes formation of stable α -synuclein polymers: Implication of nitrative and oxidative stress in the pathogenesis of neurodegenerative synucleinopathies. *Journal of Biological Chemistry* **275**(24), 18344–18349 (2000).
- [175] Norris, E. H., Giasson, B. I., Ischiropoulos, H., et al. Effects of oxidative and nitrative challenges on α -synuclein fibrillogenesis involve distinct mechanisms of protein modifications. *Journal of Biological Chemistry* **278**(29), 27230–27240 (2003).
- [176] Ruf, R. A. S., Lutz, E. A., Zigoneanu, I. G., et al. α -Synuclein conformation affects its tyrosine-dependent oxidative aggregation. *Biochemistry* **47**(51), 13604–13609 (2008).
- [177] Dehay, B., Bourdenx, M., Gorry, P., et al. Targeting α -synuclein for treatment of Parkinson's disease: Mechanistic and therapeutic considerations. *The Lancet Neurology* **14**(8), 855–866 (2015).
- [178] Mirecka, E. A., Shaykhalishahi, H., Gauhar, A., et al. Sequestration of a β -hairpin for control of α -synuclein aggregation. *Angewandte Chemie - International Edition* **53**(16), 4227–4230 (2014).
- [179] Frare, E., Mossuto, M. F., Polverino de Laureto, P., et al. Identification of the Core Structure of Lysozyme Amyloid Fibrils by Proteolysis. *Journal of Molecular Biology* **361**(3), 551–561 (2006).
- [180] Masters, C. L., Simms, G., Weinman, N. A., et al. Amyloid plaque core protein in Alzheimer disease and Down syndrome. *Proceedings of the National Academy of Sciences of the United States of America* **82**(12), 4245–9 (1985).
- [181] Ross, C. A. and Poirier, M. A. Protein aggregation and neurodegenerative disease. *Nature Medicine* **10**(7), S10–S17 (2004).
- [182] Lundblad, M., Decressac, M., Mattsson, B., et al. Impaired neurotransmission caused by overexpression of α -synuclein in nigral dopamine neurons. *Proceedings of the National Academy of Sciences of the United States of America* **109**(9), 3213–9 (2012).
- [183] Lang, A. E. and Lozano, A. M. Parkinson's disease: First of Two Parts. *The New England Journal of Medicine* **339**(15), 1044–1053 (1998).

Bibliography

- [184] Groenning, M. Binding mode of Thioflavin T and other molecular probes in the context of amyloid fibril-current status. *Journal of Chemical Biology* **3**(1), 1–18 (2010).
- [185] Kellermayer, M. S. Z., Karsai, A., Benke, M., et al. Stepwise dynamics of epitaxially growing single amyloid fibrils. *Proceedings of the National Academy of Sciences of the United States of America* **105**(1), 141–4 (2008).
- [186] Serpell, L. C., Berriman, J., Jakes, R., et al. Fiber diffraction of synthetic alpha-synuclein filaments shows amyloid-like cross-beta conformation. *Proceedings of the National Academy of Sciences of the United States of America* **97**(9), 4897–4902 (2000).
- [187] Ogi, H., Fukukushima, M., Hamada, H., et al. Ultrafast propagation of β -amyloid fibrils in oligomeric cloud. *Scientific reports* **4**, 6960 (2014).
- [188] Esler, W. P., Stimson, E. R., Jennings, J. M., et al. Alzheimer's disease amyloid propagation by a template-dependent dock-lock mechanism. *Biochemistry* **39**(21), 6288–6295 (2000).
- [189] Grüning, C. S. R., Klinker, S., Wolff, M., et al. The off-rate of monomers dissociating from amyloid- β protofibrils. *Journal of Biological Chemistry* **288**(52), 37104–37111 (2013).
- [190] Narayan, P., Orte, A., Clarke, R. W., et al. The extracellular chaperone clusterin sequesters oligomeric forms of the amyloid- β 1-40 peptide. *Nature Structural & Molecular Biology* **19**(1), 79–83 (2012).
- [191] Qiang, W., Kelley, K., and Tycko, R. Polymorph-specific kinetics and thermodynamics of β -amyloid fibril growth. *Journal of the American Chemical Society* **135**(18), 6860–6871 (2013).
- [192] Xue, W. F. and Radford, S. E. An imaging and systems modeling approach to fibril breakage enables prediction of amyloid behavior. *Biophysical Journal* **105**(12), 2811–2819 (2013).
- [193] Baldwin, A. J., Knowles, T. P. J., Tartaglia, G. G., et al. Metastability of native proteins and the phenomenon of amyloid formation. *Journal of the American Chemical Society* **133**(36), 14160–14163 (2011).
- [194] Der-Sarkissian, A., Jao, C. C., Chen, J., et al. Structural organization of α -synuclein fibrils studied by site-directed spin labeling. *Journal of Biological Chemistry* **278**(39), 37530–37535 (2003).
- [195] Hall, D., Hirota, N., and Dobson, C. M. A toy model for predicting the rate of amyloid formation from unfolded protein. *Journal of Molecular Biology* **351**(1), 195–205 (2005).
- [196] Lee, C. F., Loken, J., Jean, L., et al. Elongation dynamics of amyloid fibrils: A rugged energy landscape picture. *Physical Review E - Statistical, Nonlinear, and Soft Matter Physics* **80**(4), 1–6 (2009).
- [197] Murray, I. V. J., Giasson, B. I., Quinn, S. M., et al. C-terminal truncation: Role of alpha-synuclein carboxy-terminus on fibril formation in vitro. *Biochemistry* **42**(28), 8530–8540 (2003).
- [198] Burré, J., Vivona, S., Diao, J., et al. Properties of native brain α -synuclein. *Nature* **477**(2011), 107–110 (2013).
- [199] Fauvet, B., Mbefo, M. K., Fares, M. B., et al. α -Synuclein in central nervous system and from erythrocytes, mammalian cells, and *Escherichia coli* exists predominantly as disordered monomer. *Journal of Biological Chemistry* **287**(19), 15345–15364 (2012).
- [200] Bertoncini, C. W., Jung, Y.-S., Fernandez, C. O., et al. Release of long-range tertiary interactions potentiates aggregation of natively unstructured alpha-synuclein. *Proceedings of the National Academy of Sciences of the United States of America* **102**(5), 1430–5 (2005).
- [201] Dedmon, M. M., Lindorff-Larsen, K., Christodoulou, J., et al. Mapping long-range interactions in α -synuclein using spin-label NMR and ensemble molecular dynamics simulations. *Journal of the American Chemical Society* **127**(2), 476–477 (2005).
- [202] Lee, J. C., Langen, R., Hummel, P. A., et al. Alpha-Synuclein structures from fluorescence energy-transfer kinetics: Implications for the role of the protein in Parkinson's disease. *Proceedings of the National Academy of Sciences* **101**(47), 16466–16471 (2004).
- [203] Nath, A., Sammalkorpi, M., Dewitt, D. C., et al. The conformational ensembles of α -synuclein and tau: Combining single-molecule FRET and simulations. *Biophysical Journal* **103**(9), 1940–1949 (2012).

-
- [204] Ullman, O., Fisher, C. K., and Stultz, C. M. Explaining the structural plasticity of α -synuclein. *Journal of the American Chemical Society* **133**(48), 19536–19546 (2011).
- [205] Waxman, E. A., Mazzulli, J. R., and Giasson, B. I. Characterization of hydrophobic residue requirements for α -synuclein fibrillization. *Biochemistry* **48**(40), 9427–9436 (2009).
- [206] Chen, M., Margittai, M., Chen, J., et al. Investigation of α -synuclein fibril structure by site-directed spin labeling. *Journal of Biological Chemistry* **282**(34), 24970–24979 (2007).
- [207] Comellas, G., Lemkau, L. R., Nieuwkoop, A. J., et al. Structured regions of α -Synuclein fibrils include the early-onset Parkinson's disease mutation sites. *Journal of Molecular Biology* **411**(4), 881–895 (2011).
- [208] Ghosh, D., Sahay, S., Ranjan, P., et al. The newly discovered Parkinsons disease associated finnish mutation (A53E) attenuates α -synuclein aggregation and membrane binding. *Biochemistry* **53**(41), 6419–6421 (2014).
- [209] Paslawski, W., Mysling, S., Thomsen, K., et al. Co-existence of two different α -synuclein oligomers with different core structures determined by hydrogen/deuterium exchange mass spectrometry. *Angewandte Chemie - International Edition* **53**(29), 7560–7563 (2014).
- [210] Guo, J. L., Covell, D. J., Daniels, J. P., et al. Distinct α -synuclein strains differentially promote tau inclusions in neurons. *Cell* **154**(1), 103–117 (2013).
- [211] Schmidt, B., Ho, L., and Hogg, P. J. Allosteric Disulfide Bonds. *Biochemistry* **45**(24), 7429–7433 (2006).
- [212] Harpaz, Y., Gerstein, M., and Chothia, C. Volume changes on protein folding. *Structure* **2**(7), 641–649 (1994).
- [213] Lendel, C., Bjerring, M., Dubnovitsky, A., et al. A hexameric peptide barrel as building block of amyloid- β protofibrils. *Angewandte Chemie - International Edition* **53**(47), 12756–12760 (2014).
- [214] Sandberg, A., Luheshi, L. M., Sollvander, S., et al. Stabilization of neurotoxic Alzheimer amyloid- oligomers by protein engineering. *Proceedings of the National Academy of Sciences* **107**(35), 15595–15600 (2010).
- [215] Kyte, J. and Doolittle, R. F. A simple method for displaying the hydrophatic character of a protein. *Journal of Molecular Biology* **157**(1), 105–132 (1982).
- [216] Macao, B., Hoyer, W., Sandberg, A., et al. Recombinant amyloid beta-peptide production by coexpression with an affibody ligand. *BMC biotechnology* **8**, 82 (2008).
- [217] Andreetto, E., Yan, L. M., Taterek-Nossol, M., et al. Identification of hot regions of the A β -IAPP Interaction interface as high-affinity binding sites in both cross- and self-association. *Angewandte Chemie - International Edition* **49**(17), 3081–3085 (2010).
- [218] Serrano-pozo, A., Frosch, M. P., Masliah, E., et al. Neuropathological Alterations in Alzheimer Disease. *Cold Spring Harbor Perspectives in Medicine* **1**(a006189), 1–24 (2011).
- [219] Jackson, K., Barisone, G. A., Diaz, E., et al. Amylin deposition in the brain: A second amyloid in Alzheimer disease? *Annals of Neurology* **74**(4), 517–526 (2013).
- [220] Park, S. M., Jung, H. Y., Kim, T. D., et al. Distinct roles of the N-terminal-binding domain and the C-terminal-solubilizing domain of α -synuclein, a molecular chaperone. *Journal of Biological Chemistry* **277**(32), 28512–28520 (2002).
- [221] Souza, J. M., Giasson, B. I., Lee, V. M., et al. Chaperone-like activity of synucleins. *FEBS Lett* **474**(1), 116–119 (2000).
- [222] Härd, T. and Lendel, C. Inhibition of amyloid formation. *Journal of Molecular Biology* **421**(4-5), 441–465 (2012).
- [223] Jiang, C. and Chang, J. Y. Isomers of human α -synuclein stabilized by disulfide bonds exhibit distinct structural and aggregative properties. *Biochemistry* **46**(2), 602–609 (2007).
- [224] Walsh, D. M., Thulin, E., Minogue, A. M., et al. A facile method for expression and purification of the Alzheimer's disease-associated amyloid β -peptide. *FEBS Journal* **276**(5), 1266–1281 (2009).
- [225] Roberts, A. N., Leighton, B., Todd, J. A., et al. Molecular and functional characterization of amylin, a peptide associated with type 2 diabetes mellitus. *Proc Natl Acad Sci U S A* **86**(24), 9662–9666 (1989).

Bibliography

- [226] Solyom, Z., Schwarten, M., Geist, L., et al. BEST-TROSY experiments for time-efficient sequential resonance assignment of large disordered proteins. *Journal of Biomolecular NMR* **55**(4), 311–321 (2013).
- [227] Delaglio, F., Grzesiek, S., Vuister, G. W., et al. NMRPipe: A multidimensional spectral processing system based on UNIX pipes. *Journal of Biomolecular NMR* **6**(3), 277–293 (1995).
- [228] Vranken, W. F., Boucher, W., Stevens, T. J., et al. The CCPN data model for NMR spectroscopy: Development of a software pipeline. *Proteins: Structure, Function and Genetics* **59**(4), 687–696 (2005).
- [229] Kjaergaard, M. and Poulsen, F. M. Sequence correction of random coil chemical shifts: Correlation between neighbor correction factors and changes in the Ramachandran distribution. *Journal of Biomolecular NMR* **50**(2), 157–165 (2011).
- [230] Kjaergaard, M., Brander, S., and Poulsen, F. M. Random coil chemical shift for intrinsically disordered proteins: Effects of temperature and pH. *Journal of Biomolecular NMR* **49**(2), 139–149 (2011).
- [231] Jucker, M. and Walker, L. C. Self-propagation of pathogenic protein aggregates in neurodegenerative diseases. *Nature* **501**(7465), 45–51 (2013).
- [232] Gitler, A. D., Bevis, B. J., Shorter, J., et al. The Parkinson's disease protein alpha-synuclein disrupts cellular Rab homeostasis. *Proceedings of the National Academy of Sciences of the United States of America* **105**(1), 145–50 (2008).
- [233] Bellani, S., Sousa, V. L., Ronzitti, G., et al. The regulation of synaptic function by α -synuclein. *Communicative & Integrative Biology* **3**(2), 106–109 (2010).
- [234] Diao, J., Burré, J., Vivona, S., et al. Native α -synuclein induces clustering of synaptic-vesicle mimics via binding to phospholipids and synaptobrevin-2/VAMP2. *eLife* **2013**(2), 1–17 (2013).
- [235] Fusco, G., Pape, T., Stephens, A. D., et al. Structural basis of synaptic vesicle assembly promoted by α -synuclein. *Nature communications* **7**, 12563 (2016).
- [236] Zhu, M., Li, J., and Fink, A. L. The association of α -synuclein with membranes affects bilayer structure, stability, and fibril formation. *Journal of Biological Chemistry* **278**(41), 40186–40197 (2003).
- [237] Dikiy, I. and Eliezer, D. Folding and misfolding of alpha-synuclein on membranes. *Biochimica et Biophysica Acta - Biomembranes* **1818**(4), 1013–1018 (2012).
- [238] Butterfield, S. M. and Lashuel, H. A. Amyloidogenic protein-membrane interactions: Mechanistic insight from model systems. *Angewandte Chemie - International Edition* **49**(33), 5628–5654 (2010).
- [239] Auluck, P. K., Caraveo, G., and Lindquist, S. α -Synuclein: Membrane Interactions and Toxicity in Parkinson's Disease. *Annu. Rev. Cell Dev. Biol* **26**, 211–33 (2010).
- [240] Nemani, V. M., Lu, W., Berge, V., et al. Increased Expression of α -Synuclein Reduces Neurotransmitter Release by Inhibiting Synaptic Vesicle Reclustering after Endocytosis. *Neuron* **65**(1), 66–79 (2010).
- [241] Dikiy, I. and Eliezer, D. N-terminal Acetylation stabilizes N-terminal Helicity in Lipid- and Micelle-bound α -Synuclein and increases its affinity for Physiological Membranes. *Journal of Biological Chemistry* **289**(6), 3652–3665 (2014).
- [242] Bodner, C. R., Dobson, C. M., and Bax, A. Multiple Tight Phospholipid-Binding Modes of α -Synuclein Revealed by Solution NMR Spectroscopy. *Journal of Molecular Biology* **390**(4), 775–790 (2009).
- [243] Bodner, C. R., Maltsev, A. S., Dobson, C. M., et al. Differential phospholipid binding of α -synuclein variants implicated in Parkinson's disease revealed by solution NMR spectroscopy. *Biochemistry* **49**(5), 862–871 (2010).
- [244] Jao, C. C., Hegde, B. G., Chen, J., et al. Structure of membrane-bound alpha-synuclein from site-directed spin labeling and computational refinement. *Proceedings of the National Academy of Sciences of the United States of America* **105**(50), 19666–19671 (2008).
- [245] Drescher, M., Veldhuis, G., Van Rooijen, B. D., et al. Antiparallel arrangement of the helices of vesicle-bound α -synuclein. *Journal of the American Chemical Society* **130**(25), 7796–7797 (2008).

-
- [246] Fusco, G., De Simone, A., Gopinath, T., et al. Direct observation of the three regions in α -synuclein that determine its membrane-bound behaviour. *Nature communications* **5**(May), 3827 (2014).
- [247] Drescher, M., Godschalk, F., Veldhuis, G., et al. Spin-label EPR on α -synuclein reveals differences in the membrane binding affinity of the two antiparallel helices. *ChemBioChem* **9**(15), 2411–2416 (2008).
- [248] Zhu, M. and Fink, A. L. Lipid binding inhibits α -synuclein fibril formation. *Journal of Biological Chemistry* **278**(19), 16873–16877 (2003).
- [249] Zhao, H., Tuominen, E. K. J., and Kinnunen, P. K. J. Formation of amyloid fibers triggered by phosphatidylserine-containing membranes. *Biochemistry* **43**(32), 10302–10307 (2004).
- [250] Bayburt, T. H., Grinkova, Y. V., and Sligar, S. G. Self-Assembly of Discoidal Phospholipid Bilayer Nanoparticles with Membrane Scaffold Proteins. *Nano Letters* **2**(8), 853–856 (2002).
- [251] Zhang, Z., Dai, C., Bai, J., et al. Ca²⁺ modulating α -synuclein membrane transient interactions revealed by solution NMR spectroscopy. *Biochimica et Biophysica Acta - Biomembranes* **1838**(3), 853–858 (2014).
- [252] Thomaier, M., Gremer, L., Dammers, C., et al. High-Affinity Binding of Monomeric but Not Oligomeric Amyloid- β to Ganglioside GM1 Containing Nanodiscs. *Biochemistry* **55**(48), 6662–6672 (2016).
- [253] Viegas, A., Viennet, T., and Etzkorn, M. The power, pitfalls and potential of the nanodisc system for NMR-based studies. *Biological Chemistry* **397**(12), 1335–1354 (2016).
- [254] Denisov, I. G., Grinkova, Y. V., Lazarides, A. A., et al. Directed Self-Assembly of Monodisperse Phospholipid Bilayer Nanodiscs with Controlled Size. *Journal of the American Chemical Society* **126**, 3477–3487 (2004).
- [255] Her, C., Filoti, D. I., McLean, M. A., et al. The Charge Properties of Phospholipid Nanodiscs. *Biophysical Journal* **111**(5), 989–998 (2016).
- [256] Inagaki, S., Ghirlando, R., White, J. F., et al. Modulation of the interaction between neurotensin receptor NTS1 and Gq protein by lipid. *Journal of Molecular Biology* **417**(1-2), 95–111 (2012).
- [257] Eichmann, C., Campioni, S., Kowal, J., et al. Preparation and characterization of stable α -synuclein lipoprotein particles. *Journal of Biological Chemistry* **291**(16), 8516–8527 (2016).
- [258] Hagn, F., Etzkorn, M., Raschle, T., et al. Optimized Phospholipid Bilayer Nanodiscs Facilitate High-Resolution Structure Determination of Membrane Proteins. *Journal of the American Chemical Society* **136**, 1919–1925 (2013).
- [259] Etzkorn, M., Raschle, T., Hagn, F., et al. Cell-free expressed bacteriorhodopsin in different soluble membrane mimetics: Biophysical properties and NMR accessibility. *Structure* **21**(3), 394–401 (2013).
- [260] Iyer, A., Roeters, S. J., Schilderink, N., et al. The impact of N-terminal acetylation of α -synuclein on phospholipid membrane binding and fibril structure. *Journal of Biological Chemistry* **291**(40), 21110–21122 (2016).
- [261] Rabe, M., Soragni, A., Reynolds, N. P., et al. On-surface aggregation of α -synuclein at nanomolar concentrations results in two distinct growth mechanisms. *ACS Chemical Neuroscience* **4**, 408–417 (2013).
- [262] Vácha, R., Linse, S., and Lund, M. Surface Effects on Aggregation Kinetics of Amyloidogenic Peptides. *Journal of the American Chemical Society* **136**, 11776–11782 (2014).
- [263] Campioni, S., Carret, G., Jordens, S., et al. The Presence of an Air-Water Interface Affects Formation and Elongation of α -Synuclein Fibrils. *Journal of the American Chemical Society* **136**, 2866–2875 (2014).
- [264] Pervushin, K., Riek, R., Wider, G., et al. Attenuated T2 relaxation by mutual cancellation of dipole–dipole coupling and chemical shift anisotropy indicates an avenue to NMR structures of very large biological macromolecules in solution. *Proceedings of the National Academy of Sciences* **94**(23), 12366–12371 (1997).
- [265] Siemer, A. B., Huang, K. Y., and McDermott, A. E. Protein Linewidth and Solvent Dynamics in Frozen Solution NMR. *PLoS ONE* **7**(10) (2012).
- [266] Hong, M. and Jakes, K. Selective and extensive C-13 labeling of a membrane protein for solid-state NMR investigations. *Journal of Biomolecular NMR* **14**(1), 71–74 (1999).

Bibliography

- [267] Alvarez, F. J. D., Orelle, C., and Davidson, A. L. Functional reconstitution of an ABC transporter in nanodiscs for use in electron paramagnetic resonance spectroscopy. *Journal of the American Chemical Society* **132**(28), 9513–9515 (2010).
- [268] Iyer, A., Petersen, N. O., Claessens, M. M. A. E., et al. Amyloids of alpha-synuclein affect the structure and dynamics of supported lipid bilayers. *Biophysical Journal* **106**(12), 2585–2594 (2014).
- [269] Buell, A. K., Galvagnion, C., Gaspar, R., et al. Solution conditions determine the relative importance of nucleation and growth processes in α -synuclein aggregation. *Proceedings of the National Academy of Sciences of the United States of America* **111**(21), 7671–7676 (2014).
- [270] Maltsev, A. S., Ying, J., and Bax, A. Impact of N-terminal acetylation of α -synuclein on its random coil and lipid binding properties. *Biochemistry* **51**(25), 5004–5013 (2012).
- [271] Bartels, T., Kim, N. C., Luth, E. S., et al. N-alpha-acetylation of α -synuclein increases its helical folding propensity, GM1 binding specificity and resistance to aggregation. *PLoS ONE* **9**(7), 1–10 (2014).
- [272] Kang, L., Janowska, M. K., Moriarty, G. M., et al. Mechanistic Insight into the Relationship between N-Terminal Acetylation of α -Synuclein and Fibril Formation Rates by NMR and Fluorescence. *PLoS ONE* **8**(9), 1–10 (2013).
- [273] Perni, M., Galvagnion, C., Maltsev, A. S., et al. A natural product inhibits the initiation of alpha-synuclein aggregation by displacing it from lipid membranes and suppresses its toxicity. *Proceedings of the National Academy of Sciences of the United States of America* **114**(6), E1009–E1017 (2017).
- [274] Johnson, M., Coulton, A. T., Geeves, M. A., et al. Targeted Amino-Terminal Acetylation of Recombinant Proteins in *E. coli*. *PLoS ONE* **5**(12), e15801 (2010).
- [275] Bayburt, T. H., Carlson, J. W., and Sligar, S. G. Reconstitution and imaging of a membrane protein in a nanometer-size phospholipid bilayer. *Journal of structural biology* **123**(1), 37–44 (1998).
- [276] Sauvée, C., Rosay, M., Casano, G., et al. Highly efficient, water-soluble polarizing agents for dynamic nuclear polarization at high frequency. *Angewandte Chemie - International Edition* **52**(41), 10858–10861 (2013).
- [277] Lindorff-Larsen, K., Piana, S., Palmo, K., et al. Improved side-chain torsion potentials for the Amber ff99SB protein force field. *Proteins: Structure, Function and Bioinformatics* **78**(8), 1950–1958 (2010).
- [278] Jämbeck, J. P. M. and Lyubartsev, A. P. Derivation and systematic validation of a refined all-atom force field for phosphatidylcholine lipids. *Journal of Physical Chemistry B* **116**(10), 3164–3179 (2012).
- [279] Jorgensen, W. L., Chandrasekhar, J., Madura, J. D., et al. Comparison of simple potential functions for simulating liquid water. *The Journal of Chemical Physics* **79**(2), 926 (1983).
- [280] Hess, B., Kutzner, C., Van Der Spoel, D., et al. GROMACS 4: Algorithms for highly efficient, load-balanced, and scalable molecular simulation. *Journal of Chemical Theory and Computation* **4**(3), 435–447 (2008).
- [281] Carr, M. and MacPhee, C. E. Membrainy: a ‘smart’, unified membrane analysis tool. *Source Code for Biology and Medicine* **10**(1), 3 (2015).
- [282] Lee, J., Cheng, X., Swails, J. M., et al. CHARMM-GUI Input Generator for NAMD, GROMACS, AMBER, OpenMM, and CHARMM/OpenMM Simulations Using the CHARMM36 Additive Force Field. *Journal of Chemical Theory and Computation* **12**(1), 405–413 (2016).
- [283] Jämbeck, M. J. P., Lyubartsev, P. A., Jämbeck, J. P. M., et al. Another Piece of the Membrane Puzzle: Extending Slipids Further. *Journal of chemical theory and computation* **9**(1), 774–784 (2013).
- [284] Smith, D. E. and Dang, L. X. Computer simulations of NaCl association in polarizable water. *The Journal of Chemical Physics* **100**(5), 3757 (1994).
- [285] Bussi, G., Donadio, D., and Parrinello, M. Canonical sampling through velocity rescaling. *Journal of Chemical Physics* **126**(1) (2007).
- [286] Nosé, S. A molecular dynamics method for simulations in the canonical ensemble. *Molecular Physics* **52**(2), 255–268 (1984).

-
- [287] Hoover, W. G. Canonical Dynamics: Equilibrium Phase-Space Distributions. *Phys. Rev. A* **31**(3), 1695 (1985).
- [288] Parrinello, M. and Rahman, A. Polymorphic transitions in single crystals: A new molecular dynamics method. *Journal of Applied Physics* **52**(12), 7182–7190 (1981).
- [289] Hess, B., Bekker, H., Berendsen, H. J. C., et al. LINCS: A linear constraint solver for molecular simulations. *Journal of Computational Chemistry* **18**(12), 1463–1472 (1997).
- [290] Darden, T., York, D., and Pedersen, L. Particle mesh Ewald: An N log(N) method for Ewald sums in large systems. *The Journal of Chemical Physics* **98**(12), 10089 (1993).
- [291] Essmann, U., Perera, L., Berkowitz, M. L., et al. A smooth particle mesh Ewald method. *J Chem Phys* **103**(1995), 8577–8593 (1995).
- [292] Hirtz, D., Thurman, D. J., Gwinn-Hardy, K., et al. How common are the "common" neurologic disorders? *Neurology* **68**(5), 326–337 (2007).
- [293] Scott, D. and Roy, S. A-Synuclein Inhibits Intersynaptic Vesicle Mobility and Maintains Recycling-Pool Homeostasis. *Journal of Neuroscience* **32**(30), 10129–10135 (2012).
- [294] Hsu, L. J., Sagara, Y., Arroyo, A., et al. α -Synuclein Promotes Mitochondrial Deficit and Oxidative Stress. *The American Journal of Pathology* **157**(2), 401–410 (2000).
- [295] Chen, L., Jin, J., Davis, J., et al. Oligomeric α -synuclein inhibits tubulin polymerization. *Biochemical and Biophysical Research Communications* **356**(3), 548–553 (2007).
- [296] Lee, H. J., Khoshaghideh, F., Lee, S., et al. Impairment of microtubule-dependent trafficking by overexpression of α -synuclein. *European Journal of Neuroscience* **24**(11), 3153–3162 (2006).
- [297] Colla, E., Coune, P., Liu, Y., et al. Endoplasmic reticulum stress is important for the manifestations of alpha-synucleinopathy in vivo. *Journal of Neuroscience* **32**(10), 3306–3320 (2012).
- [298] Schapira, A. H. Mitochondria in the aetiology and pathogenesis of Parkinson's disease. *The Lancet Neurology* **7**(1), 97–109 (2008).
- [299] Raha, S. and Robinson, B. H. Mitochondria, oxygen free radicals, disease and ageing. *Trends in Biochemical Sciences* **25**(10), 502–508 (2000).
- [300] Valente, E. M., Abou-sleiman, P. M., Caputo, V., et al. Hereditary Early-Onset Parkinson's Disease Caused by Mutations in PINK1. *Science* **304**(May), 1158–1161 (2004).
- [301] Kitada, T., Asakawa, S., Hattori, N., et al. Mutations in the parkin gene cause autosomal recessive juvenile parkinsonism. *Nature* **392**(6676), 605–608 (1998).
- [302] Bonifati, V., Rizzu, P., van Baren, M. J., et al. Mutations in the DJ-1 gene associated with autosomal recessive early-onset parkinsonism. *Science* **299**(5604), 256–259 (2003).
- [303] Kim, R. H., Smith, P. D., Aleyasin, H., et al. Hypersensitivity of DJ-1-deficient mice to 1-methyl-4-phenyl-1,2,3,6-tetrahydropyridine (MPTP) and oxidative stress. *Proc Natl Acad Sci U S A* **102**(14), 5215–5220 (2005).
- [304] Joselin, A. P., Hewitt, S. J., Callaghan, S. M., et al. ROS-dependent regulation of parkin and DJ-1 localization during oxidative stress in neurons. *Human Molecular Genetics* **21**(22), 4888–4903 (2012).
- [305] Hensley, K., Maidt, M. L., Yu, Z., et al. Electrochemical analysis of protein nitrotyrosine and dityrosine in the Alzheimer brain indicates region-specific accumulation. *The Journal of neuroscience : the official journal of the Society for Neuroscience* **18**(20), 8126–8132 (1998).
- [306] Matsuzaki, M., Hasegawa, T., Takeda, A., et al. Histochemical features of stress-induced aggregates in α -synuclein overexpressing cells. *Brain Research* **1004**(1-2), 83–90 (2004).
- [307] Pennathur, S., Jackson-Lewis, V., Przedborski, S., et al. Mass spectrometric quantification of 3-nitrotyrosine, ortho-tyrosine, and o,o'-dityrosine in brain tissue of 1-methyl-4-phenyl-1, 2, 3, 6-tetrahydropyridine-treated mice, a model of oxidative stress in Parkinson's disease. *Journal of Biological Chemistry* **274**(49), 34621–34628 (1999).

Bibliography

- [308] Takahashi, T., Yamashita, H., Nakamura, T., et al. Tyrosine 125 of α -synuclein plays a critical role for dimerization following oxidative stress. *Brain Research* **938**(1-2), 73–80 (2002).
- [309] van Maarschalkerweerd, A., Pedersen, M., Peterson, H., et al. Formation of covalent di-tyrosine dimers in recombinant α -synuclein. *Intrinsically Disordered Proteins* **3**(1), 1–12 (2015).
- [310] Kerwin, B. A. and Remmele, R. L. Protect from light: Photodegradation and protein biologics, (2007).
- [311] Balasubramanian, D. and Kanwar, R. Molecular pathology of dityrosine cross-links in proteins: Structural and functional analysis of four proteins. *Molecular and Cellular Biochemistry* **234-235**(2), 27–38 (2002).
- [312] Grüning, C. S. R., Mirecka, E. A., Klein, A. N., et al. Alternative conformations of the tau repeat domain in complex with an engineered binding protein. *Journal of Biological Chemistry* **289**(33), 23209–23218 (2014).
- [313] Porcari, R., Proukakis, C., Waudby, C. A., et al. The H50Q mutation induces a 10-fold decrease in the solubility of α -synuclein. *Journal of Biological Chemistry* **290**(4), 2395–2404 (2015).
- [314] Wolff, M., Mittag, J. J., Herling, T. W., et al. Quantitative thermophoretic study of disease-related protein aggregates. *Scientific Reports* **6**(22829) (2016).
- [315] Koide, S. and Sidhu, S. S. The importance of being tyrosine: Lessons in molecular recognition from minimalist synthetic binding proteins. *ACS Chemical Biology* **4**(5), 325–334 (2009).
- [316] Brown, A. H., Rodger, P. M., Evans, J. S., et al. Equilibrium conformational ensemble of the intrinsically disordered peptide n16N: Linking subdomain structures and function in nacre. *Biomacromolecules* **15**(12), 4467–4479 (2014).
- [317] Zeskind, B. J., Jordan, C. D., Timp, W., et al. Nucleic acid and protein mass mapping by live-cell deep-ultraviolet microscopy. *Nature Methods* **4**(7), 567–569 (2007).
- [318] Pedersen, J. T., Chen, S. W., Borg, C. B., et al. Amyloid- β and α -Synuclein Decrease the Level of Metal-Catalyzed Reactive Oxygen Species by Radical Scavenging and Redox Silencing. *Journal of the American Chemical Society* **138**(12), 3966–3969 (2016).
- [319] Hashimoto, M., Hsu, L. J., Xia, Y., et al. Oxidative stress induces amyloid-like aggregate formation of NACP/ α -synuclein in vitro. *Neuroreport* **10**(4), 717–721 (1999).
- [320] Jonsson, T., Atwal, J. K., Steinberg, S., et al. A mutation in APP protects against Alzheimer's disease and age-related cognitive decline. *Nature* **488**(7409), 96–99 (2012).
- [321] Salloway, S., Sperling, R., Keren, R., et al. A phase 2 randomized trial of ELND005, scyllo-inositol, in mild to moderate Alzheimer disease. *Neurology* **77**(13), 1253–1262 (2011).
- [322] Sevigny, J., Chiao, P., Bussière, T., et al. The antibody aducanumab reduces A β plaques in Alzheimer's disease. *Nature* **537**(7618), 50–56 (2016).
- [323] Takamori, S., Holt, M., Stenius, K., et al. Molecular Anatomy of a Trafficking Organelle. *Cell* **127**(4), 831–846 (2006).
- [324] Devaux, P. F. and Morris, R. Transmembrane asymmetry and lateral domains in biological membranes. *Traffic* **5**(4), 241–246 (2004).
- [325] Ferreon, A. C. M., Gambin, Y., Lemke, E. A., et al. Interplay of α -synuclein binding and conformational switching probed by single-molecule fluorescence. *Proceedings of the National Academy of Sciences* **106**(14), 5645–5650 (2009).
- [326] Lorenzen, N., Nielsen, S. B., Yoshimura, Y., et al. How epigallocatechin gallate can inhibit α -synuclein oligomer toxicity in vitro. *Journal of Biological Chemistry* **289**(31), 21299–21310 (2014).

Appendix

Declaration of Contributions

Article One: Single fibril growth kinetics of α -Synuclein

Michael M. Wördehoff¹, Oliver Bannach^{1,2,*}, Hamed Shaykhalishahi¹, Andreas Kulawik^{1,2}, Stephanie Schiefer¹, Dieter Willbold^{1,2}, Wolfgang Hoyer^{1,2}, and Eva Birkmann^{1,2}

Published in: **Journal of Molecular Biology**, Vol. 427, Issue 6, Part B, pp. 1428–1435, 2015 [64]

DOI: [10.1016/j.jmb.2015.01.020](https://doi.org/10.1016/j.jmb.2015.01.020)

Journal Impact Factor (2015): 4.517.

Contribution: 75%

Oliver Bannach, Michael M. Wördehoff, Wolfgang Hoyer, Eva Birkmann and Dieter Willbold designed the experiments. M.M.W. performed the experiments shown in the article and evaluated and plotted the data. The AFM micrographs have been recorded by Stephanie Schiefer. Hamed Shaykhalishahi provided α -synuclein and assisted in producing it. Wolfgang Hoyer, Oliver Bannach and Andreas Kulawik participated in evaluation of the data. M.M.W., W.H. and O.B. wrote the manuscript. All authors commented on the manuscript.

Article Two: Contact Between the β 1 and β 2 Segments of α -Synuclein that Inhibits Amyloid Formation

Hamed Shaykhalishahi¹, Aziz Gauhar¹, Michael M. Wördehoff¹, Clara S. R. Grüning¹, Antonia N. Klein², Oliver Bannach^{1,2}, Matthias Stoldt^{1,2}, Dieter Willbold^{1,2}, Torleif Härd³, and Wolfgang Hoyer^{1,2,#}

Published in: **Angewandte Chemie International Edition**, Vol. 54, pp. 8837-8840, 2015 [139]

DOI: [10.1002/anie.201503018](https://doi.org/10.1002/anie.201503018)

Journal Impact Factor (2015): 11.709.

Contribution: 20%

Michael M. Wördehoff designed and performed the TIRF microscopy experiments shown in [fig. 2.11](#) and evaluated/plotted the data. He wrote method sections for and commented on the manuscript.

Article Three: A structural and kinetic link between membrane association and amyloid fibril formation of α -Synuclein

Thibault Viennet^{1,2}, Michael M. Wördehoff¹, Boran Uluca^{1,2}, Chetan Poojari^{2,4,5}, Hamed Shaykhalishahi¹, Dieter Willbold^{1,2}, Birgit Strodel², Henrike Heise^{1,2}, Alexander K. Buell¹, Wolfgang Hoyer^{1,2} & Manuel Etzkorn^{1,2,§}

Submitted to: **Nature Chemical Biology**, 12.05.2017. Journal Impact Factor (2016/2017): 15.066.

Contribution: 35%

Michael M. Wördehoff prepared unlabelled and ¹⁵N-labelled acetylated and non-acetylated α -synuclein for the experiments. M.M.W. performed all Thioflavin T aggregation assays and SDS gels and evaluated and plotted the data. He wrote method sections for and commented on the manuscript.

Article Four: Opposed Effects of Dityrosine Formation in Soluble and Aggregated α -Synuclein on Fibril Growth

Michael M. Wördehoff¹, Hamed Shaykhalishahi¹, Luca Groß¹, Lothar Gremer^{1,2}, Mathias Stoldt^{1,2}, Alexander K. Buell¹, Dieter Willbold^{1,2} and Wolfgang Hoyer^{1,2,#}

Submitted to: **Journal of Molecular Biology**, 30.06.2017. Journal Impact Factor (2016/2017): 4.632.

Contribution: 75%

Wolfgang Hoyer, Michael M. Wördehoff, Alexander K. Buell, Lothar Gremer, and Dieter Willbold designed the experiments. M.M.W. performed the experiments shown in the manuscript, evaluated and plotted the data. Additionally, AFM micrographs have been made by Luca Groß, NMR measurements were performed by Mathias Stoldt. Hamed Shaykhalishahi performed preliminary experiments. M.M.W., W.H. and A.K.B wrote the manuscript. All authors commented on the manuscript.

¹Institut für Physikalische Biologie, Heinrich-Heine-Universität Düsseldorf, Universitätsstr. 1, 40225 Düsseldorf, Germany

²Institute of Complex Systems (ICS-6), Research Centre Jülich, Wilhelm-Johnen-Straße, 52428 Jülich, Germany

³Department of Chemistry and Biotechnology, Swedish University of Agricultural Sciences (SLU), 750 07 Uppsala, Sweden

⁴Department of Physics, Tampere University of Technology, Finland

⁵Department of Physics, University of Helsinki, Finland

corresponding authors: *bannacho@hhu.de, #wolfgang.hoyer@hhu.de, §manuel.etzkorn@hhu.de

List of Abbreviations

^1H - ^{15}N	Hydrogen-1-Nitrogen-15 (in respect to NMR spectra)
2YT	Yeast extract tryptone medium, double strength
Å	Ångström (unit), 1 Å = 0.1 nm
A30P	Alanine at position 30 mutated to proline (α -synuclein)
A53T	Alanine at position 53 mutated to threonine (α -synuclein)
A β	Amyloid- β peptide
A β CC	Amyloid- β peptide with intramolecular disulfide bridge
AD	Alzheimer's disease
AFM	Atomic force microscopy
α S, α -Syn	α -Synuclein
α -SynCC	α -Synuclein with intramolecular disulfide bridge
α -Syn-A140C	α -Synuclein, alanine at position 140 mutated to cysteine
ALS	Amyotrophic lateral sclerosis
AMUPOL	15-[(7-oxyl-3,11-dioxa-7-azadispiro[5.1.5.3]hexadec-15-yl)carbamoyl][2-(2,5,8,11-tetraoxatridecan-13-ylamino)-[3,11-dioxa-7-azadispiro[5.1.5.3]hexadec-7-yl)]oxidanyl
ANS	8-Anilino-1-naphthalenesulfonic acid
AS69	β -wrapin affibody AS69
BBB	Blood brain barrier
BEST	Band-selective excitation short-transient (NMR technique)
BL21DE3	Special protein expression strain of <i>Escherichia coli</i>
BLI	Bio-layer interferometry
C-term	Carboxyterminus of a protein
CNS	Central nervous system
Cryo-EM	Electron microscopy, samples are deep frozen in liquid nitrogen
DBS	Deep brain stimulation
DCVJ	9-(2,2-Dicyanovinyl)julolidine
DiY	Dityrosine
DiY- α -syn	Dityrosine-crosslinked α -synuclein
DJ-1	Parkinsonism-associated deglycase
DLB	Dementia with Lewy bodies
DLS	Dynamic light scattering
DMPC	1,2-Dimyristoyl-sn-glycero-3-phosphocholine
DMPG	1,2-Dimyristoyl-sn-glycero-3-phosphorylglycerol
DMPS	1,2-Dimyristoyl-sn-glycero-3-phosphoserine

List of Abbreviations

DNA	Deoxyribonucleic acid
DNP	Dynamic nuclear polarization
DOPA	3,4-dihydroxyphenylalanine
DSC	Differential scanning calorimetry
dSTORM	Direct stochastic optical reconstruction microscopy
DTT	Dithiothreitol
<i>E. coli</i>	<i>Escherichia coli</i>
E46K	Glutamate at position 46 mutated to lysine (α -synuclein)
EDC/NHS	1-Ethyl-3-(3-dimethylaminopropyl)carbodiimid/N-Hydroxysulfosuccinimid
EDTA	Ethylenediaminetetraacetic acid
EM	Electron microscopy
ER	Endoplasmatic reticulum
<i>g</i>	G-force
G2019S	Glycine at position 2019 mutated to serine (LRRK2)
G51D	Glycine at position 51 mutated to aspartate (α -synuclein)
GdnHCl	Guanidine hydrochloride
GRAVY	Grand average of hydropathy
H50Q	Histidine at position 50 mutated to glutamine
HSQC	Heteronuclear single quantum coherence (NMR)
IAPP	Islet amyloid polypeptide
IDP	Intrinsically disordered protein
IgG	Immunoglobulin G
IMAC	Immobilized metal ion affinity chromatography
IPTG	Isopropyl β -D-1-thiogalactopyranoside
$k_{on}, k_1, k_2, k_+, k_-$	Several kinetic rate constants
K_D	Equilibrium dissociation constant
kDa	Kilodalton
$\lambda_{Ex/Em}$	Excitation-/Emissionwavelength
<i>LRRK2</i>	Gene coding for leucine-rich repeat kinase 2
M	Molar, mol/l ⁻¹
MAS	Magic angle spinning (NMR)
MD	Molecular dynamics (simulation)
MES	2-(N-morpholino)ethanesulfonic acid
Milli-Q H ₂ O	Ultrapure water by Millipore (18.2 M Ω x cm at 25 °C)
M.M.W.	Michael Marius Wördehoff
MPTP	1-methyl-4-phenyl-1,2,3,6-tetrahydropyridine

MSA	Multiple system atrophy
MSP	Membrane scaffold protein
MSP1D1ΔH5	Membrane scaffold protein, helix 5 deleted
MTT	3-(4,5-dimethylthiazol-2-yl)-2,5-diphenyltetrazolium bromide
MWCO	Molecular weight cutoff
N-term	Amino-terminus of a protein
NA	Natural abundance (in terms of isotopes)
NAC	non-amyloid-β component region of α-synuclein
NaPi	Sodium phosphate (buffer)
ND	Nanodisc
NMDA	N-methyl-D-aspartate
NMR	Nuclear magnetic resonance (spectroscopy)
NPT	Isothermal–isobaric ensemble (in MD simulations)
OD	Optical density
OS	Oxidative stress
p_-	Probability of being in a stop state
p_+	Probability of being in a growth state
<i>PARK7</i>	Gene coding for Parkinsonism-associated deglycase
PC	Phosphatidylcholine
PCR	Polymerase chain reaction
PD	Parkinson's disease
PDB	Protein data bank
PDSD	Proton-driven spin diffusion
PG	Phosphatidylglycerol
pH	potentia Hydrogenii
<i>PINK1</i>	Gene coding for PTEN-induced putative kinase 1
PMD(s)	Protein misfolding disease(s)
PME	Particle mesh ewald (MD simulations)
Pmel17	premelanosome protein
POPC	1-palmitoyl-2-oleoyl-sn-glycero-3-phosphocholine
POPG	1-palmitoyl-2-oleoyl-sn-glycero-3-phosphoglycerol
<i>PRKN</i>	Gene encoding for parkin RBR E3 ubiquitin protein ligase
PTEN	Phosphatase and tensin homolog
QCM	Quartz crystal microbalance
RBD	Rapid eye movement sleep behavior disorder
ROS	Reactive oxygen species
S87E	Serine at position 87 mutated to glutamate

List of Abbreviations

SAXS	Small-angle X-ray scattering
SDS-PAGE	Sodium dodecyl sulfate polyacrylamide gel electrophoresis
SEC	Size exclusion chromatography
SH-S5Y5	Human neuroblastoma cell line
SNARE	Soluble NSF attachment protein receptor
<i>SNCA</i>	Gene coding for α -synuclein
SOD1	Superoxide dismutase
ssNMR	Solid-state nuclear magnetic resonance spectroscopy
Sup35	Eukaryotic peptide chain release factor GTP-binding subunit
SUV(s)	Small unilamellar vesicle(s)
T2D	Type 2 diabetes mellitus
TCI	Triple resonance cryoprobe (NMR)
TEM	Transmission electron microscopy
TEV	Tobacco etch virus
ThT	Thioflavin T
TIRFM	Total internal reflection fluorescence microscopy
T_m	Melting temperature
Tris-HCl	tris(hydroxymethyl)aminomethane, pH adjusted with hydrochloric acid
TROSY	Transverse relaxation optimized spectroscopy
TSE(s)	Transmissible spongiform encephalopathies(s)
Tyr	Tyrosine
Tyr KO	Tyrosine knockout
$U\text{-}^{15}\text{N}$	Uniformly labeled with nitrogen-15 (NMR)
UV	Ultraviolet (light)
UV/VIS	Ultraviolet–visible (spectroscopy)
v/v	Volume/volume (ratio)
w/w	Weight/weight (ratio)
WT, wt	Wildtype (protein)
Y-to-A	Tyrosine-to-alanine (mutants of α -syn)
Y39A, Y125A, Y133A, Y136A	Four tyrosine-to-alanine mutants of α -syn
ZA β 3	β -Wrapin affibody binder for amyloid- β

Danksagung

Zunächst möchte ich meinem Erstgutachter Prof. Dr. Dieter Willbold danken, der mir die Doktorarbeit in seinem Institut für Physikalische Biologie ermöglicht hat. Die Arbeit im Institut hat mir durch die lockere und produktive Atmosphäre immer Spaß gemacht. Bei Fragen und Problemen hatte er immer ein offenes Ohr und verstand es, Projekte wieder auf den richtigen Weg zu bringen. Natürlich danke ich ihm auch für die Übernahme der Erstkorrektur meiner Arbeit.

Zweitens möchte ich Dr. Wolfgang Hoyer danken. Die Zusammenarbeit war und ist für mich lehrreich und führte zu vielen interessanten Projekten und Diskussionen, aus denen ich immer etwas gelernt habe, nicht nur auf intellektueller Ebene, sondern auch was erfolgreiche Kooperation ausmacht. Ich danke dir für die Übernahme der Zweitkorrektur und für die entspannte und professionelle Arbeitsatmosphäre, die deutlich zur Erreichung meiner wissenschaftlichen Ziele beigetragen hat.

Dr. Oliver Bannach und Dr. Eva Birkmann danke ich für die Betreuung meiner Promotion in der Anfangsphase und die Einführung ins Institutsleben.

Dr. Hamed Shaykhalishahi möchte ich für die anfängliche Betreuung im Labor, viele bereitgestellte Proben und den fruchtbaren wissenschaftlichen Austausch danken. Dr. Steffen Hübinger, Dr. Lars Luers, Dr. Tommy Agyenim und Dr. Jendrik Marbach danke ich für die vortreffliche Stimmung im Büro 1.0 und unterhaltsame und lehrreiche Gespräche. Julian Victor, Hannah Rosenbach und Lisa Galle danke ich für die vortreffliche Stimmung im Büro 2.0. Frederike Klaus danke ich für die sehr angenehme Zusammenarbeit während ihrer Bachelorarbeit und die vielen unterhaltsamen Gespräche. Desweiteren danke ich den Mitgliedern des Instituts für Physikalische Biologie für die Hilfsbereitschaft. Insbesondere seien hier Heidi Gruber, Astrid Wies und Elke Reinartz erwähnt, die immer mit Rat und Tat zur Seite standen. Ich danke auch für die sehr angenehme Stimmung im Institut und viele unvergessliche Weihnachtsfeiern, Institutsausflüge etc.

Meinen Institutsbandkollegen Dr. Mario Schneider, Dr. Manuel Etzkorn und Dr. Oliver Bannach danke ich für die vielen super Bandproben, Konzerte, Weihnachtsfeiern und Sommerfeste. Dass wir zusammen eine stattliche, Uni-weit bekannte (:D) Rockband aufgezogen haben, ist einfach mega. The Aggregates waren stets ein wunderbarer Ausgleich zur wissenschaftlichen Arbeit. The Legend will return!

Meinen Freunden danke ich für die vielen schönen Momente neben der Arbeit (teilweise auch bei der Arbeit) und der Unterstützung auf vielfältige Weise. Neben meinen langjährigen Freunden Manuel Schnee und Maximilian Juncker seien besonders Julian Victor, Felix Arntz, Laura Reiche, Katharina Koch und Hannah Rosenbach erwähnt. Ohne euch hätte ich echt wenig Spaß gehabt. :)

Thomas Maurer danke ich für die unterhaltsame Zeit in Wuppertal und seine kontinuierliche Bekräftigung, dass \LaTeX das einzig wahre Textverarbeitungsprogramm ist, um eine Dissertation zu verfassen. Zum Glück habe ich mir das zu Herzen genommen und kann das jetzt bestätigen.

Meinen Eltern, insbesondere meinem Vater Alfred Wördehoff, verdanke ich natürlich hauptsächlich, dass ich meine Ziele und Wünsche verwirklichen konnte. Du hast in mir früh die Motivation geweckt, mich mit Naturwissenschaft zu beschäftigen und zu experimentieren und mich immer in meinem Weg unterstützt. Außerdem danke ich dir für die musikalische Erziehung, die mir immer viel Freude bereitet und ein wunderbarer Ausgleich im Leben ist! Meiner großartigen Familie möchte ich für die vielen schönen Momente danken! Insbesondere meiner Großmutter, Marga Wördehoff, danke ich für die guten Gespräche, das gute Essen und die Unterstützung in vielen Lebenssituationen.

„Geil ist, wer Geiles tut.“

Julian Victor

Erklärung

Ich versichere an Eides Statt, dass die Dissertation von mir selbständig und ohne unzulässige fremde Hilfe unter Beachtung der „Grundsätze zur Sicherung guter wissenschaftlicher Praxis an der Heinrich-Heine-Universität Düsseldorf“ erstellt worden ist.

Die Dissertation wurde in der vorgelegten oder in ähnlicher Form noch bei keiner anderen Institution eingereicht. Ich habe bisher keine erfolglosen Promotionsversuche unternommen.

Ort, Datum

Michael M.W. Wördehoff